TECHNICAL REPORT STANDARD TITLE PAGE

1. Report No.	2. Government Accession No.	3. Recipient's Catalog No.
FHWA/TX-82/34+256-2		

4. Title and Subtitle	5. Report Date
DETERMINATION OF IN SITU SHEAR WAVE VELOCITIES FROM SPECTRAL ANALYSIS OF SURFACE WAVES	December 1982
	6. Performing Organization Code
7. Author(s) J. Scott Heisey, Kenneth H. Stokoe, W. Ronald Hudson, and A. H. Meyer	8. Performing Organization Report No. Research Report 256-2
9. Performing Organization Name and Address Center for Transportation Research The University of Texas at Austin Austin, Texas 78712-1075	10. Work Unit No.
	11. Contract or Grant No. Research Study 3-8-80-256
12. Sponsoring Agency Name and Address Texas State Department of Highways and Public Transportation; Transportation Planning Division P. O. Box 5051 Austin, Texas 78763	13. Type of Report and Period Covered Interim
	14. Sponsoring Agency Code

15. Supplementary Notes

Study conducted in cooperation with the U. S. Department of Transportation Federal Highway Administration

Research Study Title: "The Study of New Technologies for Pavement Evaluation"

16. Abstract

A method for determining elastic moduli at soil and pavement sites was proposed and tested. Surface receivers were utilized to evaluate the Rayleigh wave motion created by a vertical, impulsive source that could excite a wide range of frequencies with a single impact. Analysis was facilitated by using a portable spectral analyzer to study the magnitude and phase of the frequency content of the recorded wave pulse.

Results from field testing at two flexible pavement sites and two soil sites indicate that the spectral analysis of surface waves provides an accurate estimation of the velocity (and hence modulus) profile at a site. Moduli calculated from wave propagation velocities were generally comparable to moduli calculated by deflection measurements from Dynaflect testing.

17. Key Words	18. Distribution Statement
pavement evaluation, elastic modulus, nondestructive testing, seismic waves	No restrictions. This document is available to the public through the National Technical Information Service, Springfield, Virginia 22161.

19. Security Classif. (of this report)	20. Security Classif. (of this page)	21. No. of Pages	22. Price
Unclassified	Unclassified	292	

Form DOT F 1700.7 (8-69)

DETERMINATION OF IN SITU SHEAR WAVE VELOCITIES FROM SPECTRAL ANALYSIS OF SURFACE WAVES

by

J. Scott Heisey
Kenneth H. Stokoe
W. Ronald Hudson
A. H. Meyer

Research Report Number 256-2

The Study of New Technologies for Pavement Evaluation
Research Project 3-8-80-256

conducted for

Texas
State Department of Highways and Public Transportation

in cooperation with the
U. S. Department of Transportation
Federal Highway Administration

by the

CENTER FOR TRANSPORTATION RESEARCH
BUREAU OF ENGINEERING RESEARCH
THE UNIVERSITY OF TEXAS AT AUSTIN

December 1982

The contents of this report reflect the views of the authors, who are responsible for the facts and the accuracy of the data presented herein. The contents do not necessarily reflect the official views or policies of the Federal Highway Administration. This report does not constitute a standard, specification, or regulation.

PREFACE

This report summarizes the results to date of an experimental study to evaluate the use of spectral analysis of wave forces a a nondestructive method of determining elastic moduli of pavement layers.

The project is being conducted at the Center for Transportation Research, The University of Texas at Austin, as part of the Cooperative Highway Research Program sponsored by the Texas State Department of Highways and Public Transportation and the Federal Highway Administration.

Special appreciation is due Richard Rogers, Harett Hakins, Jim Long, and Leon Snyder for their assistance concerning this project.

J. Scott Heisey

Kenneth H. Stokoe, II

W. Ronald Hudson

A. H. Meyer

LIST OF REPORTS

Report No. 256-1, "Comparison of the Falling Weight Deflectometer and the Dynaflect for Pavement Evaluation," by Bary Eagleson, Scott Heisey, W. Ronald Hudson, Alvin H. Meyer, and Kenneth H. Stokoe, presents the results of an analytical study undertaken to determine the best model for pavement evaluation using the criteria of cost, operational characteristics, and suitability.

Report No. 256-2, "Determination of In Situ Shear Wave Velocities From Spectral Analysis of Surface Waves," by J. Scott Heisey, Kenneth H. Stokoe II, W. Ronald Hudson, and A. H. Meyer, presents a method for determining elastic moduli at soil and pavement sites. Criteria considered in developing this method included the restraint of nondestructive testing, accuracy of moduli for all layers regardless of thickness, and quickness and effeciency for rapid, extensive testing.

ABSTRACT

A method for determining elastic moduli at soil and pavement sites was proposed and tested. Surface receivers were utilized to evaluate the Rayleigh wave motion created by a vertical, impulsive source that could excite a wide range of frequencies with a single impact. Analysis was facilitated by using a portable spectral analyzer to study the magnitude and phase of the frequency content of the recorded wave pulse.

Results from field testing at two flexible pavement sites and two soil sites indicate that the spectral analysis of surface waves provides an accurate estimation of the velocity (and hence modulus) profile at a site. Moduli calculated from wave propagation velocities were generally comparable to moduli calculated by deflection measurements from Dynaflect testing.

KEYWORDS: Pavement evaluation, elastic modulus, nondestructive testing, seismic waves.

SUMMARY

A method for determining elastic moduli at soil and pavement sites was proposed and tested. Criteria considered in developing this method included the restraint of nondestructive testing, accuracy of moduli for all layers regardless of thicknesses, and quickness and efficiency for rapid, extensive testing. To meet these criteria, surface receivers were utilized to evaluate the Rayleigh wave motion created by a vertical, impulsive source that could excite a wide range of frequencies with a single impact. Analysis was facilitated by using a portable spectral analyzer to study the magnitude and phase of the frequency content of the recorded wave pulse.

Phase information from the cross spectrum function was used to calculate Rayleigh wave velocities from which shear wave velocities were calculated. Elastic moduli (shear moduli and Young's moduli) were then calculated from the shear wave velocities. Results from field testing at two pavement sites and two soil sites indicate that the spectral analysis of surface waves provides an accurate estimation of the velocity (and hence modulus) profile at a site. Moduli calculated from wave propagation velocities were generally comparable to moduli calculated by deflection measurements from Dynaflect testing.

IMPLEMENTATION STATEMENT

The procedure described in this report should not be implemented at the present time. The equipment and procedures are not sufficiently refined, and the data are not adequate to establish standard tests.

TABLE OF CONTENTS

PREFACE iii

LIST OF REPORTS v

ABSTRACT vii

SUMMARY ix

IMPLEMENTATION STATEMENT xi

CHAPTER 1. INTRODUCTION 1

CHAPTER 2. MEASUREMENT OF ELASTIC PROPERTIES BY WAVE PROPAGATION

Review of Wave Propagation Theory 5
Wave Propagation in an Elastic Half-Space 5
Wave Propagation in a Layered System 13
Field Techniques for Determining Elastic Properties 15
Investigation of Soil Profiles 15
Evaluation of Pavements 22
Application of Spectral Analysis 25

CHAPTER 3. DIGITAL SIGNAL AND SPECTRAL ANALYSES

Time Domain Measurements 29
Averaging 29
Correlation 30
Frequency Domain Measurements 33
Advantages of Spectral Analysis 33
The Fourier Transform 36
Measurements in the Frequency Domain 40
Linear Spectrum 40
Auto Spectrum 40
Cross Spectrum 41
Transfer Function 42
Coherence Function 42
Additional Considerations for Digital Signal Analysis 44

CHAPTER 4. SOIL TESTING AT WALNUT CREEK SITE

Site Description 47
Experimental Procedure 47
Test Series WC-1 50
Test Series WC-2 52
Recording of Spectral Measurements 59
Description of Sources 60
Drop Hammer 60
Drop Hammer on Embedded Steel Wedge 61
Sledge Hammer on Embedded Concrete Cylinder 61
Small Hammer on Wooden Plate 63
Comparison of Significant Parameters 63
Number of Averages 63
Measurement Bandwidth 66
Sources 74
Test Series WC-1 74
Test Series WC-2 76
Spatial Distribution of Geophones 84
Shear Wave Velocity Profile 96
Crosshole Test Results 96
Velocity Profile from Cross Spectrum Measurements 99
Comparisons Between Cross Spectrum Measurements and Crosshole Results 101
Attenuation Measurements 105
Summary 116

CHAPTER 5. SOIL TESTING AT THE CROSSING SITE

Site Description 119
Experimental Procedure 121
Shear Wave Velocity Profile 123
Velocity Profiles From Cross Spectrum Measurements 126
Comparison Between Cross Spectrum Measurements and Crosshole Results 134
Attenuation 138
Summary 148

CHAPTER 6. PAVEMENT EVALUATION AT AUSTIN SITE

Site Description 151
Experimental Procedure 154
Equipment 154
Measurement Setup and Analysis 156

Results from Surface Measurements 158
Comparison of Horizontal and Vertical Geophones 160
Analysis of the Falling Weight Deflectometer 166
Analysis of the Drop Hammer 172
Comparison of the FWD and the Drop Hammer 178
Results from Crosshole Testing 184
Description of Test Procedure 184
Analysis of Crosshole Data 186
Determination of Moduli 193
Summary 194

CHAPTER 7. PAVEMENT EVALUATION OF GRANGER SITE

Site Description 197
Experimental Procedure 200
Determination of Velocity Profile 202
Determination of Moduli 216
Summary 218

CHAPTER 8. SUMMARY, CONCLUSIONS, AND RECOMMENDATIONS

Summary 221
General Conclusions Regarding Test-Related Variables 222
Conclusions and Recommendations for Soil Investigation 224
Conclusions and Recommendations for Pavement Evaluation 226

REFERENCES 229

APPENDICIES

Appendix A. Discussion of Experimental Procedures and Data Analysis 235

Appendix B. Computer Programs and Plot Routines 255

THE AUTHORS 275

CHAPTER 1. INTRODUCTION

Wave propagation velocities are used to determine material properties which characterize the response of systems undergoing low-strain, dynamic loading. Examples of such systems are foundations which support vibrating machinery and pavements which support repetitive traffic loads. In the dynamic design of foundations, material properties are generally characterized by the shear modulus. For the design of pavement systems, material properties are characterized by the elastic (Young's) modulus. Both moduli can be easily calculated if the shear wave velocities of the materials of concern are known.

In this study, a method was investigated to determine shear wave velocities from the frequency spectrum of surface waves. Both the source of surface wave energy and the receivers to detect wave motion are located on the surface. This approach eliminates the need for drilling and coring. As a result, the time and costs of a site investigation are greatly reduced. The method is quick and nondestructive, thereby making it feasible for the evaluation of existing pavement systems. In addition, the analysis of the frequency spectrum of the surface wave(s) provides data for individual layers in a multilayered system.

Basic theory of wave propagation pertinent to this method is briefly reviewed in Chapter 2. Conventional techniques for site investigation and pavement evaluation are also discussed. The spectral analysis method is

presented and discussed in relation to the theory and in comparison with other methods. Chapter 3 introduces the reader to the theory and mathematics of the Fourier transform, which provides the framework for spectral analysis. Various functions derived from frequency spectrums are defined and their general uses are described.

Field investigations were conducted at two sites where the profile included a flexible pavement surface, a base course, and subgrade soil (referred to as pavement sites) and at two sites where the profile included only soil (referred to as soil sites). The soil sites were investigated to determine the influence of the relatively stiff layers at the surface of a pavement system on the propagation of surface waves through the underlying soil. The soil sites which were selected had previously been investigated by crosshole seismic testing and thereby provided additional test sites to verify the applicability and accuracy of the spectral analysis method.

Results from the soil sites, Walnut Creek and the Crossing, are presented in Chapters 4 and 5, respectively. Test-related variables which were studied include type of source, number of averages in the measurement, frequency range of the measurement bandwidth, location of the receivers from the source, and the appropriate depth factor to correlate the measured velocity profile with known field conditions.

Results from the pavement sites, IH 35 in Austin, Texas, and FM 971 near Granger, Texas, are presented in Chapters 6 and 7, respectively. At the Austin site, comparison measurements were made between the Falling Weight Deflectometer and a small, hand-held drop hammer. Other test-related variables included: orientation of the receivers (for horizontal or vertical motion), location of the receivers from the source, and frequency range of the measurement.

At all four sites, data from crosshole seismic testing either available or were gathered for comparison purposes. Comparisons between the velocity profiles obtained from crosshole testing and those obtained from spectral analysis of surface waves indicate that, in general, the spectral analysis method provides an accurate estimation of the velocity (and, hence, modulus) profile of a site. However, further investigation of some of the test-related variables is necessary to refine the method and to reinforce the conclusions of this study. Conclusions and recommendations for future research are summarized in Chapter 8.

For the benefit of the reader, a detailed discussion of the experimental procedure and useful data reduction is presented in Appendix A. The computer programs used for data reduction and analysis are listed in Appendix B.

CHAPTER 2. MEASUREMENT OF ELASTIC PROPERTIES BY WAVE PROPAGATION

REVIEW OF WAVE PROPAGATION THEORY

Since the stress-strain properties of a material govern wave propagation velocities in that material, dynamic (also called seismic) testing can be used to determine wave propagation velocities from which moduli of the material can be calculated. These moduli characterize behavior in the "elastic" range, where the material is undergoing very small strains. Relationships between moduli and wave propagation velocities are presented in the following sections. A more complete and rigorous discussion on wave propagation in elastic media can be found in the textbooks by Richart, Hall, and Woods (1970) and Ewing, Jardetzky, and Press (1957).

WAVE PROPAGATION IN AN ELASTIC HALF-SPACE

Wave motion created by a disturbance within an infinite, isotopic, elastic medium, usually called a "whole space," can be described by two kinds of waves: compression waves and shear waves. These waves are called body waves because they propagate within the body of the medium. When the elastic medium forms a half-space with an upper surface of infinite extent, a third type of wave motion occurs. This third type of wave occurs in a zone near

the surface of the half-space. The surface wave is named after its first investigator, Lord Rayleigh (1885). Each of these three waves displays a different type of motion and travels at a different velocity.

The compression wave exhibits a "push-pull" motion and, hence, is referred to as a dilatational wave. This dilatational motion occurs in the same direction as the direction of wave propagation. The compression wave travels with a faster velocity than either the shear wave or the Rayleigh wave. Since the compression wave appears first in a travel time record of wave motions, it is commonly called the primary wave, or P-wave. The velocity of the P-wave, V_P, is given by

$$V_P = \sqrt{\frac{\lambda + 2G}{\rho}} = \sqrt{\frac{M}{\rho}} \tag{2.1}$$

where

$$\lambda \text{ (Lame's constant)} = \frac{\nu E}{(1 + \nu)(1 - 2\nu)} \tag{2.2}$$

$$G \text{ (shear modulus)} = \frac{E}{2(1 + \nu)} \tag{2.3}$$

$$M \text{ (constrained modulus)} = \frac{1 - \nu}{(1 + \nu)(1 - 2\nu)} E \tag{2.4}$$

$$\rho \text{ (mass density)} = \frac{\gamma}{g}, \text{ and} \tag{2.5}$$

E, ν, and γ, are the Young's modulus, Poisson's ratio, and total unit weight, respectively, of the elastic material. The constant g, the standard acceleration of gravity, has a value of 32.17 ft/sec^2 (9.81 m/sec^2).

The shear wave, also called a distortional wave, exhibits shearing motion which is perpendicular to the direction of wave propagation. The shear wave travels significantly slower than the P-wave and, as a result, appears later in a travel time record. It is commonly called the secondary wave, or S-wave, because it arrives after the P-wave. The velocity of the S-wave, V_S , is given by

$$V_S = \sqrt{\frac{G}{\rho}} \tag{2.6}$$

Unlike P-waves, whose velocities can vary with the degree of saturation of a porous medium, S-waves have essentially the same velocities in a saturated medium as in an unsaturated medium because the fluid cannot transmit shearing motion.

The Rayleigh wave, or R-wave, does not propagate into the body of the elastic medium but travels along the surface of the half-space. The wave motion causes both horizontal and vertical particle displacements, which describe a retrograde ellipse at the surface. The amplitude of the wave decays quickly with depth such that at a depth of one wavelength, the amplitude of particle motion is only about 30 percent of the original amplitude at the surface. The velocity of the R-wave, V_R , is nearly equal to the S-wave velocity, particularly for values of Poisson's ratio above 0.40. In addition, R-wave velocity is independent of frequency in a homogeneous half-space. Since an ideal elastic half-space has a unique R-wave velocity, each frequency has a corresponding wavelength according to the relationship

$$V_R = f \cdot L_R \tag{2.7}$$

where f is the input frequency of excitation that generates a Rayleigh wave of wavelength L_R. The frequency-independent nature of the R-wave is the basis for certain types of dynamic testing.

The propagation of wave energy away from a vertically vibrating, circular footing resting on the surface of an elastic half-space is shown in Fig 2.1a. This figure illustrates the three types of waves just discussed. Miller and Pursey (Ref 18) found that, for the vertically oscillating, circular, energy source shown in Fig 2.1a, 67 percent of the input energy propagates away in the form of Rayleigh wave energy while 26 percent is carried by the shear wave and 7 percent is carried by the compression wave. Body waves, P- and S-waves, propagate radially outward along a hemi spherical wave front, while the Rayleigh wave propagates radially outward along a cylindrical wave front at the surface.

The propagation velocities of all of these waves relative to the shear wave velocity are shown as a function of Poisson's ratio in Fig 2.1b. For the range of Poisson's ratio of most soils and pavement materials ($0.25 \leq \nu \leq 0.45$), V_R is generally approximated as $0.95\ V_S$. The exact relationships between V_P, V_R, and V_S over the entire range of Poisson's ratios are listed in Table 2.1.

It should be noted that the velocities V_P, V_R, and V_S are the <u>propagation</u> velocities of the respective wave fronts, and not the <u>particle</u> velocities of the medium itself due to the wave energy. Figure 2.2 illustrates the particle motion caused by the various waves propagating in an elastic half-space.

As wave fronts propagate away from a source, they encounter a greater volume of the half-space, which causes the wave energy to dissipate with distance from the source. This phenomenon is referred to as geometrical

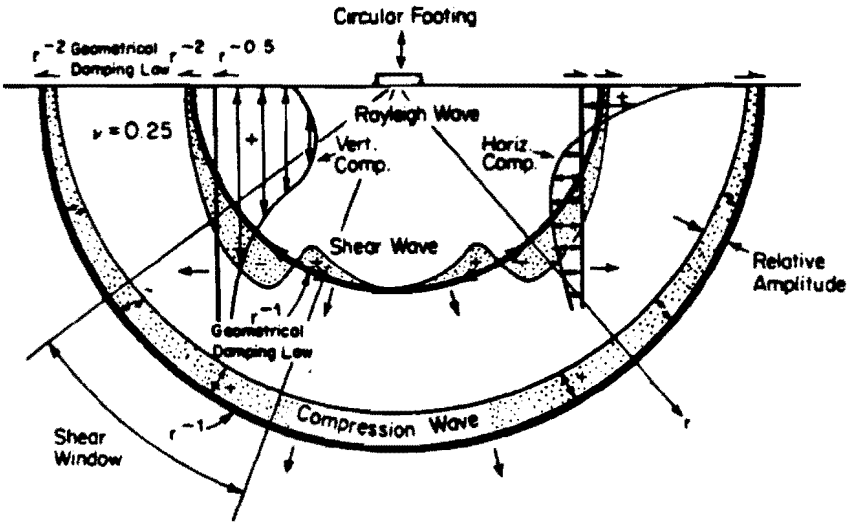

(a) Distribution of waves from a vertically vibrating footing on a homogeneous, isotropic, elastic half-space (Ref 23).

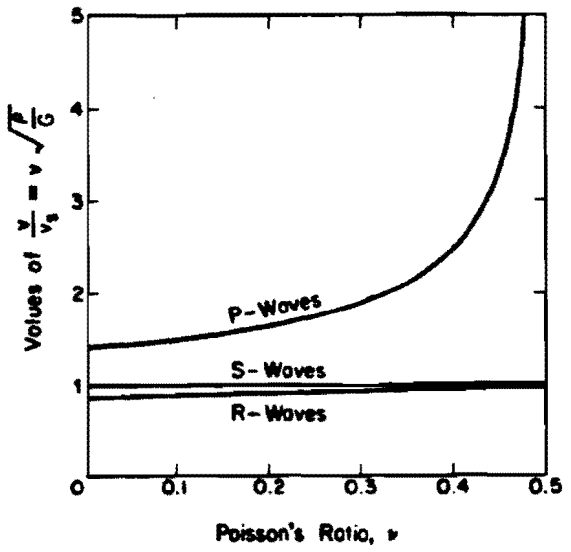

(b) Relationship between Poisson's ratio and wave velocities in an elastic half-space (Ref 23).

Fig 2.1. Propagation of waves in an elastic half-space.

TABLE 2.1. RELATIONSHIPS BETWEEN WAVE VELOCITIES AS A FUNCTION OF POISSON'S RATIO

Poisson's Ratio	V_S/V_P	V_R/V_S	V_R/V_P
.00	.7071	.8740	.6180
.01	.7035	.8760	.6163
.02	.6999	.8780	.6145
.03	.6961	.8798	.6124
.04	.6922	.8818	.6104
.05	.6882	.8837	.6082
.06	.6842	.8856	.6059
.07	.6800	.8875	.6035
.08	.6757	.8894	.6010
.09	.6712	.8912	.5982
.10	.6667	.8931	.5954
.11	.6620	.8949	.5924
.12	.6571	.8968	.5893
.13	.6521	.8986	.5860
.14	.6470	.9004	.5826
.15	.6417	.9022	.5789
.16	.6362	.9040	.5751
.17	.6305	.9058	.5711
.18	.6247	.9075	.5669
.19	.6186	.9093	.5625
.20	.6124	.9110	.5579
.21	.6059	.9127	.5530
.22	.5991	.9144	.5478
.23	.5922	.9161	.5425
.24	.5849	.9178	.5368
.25	.5774	.9194	.5309
.26	.5695	.9210	.5245
.27	.5613	.9227	.5179
.28	.5528	.9243	.5110
.29	.5439	.9259	.5036
.30	.5345	.9274	.4957
.31	.5247	.9290	.4874
.32	.5145	.9305	.4787
.33	.5037	.9320	.4694
.34	.4924	.9335	.4597
.35	.4804	.9350	.4492
.36	.4677	.9365	.4380
.37	.4543	.9379	.4261
.38	.4399	.9394	.4132
.39	.4247	.9408	.3996
.40	.4082	.9423	.3846
.41	.3906	.9436	.3686
.42	.3714	.9449	.3510
.43	.3504	.9463	.3316
.44	.3273	.9476	.3101
.45	.3015	.9489	.2861
.46	.2722	.9503	.2587
.47	.2379	.9515	.2264
.48	.1961	.9528	.1868
.49	.1400	.9541	.1336

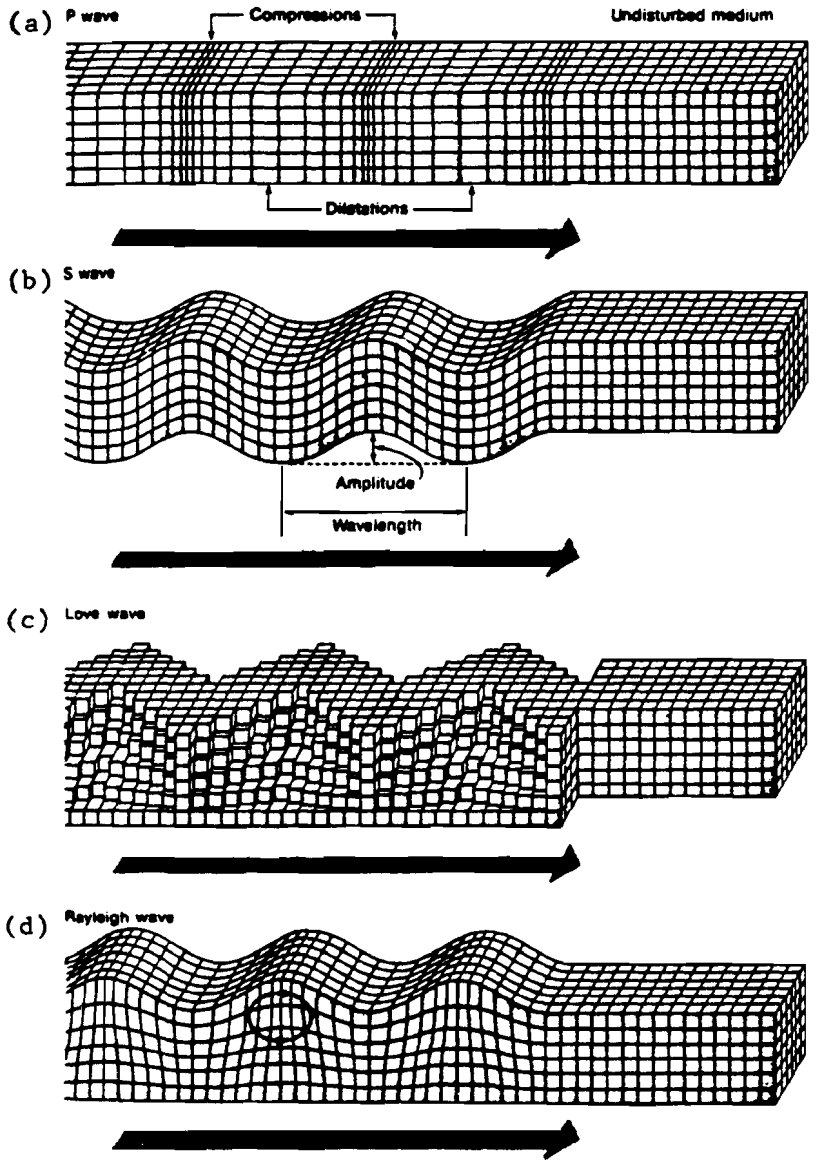

Fig 2.2. Forms of wave motion in an elastic half-space (Ref 4).

damping or geometrical attenuation. The relationships governing geometrical damping of wave energy as a function of distance from the source (r) are shown in Fig 2.1a. At the surface, the amplitudes of P- and S-waves decrease as $1/r^2$, whereas the R-wave amplitude decreases only as $1/\sqrt{r}$. As a result, in a relatively short distance from the source, most of the energy (at the surface) is R-wave energy.

Besides geometrical damping, material damping causes energy dissipation since soil and rock are not perfectly elastic. Material damping can be expressed in terms of a coefficient of attenuation, which is related to R-wave attenuation as follows

$$\frac{A_2}{A_1} = \sqrt{\frac{r_1}{r_2}} \quad \exp \left[-\alpha \, (r_2 - r_1)\right] \tag{2.8}$$

where

A_1 = amplitude of the vertical component of the R-wave at a distance r_1 from the source,

A_2 = amplitude of the vertical component of the R-wave at a distance r_2 from the source, and

α = coefficient of attenuation, with dimensions of 1/distance and the same units as r_1 and r_2 .

Material damping can also be expressed in terms of the logarithmic decrement δ which is related to α as follows

$$\delta = \alpha \cdot \frac{V_R}{f} = \alpha \cdot L_R \tag{2.9}$$

Damping is most often expressed in terms of a damping ratio D, which is related to δ as follows

$$D = \frac{\delta}{\sqrt{4\pi^2 + \delta^2}} \tag{2.10}$$

Material damping (D or δ) in earth materials is usually assumed to be independent of frequency. Therefore, the coefficient of attenuation α must be a function of frequency. McDonal, et al (Ref 17)) and Kudo and Shima (Ref 14) showed α to be a linear function of frequency. Szendrei and Freeme (Ref 26) detected different values of α corresponding to individual layers in a pavement system.

Wave Propagation in a Layered System

The previous section dealt with body and surface waves in an elastic half-space. However, in the case of a pavement section, these waves propagate through a layered system, which complicates the problem. When body waves reach an interface between two layers, some of the body wave energy is reflected back into the first layer and some is transmitted by refraction into the second layer. The combination of reflected and refracted body waves from a layered system greatly increases the complexity in analyzing wave arrivals.

In a horizontally layered system, an initial complication occurs because the incident shear wave may actually be composed of two components, SV-waves and SH-waves. The SV-wave propagates in a plane perpendicular to the plane of the interface, while the SH-wave propagates in a plane parallel to the

interface. An incident SV-wave creates reflected P- and SV-waves and refracted P- and SV-waves. In addition to the shear waves, each incident P-wave results in a reflected P-wave, a refracted P-wave, a reflected SV-wave, and a refracted SV-wave. In just a horizontal, two-layered system, three incident body waves have generated ten new waves.

The redistribution of body wave energy is influenced by three variables

(1) the angle of incidence of the incident wave,

(2) the ratio of wave velocities in the two media, and

(3) the ratio of densities in the two media.

Therefore, the redistribution of wave energy becomes quite complicated in a simple two-layered system. Wave detection becomes even more difficult in multi-layered systems.

Special cases of reflected and refracted body waves may also occur. When a reflected SH-wave in the upper layer reaches the surface, it will be totally reflected. Multiple <u>total</u> reflections of SH-waves from the layer interface can generate another type of surface wave, a Love wave. Love waves are horizontally polarized shear waves confined to a surface layer. Such a wave cannot occur if the upper layer has a higher velocity than the lower layer. Love waves travel at a velocity which is between the shear wave velocities of the two layers and is dependent on the wavelength.

In addition, surface waves can be complicated in a layered system. First, depending on the frequency of excitation and material properties at a given site, higher order modes of Rayleigh wave vibration may occur. Second, waves can exist at the boundaries between layers; they are Stoneley (Ref 25) waves. These waves are analogous to Rayleigh waves in that they occur at the interface of two materials and travel at a velocity approximately equal to

the S-wave velocity. However, Stoneley wave energy is dissipated without any appreciable surface displacement.

FIELD TECHNIQUES FOR DETERMINING ELASTIC PROPERTIES

There are many in situ tests used to determine various moduli of materials. Depending on the application, these tests may involve static or dynamic loading. Some of the most widely used techniques in soil site investigations and pavement evaluations are discussed in the following sections.

Investigation of Soil Profiles

Various techniques are used for in situ measurement of wave velocities. The type of wave that is generated and recorded depends on the source of vibration as well as the location of the receivers. Site conditions may also govern which technique is most effective.

Steady-state techniques generally use a vertically oscillating mass placed on the surface to excite the system with primarily Rayleigh waves. Vertical motion transducers are then moved along the surface until the distance between successive troughs or peaks of the wave is established. This distance is the wavelength of the Rayleigh wave, L_R, and, knowing the frequency of vibration of the source, the velocity is readily determined from Eq 2.7. This technique is illustrated in Fig 2.3.

For each excitation frequency, the transducers must be moved to determine the corresponding wavelength. Depending on the range of frequencies to be excited, this approach can be quite time consuming.

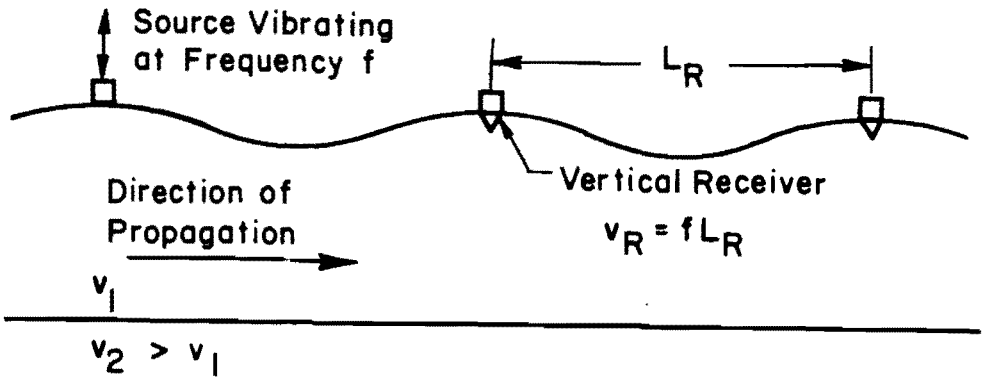

(a) Measurement of steady-state, Rayleigh - wave motion.

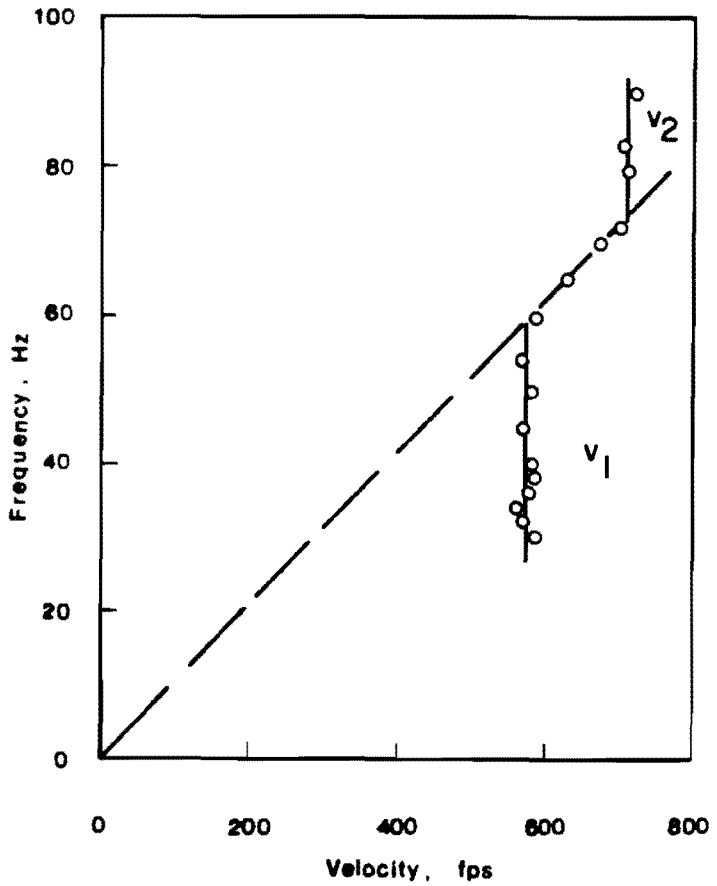

(b) Typical results.

Fig 2.3. Steady-state, Rayleigh-wave testing in layered systems.

Since most of the Rayleigh wave energy travels through a zone within about one wavelength of the surface, the velocity of the Rayleigh wave is influenced primarily by material properties to a depth of one wavelength. When the steady-state technique shown in Fig 2.3 is used at a given site, low frequencies generate long wavelengths corresponding to deep "sampling" of the site. Conversely, high frequencies generate short wavelengths corresponding to shallow sampling. In an ideal, homogeneous, elastic half-space, the material properties do not change with depth. Therefore, the Rayleigh wave velocity is independent of frequency (or wavelength). However, if the properties vary with depth, the Rayleigh wave will become dispersed, i.e., different frequencies will travel at different velocities. As such, different wavelengths will be sampling different elastic properties.

It is apparent that a given wavelength will sample the <u>average</u> properties within about one wavelength of the surface. (In addition, lateral variation in soil properties will be averaged over the distance of the particular measurement.) It is not clear, however, at what depth the measured velocity (or modulus) should be assigned. As a first approximation, this depth could be taken as one-half the wavelength ($L_R/2$), assuming that the average properties are equally weighted over the full wavelength. Fry (Ref 7), Ballard (Ref 1), and Ballard and Casagrande (Ref 2) reported field tests that showed good correlation between measured wave velocities plotted at a depth of $L_R/2$ and the soil profile at the test site.

However, the displacement amplitude (and, hence, wave energy) is not equally distributed over the full wavelength, as indicated by the curves shown in Fig 2.4. For the vertical component of wave motion, the wave energy is more concentrated toward the surface. As can be seen in Fig 2.4, the amplitude function W(z) varies slightly with the Poisson's ratio of the

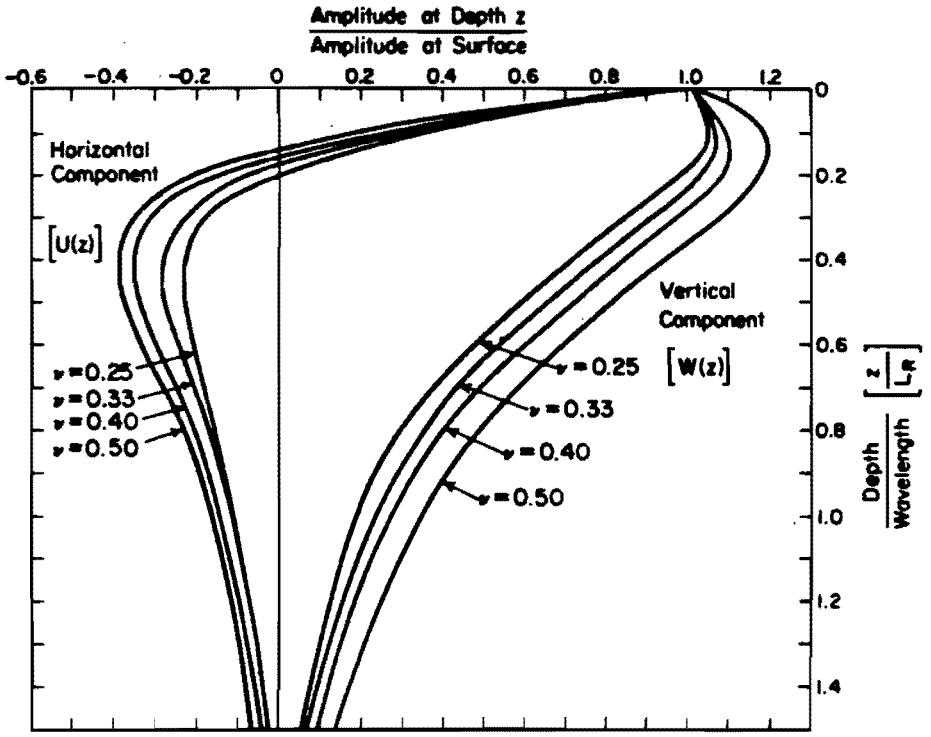

Fig 2.4. Variation of Rayleigh-wave amplitude as a function of depth normalized to wavelength (Ref 23).

material. For the range of Poisson's ratios of most earth materials, the "centroid" of wave energy distribution is located at a depth approximately equal to $L_R/3$, suggesting that measured wave velocities may more nearly correspond to properties at a depth of one-third of the wavelength rather than one-half of the wavelength.

Using the $L_R/3$ criterion, the data presented by Fry (Ref 7) for the Eglin Field test site were reexamined. Figure 2.5 shows a comparison of the measured Rayleigh-wave velocity profile (using both $L_R/2$ and $L_R/3$ as criteria for depth) with the theoretical variation of Rayleigh-wave velocity with depth. The theoretical curve for the Eglin Field site was determined by Richart, Hall, and Woods (Ref 23). They calculated shear wave velocities as a function of depth based on an empirical relationship incorporating void ratio ($e = 0.70$) and effective confining pressure ($\bar{\sigma}_o$) as a function of depth. Shear wave velocities were converted to Rayleigh wave velocities using the relationship of $V_R = 0.933\ V_s$ for $\nu = 1/3$. Figure 2.5 indicates that the measured velocities, when plotted at a depth of $L_R/3$, correlate better with the theoretical curve than when plotted at a depth of $L_R/2$.

Other surface measurement techniques utilize an impulsive source. Several types of surface techniques are shown in Fig 2.6. Usually, velocities of P-waves are determined in these surveys. Travel times and travel distances to the receiver may be determined for the direct arrival or for an initial reflection in the upper layer. However, refracted waves are normally encountered and care must be taken not to identify refracted waves as direct waves. To overcome this problem, refraction surveys are performed which take advantage of the faster-travelling refracted waves to develop the profile and corresponding velocities for a layered system. Such an analysis

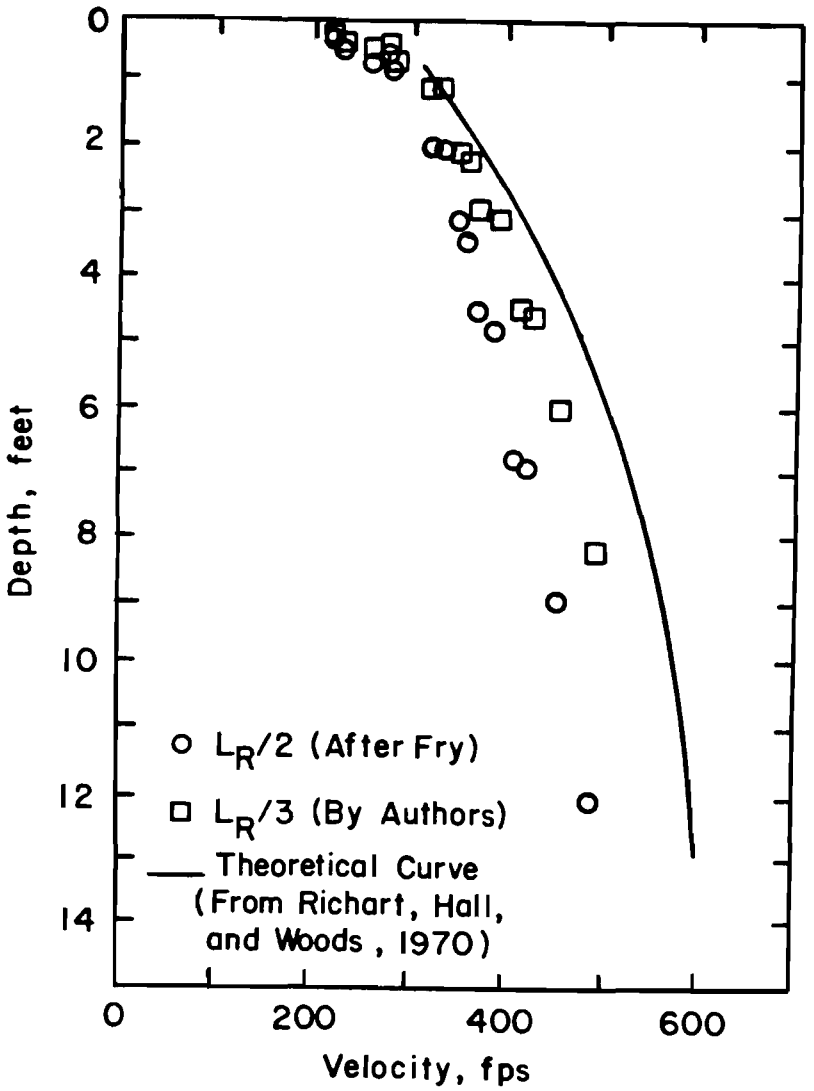

Fig 2.5. Comparison of depth criteria using data from Eglin Field site (Ref 7).

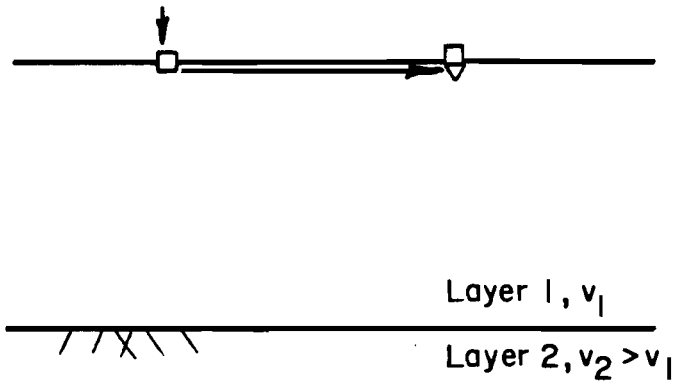

(a) Direct arrival survey.

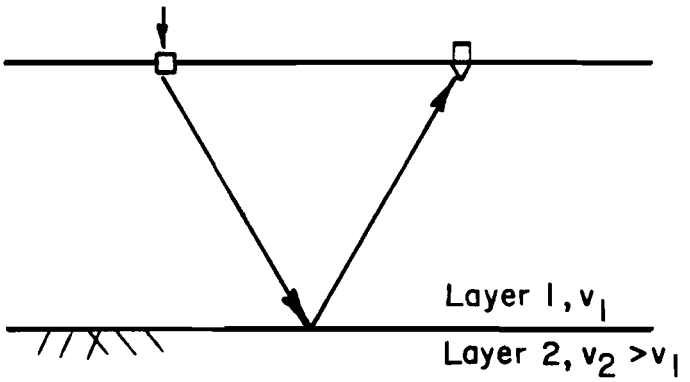

(b) Reflection survey.

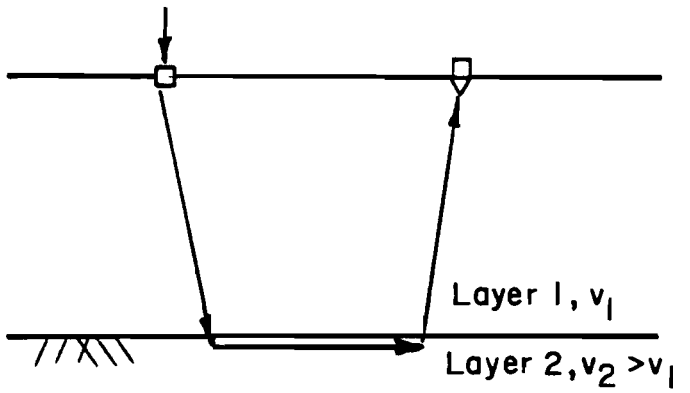

(c) Refraction survey.

Fig 2.6. Surface measurements based on arrival times of various body waves.

is greatly complicated for a site with many layers or dipping strata. Refraction surveys are also hindered when a higher-velocity layer overlays a lower-velocity layer, as in the case of a pavement surface overlaying a base course or subgrade.

An alternative to surface measurement techniques is crosshole seismic testing. This method is discussed in detail by Stokoe and Hoar (Ref 24). The source and receivers are placed in drilled holes so that direct arrivals of waves can be determined. Both P- and S-wave velocities are measured in this type of test. Layering and velocities are accurately determined. Proper spacing of the boreholes eliminates or minimizes problems caused by refracted waves. A major drawback of the crosshole test is the high cost associated with the drilling of several boreholes.

Downhole seismic testing utilizes an impulsive source at the surface and requires only one borehole for placement of receivers. This method has been investigated extensively by Patel (Ref 20). In general, only S-wave velocities are determined from downhole testing. The necessity for boreholes prevents use of both the downhole test and the crosshole test in normal pavement evaluations.

Evaluation of Pavements

Lytton, Moore, and Mahoney (Ref 16), in a state-of-the-art report, discuss four general methods used to evaluate elastic moduli of pavement systems: static deflections, steady-state dynamic deflections, impact load response, and wave propagation methods. Each of these methods is briefly summarized in the following paragraphs.

Static deflection methods include the plate bearing test, curvature meter, Benkelman beam, travelling deflectometer, and LaCroix deflectograph. Each of these methods measures pavement deflection under static loading. Elastic layer theory is then used with the measurements to calculate moduli indirectly on the basis of the measured deflections. In general, static methods require some reference to establish a datum for the deflection measurements.

Steady-state dynamic deflection methods measure deflections caused by steady-state vibrations. Current equipment includes the Road Rater, the Dynaflect device, and the WES Vibrator, among others. Moduli are then calculated on the basis of the measured deflection basin using elastic layer theory. The major drawback of the steady-state method is that the stiffness of the entire pavement system is measured. Separation of the properties of the individual layers is extremely difficult unless measurements are performed at many different frequencies. This integrating effect also prevents determination of the modulus of the relatively thin surface layer.

Impact load response methods involve monitoring the displacement-time response, $x(t)$, at the pavement surface due to a transient impulse force, $f(t)$. If the pavement is approximated as a single-degree-of-freedom mechanical system with a mass, spring, and dashpot, the pavement stiffness is an overall stiffness of the pavement system. Impact testing, however, does offer the advantage of exciting a wide range of frequencies with just one impulse. This type of excitation provides a quick and thorough technique for extensive field testing.

Wave propagation methods measure the velocities of elastic waves travelling through the pavement system, rather than the deflections caused by the vibration source. Elastic waves can be generated by steady-state

vibrations or transient impulses, and they can propagate through individual layers or the entire pavement system. Wave propagation methods, although not widely used, offer the most direct approach to determining elastic moduli of pavement systems.

Among wave propagation methods, the steady-state technique is most widely used in nondestructive pavement testing. In multilayered systems, the Rayleigh wave propagates at a velocity which reflects the material properties of the layer(s) that the wavelength samples. Short wavelengths within the surface layer will measure properties in that layer only. Long wavelengths (relative to the depth of the surface and base courses) will travel predominantly through the subgrade. Intermediate wavelengths will sample the base course or average the properties of all three materials: surface, base, and subgrade. Each wavelength will then have a corresponding phase velocity, depending on how much of each layer the wave samples.

The mathematical analysis required to interpret the phase velocity-wavelength relationship for several typical pavement sections was studied by Jones (Ref 13). Jones assumed homogeneous, elastic layers while treating the subgrade as a semi-infinite medium and showed that at infinitely long wavelengths, the phase velocity approached the R-wave velocity of the semi-infinite medium. Similarly, at very short wavelengths, the phase velocity approached the R-wave velocity of the surface layer. Theoretical solutions for an intermediate layer required more assumptions.

Although earth materials are neither perfectly homogeneous or elastic, field investigations indicate that such assumptions are reasonable. Heukelom and Foster (Ref 8) reported a profile of velocity versus depth that showed good correlation with the pavement profile when the effective sampling depth was taken as one-half of the Rayleigh wavelength. Szendrei and Freeme

(Ref 26) found a similar correlation by using an effective sampling depth of approximately one-third of the Rayleigh wavelength. Heukelom (Ref 8) suggested that the sampling depth may vary from one-half to one-third the Rayleigh wavelength, depending on the particular properties at a given site. It should be emphasized that the use of any such depth criterion is primarily empirical.

APPLICATION OF SPECTRAL ANALYSIS

Based on the preceeding review of results published in the literature, it appears that the steady-state vibration technique is a valid means of determining wave velocities and moduli of both soil profiles and pavement systems. Because individual layers can be identified by contrasting velocities, determination of moduli directly from wave propagation velocities is more desirable than indirect calculation based on deflection measurements and elastic layer theory. However, there are two drawbacks to the conventional steady-state technique.

First, determination of wavelength requires measurement of the phase difference between signals at two motion transducers. The conventional approach was to move one transducer relative to the other until the signals were "in phase," i.e., the distance between transducers was an integral multiple of the wavelength generated by the particular frequency. This trial-and-error approach resulted in excessive time to complete the test. With the advent of more sophisticated equipment, the phase difference between sinusoidal waveforms could be identified regardless of the spacing between transducers. Using such a phase computer in conjunction with steady-state

sources, Rao and Harnage (Ref 21) reported moderate success for vibration tests on a rigid pavement test section and indicated that investigations should be extended to actual field sites.

Secondly, the conventional steady-state technique uses a vertically oscillating mass that excites only one frequency at a time. However, a wide range of frequencies is required to generate the appropriate wavelengths needed to sample a site. Again, this approach resulted in excessive time to complete the test.

If the steady-state technique is modified to use an impulsive source to propagate a transient wave pulse through the materials to be tested, a wide range of frequencies can be excited at one time. This approach requires that the time domain waveform be transformed into its frequency spectrum. Spectral analysis instrumentation is required to record, transform, and analyze signals for their frequency and phase relationships. (An introduction to the theory and mathematics involved in spectral analysis is presented in Chapter 3.) The goal of this study was to implement such instrumentation to develop a transient technique to determine a profile of wave velocity (modulus) versus depth. The main advantage of the transient technique is that it is significantly quicker and more efficient than the conventional steady-state technique.

In this study, various parameters were investigated to determine their influence on the measurement of an accurate velocity profile. These parameters included the number of averages (transient events) needed to obtain a representative measurement, the appropriate frequency bandwidth(s) to be analyzed, the type of source required to generate Rayleigh wave energy, the appropriate location of the geophone nearer to the source, and the

appropriate spacing between geophones. In addition, the empirical depth criteria (L_R /2 and L_R /3) were reexamined.

Data from surface measurements were also compared with data from crosshole tests. No published data could be found in the literature where results from the two techniques are compared. Previous comparisons were based on other types of modulus tests, theoretical velocity profiles calculated from laboratory soil properties and empirical relationships, or solely on correlation between known layer boundaries and velocity contrasts in different materials. The direct comparison of velocities obtained from both surface measurements and crosshole tests indicates that the spectral analysis of surface waves is a valuable method for determining shear wave velocities and elastic moduli.

CHAPTER 3. DIGITAL SIGNAL AND SPECTRAL ANALYSES

TIME DOMAIN MEASUREMENTS

Conventional travel time methods usually employ a single-channel, dual-channel, or multi-channel recorder to determine direct arrival or interval travel times. Often it is difficult to detect sharp arrivals of the various elastic waves in the waveform. Digital analysis of time domain measurements introduces two additional techniques to analyze poorly defined signals: averaging and correlation.

Averaging

Averaging clarifies the signal by reinforcing the desired waveform and by reducing background noise that obscures the signal. A trigger is required to synchronize the averaging of measurements. If the system input is perfectly repeatable and the system in linear, then ideally the response for each measurement will be identical. In the case of waves propagating through elastic media, an input source that can be adequately reproduced does reasonably duplicate the output waveform. Sufficient averaging causes any slight variances to be "cleaned out" so the remaining signal approaches its mean value. Since noise is essentially random , it will average to a mean

value of zero. The benefit of averaging in signal recognition is shown in Fig 3.1.

There are several types of averaging. Stable averaging weighs each measurement equally, which is the conventional definition of "average." Exponential decay averaging weighs newer measurements more heavily than older ones. Exponential decay averaging is useful for systems with behavior that is changing with time while the measurements are being taken. Since the behavior of a pavement system does not change with time (within the time frame that measurements are made), stable averaging is the better technique. Stable averaging of time domain measurements is referred to as time record averaging.

Correlation

Two random variables that display a definite pattern or relationship are said to be correlated. When a linear least-squares fit is performed, the deviation of the data from the regression line is measured by the normalized covariance or correlation coefficient, ρ_{xy}. Data for which ρ_{xy} equals unity are perfectly correlated, while data for which ρ_{xy} equals zero contain no (linear) correlation.

Generally, correlation is associated with sets of discrete pairs of data, but it is also applicable to continuous functions of time. A collection of data is an ensemble of time records instead of discrete points. The correlation function is actually a type of time average that measures the similarity of two signals.

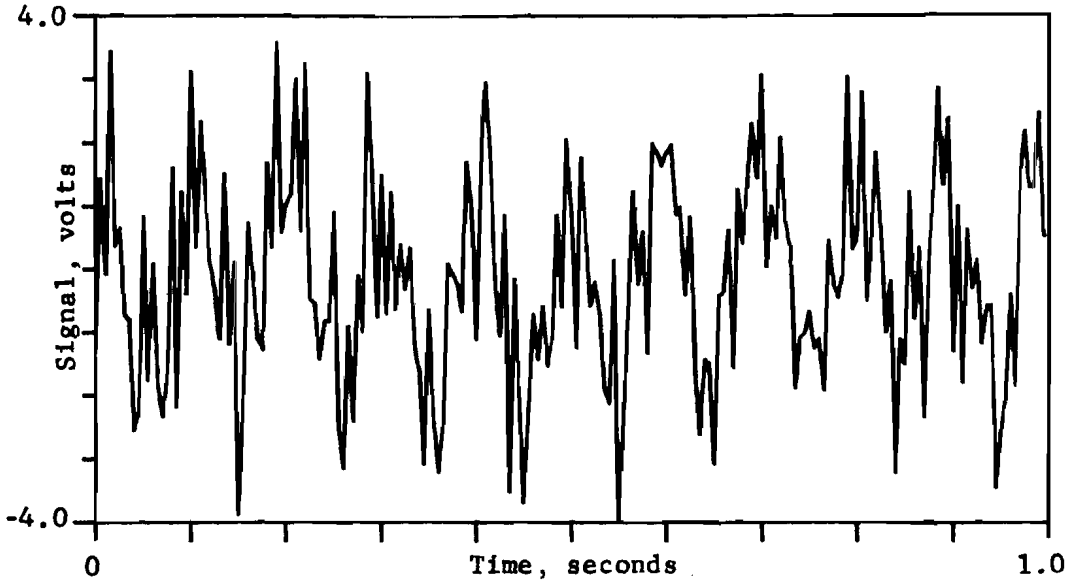

(a) Single time record with signal buried in noise.

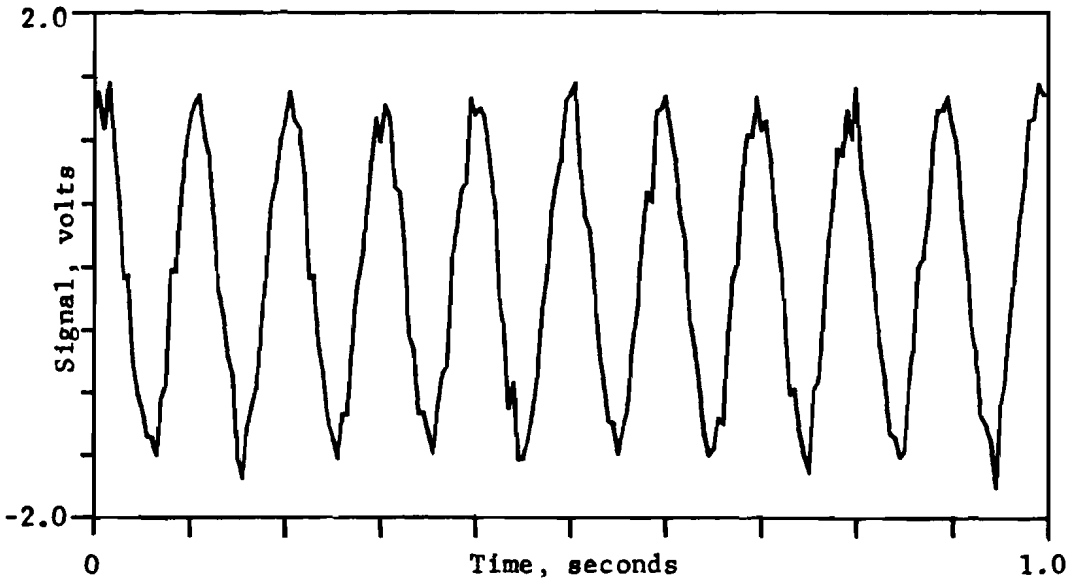

(b) 10-Hz signal after 100 averages.

Fig 3.1. Extraction of a periodic signal from noise by averaging.

The autocorrelation function is the special case where the signal is correlated with itself. In integral form, the autocorrelation function is given by

$$R_{xx}(\tau) = \lim_{T\to\infty} \frac{1}{T} \int_0^T x(t)\cdot x(t+\tau)dt \tag{3.1}$$

where x(t) is a time record of length T. The signal is multiplied by the same signal shifted by time τ, and the product is integrated to yield a value of $R_{xx}(\tau)$ for that particular shift τ. This procedure is continued for all values of τ. (For digitized signals, a finite number of products are summed for a finite number of values of τ .) As expected, the autocorrelation function is maximum at $\tau = 0$, when the two signals are "lined up" perfectly. Large values of $R_{xx}(\tau)$ will also occur at $\tau_o \neq 0$ if the signal is periodic, where τ_o is the period of both the signal and the autocorrelation. Autocorrelation is used to detect periodicity, particularly in a noisy background, since random noise correlates only at $\tau = 0$.

Cross-correlation measures similarity between two different signals. The cross-correlation function in integral from is given by

$$R_{xy}(\tau) = \lim_{T\to\infty} \frac{1}{T} \int_0^T x(t)\cdot y(t+\tau)dt \tag{3.2}$$

where x(t) and y(t) are time records of length T. Although x(t) and y(t) may appear very dissimilar at $\tau = 0$, they may be quite alike when one is shifted

with respect to the other. Thus, the cross-correlation function is very useful for determining time delays or travel path delays between two signals. Figure 3.2 illustrates the concept of cross-correlation by displaying similarity between signals for various time shifts.

FREQUENCY DOMAIN MEASUREMENTS

In the past ten to fifteen years, the development of microprocessors and the Fast Fourier Transform (FFT) algorithm has greatly extended the capability to measure and analyze dynamic systems in the frequency domain. Instrumentation now exists that rapidly filters and converts an analog signal to a digitized signal, transforms the signal from its representation in the time domain into its frequency components, and analyzes the data in various formats. Consequently, frequency spectral analysis provides a quick and feasible approach to evaluating the propagation of elastic waves through layered systems.

Advantages of Spectral Analysis

The primary reason for utilizing spectral analysis is that information can be extracted from the data that was not apparent from the time domain representation of the signal. For example, the components of the signal in Fig 3.3a are indistinguishable in the time record, but each wave and its relative contribution to the overall waveform are easily observed in the frequency spectrum shown in Fig 3.3b. The amplitude and phase of each frequency component in the waveform can be determined. In addition, relationships between two signals can be easily identified.

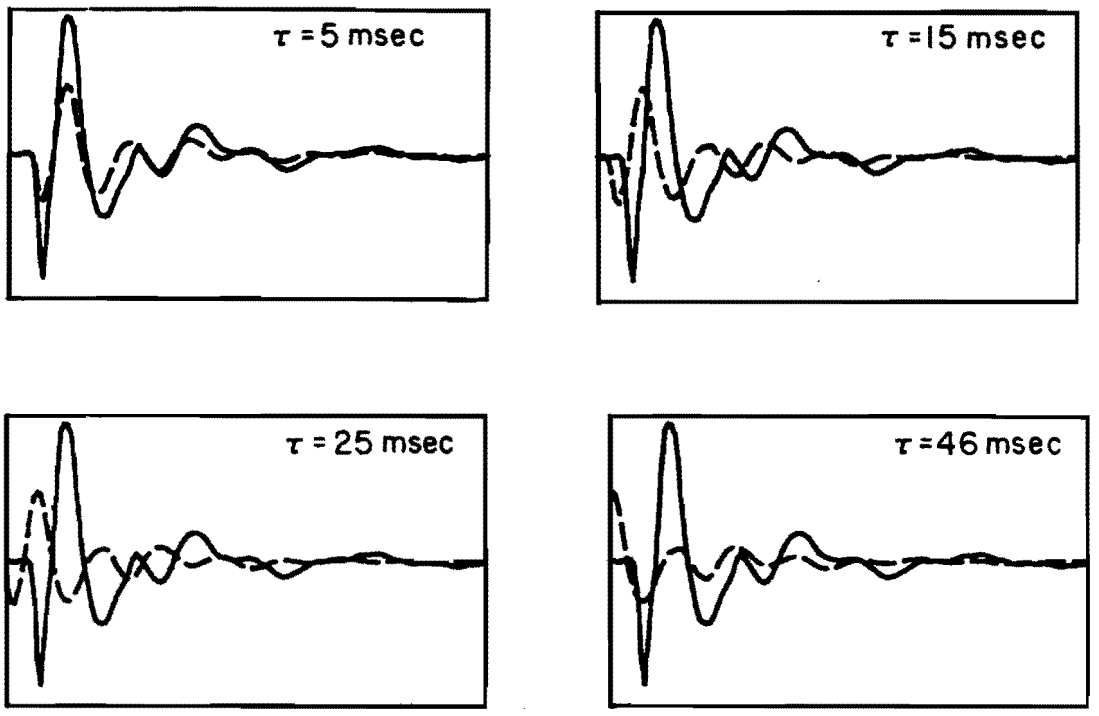

(a) Relative similarities in waveforms for various time shifts.

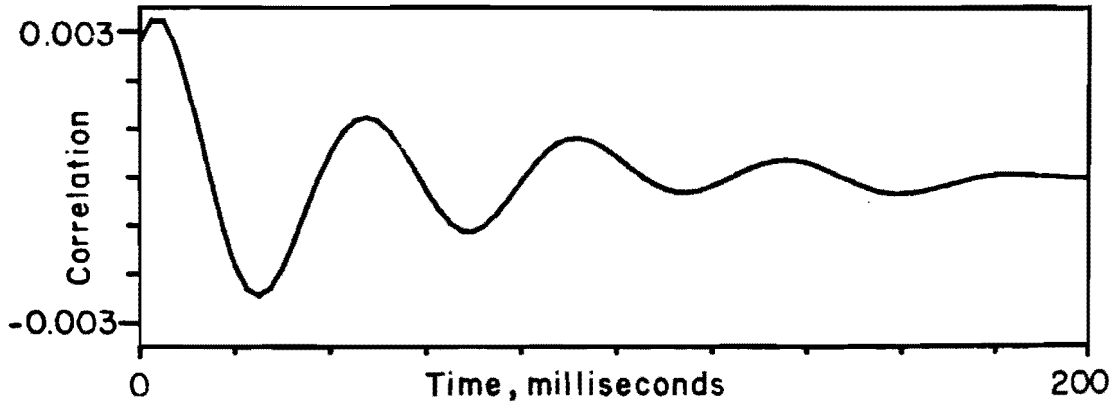

(b) Resultant cross-correlation function having a peak at τ = 5 msec.

Fig 3.2. Illustration of how a cross-correlation function is generated.

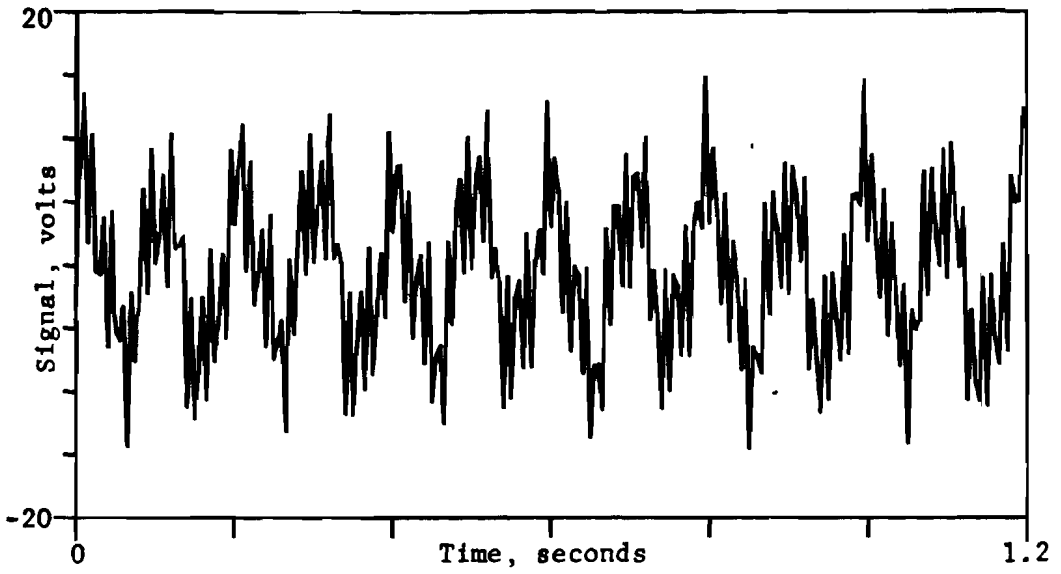

(a) Signal in the time domain.

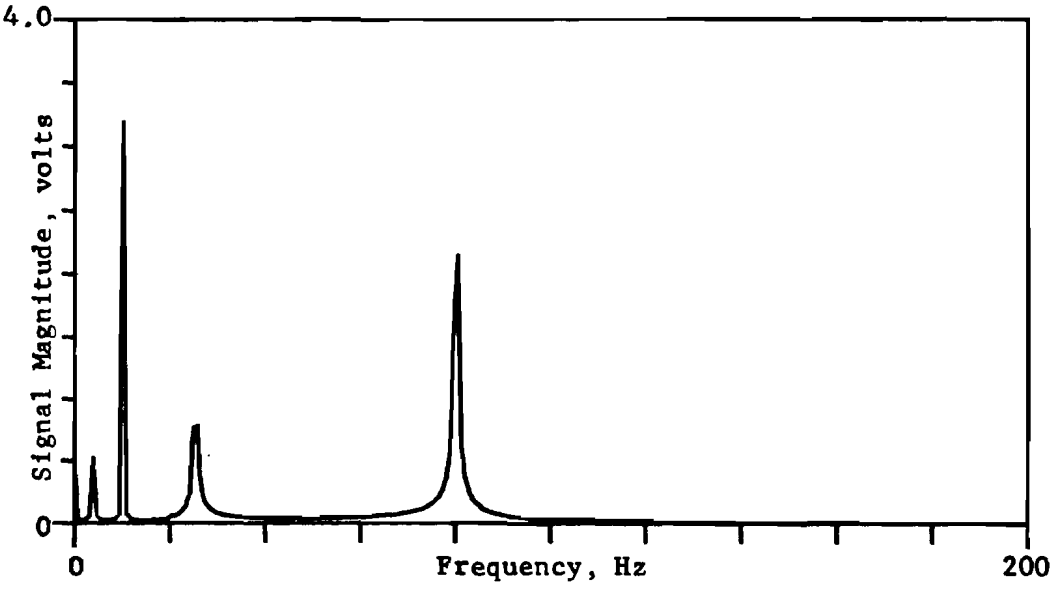

(b) Signal in the frequency domain.

Fig 3.3. Representation of a complex time signal by its frequency spectrum.

Second, handling of data in the frequency domain permits ease of operations. For example, integration of a signal in the time domain simplifies to just one division of the corresponding spectrum in the frequency domain. The advantage of spectral analysis is similar to that of using logarithms to solve a problem involving noninteger exponents.

Last, most of the measurements made in the frequency domain do not require a synchronized signal. As such, a trigger condition for averaging signals is not necessarily required. Unknown trigger delays that can affect time domain measurements are not a factor in most spectral analyses.

The Fourier Transform

Fourier analysis is central to the theory and mathematics involved in transforming a signal from a time record to its spectrum. The discussion that follows provides only a framework in which to introduce the types and usefulness of various spectral measurements. A more rigorous and complete presentation of the theory can be found in Brigham (Ref 5) or Newland (Ref 19).

The concept of the Fourier transform is an extension of the Fourier series representation of a periodic function. If x(t) is a periodic function of time with period T, then that function can be represented by an infinite trigonometric series (Fourier series) of the form

$$x(t) = a_0 + \sum_{n=1}^{\infty} a_n \cos \frac{2\pi nt}{T} + \sum_{n=1}^{\infty} b_n \sin \frac{2\pi nt}{T} \qquad (3.3)$$

where the a_o, a_n's, and b_n's are called Fourier coefficients. In the case where $T \to \infty$ (such as a waveform with no apparent periodicity), x(t) is no longer periodic and cannot be represented by discrete frequency components. However, the approach of representing waveforms by frequency components is still valid for practically all engineering problems except that the discrete Fourier series becomes a continuous Fourier integral and the discrete Fourier coefficients become a continuous function of frequency called the Fourier transform. The Fourier transform of x(t) is then defined as

$$X(f) = \int_{-\infty}^{\infty} x(t)\ e^{-j2\pi ft} dt \tag{3.4}$$

and the Fourier integral or inverse Fourier transform is

$$x(f) = \int_{-\infty}^{\infty} X(f)\ e^{j2\pi ft} df \tag{3.5}$$

where X(f) and x(t) are called a transform pair. By convention, the integrals are defined from $-\infty$ to $+\infty$, although "negative" time or "negative" frequencies do not have physical meaning. Such a convention simplifies some of the mathematics and allows for convenient interchange of various forms of the equations.

Various forms of the Fourier coefficients are used to aid the analysis of frequency measurements. The definition of X(f) indicates that the Fourier transform exists in complex form. Using Euler's identity,

$$e^{j2\pi fnt} = \cos(2\pi fnt) + j \cdot \sin(2\pi fnt) \tag{3.6}$$

yields

$$\cos(2\pi fnt) = \frac{e^{j2\pi fnt} + e^{-j2\pi fnt}}{2} \tag{3.7}$$

and

$$\sin(2\pi fnt) = \frac{e^{j2\pi fnt} - e^{-j2\pi fnt}}{2\,j} \tag{3.8}$$

Substituting Eqs 3.7 and 3.8 into 3.3, and rearranging, gives the form

$$x(t) = a_0 + \sum \frac{a_n - jb_n}{2} e^{j2\pi fnt} + \frac{a_n + jb_n}{2} e^{-j2\pi fnt} \tag{3.9}$$

In this form, the a_n (or cosine) terms become the real part and the b_n (or sine) terms become the imaginary part in the representation of the spectrum. The amplitudes of these coefficients are half the amplitudes in Eq 3.3 due to the introduction of "negative" frequencies.

Using real and imaginary components, Fourier coefficients can be treated as rotating phasors in the complex plane. Such a representation is illustrated in Fig 3.4. Each pair of coefficients (a_n, b_n) is represented by a phasor with magnitude A_n and phase θ_n where

$$A_n = \sqrt{a_n^2 + b_n^2} \tag{3.10}$$

and

$$\theta_n = -\tan^{-1}\left(\frac{b_n}{a_n}\right) \tag{3.11}$$

Magnitude and phase are often convenient ways to examine spectral data.

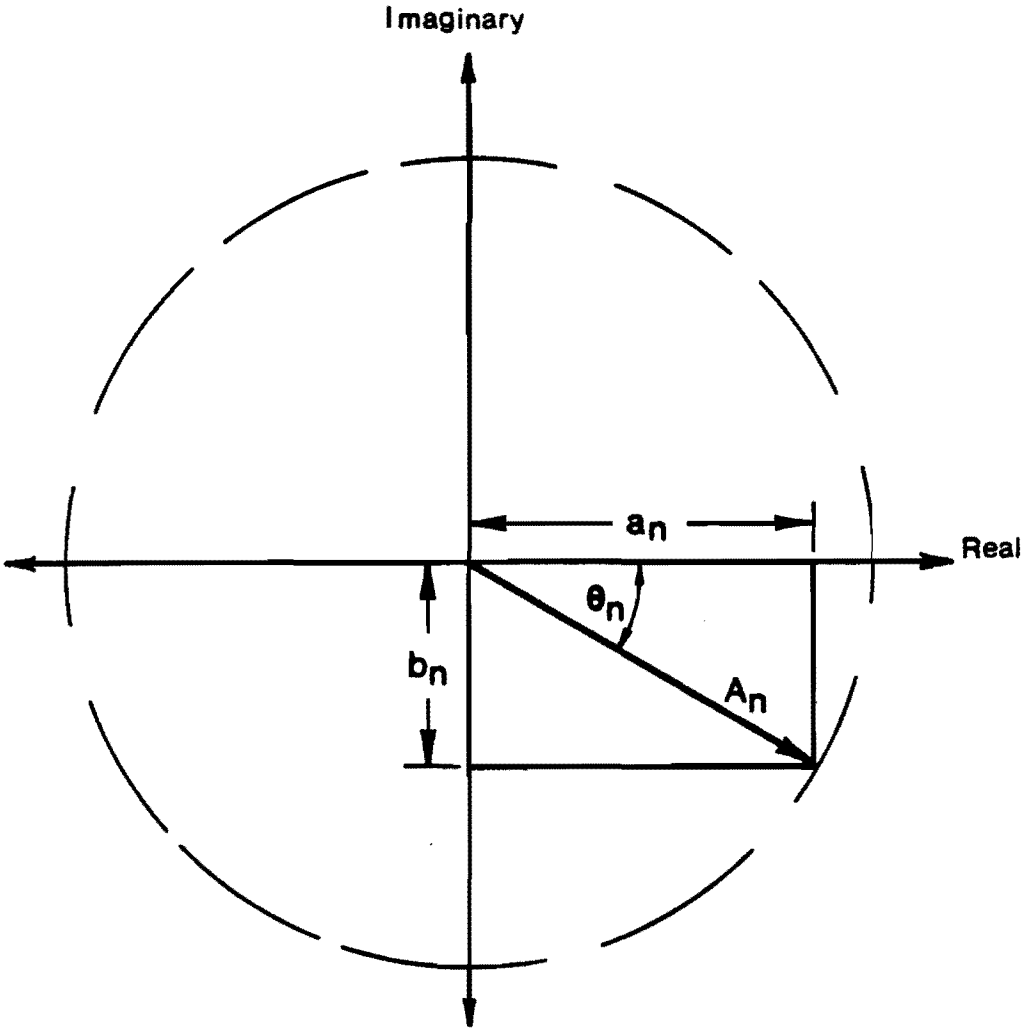

Fig 3.4. Representation of Fourier coefficients by a rotating phasor in the complex plane.

Measurements in the Frequency Domain

Several types of measurements can be made directly with most of the spectral analyzers that are currently available. The basic measurement is the linear spectrum, generally of both an "input" signal and an "output" signal. Other functions are defined using these two spectrums or their complex conjugates.

Linear Spectrum. The linear spectrum, denoted by $S_x(f)$, is simply the Fourier transform of the signal. From Eq 3.8,

$$S_x(f) = \int_{-\infty}^{\infty} x(t)\, e^{-j2\pi ft} dt \tag{3.12}$$

The linear spectrum provides both magnitude and absolute phase information for all frequencies within the bandwidth for which the measurement was taken. Since the absolute phase is measured, a trigger is required to synchronize the signal for averaging. Linear spectrum averaging is useful for determining predominant frequencies of excitation, identifying fundamental modes and harmonics of a dynamic system, or extracting a "true" signal out of background noise.

Auto Spectrum. The autospectral density function, $G_{xx}(f)$, commonly called the autospectrum, is defined as the linear spectrum, $S_x(f)$, multiplied by its own complex conjugate, $S_x^*(f)$. That is:

$$G_{xx}(f) = S_x(f) \cdot S_x^*(f) \tag{3.13}$$

The magnitude of the autospectrum is the magnitude squared of the linear spectrum. This magnitude can be thought of as the power (or energy of a

transient, impulse signal) at each frequency in the measurement bandwidth. However, multiplication by the complex conjugate eliminates the imaginary components of the spectrum, so no phase information is provided by the autospectrum. The advantage of the autospectrum is that it provides information similar to that of the linear spectrum but does not require a trigger to synchronize the averaging of signals. The autospectrum is the Fourier transform of the autocorrelation function in the time domain.

Cross Spectrum. The cross-spectral density function, $G_{yx}(f)$, or cross spectrum, is the Fourier transform of the cross-correlation function between two different signals x(t) and y(t). The cross spectrum is defined by

$$G_{yx}(f) = S_y(f) \cdot S_x^*(f)$$

where $S_y(f)$ is the linear spectrum of the output and $S_x^*(f)$ is the complex conjugate of the linear spectrum of the input. The magnitude of $G_{yx}(f)$ is a measure of the mutual power between the two signals, making the cross spectrum an excellent means of identifying predominant frequencies that are present in both the input and output signals. The phase of $G_{yx}(f)$ is the relative phase between the signals at each frequency in the measurement bandwidth. Since the phase is a relative phase, the cross spectrum measurement can be made without a synchronizing trigger. The cross spectrum is used primarily to determine the phase relationships between two signals which may be caused by time delays, propagation delays, or varying wave paths between receivers.

Transfer Function. The transfer function, H(f), or frequency response function, characterizes the input-output relationship of a dynamic system. The frequency response function is the ratio of the spectrum of the system's response (output) to the spectrum of the system's excitation (input):

$$H(f) = \frac{S_y(f)}{S_x(f)} \tag{3.15}$$

Due to statistical variance of $S_y(f)$ and $S_x(f)$ for certain systems, a better measure of H(f) can be obtained by using the autospectrum and cross-spectrum functions. If both numerator and denominator are multiplied by $S_x^*(f)$,

$$H(f) = \frac{S_y(f) \cdot S_x^*(f)}{S_x(f) \cdot S_x^*(f)} = \frac{G_{yx}(f)}{G_{xx}(f)} \tag{3.16}$$

Thus, the transfer function is similar to the cross spectrum. Both provide the same information; the magnitude of the transfer function is normalized by the autospectrum of the input $G_{xx}(f)$ relative to the magnitude of the cross spectrum. Consequently, the transfer function of a given system should be constant regardless of the input (if the system does not undergo nonlinear behavior). Generally, the input is a force measurement derived from the signal of a load cell mounted on the source of excitation. Depending on the quality which is measured as output, the transfer function may provide a measurement of impedance, dynamic stiffness, or one of several other system properties. The transfer function is frequently used to identify natural frequencies and damping coefficients of a dynamic system.

Coherence Function. The coherence function, $|\gamma^2(f)|$, is a measurement made in conjunction with the transfer function. Coherence is defined as,

$$\gamma^2(f) = \frac{G_{yx}(f) \cdot G_{yx}^*(f)}{G_{xx}(f) \cdot G_{yy}(f)} \tag{3.17}$$

The coherence is a real-valued function which is the ratio of the response (output) power caused by the measured input to the total measured response power. Therefore, $|\gamma^2(f)| = 1$, all of the output at the particular frequency of interest, is due to the measured inputs. Reasons why the coherence function may be less than unity are:

(1) there are multiple input signals in the system which are not being measured,
(2) background noise is present in the measurement,
(3) the frequency response function is nonlinear for the system,
(4) there are closely spaced resonant peaks which cannot be detected with the given frequency resolution inherent in the digitization of the signal, and
(5) waves in the frequency range of poor coherence are not adequately excited.

The coherence function is often used in the form of the signal-to-noise ratio (S/N):

$$S/N = \frac{S(f)}{N(f)} = \frac{|\gamma^2(f)|}{1 - |\gamma^2(f)|} \tag{3.18}$$

In addition, the coherence function can be used to weigh the output autospectrum $G_{yy}(f)$ to reflect the output power caused only by the input. This weighted spectrum is called the coherent output power and is given by $G_{yy}(f) \cdot |\gamma^2(f)|$. The relative contributions of several inputs can be separated using the coherent output power function. In general, the coherence function indicates the "quality" of the measurement at each frequency. A low value of coherence does not necessarily indicate that the

measurement is invalid for a particular frequency but may suggest that more averaging is required to improve the signal-to-noise ratio.

Additional Considerations for Digital Signal Analysis

Digital signal processes offer the advantages of quick and efficient data measurement, analysis, and storage. The capability to average a series of records enhances data measurement since noise and non-synchronized signals will approach a mean value of zero. Digitization also permits convenient manipulation of data for calculations and interpretation. However, the conversion of an analog signal to a digital signal includes some drawbacks.

First, to ensure that the digitized signal accurately represents the analog signal, the sampling rate of the "function" which converts the signal must be at least twice the frequency of the highest frequency present in the waveform being sampled. If the sampling rate is too low, higher frequencies will "alias", or appear as lower frequencies in the spectrum. This potential problem is demonstrated graphically for the time record shown in Fig 3.5. Generally, the instrumentation is designed so that the selection of the bandwidth for the measurement automatically adjusts the necessary filtering and sampling rate.

Secondly, since computers or microprocessors can handle only a finite amount of data, the signal must be truncated. Truncation is accomplished with a function called a window. The simplest type of window is a rectangular box. When the window "examines" an exact integral number of cycles of all the frequency components, the resulting spectrum is accurate. If a noninteger number of cycles occurs in the window, some of the magnitude of a given frequency component may appear at adjacent frequencies. This

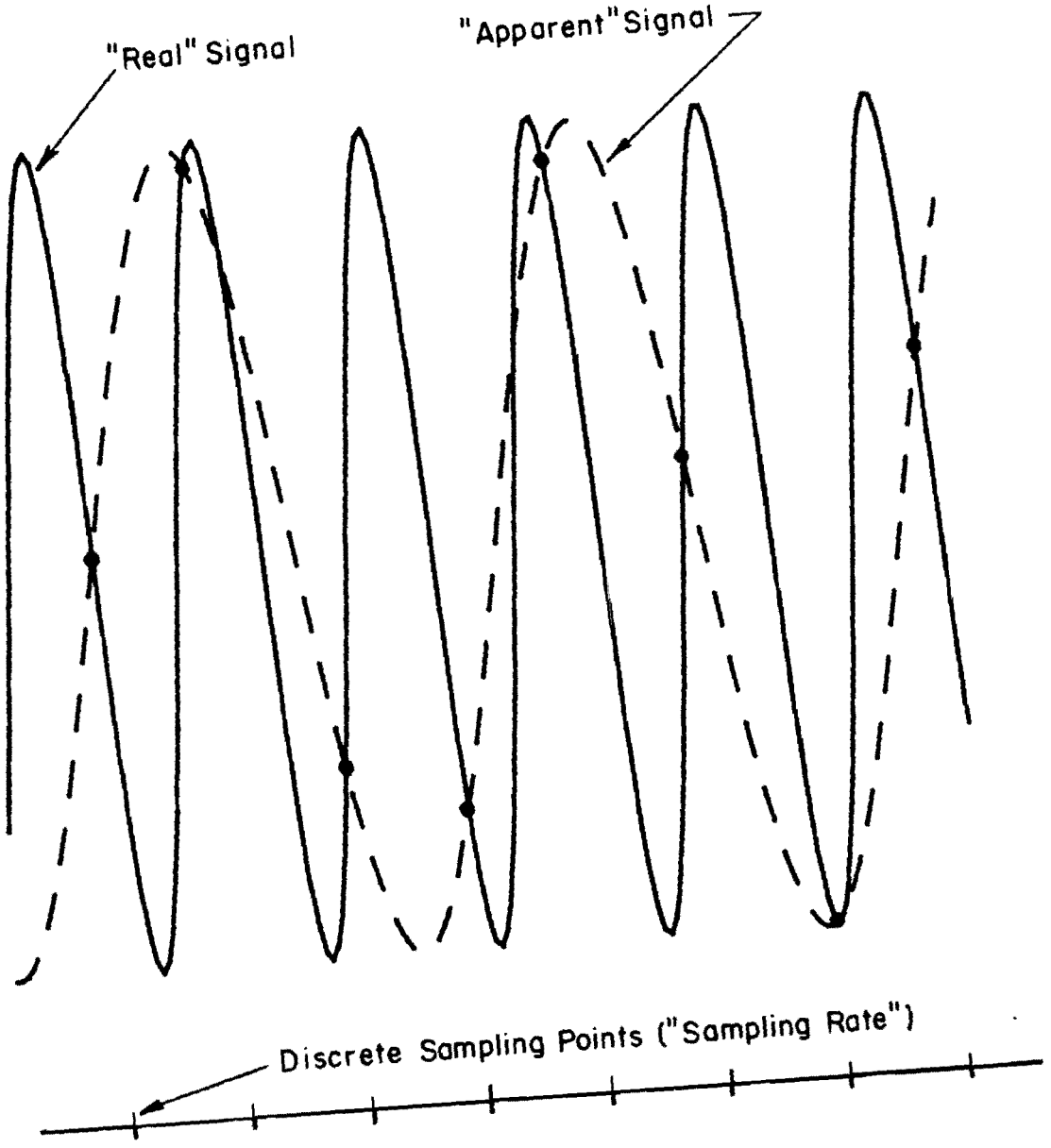

Fig 3.5. Low-frequency alias resulting from insufficient sampling of a high-frequency signal.

phenomenon is known as leakage. Invariably, some leakage is going to occur for some frequencies in most signals. The type of signal (e.g., sinusoidal, random, or transient) governs the type of window employed to minimize the effects of leakage.

Lastly, the inherent inverse relationship between period, or length of the time signal, and frequency creates problems with resolution, particularly when the digital signal consists of a fixed number of data points. As the time length of the signal increases, the bandwidth of the measurement in the frequency domain narrows. Conversely, wider bandwidths require shorter time records and provide less frequency resolution. Some instruments include capabilities to overcome this dilemma. Rather than make a wide baseband measurement from zero to some high frequency, the measurement is centered about the high frequency with a narrow band. The band selectable analysis, or "zoom" measurement, allows high frequency resolution in a high frequency range.

CHAPTER 4. SOIL TESTING AT WALNUT CREEK SITE

SITE DESCRIPTION

The Walnut Creek site is located about 5 miles (8 km) east of the campus of The University of Texas at Austin, as shown in Fig 4.1. The land at the site is part of the Walnut Creek Wastewater Treatment Plant, which is operated by the City of Austin. The site is located about 600 ft (180 m) from the public road in front of the treatment plant. As a result, traffic movement or high tension wires do not contribute to the background noise level. Power to operate electrical equipment is conveniently available from a nearby storage building.

The topography at the site is relatively flat. The soil profile consists of a deep clay deposit with a thin seam of gravelly material within a few feet of the surface. The natural water content of the clay ranges from 16 percent at the surface to 30 percent at a depth of 30 ft (9 m). Subsurface exploration by Patel (Ref 20) is recorded in the boring log shown in Fig 4.2.

EXPERIMENTAL PROCEDURE

Two series of tests were performed on two different occasions at the Walnut Creek site, hereafter they are referred to as WC-1 and WC-2. Test

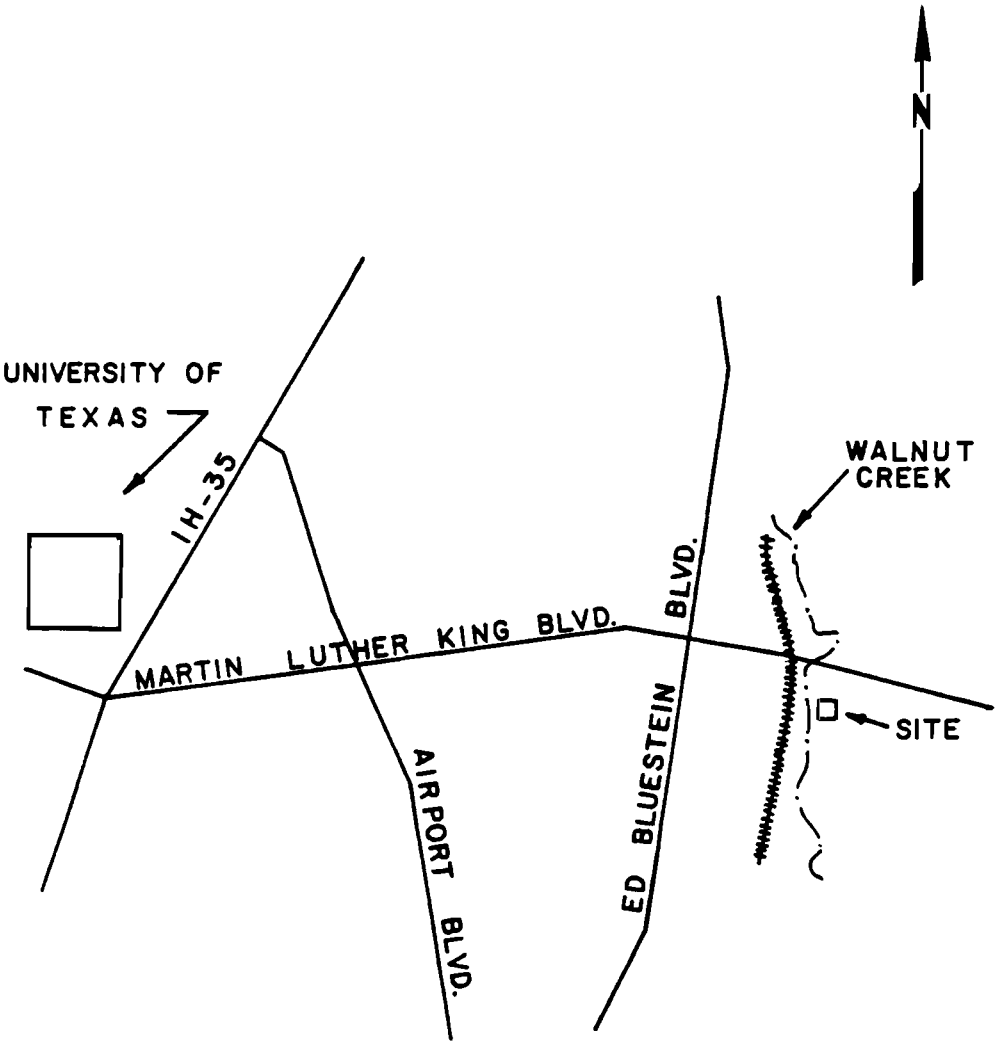

Fig 4.1. Location of Walnut Creek test site.

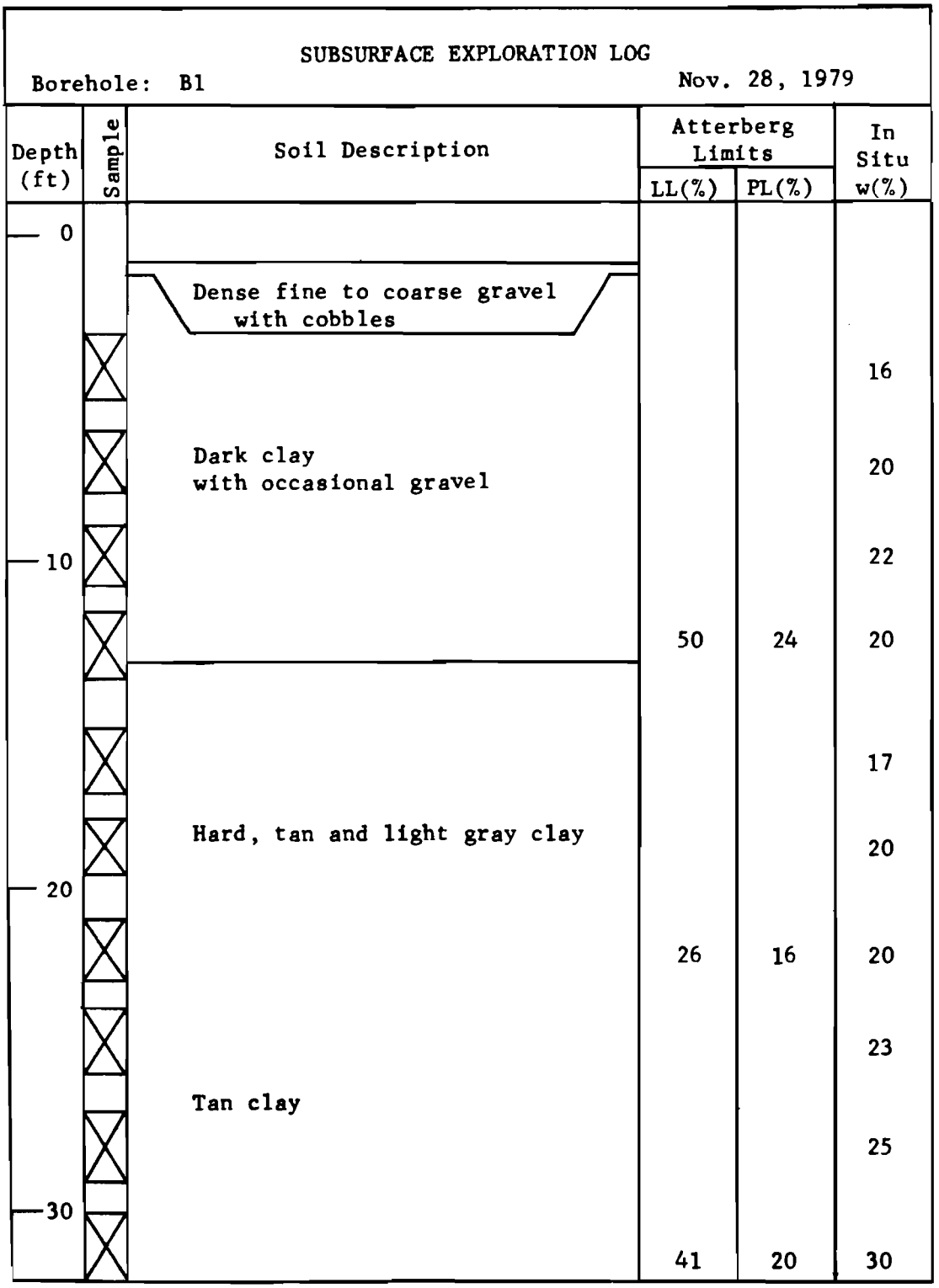

Fig 4.2. Soil profile at Walnut Creek site (Ref 20).

Series WC-1 was performed on October 23, 1980, while WC-2 was performed on March 19, 1981. Both series of tests included similar spectral measurements. The primary differences between the two series of tests were the types of sources employed, the resonant frequency of the geophones, and the spatial configuration of the geophones.

Test Series WC-1

The only source used in this first series of tests was a steel drop hammer. (The steel drop hammer and subsequent sources are described in detail in Section 4.3.) The drop hammer was used to impact the soil surface directly and also to strike a steel plate resting on the soil surface. In addition, the height of drop was set at both 6 in. (15.2 cm) and 24 in. (61.0 cm) for the initial set of measurements.

Two vertical geophone velocity transducers were used to capture the time domain signal of the generated waves. Each geophone had an undamped natural frequency of about 8 Hz and had a shunt resistance which provided a damping of approximately 50 percent of critical damping. The frequency response curves for the two geophones used for WC-1 were nearly identical up to 1600 Hz and were approximately linear over the range from 10 to 100 Hz, as shown in Fig 4.3. The transduction constant was in the range of 1 volt per in./sec (0.4 volt per cm/sec), although an exact calibration factor was not obtained since only wave propagation velocities (and not absolute particle velocities) were determined in this study.

The geophones were coupled to the soil surface by means of a 3-in. (7.6-cm) long steel spike attached to the bottom of the geophone case. For each measurement, the pair of geophones was located so that the distance

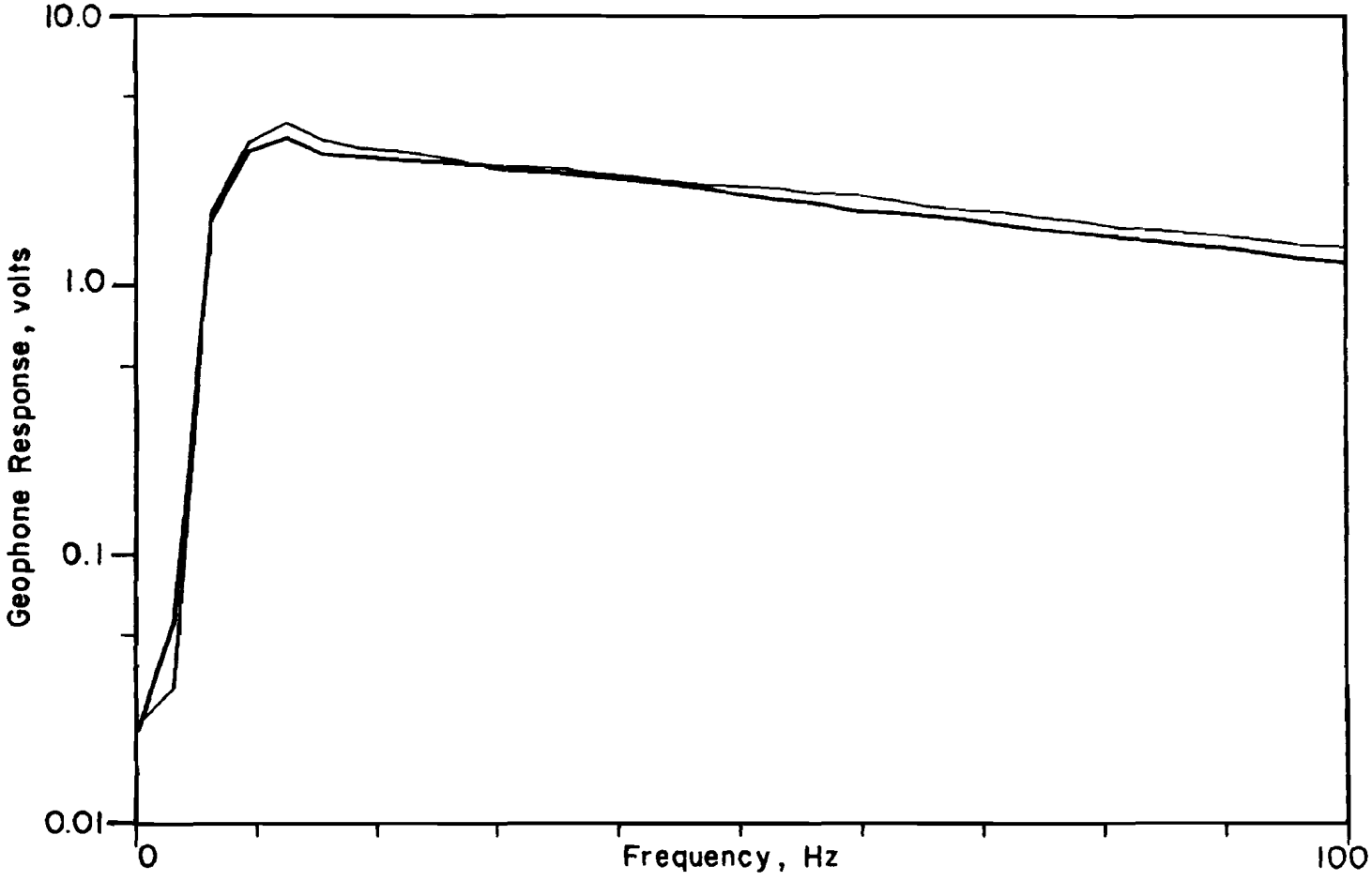

Fig 4.3. Response curves of the two vertical geophones used for test series WC-1.

between the geophones was the same as the distance from source to the first geophone. For example, for the first set of measurements, the first geophone was placed at a distance 4.0 ft (1.2 m) from the source and the second geophone was placed at a distance 8.0 ft (2.4 m) from the source, so as to maintain a spacing of 4.0 ft (1.2 m) between the two geophones. Since the geophones could be conveniently placed at the desired location with the attached spike, distances and spacings were controlled within a tolerance of + 0.02 ft (+ 0.6 cm). The geophones were aligned in a linear array extending from the source location in a direction parallel with the centerline of the cased boreholes at the site. Wave propagation was measured in the direction from borehole B1 toward borehole B5. A complete diagram of the test set-up is shown in Fig 4.4. Table 4.1 contains a summary of the measurements made during Test Series WC-1.

Test Series WC-2

Three different sources were utilized in this second series of tests: a sledge hammer striking an embedded concrete cylinder, the drop hammer striking an embedded steel wedge, and a small hammer striking a rectangular wooden plate resting on the surface. In each case, it was difficult to control the exact nature of the hammer blow, although it was possible to establish a "reproducible" hit for each source. Because of the size of the embedded concrete cylinder, the embedded steel wedge and rectangular wooden plate were located about one ft (0.3 m) closer to the geophones than the concrete cylinder in order to maintain all sources and geophones in the same linear array.

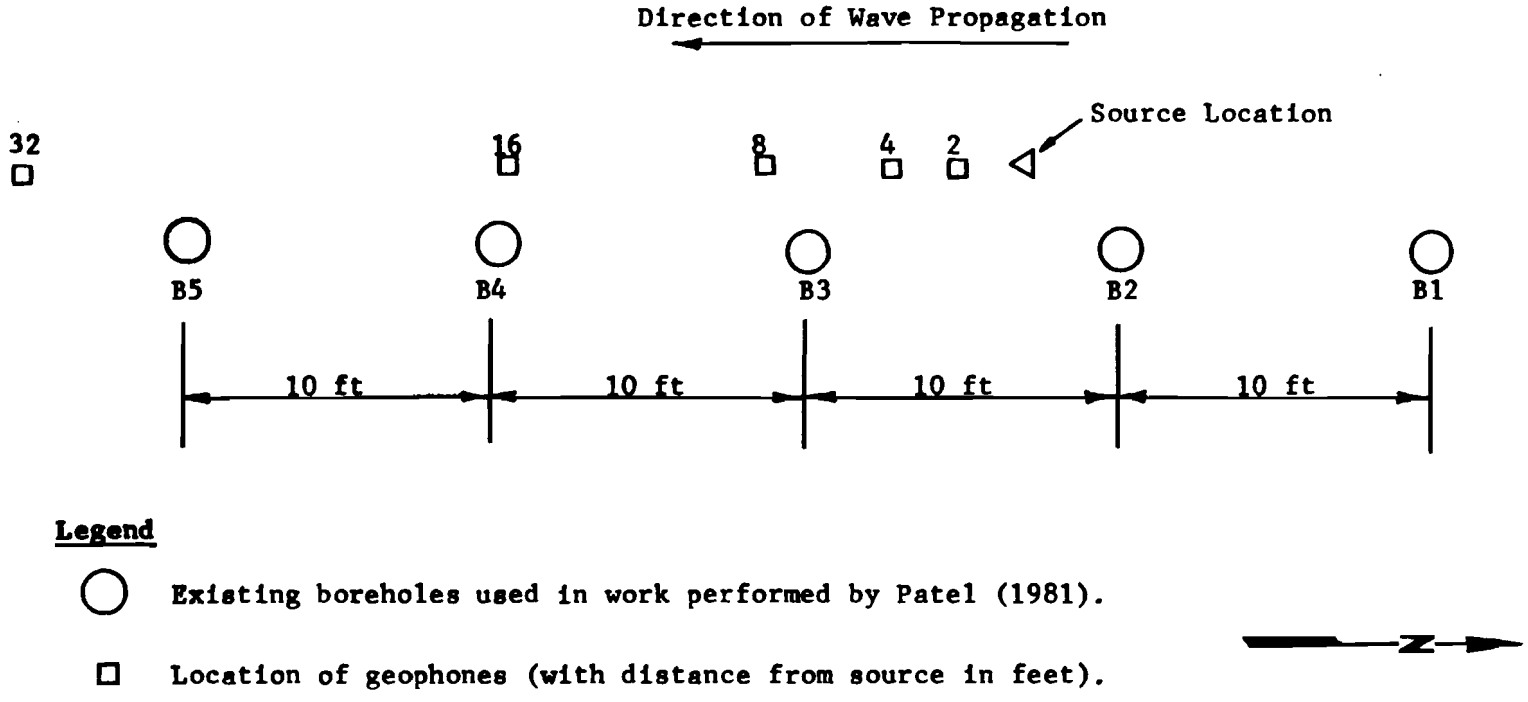

Fig 4.4. Schematic layout of the Walnut Creek site for test series WC-1.

TABLE 4.1. SUMMARY OF MEASUREMENTS AT WALNUT CREEK FOR TEST SERIES WC-1

Record No. (Track No.)	Distance from Source to Geophones (ft)		Distance between Geophones (ft)	Type of Source	Height of Drop (in)	Number of Averages	Bandwidth of Spectrum (Hz)	Computer Data File Identification
	Near	Far						
35(1)	4.0	8.0	4.0	Hammer on Plate	6	5	200	SHWC1
40(1)	4.0	8.0	4.0	" " "	6	25	200	SHWC2, SHWC6
45(1)	4.0	8.0	4.0	" " "	24	25	200	SHWC3
50(1)	4.0	8.0	4.0	" " "	24	25	1600	SHWC4
55(1)	4.0	8.0	4.0	" " "	24	5	1600	-
60(1)	8.0	16.0	8.0	" " "	24	5	1600	-
5(2)	8.0	16.0	8.0	" " "	24	5	200	-
10(2)	8.0	16.0	8.0	" " "	24	25	200	-
15(2)	8.0	16.0	8.0	Hammer on Soil	24	5	200	SHWC7
20(2)	16.0	32.0	16.0	" " "	24	5	200	SHWC5, SHWC10
25(2)	2.0	4.0	2.0	" " "	24	5	200	SHWC8
30(2)	2.0	4.0	2.0	" " "	24	25	200	-
35(2)	2.0	4.0	2.0	" " "	24	5	1600	SHWC9

Vertical geophones used in Test Series WC-2 had an undamped natural frequency of 4.5 Hz and a shunt resistance to provide approximately 50 percent of critical damping. The frequency response curves were nearly identical up to 800 Hz and were approximately linear over the range from 5 to 100 Hz, as shown in Fig 4.5. Again, an exact calibration factor was not determined since the calibration curves were nearly identical and particle velocities were not determined.

For Test Series WC-2, the geophones were placed in augered holes to minimize background noise and to provide better coupling between the geophones and the soil. The holes were augered to a depth of 6 to 8 in. (15.2 to 20.3 cm). The geophones were then embedded at the bottom of the hole by means of steel spikes and the remainder of the hole was backfilled with the augered soil.

For each measurement, one geophone was always located at a fixed distance of 2.25 ft (0.68 m) from the center of the concrete cylinder. This geophone served as a "reference" geophone from which the second geophone was located. The distance from the source (concrete cylinder) to the far geophone ranged from 4 ft (1.2 m) to 32 ft (9.8 m). Since the holes were augered by hand, the exact distances varied slightly from geophone to geophone. The exact spacing between geophones for each set of measurements is given in Table 4.2. The geophones were aligned in a linear array extending from the source in a direction parallel with the centerline of the boreholes. Wave propagation was measured in the direction from borehole B4 to slightly beyond borehole B1. A complete diagram of the test set-up is shown in Fig 4.6. Table 4.2 contains a summary of the measurements made during Test Series WC-2.

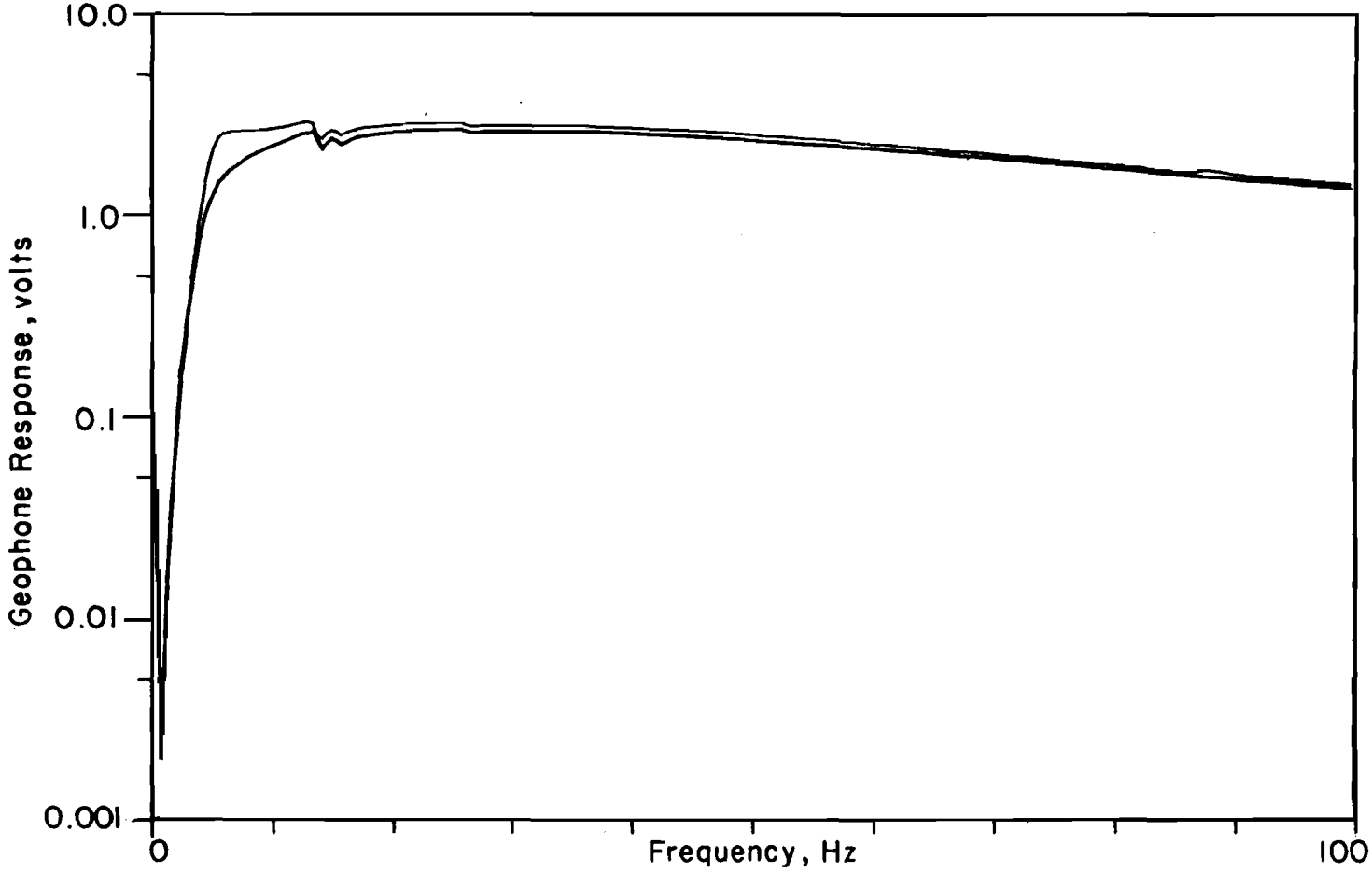

Fig 4.5. Response curves of the two vertical geophones used for test series WC-2.

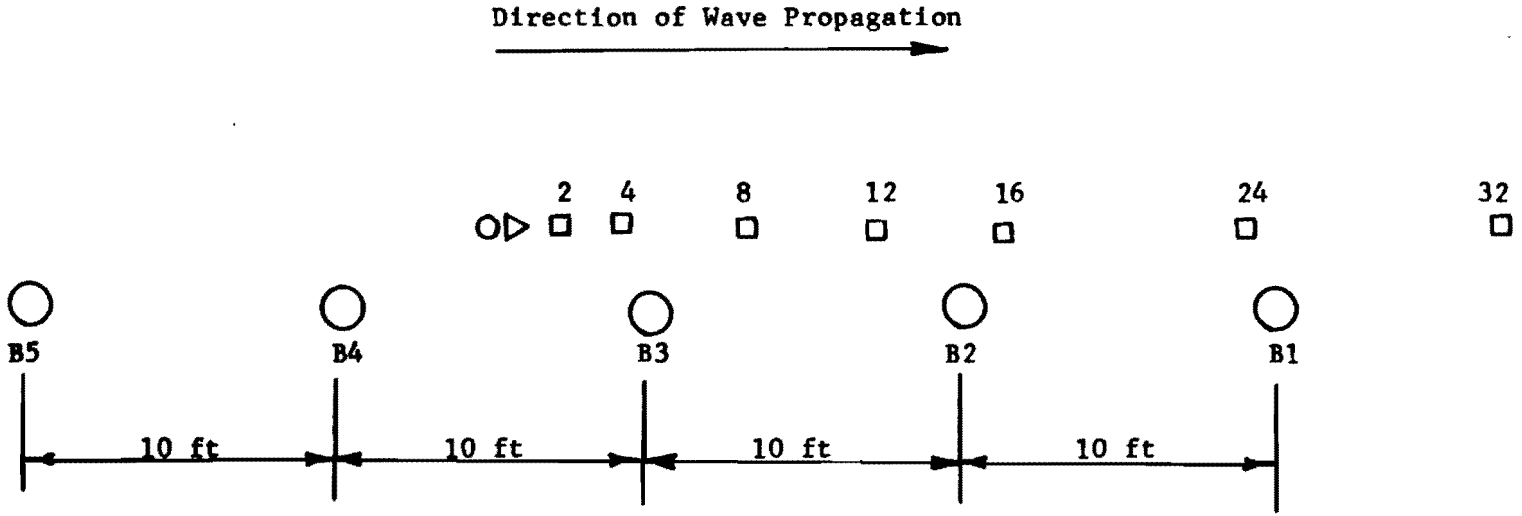

Legend

- Existing boreholes used in work performed by Patel (1981).
- Location of geophones (with distance from source in feet).
- Location of embedded concrete cylinder source.
- Location of steel wedge source and wooden plate source.

Fig 4.6. Schematic layout of the Walnut Creek site for test series WC-2.

TABLE 4.2. SUMMARY OF MEASUREMENTS AT WALNUT CREEK FOR TEST SERIES WC-2

Record No. (Track No.)	Approximate Distance from Source to Far Geophone (ft)	Exact Distance between Geophones (ft)	Type of Source	Number of Averages	Bandwidth of Spectrum (Hz)	Computer Data File Identification
11(1)	4	2.08	Sledge Hammer on Conc. Cylinder	5	1600	SHWC11
16(1)	3	2.08	Drop Hammer on Steel Wedge	5	1600	SHWC14
21(1)	4	2.08	Sledge Hammer on Conc. Cylinder	5	400	SHWC12
26(1)	4	2.08	" " " " "	5	100	SHWC13
31(1)	3	2.08	Drop Hammer on Steel Wedge	5	100	SHWC15
36(1)	3	2.08	Small Hammer on Wooden Plate	5	100	SHWC21.
41(1)	8	6.04	Sledge Hammer on Conc. Cylinder	5	400	SHWC22
46(1)	8	6.04	" " " " "	5	100	SHWC16
51(1)	7	6.04	Drop Hammer on Steel Wedge	5	100	SHWC23
56(1)	12	9.94	Sledge Hammer on Conc. Cylinder	5	100	SHWC17
61(1)	16	14.10	" " " " "	5	100	SHWC18
62(1)	16	14.10	" " " " "	5	25	SHWC24
68(1)	24	21.92	" " " " "	5	100	SHWC19
69(1)	24	21.92	" " " " "	5	25	SHWC25
5(2)	32	30.00	" " " " "	5	100	SHWC20

Recording of Spectral Measurements

Measurements were recorded and stored with a Hewlett-Packard 5423A Structural Dynamics Analyzer. The dual-channel instrument includes a set of signal filters, an analog-to-digital converter (ADC), a digital oscilloscope, and a magnetic cassette tape for storage and recall of permanent records. The analyzer can directly measure all of the time domain and frequency domain measurements previously discussed in Chapter 3. In addition, the type of signal, type and number of averages, bandwidth (or time length of the record), and trigger conditions can all be specified by the operator. The analyzer can be easily interfaced with an x-y plotter to provide a hard copy of the data.

Each set of measurements was made with a pair of geophones since the HP5423A analyzer is a dual-channel device. The measurement was triggered internally by using the input signal from the first geophone in the pair. The trigger level was adjusted to start the recording of the measurement in the first half sine wave of the impulse as it passed by the first geophone. A pre-trigger delay was used to capture the initial portion of the impulse that would have otherwise been lost prior to triggering. Both channels were programmed with the same pre-trigger delay so as not to introduce an internal time or phase delay when calculating measurements using both signals. A more detailed and complete explanation of the set-up procedure is contained in Appendix A.

Frequency measurements (in contrast to time domain measurements) were most often performed during both Test Series WC-1 and WC-2. Stable (equal weight) averaging was used for all measurements. The analyzer was programmed to perform a frequency response function, commonly called the transfer

function. This measurement additionally provided the coherence function, the cross spectrum, and the autospectrums for both signals. Hereafter, measurements will be identified by the location of the pair of geophones. For example, measurement V2-V24 identifies the measurement recorded with the vertical geophone (V) nearer to the source located at 2 ft (0.6 m) and the vertical geophone farther from the source located at 24 ft (7.3 m).

DESCRIPTION OF SOURCES

All of the sources used during both series of tests were available from past or ongoing projects at The University of Texas at Austin. Due to time and budget constraints, no new sources were developed in this particular phase of the project.

Drop Hammer

The drop hammer consists of a 2.5-in. (6.4-cm) diameter cylindrical steel mass with a length of 9 in. (23 cm) and a weight of about 12 lb (5.4 kg). The cylinder has a longitudinal center hole so that it can be released to fall from any height along the 24-in. (6.4 cm) long rod which guides the hammer to impact on a steel base which is also 2.5 in. (6.4 cm) in diameter. The amount of energy delivered by the impact is roughly proportional to the height of drop.

The drop hammer is most easily used by simply resting the base directly on the soil surface. To provide a larger striking surface, some type of plate can be placed between the soil and the base of the hammer. In Test Series WC-1, a 0.75-in. (1.9-cm) thick steel plate with a 6-in. (15.2-cm)

diameter was used as a striking surface in conjunction with the drop hammer. This arrangement is shown in Fig 4.7a.

Drop Hammer on Embedded Steel Wedge

An embedded steel wedge was selected as a typical source that could be quickly and directly coupled with the soil. The wedge consisted of a 1/4-in. (0.6-cm) thick, steel plate with a 2-in. (5.1-cm) square shape. The plate was welded to a short section of 1-in. (2.5-cm) diameter pipe, which in turn was welded to a steel head approximately 2.5 in. (6.4 cm) in diameter. The head can be struck by any hammer. The drop hammer was chosen for the following reasons:

(1) the base of the hammer is the same size as the head of the wedge,
(2) the drop hammer hit is vertical, and
(3) the magnitude of the impact can be repeated fairly consistently.

The wedge can be embedded with little difficulty by a sledge hammer. The wedge was driven such that the broad side of the plate was perpendicular to the direction of wave propagation. This orientation provided a shearing motion when the wedge was struck. As such, minimal P-wave energy was generated. The drop hammer and steel wedge are shown in Fig 4.7b.

Sledge Hammer on Embedded Concrete Cylinder

An embedded concrete cylinder already existed at the site from testing performed by Patel (Ref 20). The top of the cylinder is located slightly below the ground surface. The cylinder is approximately 16 in. (40 cm) in diameter and 13 in. (33 cm) deep. The location of the embedded cylinder at

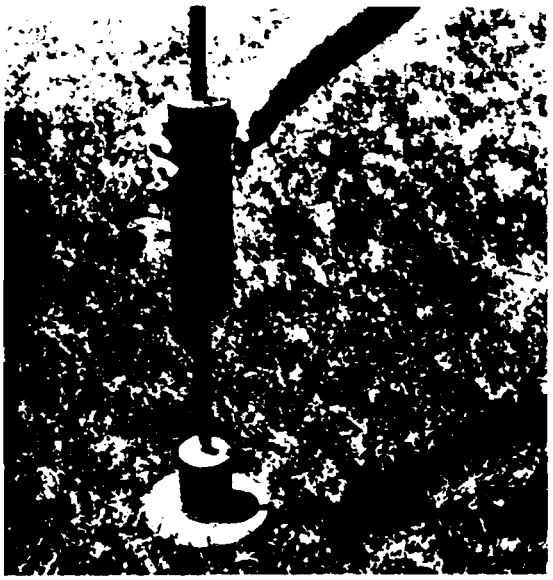

(a) Drop Hammer on Steel Plate.

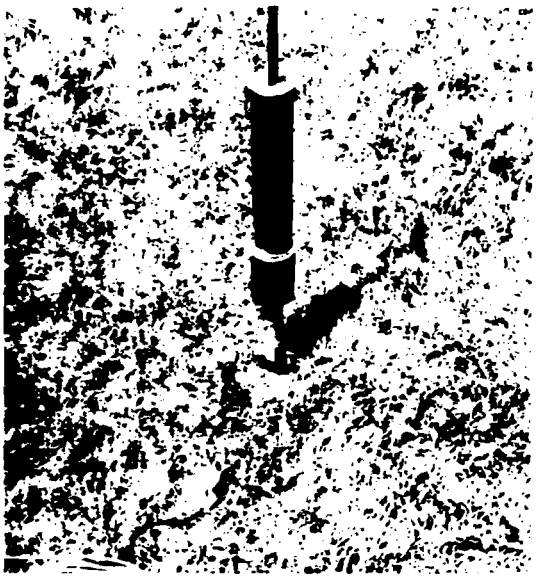

(b) Drop Hammer on Embedded Wedge.

(c) Sledge Hammer on Conc. Cylinder.

(d) Small Hammer on Wooden Plate.

Fig 4.7. Illustration of sources used at Walnut Creek.

the site is shown in Fig 4.6. The cylinder was struck near its center by a sledge hammer to generate wave energy. The source is shown in Fig 4.7c.

Small Hammer on Wooden Plate

This source was tested briefly to examine the effect of the material of the striking plate on the magnitudes and frequencies of wave energy. The plate was a 12 in. x 6 in. x 3/4 in. (30 cm x 15 cm x 2 cm) plywood section that rested directly on the ground surface. The plate was struck with a small hammer with a nearly vertical hit. The plate and hammer are shown in Fig 4.7d.

COMPARISON OF SIGNIFICANT PARAMETERS

Various parameters were investigated to determine their significance in the measurement of Rayleigh wave velocities. The parameters that were examined include

(1) number of averages to obtain a representative measurement,
(2) range of frequencies to be included in the measurement bandwidth,
(3) type or nature of source, and
(4) spatial distribution of geophones from the source point.

Number of Averages

Measurements were made during Test Series WC-1 to determine the effects of varying the number of averages to obtain a "representative" spectral measurement. The HP5423A Analyzer was set up to accept or reject a particular transient event. Events were accepted only when they were judged

to be representative of the reproducible impact of the source. A specified number of these events were included in a stable (equal weight) average.

Naturally, as the number of events of "averages" increases, the more representative the overall average or total measurement will be. However, for a method to be a quick and efficient testing technique, a small number of averages is desirable. Ideally, one representative event would be adequate. As a safeguard against capturing an event which for some reason is not representative, several averages should be taken.

Since it is not clear how many averages are necessary or when averaging has become excessive and unnecessary, sets of measurements from Test Series WC-1 were compared. Comparisons were made with measurements consisting of five averages and with measurements consisting of 25 averages. The measurements were compared directly by examining the similarities of the phases of the cross spectrum. In addition, comparisons were made indirectly by examining the coherence function for the relative quality of each measurement.

Results of these comparisons for measurement(s) V8-V16 are shown in Fig 4.8. The dashed lines represent the measurement made with five averages; the solid lines represent the measurement made with 25 averages. The plot in Fig 4.8a indicates that the phase information provided by the 5-average measurement nearly matches that provided by the 25-average measurement. There are no significant differences between the coherence functions associated with the two measurements, as shown in Fig 4.8b, suggesting that the additional averages do not contribute to a better-quality or more-valid measurement.

Similar results were obtained for other sets of measurements. The 5-average measurements provided essentially the same phase information and

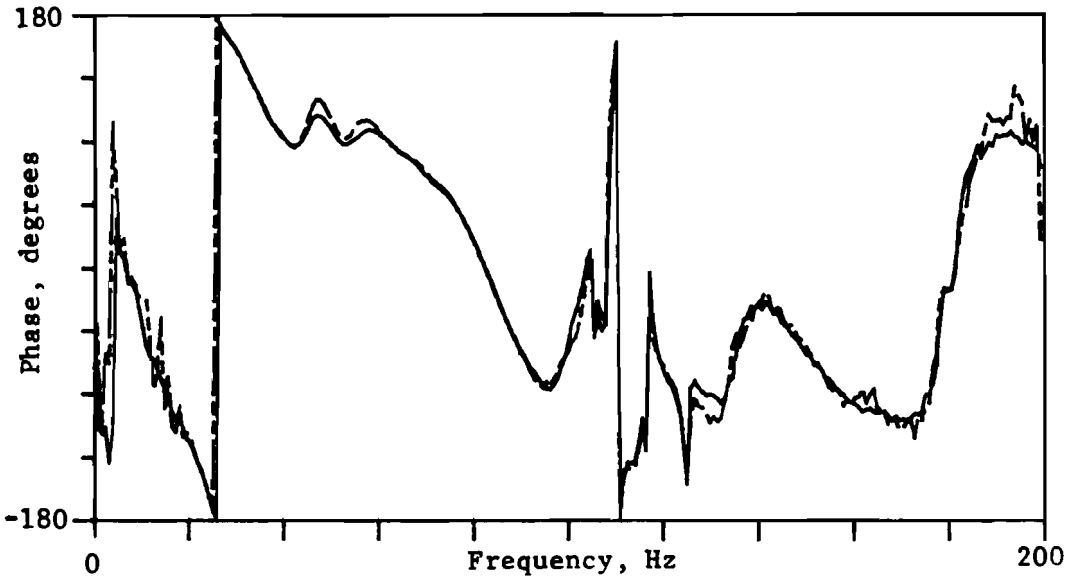

(a) Phase of the cross spectrum.

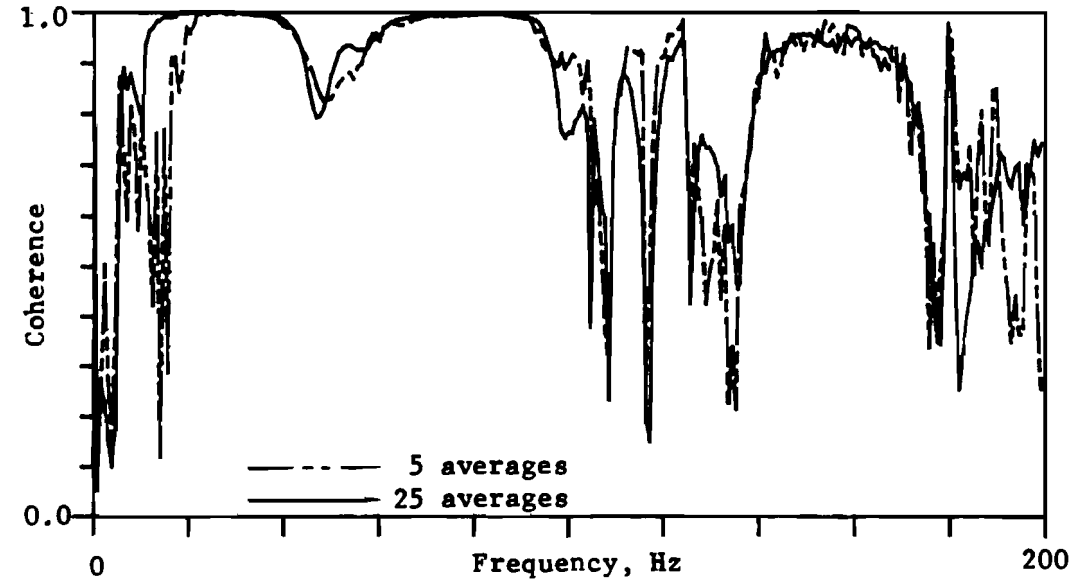

(b) Coherence function.

Fig 4.8. Comparisons of the use of the average of 5 observations with the average of 25 observations to obtain representative spectral measurements.

coherence values as the 25-average measurements regardless of the spatial distribution of the geophones, the frequency bandwidth of the measurement, or the amount of energy delivered by the drop hammer (varied by the height of drop). These results led to the conclusion that five averages provided a measurement that was as "accurate" as could be expected for any reasonable number of averages. Subsequently, measurements taken during Test Series WC-2 were compiled with only five averages.

Measurement Bandwidth

The frequency bandwidth of a measurement is a significant parameter for two reasons. First, the range of frequencies (or wavelengths) must be adequate to sample appropriate depths of the soil profile. Second, the resolution or "accuracy" of the measurement is controlled by the number of points used to convert the analog signal to a digital signal. The HP5423A Analyzer uses a fixed number of points (1024) for all measurements, regardless of bandwidth, which means that as the range of frequencies is extended, the resolution becomes poorer (Δf between points becomes larger). Inasmuch as wide bandwidths and fine resolution are in opposition with each other, some trade-offs must be made.

Comparison measurements for Test Series WC-1 included bandwidths of 200 and 1600 Hz, while comparison measurements for Test Series WC-2 included bandwidths of 25, 100, 400, and 1600 Hz. With few exceptions, no significant differences were found between values of phase of the cross spectrum function, regardless of the resolution associated with the bandwidth. Figure 4.9a shows a comparison phase plot for bandwidths of 200 and 1600 Hz for measurements V8-V16 from Test Series WC-1, while Fig 4.9b shows a similar

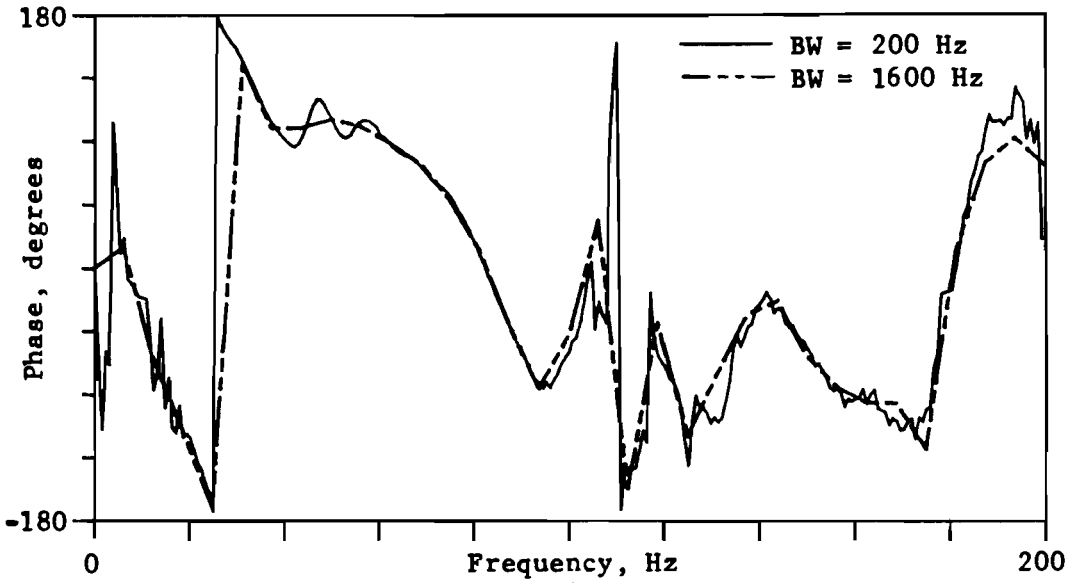

(a) Measurement V8-V16 from test series WC-1.

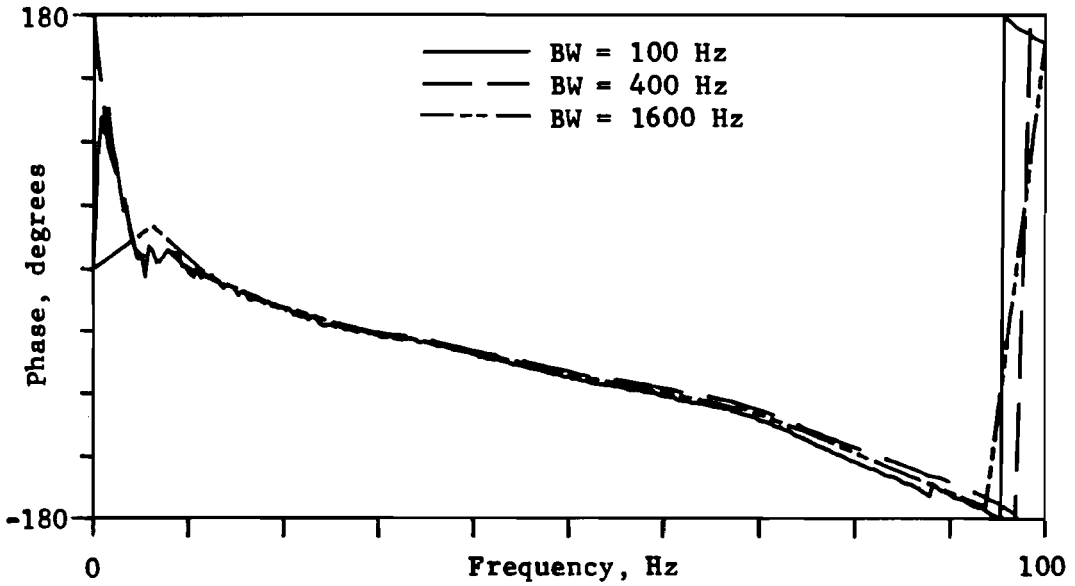

(b) Measurement V2-V4 from test series WC-2.

Fig 4.9. Comparisons of cross spectrum phase plots for different measurement bandwidths.

comparison for measurements V2-V4 from Test Series WC-2. The frequency-phase data from Fig 4.9b are reduced and plotted as a velocity-wavelength chart in Fig 4.10. The slight variations in phase translate into a difference in velocities of at most 8 percent. This difference is within the range of experimental scatter associated with velocity measurements.

Although the range of the bandwidth (and inherently the degree of resolution) is generally not a critical parameter in the cross spectrum measurement, there are a few cases where special consideration is required. First, if the measurement bandwidth is too large, the resolution may not be fine enough to measure sharp changes in frequency response that occur over a range of frequencies smaller than Δf, the degree of resolution. Such an occurrence is illustrated in Fig 4.9a, where the measurement with bandwidth (BW) equal to 1600 Hz exhibits much less sensitivity to slight variations in phase than the measurement with BW equal to 200 Hz which has a much finer resolution. Since frequency and wavelength are inversely related, increasing wavelengths correspond to decreasing frequencies. Resolution is most critical at these lower frequencies where Δf may approach the same order of magnitude as the frequencies being measured. This problem is illustrated in Fig 4.11. Measurements with 25-Hz and 100-Hz bandwidths are compared. As the wavelengths increase, the resolution becomes more critical, and the scatter in velocities (between measurements) increases.

A second consideration involves high frequencies or short wavelengths. In a material with significant damping, such as soil, high frequencies will attenuate very rapidly. Meaningful information may not be provided at high frequencies, depending on several factors, including the type of source and the spatial distribution of the geophones (to be discussed in subsequent sections). Poor coherence at high frequencies (above about 250 Hz in

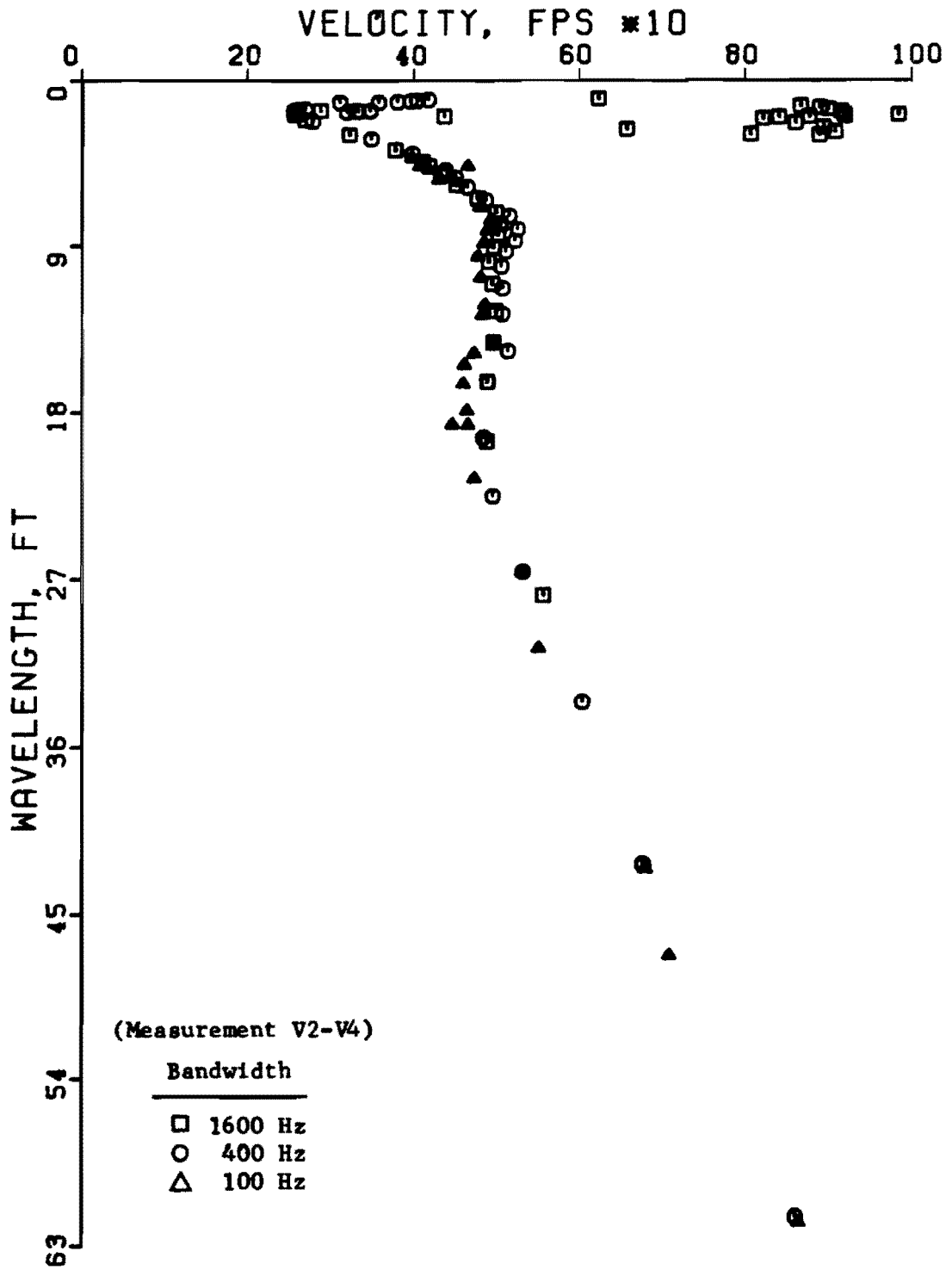

Fig 4.10. Variation in velocity-wavelength profile from differences in measurement bandwidth.

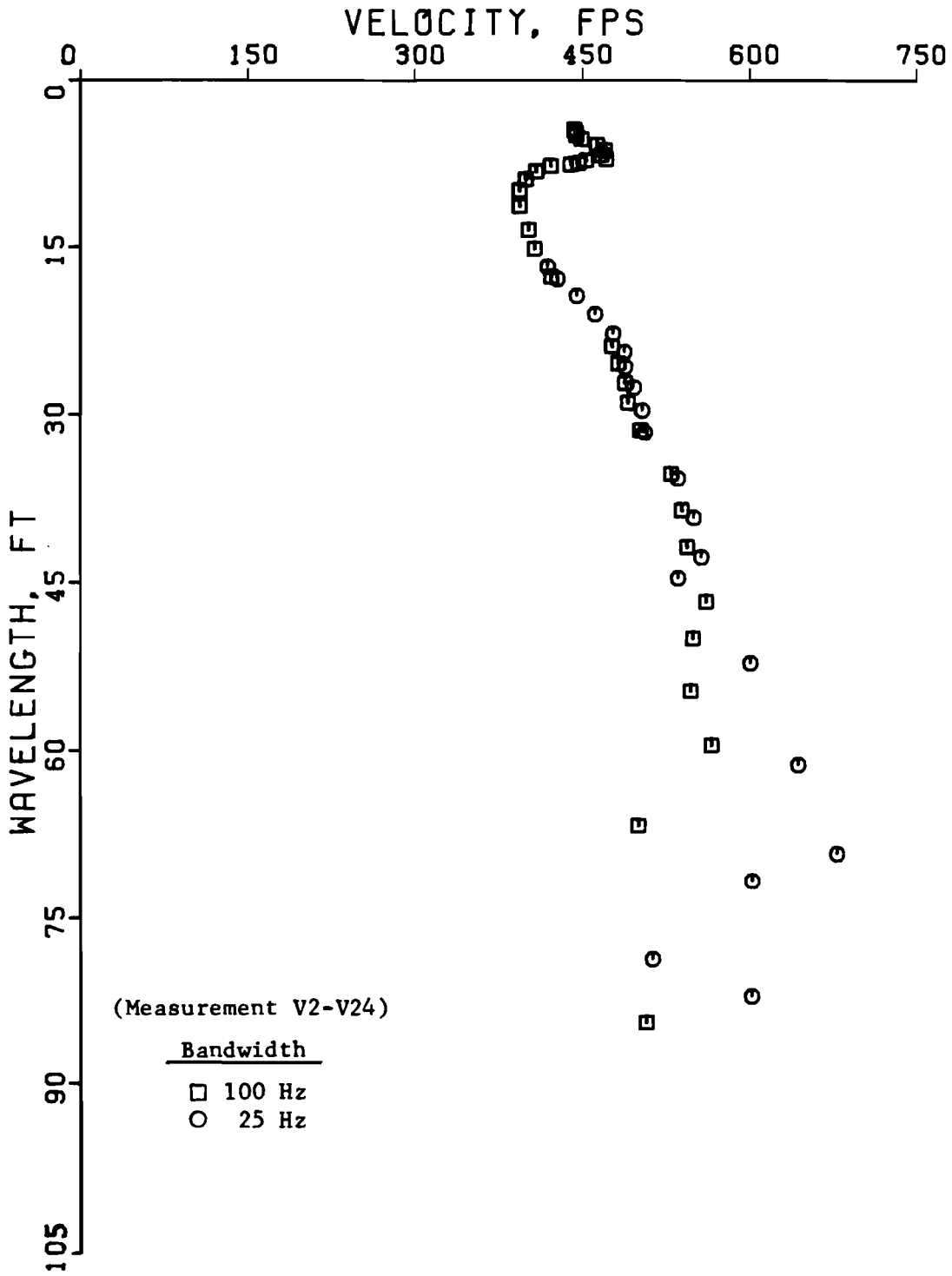

Fig 4.11. Scatter in velocities at long wavelengths caused by inadequate frequency resolution.

Fig 4.12a) indicates that significant attenuation of the short wavelengths has occurred and is generally accompanied by erratic phase information, as shown in Fig 4.12b.

Selection of an appropriate measurement bandwidth primarily depends on which frequencies are required to "sample" desired depths. Naturally, these frequencies may vary slightly from site to site depending on the soil properties, particularly the wave velocities. For a given site, it is relatively easy to develop a frequency-wavelength profile from the reduced data which will indicate the appropriate frequency bandwidth necessary to investigate the site. Such a plot for the Walnut Creek site is shown in Fig 4.13. The plot indicates that wavelengths as short as 4 ft (1.2 m) can be observed by using a measurement bandwidth of 100 Hz. If data closer to the surface is required, a larger measurement bandwidth must be used to observe the shorter wavelengths.

Typically, a bandwidth of 100 Hz will provide both an adequate range and an adequate resolution ($\Delta f \simeq 0.8$ Hz with the HP5423A) for a reasonable depth below the surface. For velocities at depths below about 25 ft (7.6 m), it may be advantageous to lower the bandwidth (say to 25 Hz) and increase the resolution. Conversely, if velocities within a foot or two of the surface are desired, it will be necessary to increase the bandwidth severalfold. Because sampling depth, or wavelength, is also related to the spacing between geophones, the appropriate bandwidth should be selected in conjunction with this spacing.

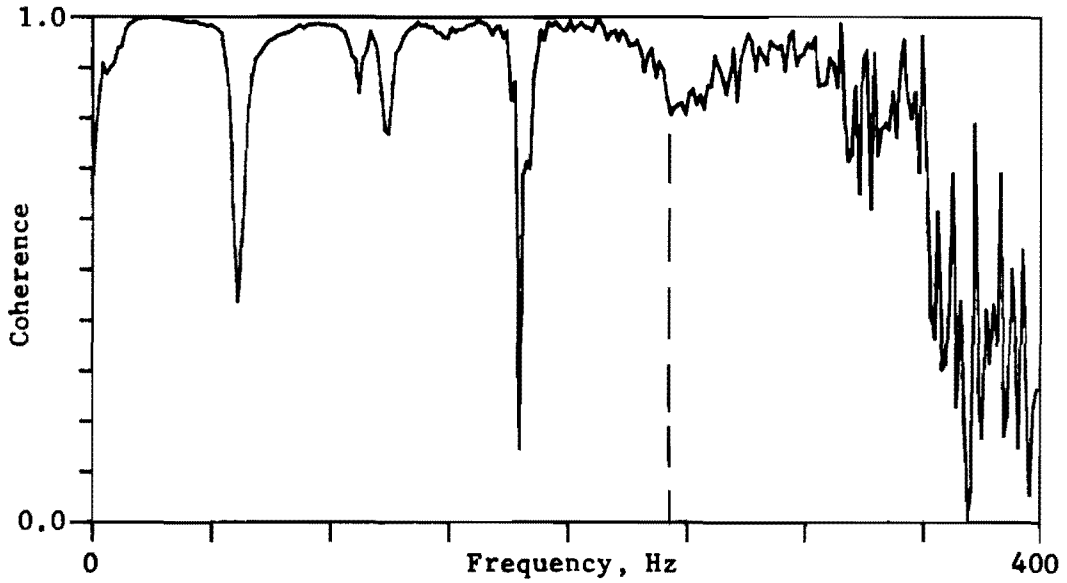

(a) Coherence function.

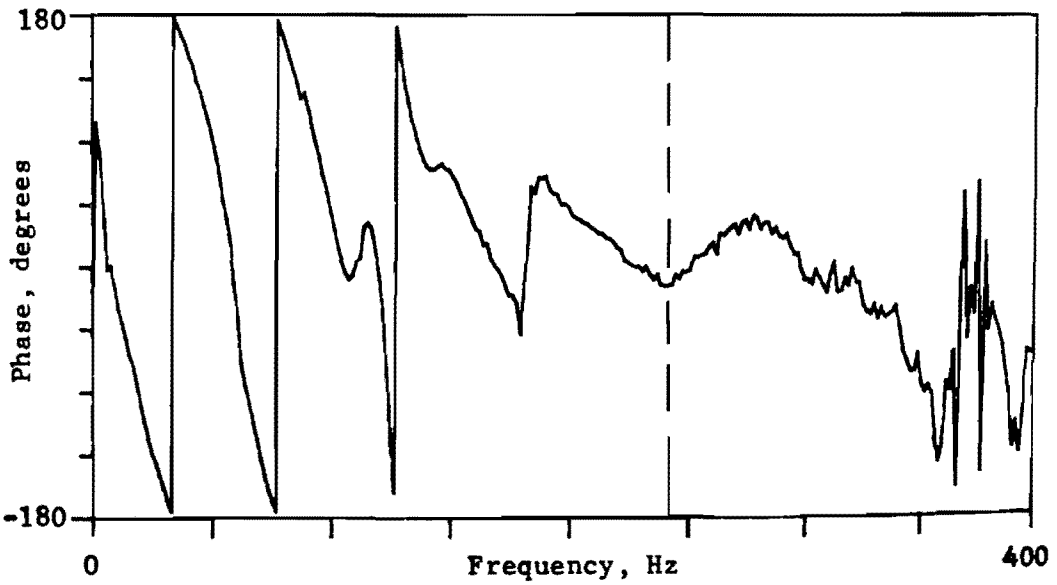

(b) Phase of the cross spectrum.

Fig 4.12. Effect of attenuation of high frequencies (short wavelengths) on spectral measurements.

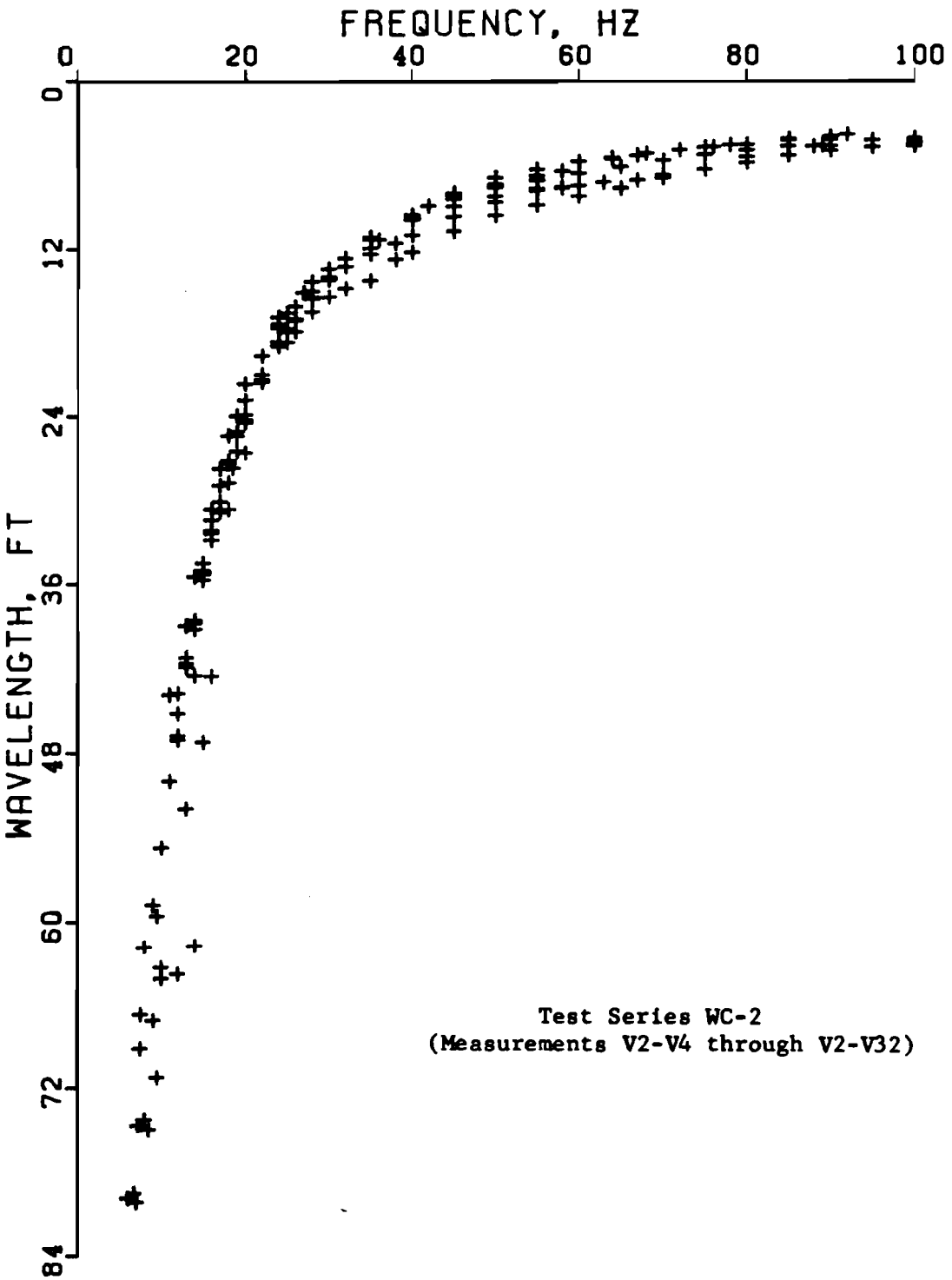

Fig 4.13. Frequency versus wavelength plot a Walnut Creek site.

Sources

There are several characteristics which are important in the evaluation of a feasible source. Among these are the magnitude of the impact, or how much energy is delivered to the soil; the coupling of the source to the soil, or how well the source transfers energy into the soil over the range of frequencies required to sample the site adequately; and, last, the type(s) of wave energy which are being generated or are at least the predominant energy type(s). All of the sources used at Walnut Creek involved a hammer blow which generated a transient impulse in the soil.

Test Series WC-1. Two sets of measurements were conducted to compare the effect of the magnitude of the impact on the cross spectrum measurement. With all other parameters held constant, one set of measurements was made with the drop hammer released at a height of 6 in. (15.2 cm) above the base (resting on the steel plate), while another set was made with the drop hammer released at a height of 24 in. (61 cm). The similarities of the coherence functions of these measurements are shown in Fig 4.14a and suggest that the variation in drop height did not affect the range of frequencies excited by the hammer-plate source. The relative magnitudes of the cross spectrums (expressed in voltage squared) are shown in Fig 4.14b. Both spectrums exhibit similar excitation up to about 120 Hz. The values of phase for the two measurements agree very closely, except in the range of about 40 to 80 Hz where the coherence for both measurements is relatively low. This suggests that the magnitude of the impact is not a critical factor as long as sufficient energy is input to "sample" the desired depth of a site.

Comparison measurements were also made using the drop hammer resting on the steel plate and the drop hammer resting directly on the soil at the

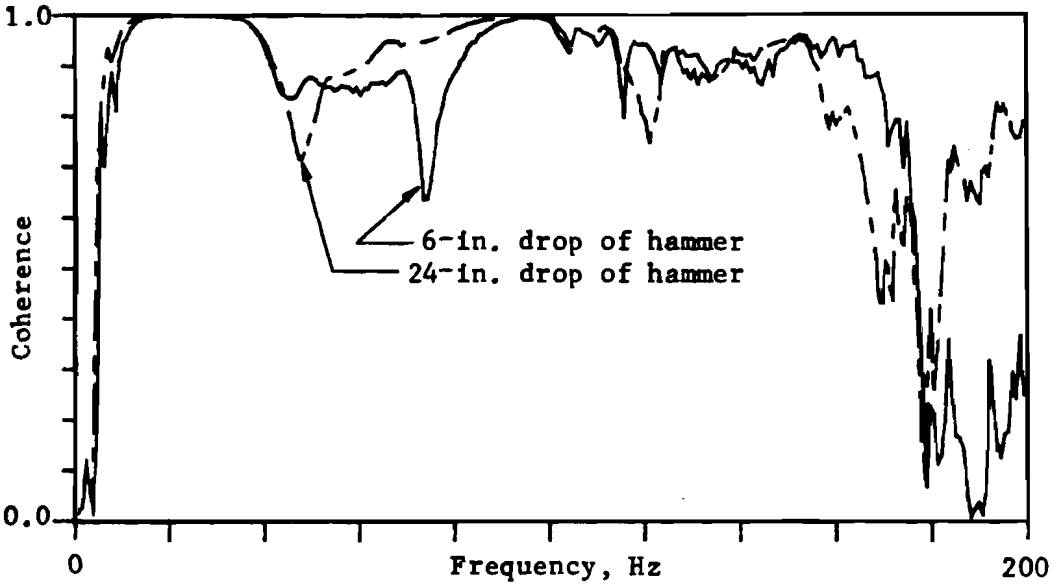

(a) Coherence function.

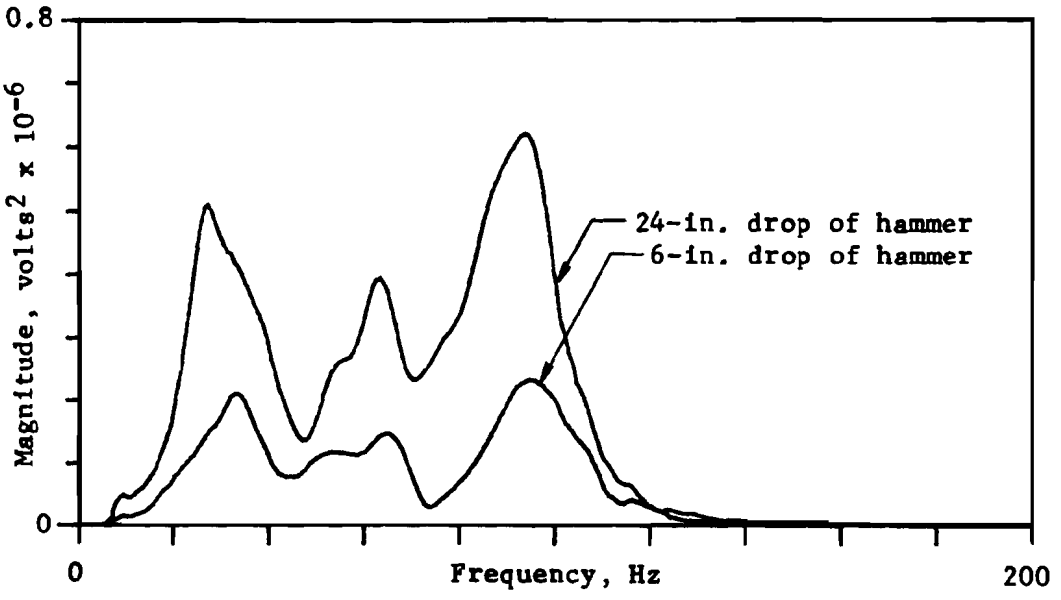

(b) Cross spectrum function.

Fig 4.14. Effect of magnitude of impact on frequency response.

ground surface. The results from measurements V8-V16 are shown in Fig 4.15. For each plot, the solid line represents the measurement with the hammer on the plate. Both source arrangements excite a similar range of frequencies and with roughly the same magnitude for any selected frequency, as indicated by the autospectrum of the signal at geophone V8, shown in Fig 4.15a. The phase plots of the cross spectrum, shown in Fig 4.15b, are quite comparable for both sources. However, the coherence for the hammer-on-soil source is significantly better over the range of 6 to 20 Hz than the coherence for the hammer-on-plate source over the same range (Fig 4.15c). This suggests that the coupling between the hammer, plate, and soil is such that low frequencies are not excited sufficiently. A source that does not transfer energy through a separate plate (source-plate-soil) seems to be more desirable for generating low frequencies and long wavelengths.

Test Series WC-2. The transient (time) signals recorded at geophone V2 (the "reference" geophone) for the sources investigated during Test Series WC-2 are shown in Fig 4.16a. The impulses generated by the sources are quite similar in both amplitude and duration. Based on the amplitude and length of the predominant wave pulse, the sledge-hammer-on-concrete-cylinder source inputs slightly more energy and excites a slightly lower predominant frequency, as shown in Fig 4.16b.

The relative energy by which any particular frequency is excited is proportional to the magnitude of the linear spectrum. The linear spectrums shown in Fig 4.16b, which are the Fourier transforms of the time signals in Fig 4.16a, provide clearer comparisons between the sources. The distribution of energy for each source indicates that the sledge-hammer-on-concrete-cylinder source provides considerably more energy

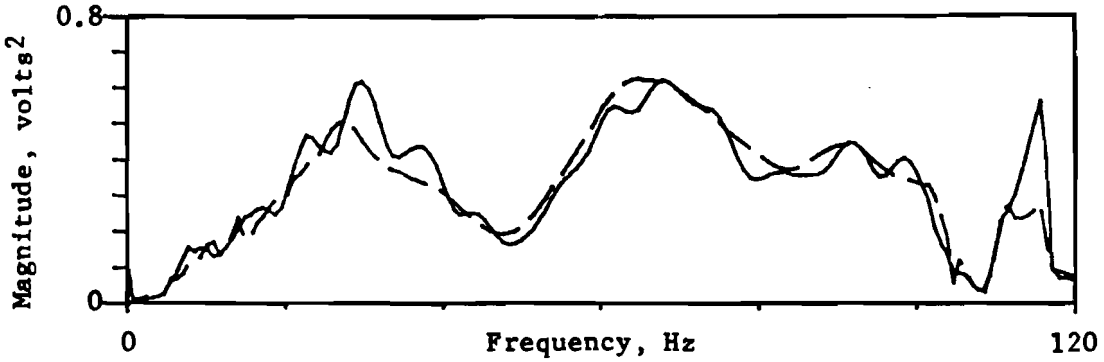

(a) Magnitude of the autospectrum function.

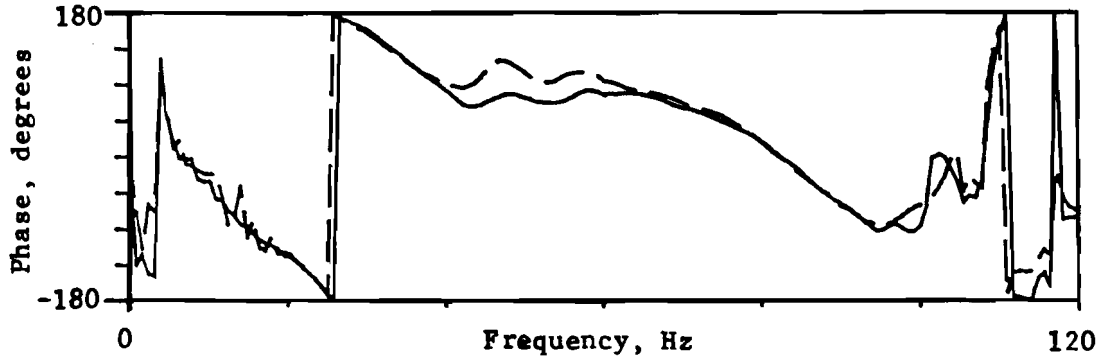

(b) Phase of the cross spectrum function.

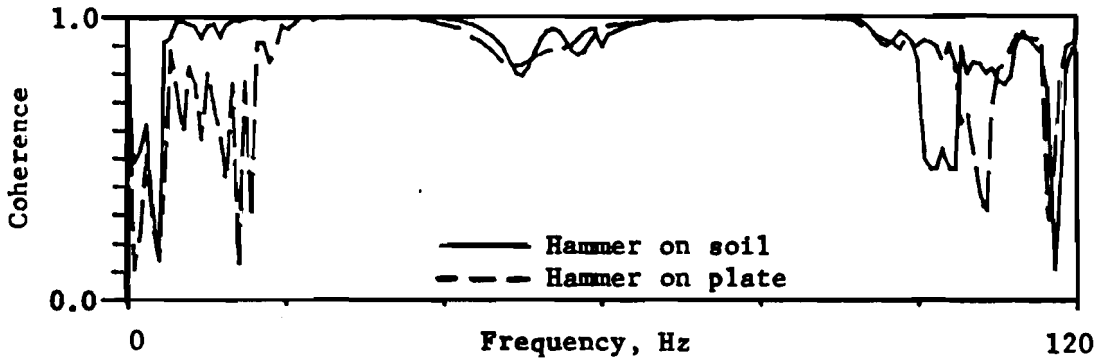

(c) Coherence function.

Fig 4.15. Comparison of frequency responses for sources used in test series WC-1.

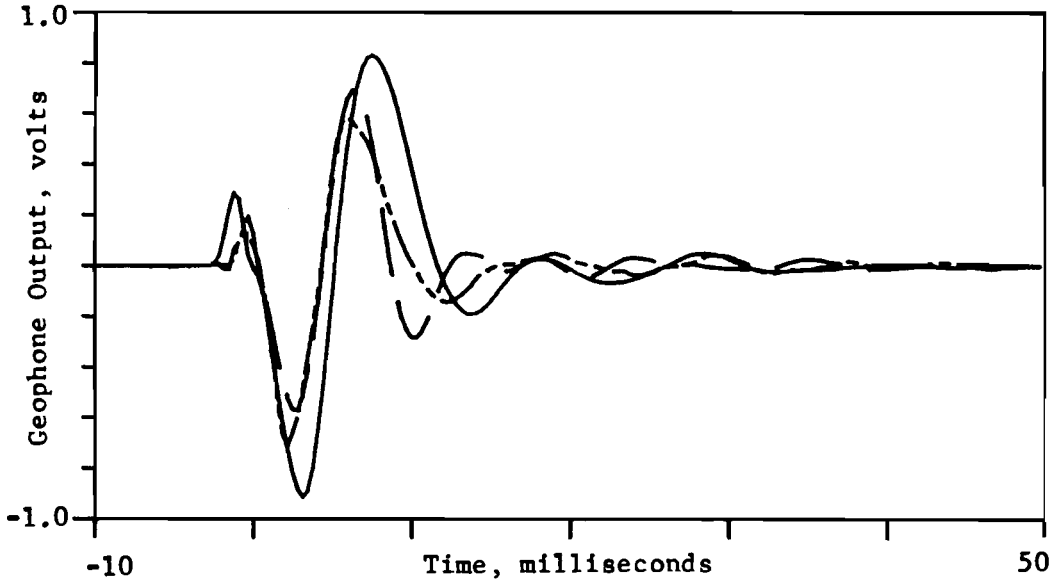

(a) Time record of generated wave pulse.

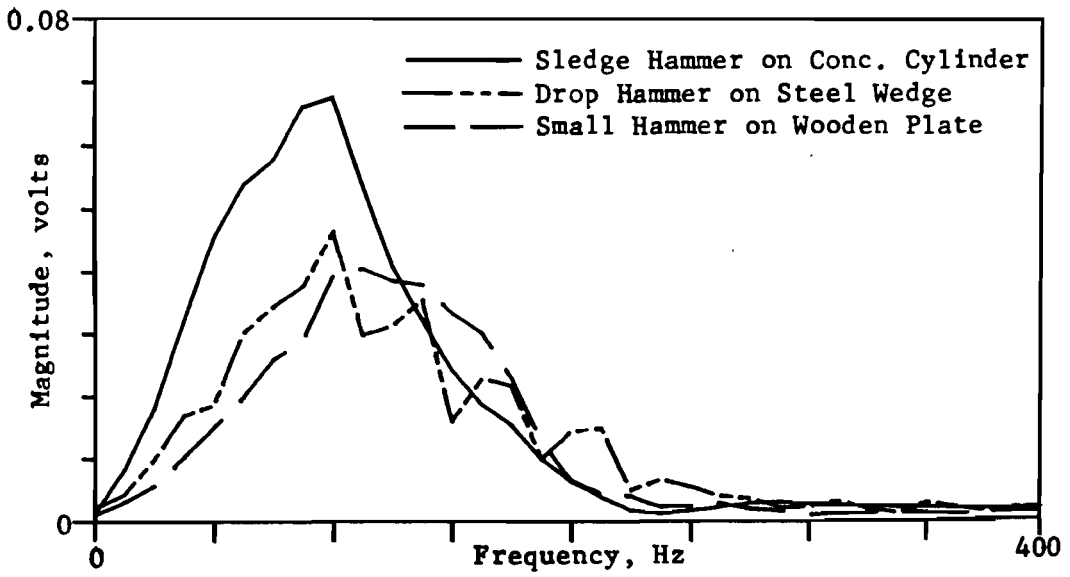

(b) Frequency spectrum of generated wave pulse.

Fig 4.16. Comparison of wave pulses and spectrums for sources used in test series WC-2.

at frequencies below about 100 Hz, which is the range of frequencies needed to investigate the Walnut Creek site (Fig 4.13). Over this range, the drop-hammer-on-steel-wedge source generates about 50 to 75 percent of the energy that the sledge-hammer-on-concrete-cylinder generates, while the small-hammer-on-wood-plate generates only 25 to 50 percent of the energy that the sledge-hammer-on-concrete-cylinder generates.

However, if the frequency response based on the transfer function is examined, a different conclusion is reached about the effectiveness of wave propagation by each source. Transfer functions based on measurements V2-V4 are shown in Fig 4.17. The magnitude of the transfer function is a dimensionless ratio of the energy of the output signal (V4) to the energy of the input signal (V2). Since the measurement is in effect "normalized" by dividing the output by the input, the amount of input energy is not critical for comparison purposes, as was the case for the linear spectrums compared in Fig 4.16b.

Any apparent differences in attenuation of wave energy (indicated by an output/input ratio less than one) must be a result of the geometric damping of the various components of wave energy in the impulse produced by the source, because the distance between the two geophones is the same and the same material properties are being measured. At the surface of an elastic half-space, body waves (P- and S-waves) follow a geometrical damping law of $1/r^2$ and R-waves follow a geometrical damping law of $1/\sqrt{r}$. Therefore, body waves attenuate more rapidly than Rayleigh waves. For the transfer functions shown in Fig 4.17, a lower output/input ratio indicates more geometrical damping, which can be interpreted as a greater percentage of body wave energy in the impulse produced by the particular source.

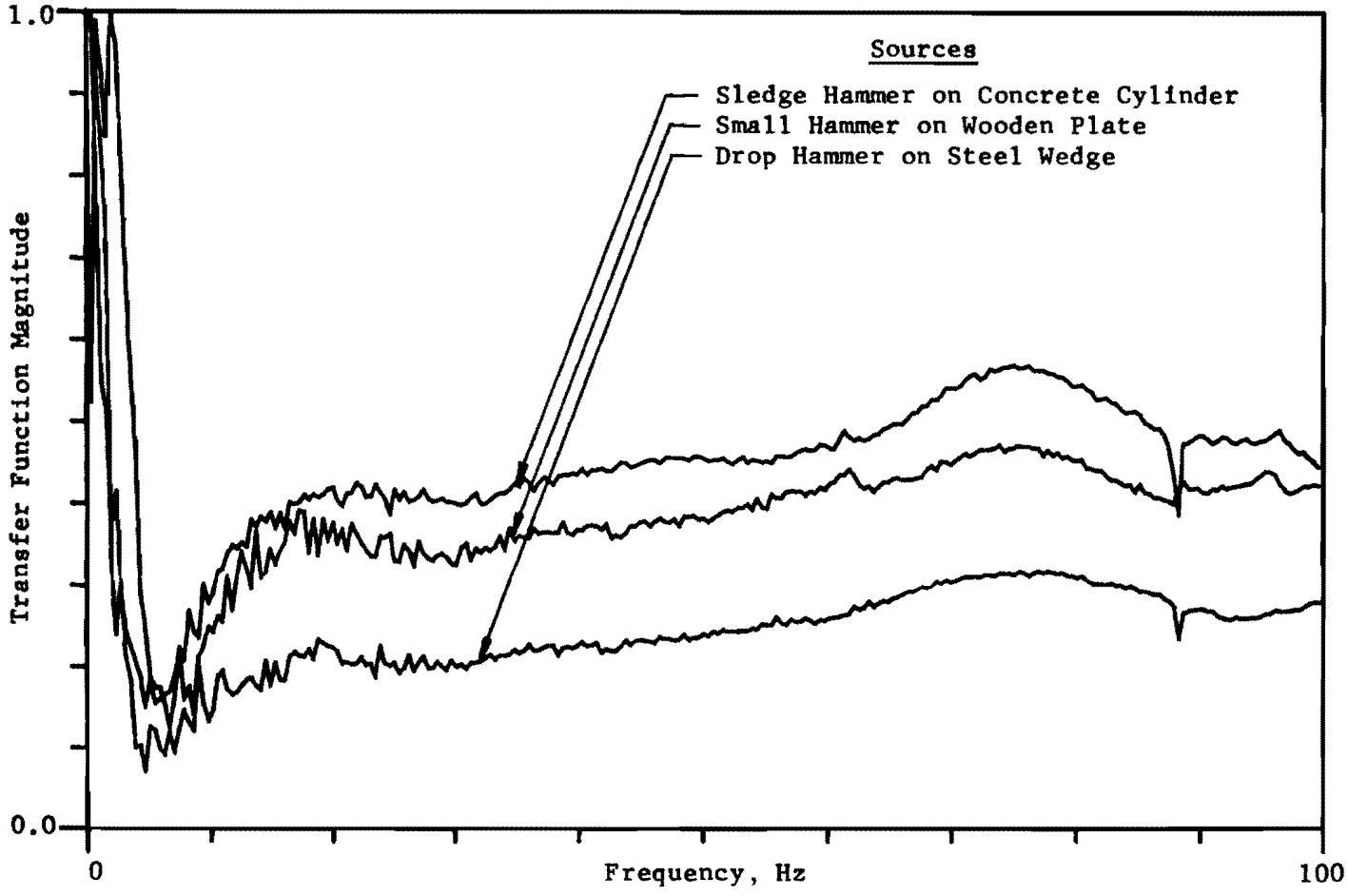

Fig 4.17. Comparison of transfer functions for sources used in test series WC-2.

The sledge-hammer-on-concrete-cylinder source exhibits the highest output/input ratio. The output/input ratio of the small-hammer-on-wood-plate source is about 80 to 90 percent of the ratio of the sledge-hammer-on-concrete-cylinder source, while the output/input ratio from the drop-hammer-on-steel-wedge is about 50 to 55 percent of the ratio of the sledge-hammer-on-concrete-cylinder. These results indicate that the drop-hammer-on-steel-wedge source contains more body wave components and is less desirable as a Rayleigh wave source. This is not unexpected, since the wedge was oriented so as to produce a shearing motion.

Based on the comparison of the sources in terms of their linear spectrums (Fig 4.16b) and their energy transfer characteristics (Fig 4.17), it can be concluded that the magnitude of energy generated by a particular source is not the most critical characteristic of the source. More important is the coupling, or energy transfer, of the source to the soil. With respect to this criterion, a large flat mass in contact with the soil (preferably without an intermediate plate) is the most desirable type of source.

Further evidence that the type of wave energy generated is an important factor is shown in Figs 4.18 and 4.19. The phase of the cross spectrum for each source (measurement V2-V4) shown in Fig 4.18a indicates that there is a fair amount of scatter in phase between the sources, particularly at larger frequencies. This translates into substantial scatter in the velocity-wavelength profile, as shown in Fig 4.19. One possible explanation of these differences in velocity may be varying percentages of body wave energy in the signal, which affects the overall velocity of the impulse.

The coherence functions, shown in Fig 4.18b, indicate that the sledge-hammer-on-concrete-cylinder source excites low-frequency (about 6 to

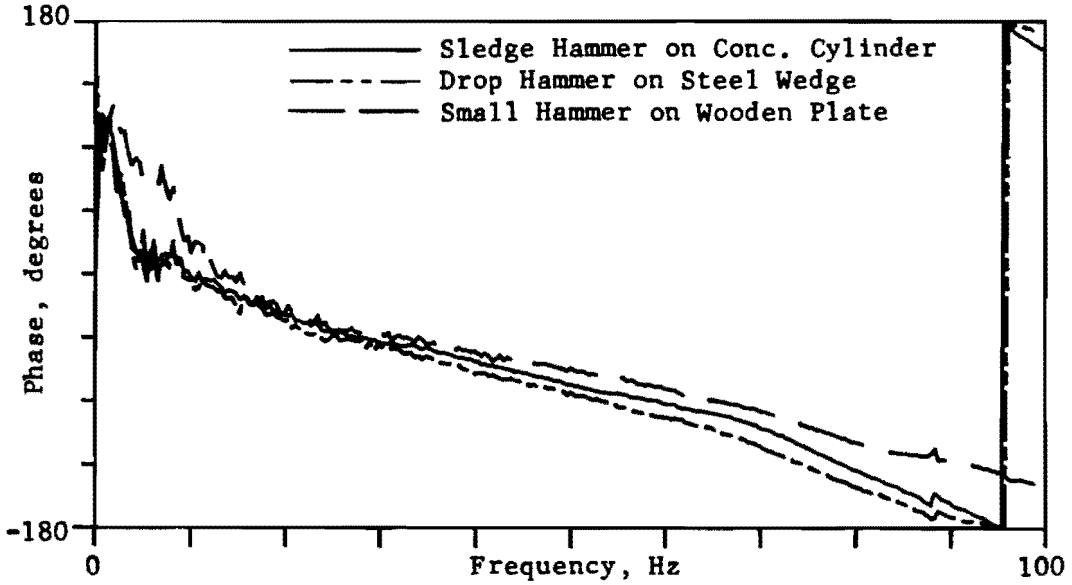

(a) Phase of the cross spectrum.

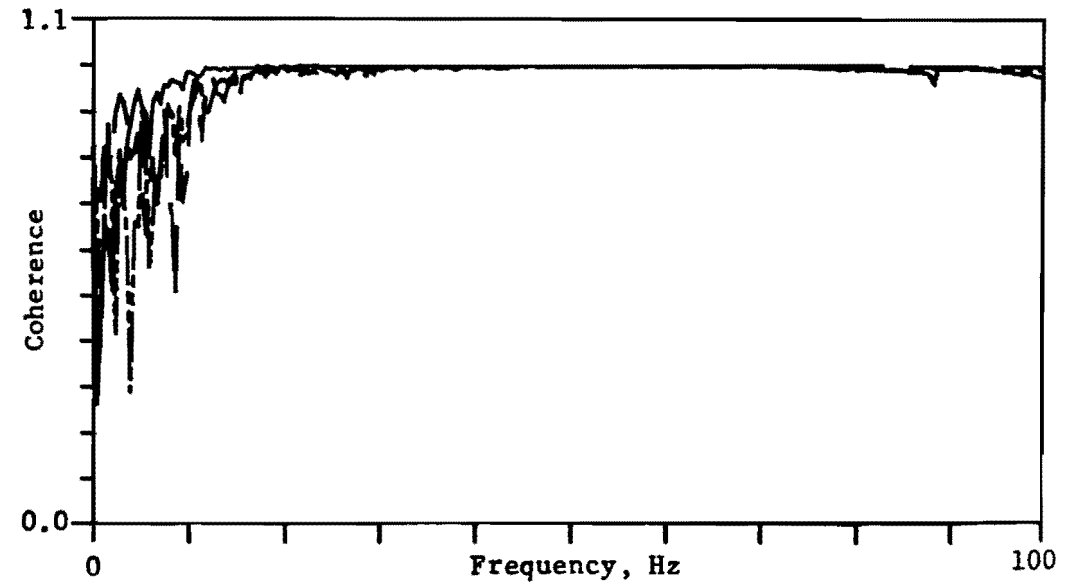

(b) Coherence function.

Fig 4.18. Comparison of cross spectrums and coherence functions for sources used in test series WC-2.

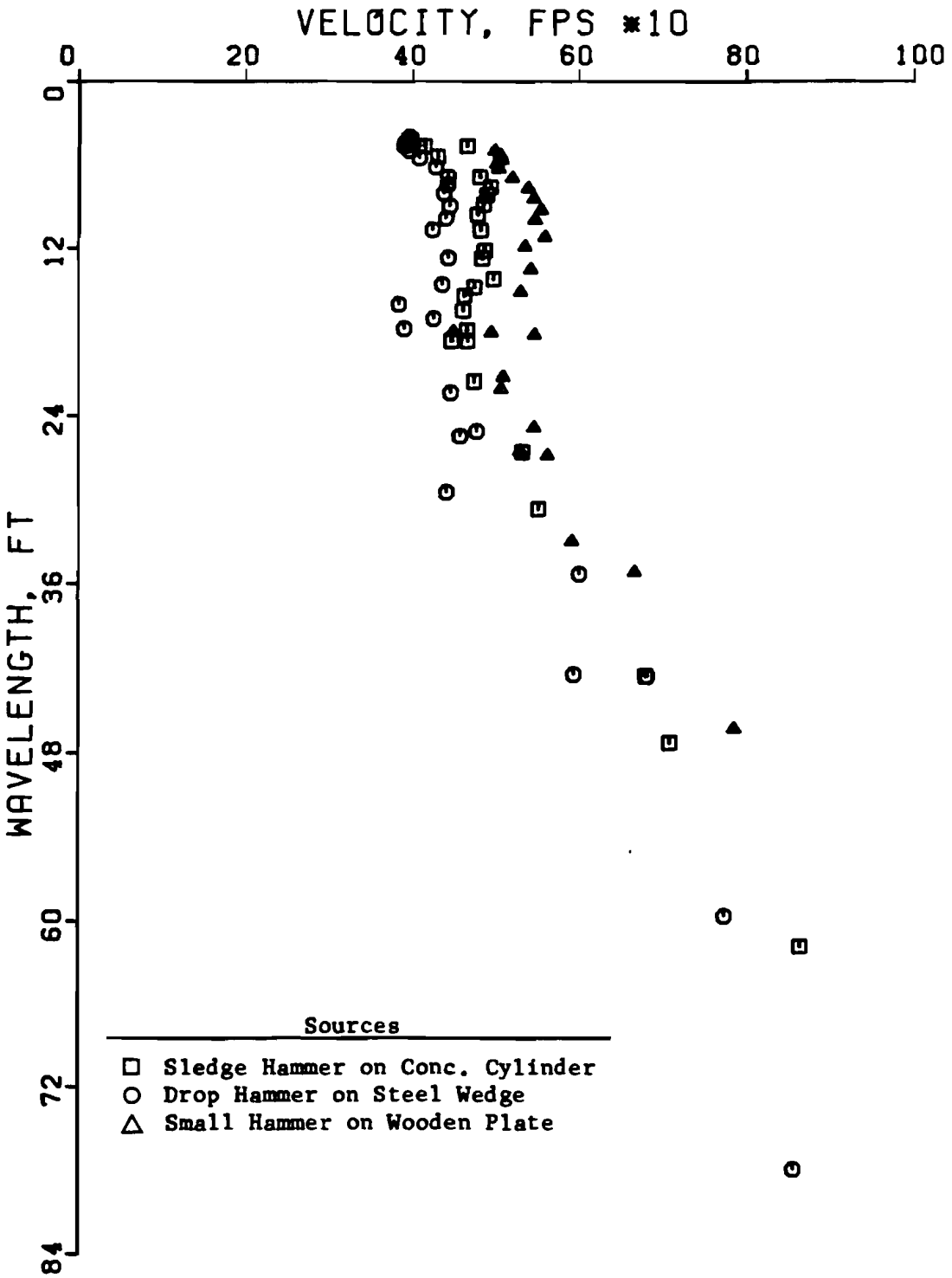

Fig 4.19. Comparison of velocity-wavelength profiles for measurement V2-V4 for sources used in test series WC-2.

20 Hz) wave energy markedly better than the other sources. Again, this is probably due to the excellent coupling of the mass with the soil.

Spatial Distribution of Geophones

The appropriate spacing of the geophones depends on the velocities of the materials found at the site and the depth to which the investigation will be conducted. The wavelengths, frequency bandwidth, and attenuation properties of the site are all interrelated and affect the necessary spacing of the geophones. Determination of upper and lower bounds for the spacing (Δx) between geophones as a function of wavelength is discussed in the following paragraphs.

Consideration is first given to an upper bound for Δx. This bound is related to the attenuation of the wave energy and can be established by examining the range of frequencies over which the coherence value (γ^2) remains near unity. Such a range indicates which frequencies have sufficient energy at the output geophone (far geophone) to be accurately measured as a response similar to that at the input geophone (near geophone). Since wave attenuation is a function of distance, variations in Δx will give different ranges of frequencies over which useful information is recorded.

The level of coherence that defines "useful information" is somewhat arbitrary. For the purposes of developing a relationship between Δx and f, a coherence of $\gamma^2 \geq 0.90$ has been selected as indicative of useful information. Relationships of frequency range (upper limit) to spacing are shown in Table 4.3 for Test Series WC-1 and in Table 4.4 for Test Series WC-2. Both sets of data indicate a marked decrease in the range of useful frequencies as the spacing increases. In other words, closer spacing is required to sample

TABLE 4.3. USEFUL FREQUENCY RANGE AS A FUNCTION OF RECEIVER SPACING FOR TEST SERIES WC-1.

Distance from Source to Geophones (ft)		Geophone Spacing,	Range of Frequencies with Coherence $\geq$ 0.9
Near	Far	Δx (ft)	(Hz)
2	4	2	800*
4	8	4	326
8	16	8	207
16	32	16	84

*Based on useful information in phase plot of cross spectrum.

TABLE 4.4. USEFUL FREQUENCY RANGE AS A FUNCTION OF RECEIVER SPACING FOR TEST SERIES WC-2.

Distance from Source Geophones (ft)		Geophone Spacing,	Range of Frequencies with Coherence $\geq$ 0.9
Near	Far	Δx (ft)	(Hz)
2	4	2	625
2	8	6	240
2	12	10	91
2	16	14	87
2	24	22	73
2	32	30	58

higher frequencies. This is particularly true for soils, which rapidly attenuate high-frequency-wave energy.

The data in Tables 4.3 and 4.4 are plotted in Fig 4.20. It appears that the relationship between Δx and f does not depend on the location of the geophone nearer the source but only on the spacing between the geophones. The data can be reasonably approximated by a straight line on a logarithmic plot and can be described by an equation of the form

$$f = k\ (\Delta x) \tag{4.1}$$

where k is a constant (the intercept at $x = 1$) and m is the slope of the line. The value of k is approximately 1360 and the slope of the line is

$$m = \tan(-44°) = -0.966 \simeq -1.0$$

Since the values of f plotted in Fig 4.20 represent an upper limit, the range of frequencies over which useful information is provided (as a function of spacing) is

$$f \leq \frac{1360}{\Delta x} \tag{4.2}$$

The constant 1360 has units of fps where f is in cps and Δx is in ft. This constant represents soil conditions at the Walnut Creek site and will most likely vary depending on the particular site profile. Note that Eq 4.2 can serve as a guide for selecting an appropriate bandwidth for a given spacing.

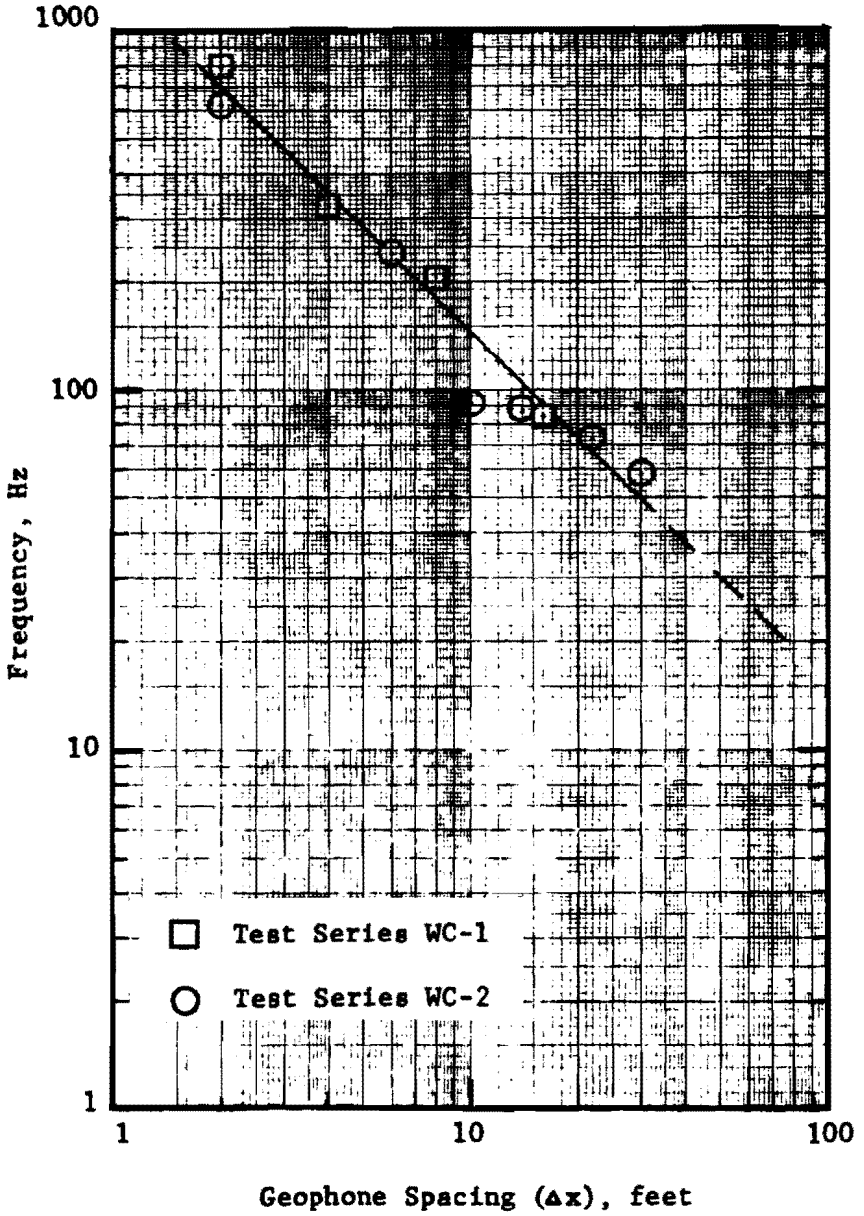

Fig 4.20. Relationship between geophone spacing and frequency range of useful information.

If the quantity V/L_R replaces f in Eq 4.2, a relationship between wavelength and spacing is obtained as follows:

$$L_R \geq \frac{V_R \cdot \Delta x}{1360} \tag{4.3}$$

where velocity, V_R, is in fps and wavelength, L_R, is in ft. For a range of S-wave (or R-wave) velocities of about 450 fps to 700 fps, which is typical of soils, Eq 4.3 yields a range of L_R greater than or equal to about one-third Δx to one-half Δx. Conversely, to insure that the wave energy of a particular wavelength does not decay excessively, the spacing between geophones should not exceed two to three times the wavelength to be sampled. This outcome verifies that excessive cycles of a particular wavelength or frequency will lead to undesirable attenuation as far as signal pickup is concerned.

The establishment of an upper bound for spacing between geophones should be guided by the wavelength(s) to be measured. Based on the foregoing discussion, it is preferable that Δx not exceed two times the wavelength to be measured. It is also reasonable to assume that the spacing between the source and the first geophone should follow a similar criterion.

Consideration is now given to the lower bound for Δx. This bound is influenced by the sensitivity of the instrumentation to measure phase differences between signals. If the wave had travelled one wavelength by the time it reached the first geophone, then, in theory, the second geophone could be located as close as possible to the first geophone to measure the relative phase differences. However, the precision of the instrumentation and the desired accuracy in the phase difference create a physical limitation that governs the proximity of the geophones to each other. The performance

specifications of the HP5423A Analyzer list the channel-to-channel phase match as + 5 degrees. Thus, a cross spectrum phase measurement of 50 degrees may potentially (though most likely will not) be in error by 10 percent. If the spacing Δx is at least one-third of the wavelength, then the phase measurement will always be at least 120 degrees, and the percent error will be less than about 4 percent. Note that this does not mean that all measurements are in error by 4 percent, but that certainly no measurement is in error by more than 4 percent.

For a given spacing, then, the longest wavelength which can be reliably measured (with certainty of no more than 4 percent error) is three times Δx. Longer wavelengths will not have travelled a distance sufficient to change the phase by at least 120 degrees leading to potential errors greater than 4 percent. This establishes the lower bound for spacing between geophones to be such that Δx is greater than or equal to $L_R/3$. It should be recognized that this is a very conservative lower bound, since it eliminates from (confident) consideration any phase measurements less than 120 degrees. In general, observed phase measurements even as low as 20 degrees for short spacings ($\Delta x \simeq 2 - 6$ ft) have provided reasonably representative wave velocities. This is probably a benefit of using several averages to make the measurement.

In summation, spacing is directly related to the wavelength(s) to be measured. Based on the preceding discussion, a particular wavelength L_R is most accurately (or confidently) measured within a range of spacings given by

$$L_R/3 \leq \Delta x \leq 2L_R \tag{4.4}$$

For application in field testing, it is more convenient to establish a particular spacing and then to consider the range of wavelengths over which a

reliable measurement was made for that spacing. This relationship is obtained by rearranging Eq 4.4 to yield

$$\frac{1}{2}\Delta x \leq L_R \leq 3\Delta x \tag{4.5}$$

For example, if the spacing in the field was selected as 10 ft (3 m), the range of wavelengths which could be measured with reasonable confidence and accuracy would be about 5 to 30 ft (1.5 to 9 m). In general, if Δx is increased geometrically—by doubling or tripling the spacing between geophones—for each successive measurement, then all wavelengths will be sampled properly during at least one measurement. More than likely, some overlap of wavelength measurements will occur, to provide continuity in the dispersion (velocity versus wavelength) curve.

The range given by Eq 4.5 can be employed to filter out those wavelengths (or frequencies) which are not appropriate for a designated spacings. By filtering out long wavelengths from close spacings and short wavelengths from far spacings, much of the scatter associated with a set of measurements is eliminated. Then only those wavelengths which fall within the appropriate range are used to develop the velocity-wavelength profile.

The benefits of such an approach are illustrated in Figs 4.21-4.24. The velocity-wavelength profile for Test Series WC-2, without filtering the inappropriate wavelengths according to Eq 4.5, is shown in Fig 4.21. As a result, there is excessive scatter for very short waves (less than 10 ft) as well as for relatively long waves (greater than 50 ft). When the inappropriate wavelengths are filtered, much of the scatter is removed, as indicated in Fig 4.22. Similar results are shown for Test Series WC-1. The velocity profile in Fig 4.23 contains unfiltered wavelengths, while the improved profile using filtered wavelengths is shown in Fig 4.24.

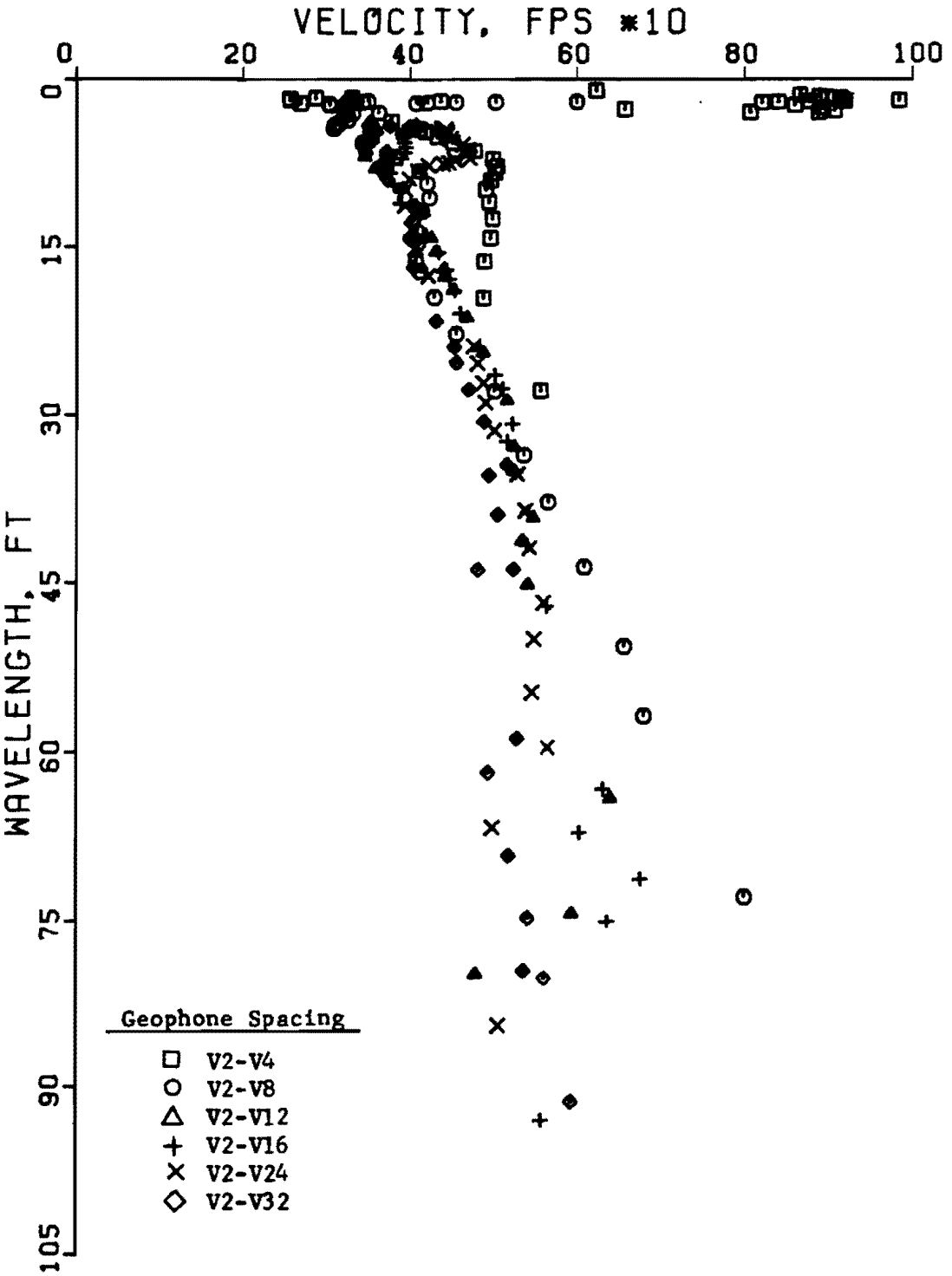

Fig 4.21. Velocity-wavelength plot without filtering for different geophone spacings from test series WC-2.

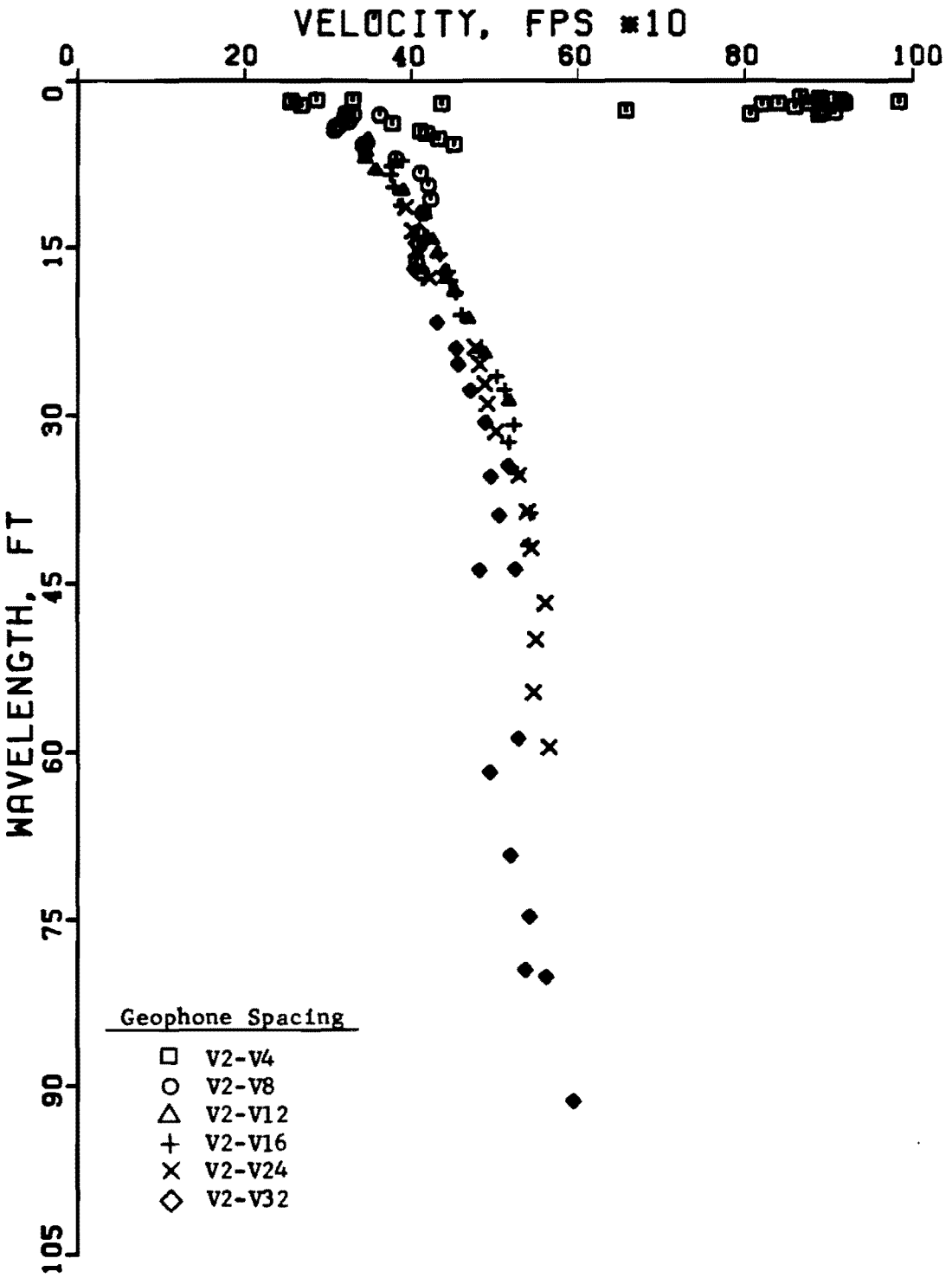

Fig 4.22. Velocity-wavelength plot with filtering for different geophone spacings from test series WC-2.

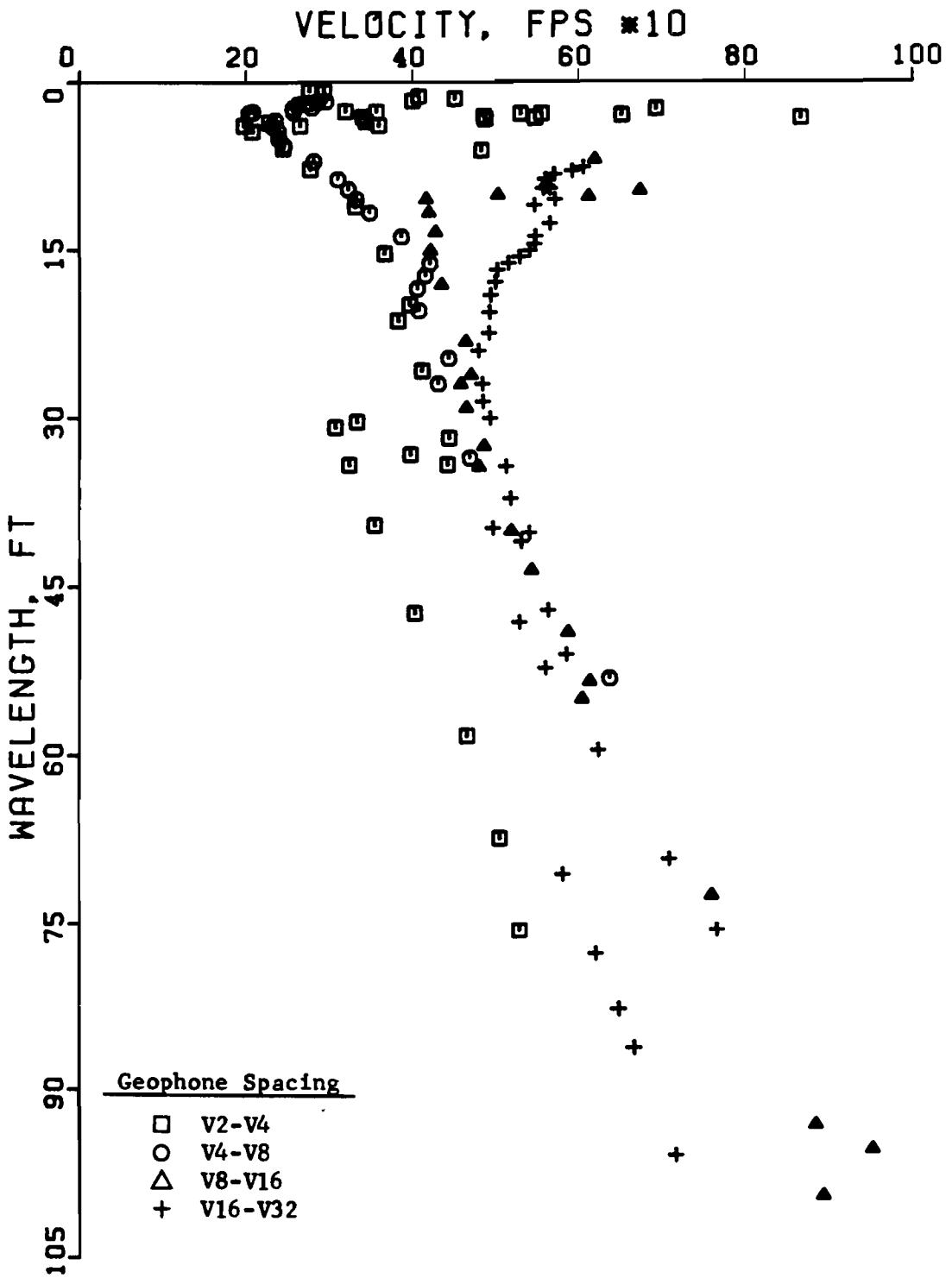

Fig 4.23. Velocity-wavelength plot without filtering for different geophone spacings from test series WC-1.

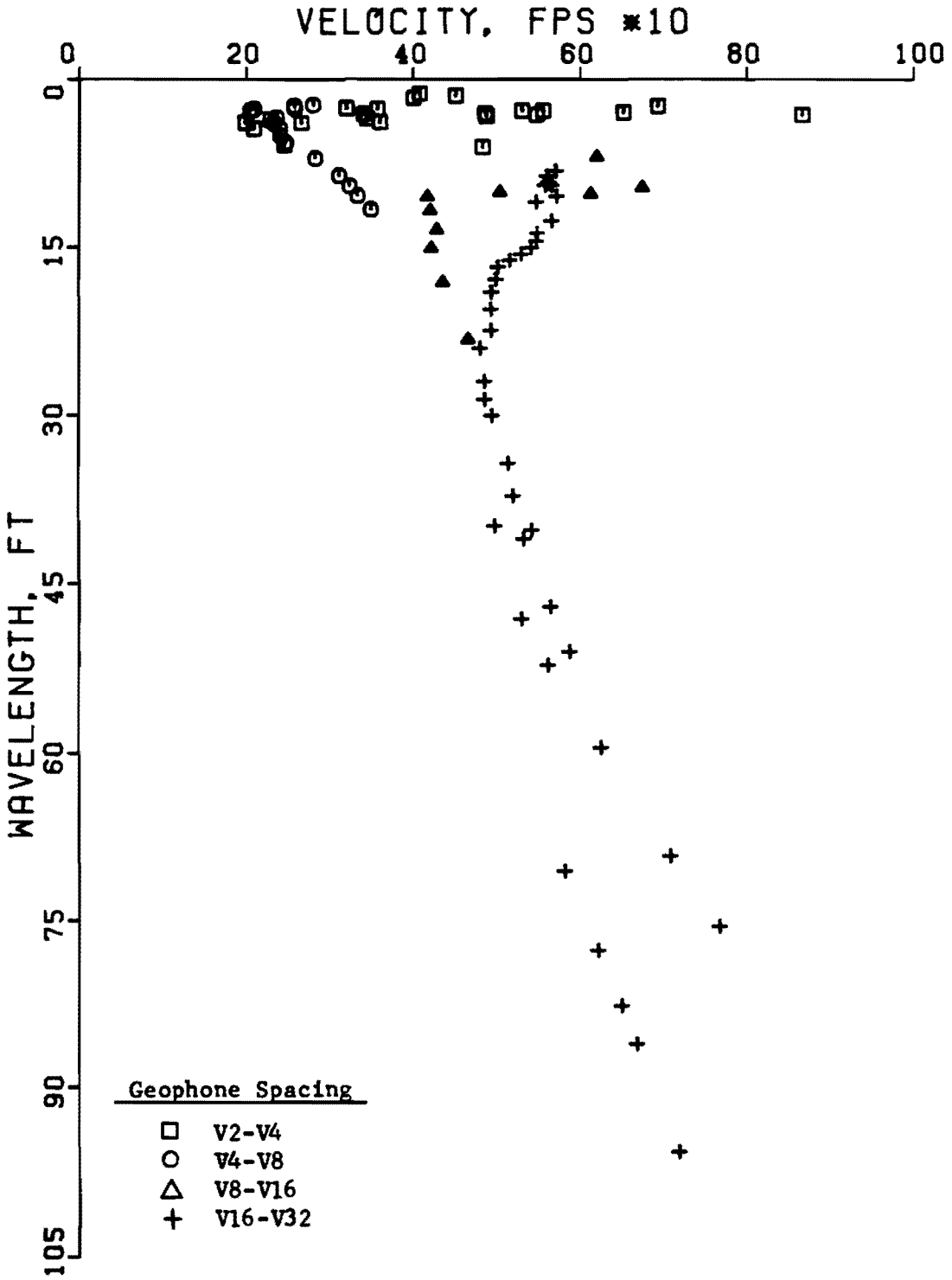

Fig 4.24. Velocity-wavelength plot with filtering for different geophone spacings from test series WC-1.

In addition to spacing Δx, the appropriate location of the first geophone from the source must be considered. Intuitively, the first geophone should be located at a distance equal to or greater than the particular wavelength to be measured. This permits ample time for the wave to propagate due to the influence of the depth to be sampled. In actual field testing, it is difficult to assess how rigorously this criterion should be followed. Certainly the first geophone should be spaced some distance away so that any body wave energy will have had sufficient opportunity to dissipate and, thus, a wave pulse that is more nearly pure Rayleigh wave energy will be captured. For that reason, the use of a reference geophone near the source is not desirable.

This distance also allows more time for the various frequencies (wavelengths) in the pulse to separate, which should enhance the ability of the spectral analyzer to transform accurately the wave pulse into its frequency spectrum. Based on the data in Tables 4.3 and 4.4, the location of the first geophone is important. For measurements where the far geophone was located at the same distance in both test series, a greater range of useful frequencies was obtained (based on $\gamma^2 \geq 0.90$) when the near geophone was located away from the source as opposed to being at the reference location V2. For example, measurement V8-V16 provided data up to 207 Hz while measurement V2-V16 provided data only up to 87 Hz. It appears that the "extra" distance from the source to the near geophone provides for a better overall measurement.

Measurements from Test Series WC-1 and WC-2 can be used to test this hypothesis. Recall that, for Test Series WC-1, both geophones were spaced at increasing distances from the source, while, for Test Series WC-2, the near geophone remained at a distance 2 ft (0.6 m) from the source and only the far

geophone was moved. Figures 4.22 and 4.23 are replotted in Fig 4.25 to compare the velocity profiles obtained by the different spacing arrangements. The profiles begin to diverge at a wavelength of about 60 ft (18 m), indicating that longer wavelengths are affected more by the difference in geophone location. Further conclusions can be drawn by comparing the profiles with shear wave velocities from crosshole tests.

SHEAR WAVE VELOCITY PROFILE

One of the main purposes of dynamic testing in the field is to determine in situ shear moduli based on measured shear wave velocities. The variation of modulus with depth can be conveniently described by the profile of the shear wave velocity versus depth. Heretofore in this chapter, only Rayleigh wave velocities have been discussed or plotted. Rayleigh wave velocities can be converted to shear wave velocities if the Poisson's ratio of the material is known or if it can be reasonably assumed.

Before developing and presenting a shear wave velocity profile from Rayleigh wave velocities, it is necessary to determine a Poisson's ratio (or several, if material properties vary significantly) for the site. Data from crosshole tests (ratios of V_S/V_P) can be used to calculate an estimate of Poisson's ratio.

Crosshole Test Results

The crosshole data presented herein were collected and presented by Patel (Ref 20). The crosshole shear wave velocity profile obtained by Patel is shown in Fig 4.26. This profile includes measurements made between

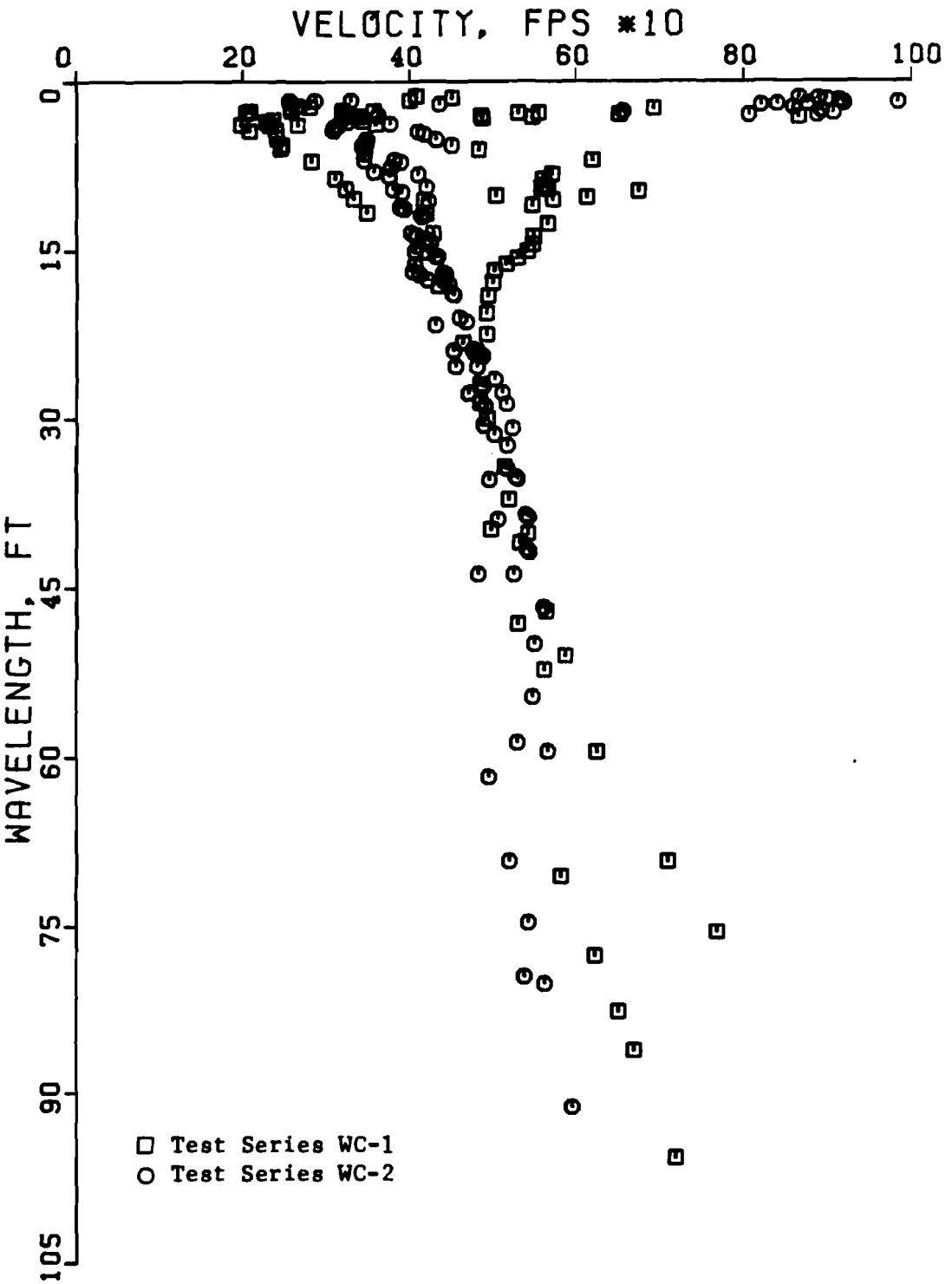

Fig 4.25. Comparison of filtered velocity-wavelength plots for geophone spacings of test series WC-1 and WC-2.

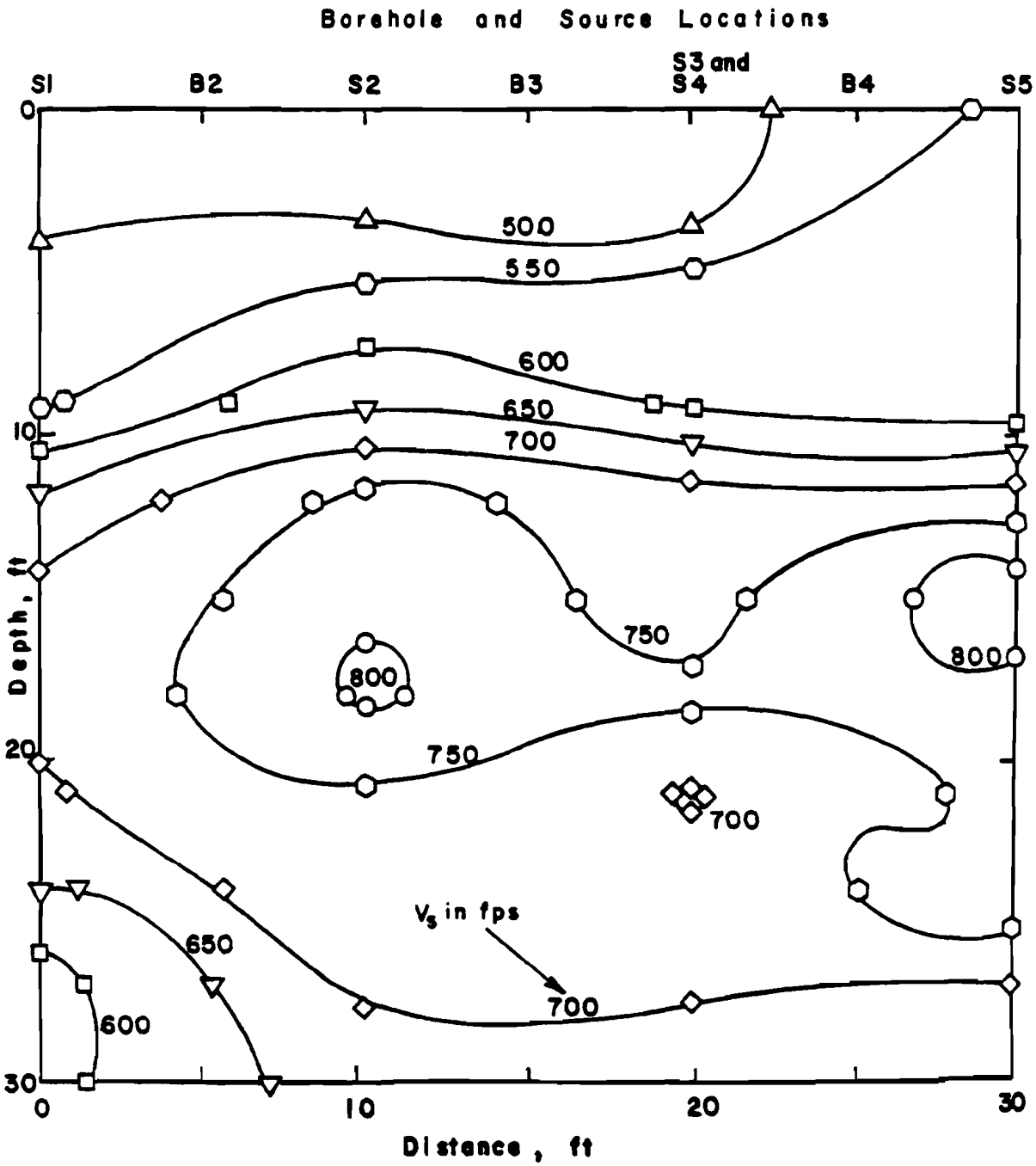

Fig 4.26. Crosshole shear wave velocity profile at Walnut Creek site (Ref 20).

boreholes B1 and B5 as depicted in Figs 4.4 and 4.6. A rather large variation in shear wave velocities exists from borehole to borehole, particularly at depths from about 15 to 20 ft (4.6 to 6.1 m).

Table 4.5 contains a summary of the S-wave and P-wave velocities (average values) obtained by Patel. Above 30 ft (9 m) the degree of saturation is less than 99 percent, so that these velocities represent properties of the soil skeleton. The ratio of V_S/V_P was calculated, and, using Table 2.1, Poisson's ratios were estimated. Finally, ratios of V_R/V_S listed in Table 4.5 were approximated on the basis of Poisson's ratios. At the Walnut Creek site, Poisson's ratios ranged from 0.31 to 0.40. The ratio of the Rayleigh wave velocity to the shear wave velocity only varies from about 0.93 to 0.94. For purposes of analysis, the value of V_R/V_S was assumed to be 0.94 over the entire profile.

Velocity Profile from Cross Spectrum Measurements

Previous discussion of sources showed the sledge-hammer-on-concrete source provided the best combination of magnitude and coupling to generate predominantly Rayleigh-wave energy over the range of wavelengths needed to sample the Walnut Creek site. The velocities plotted in Fig 4.25 as representative of Test Series WC-2 included only cross spectrum measurements made with the sledge-hammer-on-concrete source. The velocities are assumed to be Rayleigh wave velocities. Using the ratio of V_R/V_S equal to 0.94, the calculated R-wave velocities can be converted to S-wave velocities by

$$V_S = V_R/0.94$$

TABLE 4.5. SUMMARY OF CROSSHOLE TEST RESULTS AT WALNUT CREEK (REF 20)

Depth (ft)	S-Wave Velocity V_S(fps)*	P-Wave Velocity V_P(fps)*	V_S/V_P	Poisson's Ratio**	V_R/V_S**
3	540	1248	0.433	0.38	0.94
6	565	1225	0.461	0.36	0.94
9	680	1670	0.407	0.40	0.94
12	735	1775	0.414	0.40	0.94
15	765	1657	0.462	0.36	0.94
18	745	1417	0.526	0.31	0.93
21	730	1415	0.516	0.32	0.93
24	705	1667	0.423	0.39	0.94
27	665	1610	0.413	0.40	0.94
30	640	4883	(Water Table)	-	-

* S-wave velocities and P-wave velocities from Patel (1981).

** Poisson's ratios and V_R/V_S based on V_S/V_P using Table 2.1.

To obtain a profile of velocity versus depth, some criterion must be selected regarding the "effective sampling depth" of a given wavelength. The velocity versus magnitude plot shown in Fig 4.25 can, thereby, be translated into a velocity versus depth profile. Three such profiles (from measurements for Test Series WC-1), employing $L_R/2$, $L_R/3$, and $L_R/4$ criteria, are plotted together in Fig 4.27. Naturally, the profile using the greatest fraction of wavelength ($L_R/2$) will provide the deepest region of sampling or testing.

It should be emphasized that the use of a depth criterion based on wavelength is somewhat empirical. In general, a unique criterion is probably not correct for all wavelengths. A more accurate solution based on rigorous theory and numerical analysis is beyond the scope of this study. However, for typical sites and material properties, the use of a depth criterion based on wavelength appears to be satisfactory for engineering applications.

Comparisons Between Cross Spectrum Measurements and Crosshole Results

A comparison between cross spectrum measurements and crosshole measurements serves two purposes. First, it provides a basis for determining which wavelength criterion (shown in Fig 4.27) yields the most representative sampling depth at this particular site. Second, it permits a judgement on the overall ability of a surface measurement to define the shear wave velocity profile accurately.

The range of values of shear wave velocities (Ref 20) obtained at 3-ft (0.9-m) intervals to a depth of 30 ft (9 m) is graphed as a band in Fig 4.27. Based on this band, the shear wave velocity profile increases linearly from the surface to about 12 ft (3.7 m), remains relatively constant from about 12

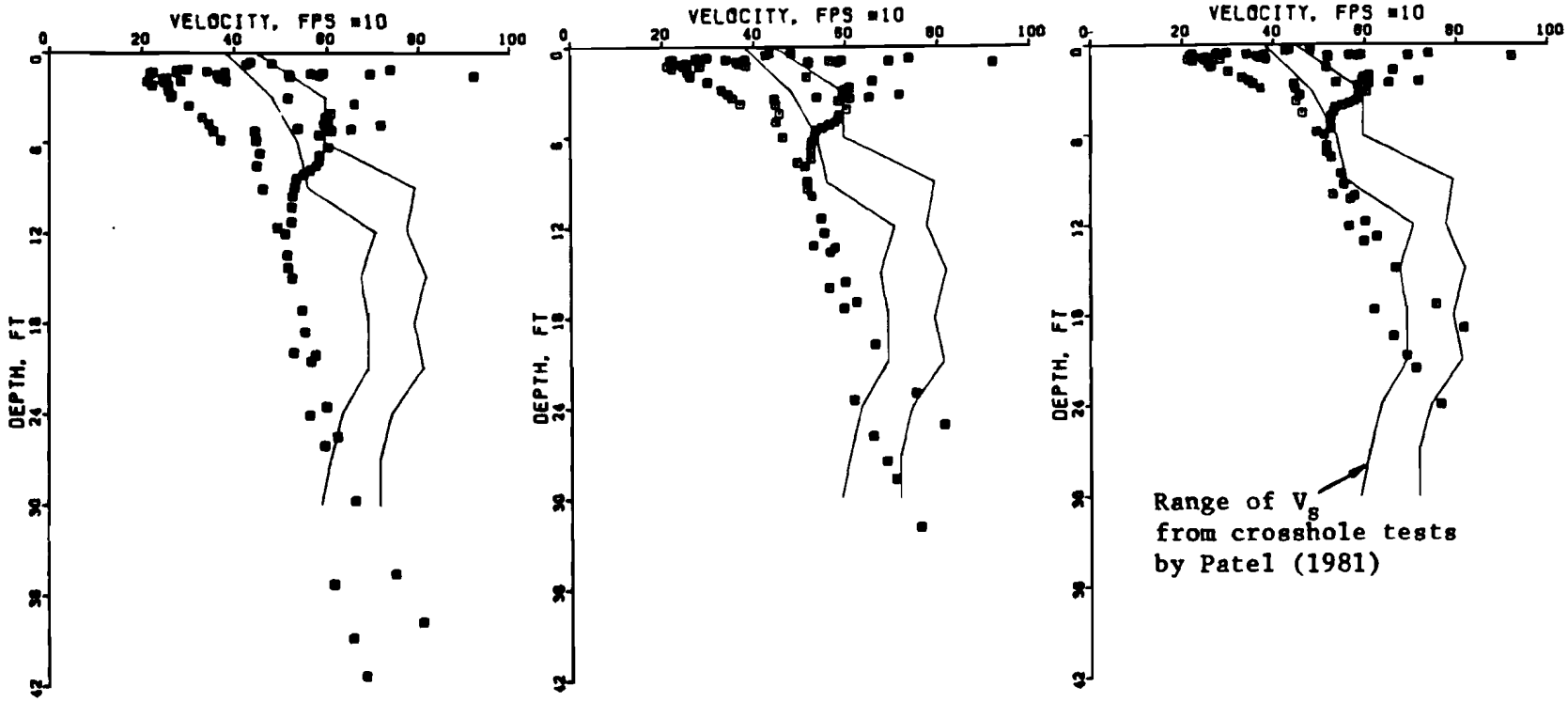

(a) Effective Depth = $L_R/2$ (b) Effective Depth = $L_R/3$ (c) Effective Depth = $L_R/4$

Fig 4.27. Comparison of various "Effective Sampling Depth" criteria with crosshole results.

to 21 ft (3.7 to 6.4 m), and then decreases slightly from about 21 to 30 ft (6.4 to 9.1 m).

If the near-surface and deepest cross spectrum measurements are ignored, the remaining cross spectrum measurements exhibit a similar trend to the crosshole results. The profile increases linearly with depth up to a certain point and then remains relatively constant. The exact depths where the profile changes depends, of course, on the fraction of wavelength equated to the effective sampling depth. It appears that most of the cross spectrum measurements are reflecting the shear wave velocity profile, although, in most cases, the velocities are lower than velocities obtained from crosshole tests. On the average, the velocities from cross spectrum measurements are 10 to 20 percent lower than velocities from crosshole tests.

Which wavelength fraction best fits or approaches the crosshole data is not evident in Fig 4.27. At depths from 0 to 10 ft (0 to 3 m), the $L_R/4$ criterion seems to provide the best agreement with the crosshole profile; at depths from 10 to 20 ft(3 to 6 m), the $L_R/3$ criterion seems to agree best; at depths from 20 to 30 ft (6 to 9 m), the $L_R/2$ criterion seems to agree best. However, there is no apparent theoretical basis for varying the depth of sampling with wavelength or frequency. Overall, the $L_R/3$ criterion seems to agree best from 0 to 30 ft (0 to 9 m).

Using the $L_R/3$ criterion, profiles from Test Series WC-1 and WC-2 are compared with crosshole results in Fig 4.28. The profiles are similar, although at depths below about 20 ft (0.6 m) the profile from Test Series WC-2 more nearly approaches the profile obtained from crosshole tests. This result again suggests that better data are obtained by spacing the near geophone at a significant distance from the source (as opposed to using the reference geophone for all measurements).

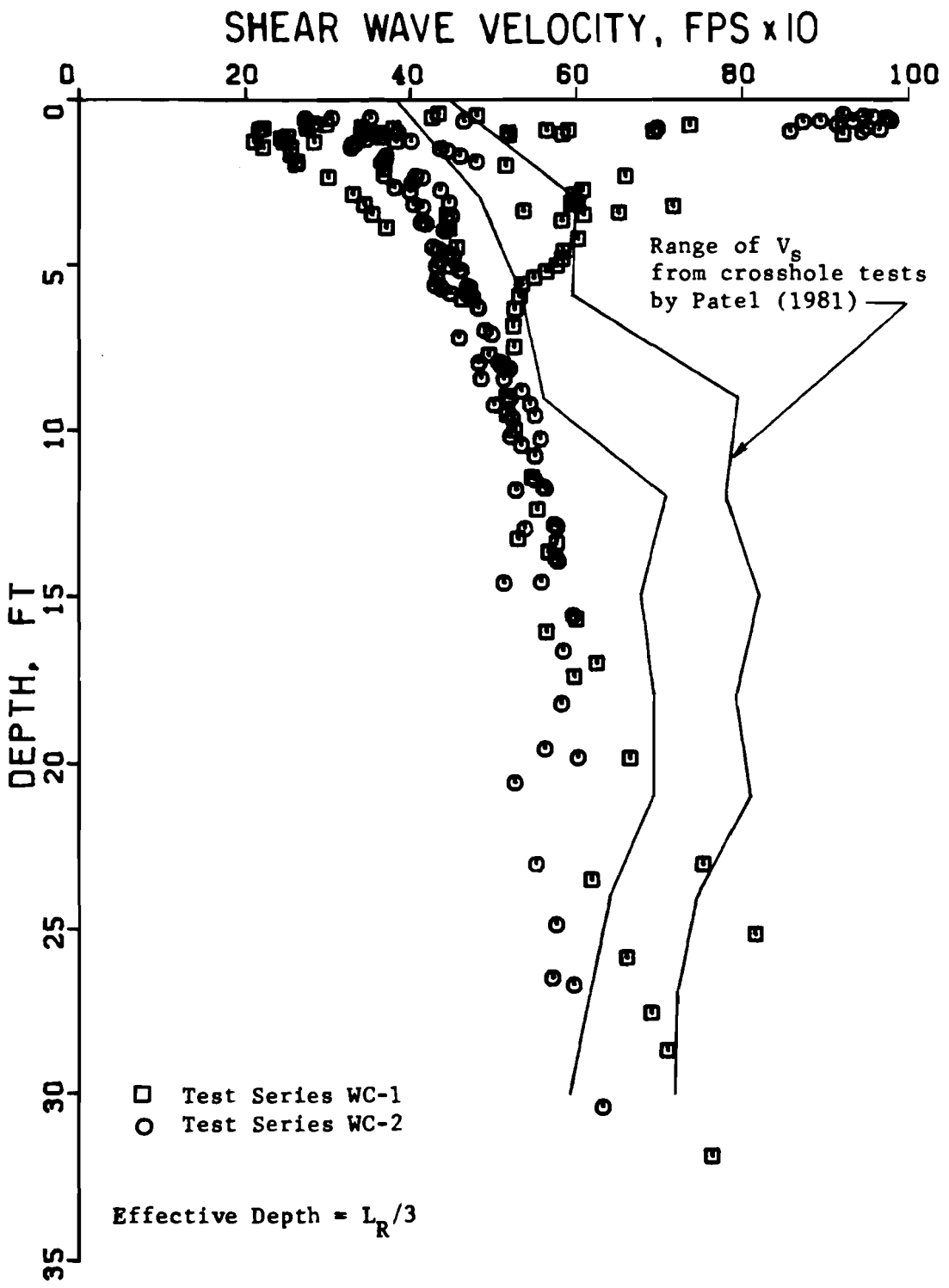

Fig 4.28. Comparison of crosshole results with shear wave velocity profiles obtained from measurements of test series WC-1 and test series WC-2.

In general, velocities from cross spectrum measurements were lower (by about 10 to 20 percent) than velocities obtained from crosshole tests. For engineering purposes, this difference is usually not significant. Some variation may have been due to different moisture conditions, since the two sets of measurements were performed at different times. Also, since the cross spectrum measurements use surface receivers, velocities determined at the greater depths will include an average of lower velocity material nearer the surface as well as deeper, higher velocity material. The overall effect of this averaging will probably yield a velocity which is somewhat lower than the velocity obtained at a specific depth using crosshole tests. The amount of variation caused by averaging will probably differ slightly from site to site, depending on the soil properties. Nevertheless, the surface (cross spectrum) measurements seem to provide a fairly accurate profile of the shear wave velocity.

ATTENUATION MEASUREMENTS

During both series of tests, transfer function measurements were recorded. The magnitude of the transfer function gives a ratio of output energy per given input energy at each frequency. The ratio provided a measure of the attenuation properties at the site as a function of frequency. Both geometric damping and material damping were included in the transfer function, thus supplying data to calculate a coefficient of attenuation, α.

Measurements made during Test Series WC-1 contained excessive scatter. Transfer functions for these measurements are shown in Fig 4.29a. In some instances, the spectrum from the farther geophone yielded amplitudes greater than those at the closer geophone (indicated by a transfer function magnitude

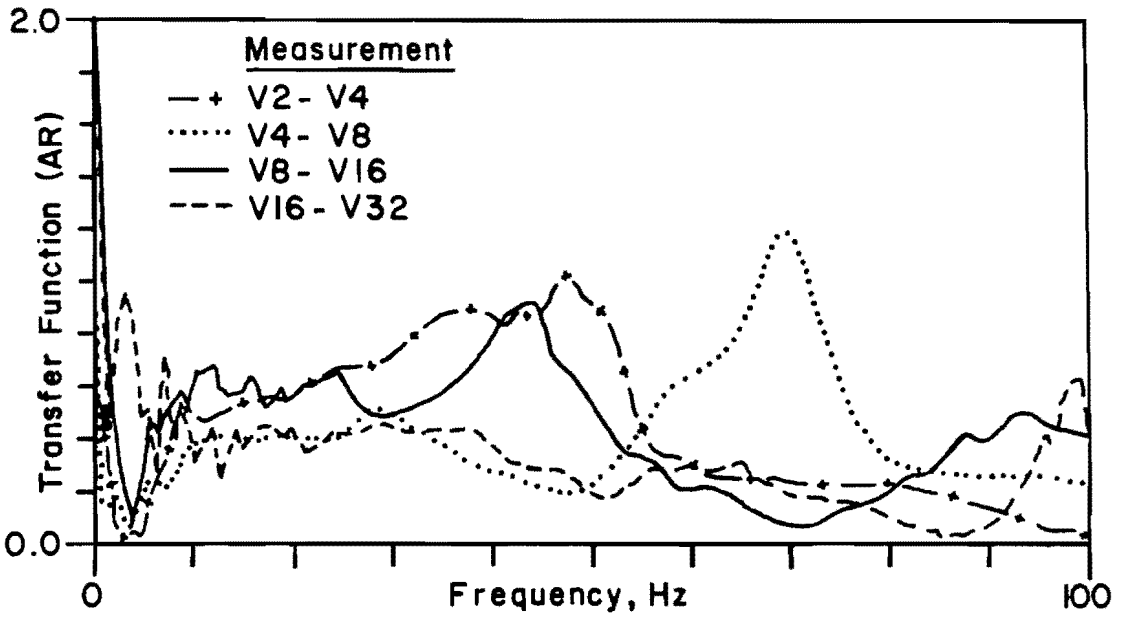

(a) Test Series WC-1

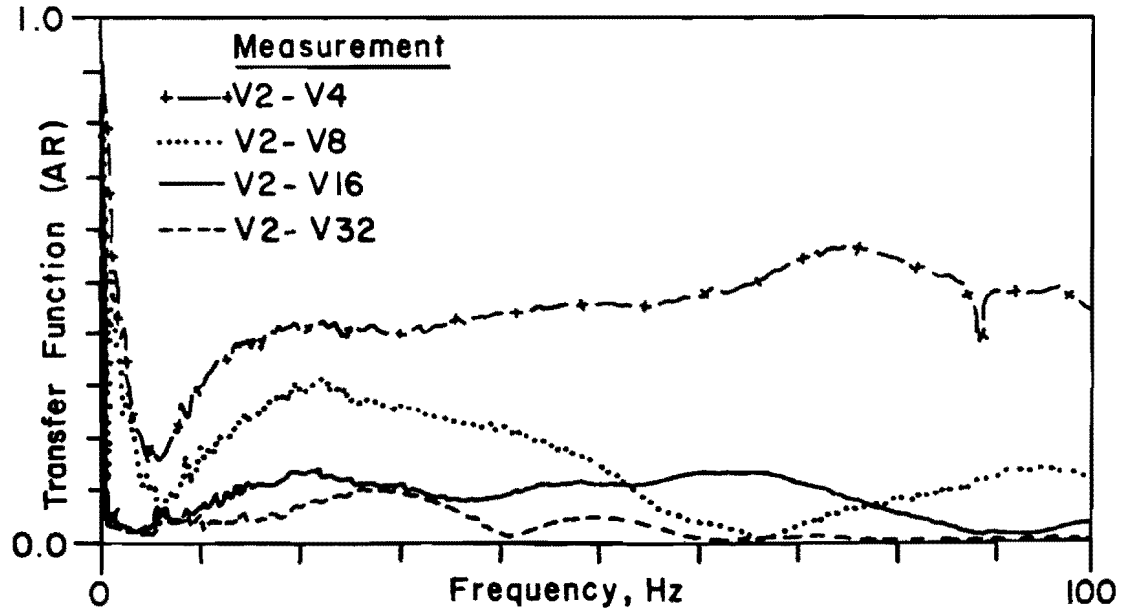

(b) Test Series WC-2

Fig. 4.29. Comparison of Transfer Function Magnitudes from Different Geophone Spacing Arrangements.

greater than unity). In various other cases, the amplitude decay was not sufficient to account for geometric damping, let alone material damping. Perhaps the cause of the extreme scatter was the variation of spacing between the source and the first geophone. As such, different amounts of attenuation occurred before the wave even reached the first geophone.

During Test Series WC-2, the first geophone was fixed at a location 2 ft (0.6 m) from the source and only the far geophone was moved to vary the spacing between geophones. Transfer functions for these measurements are shown in Fig 4.29b. As a result, there was considerably less scatter in the data. Meaningful attenuation calculations were possible, although some scatter did exist. It should be emphasized that the geophone arrangement for Test Series WC-2 (reference geophone) provided better data for calculation of attenuation than the geophone arrangement for Test Series WC-1 (equally spaced geophones), although the latter arrangement was better for determining the velocity profile.

The output/input ratios, hereafter referred to as amplitude ratios (AR), from various transfer functions are summarized in Table 4.6. The transfer functions represent measurements performed with the sledge-hammer-on-concrete source (to standardize the source) and over a measurement bandwidth of 100 Hz (to keep the resolution constant). Amplitude ratios are listed as a function of spacing (ranging from 2 to 30 ft) and as a function of frequency (6 to 100 Hz).

To compare graphically the attenuation as a function of frequency, it is necessary to establish some type of datum at which each frequency has the same initial magnitude. The reference geophone V2 is the most convenient initial point since it served as the input geophone for each measurement. However, the amount of input energy of the sledge-hammer-on-concrete source

TABLE 4.6. SUMMARY OF ATTENUATION FROM WALNUT CREEK AS A FUNCTION OF FREQUENCY AND GEOPHONE SPACING

f	L_R	L SPEC Ampl. at V2	V4, Δx = 2.08 ft			V8, Δx = 6.04 ft			V12, Δx = 9.94 ft			V16, Δx = 14.10 ft			V24, Δx = 21.92 ft			V32, Δx = 30.00 ft		
			AR*	NAR†	NoC‡	AR	NAR	NoC	AR	NAR	NoC	AR	NAR	NoC	AR	NAR	NoC	AR	NAR	NoC
10	62	0.325	.286	.880	0.034	.176	.542	0.097	.108	.332	0.160	.063	.194	0.227	.050	.154	0.354	.049	.151	0.484
12	48	0.399	.346	.867	0.043	.208	.521	0.126	.123	.308	0.207	.077	.193	0.294	.054	.135	0.457	.041	.103	0.625
15	34	0.539	.381	.707	0.061	.236	.438	0.178	.153	.284	0.292	.110	.204	0.415	.072	.134	0.645	.039	.072	0.882
20	24	0.707	.416	.588	0.087	.297	.420	0.252	.206	.291	0.414	.137	.194	0.588	.073	.103	0.913	.072	.102	1.250
25	18.4	0.952	.416	.437	0.113	.274	.288	0.328	.209	.220	0.540	.121	.127	0.767	.074	.078	1.191	.100	.105	1.630
30	14.9	1.191	.399	.335	0.140	.262	.220	0.406	.180	.151	0.667	.111	.093	0.947	.095	.080	1.471	.094	.079	2.013
40	10.9	1.838	.437	.238	0.191	.217	.118	0.554	.119	.065	0.912	.089	.048	1.294	.127	.069	2.011	.016	.009	2.752
50	8.6	2.384	.454	.190	0.242	.142	.060	0.703	.108	.045	1.156	.111	.047	1.640	.058	.024	2.548	.046	.019	3.488
60	6.6	2.873	.468	.163	0.316	.042	.015	0.915	.179	.062	1.506	.130	.045	2.137	.018	.006	3.321	.009	.003	4.545
70	5.7	3.012	.539	.179	0.365	.048	.016	1.060	.174	.058	1.744	.112	.037	2.474	.017	.006	3.845	.009	.003	5.263
80	5.1	3.310	.543	.164	0.408	.088	.027	1.185	.118	.036	1.949	.052	.016	2.765	.012	.004	4.297	.004	$.001^+$	5.882
100	4.5	3.684	.448	.122	0.463	.122	.033	1.343	.014	.004	2.208	.033	.009	3.134	.004	.001	4.870	$.002^-$	$.000^+$	6.667

* AR = Amplitude Ratio † NAR = Normalized Amplitude Ratio ‡ NoC = Number of Cycles

was not equal for each frequency (see Fig 4.16b). The amplitude of the wave energy as a function of frequency can be obtained from the spectrum of V2. The values of amplitude at V2 for selected frequencies are listed in Table 4.6. For the sake of comparison, all amplitudes are assumed to equal unity at V2. To "normalize" the amplitude ratios at other distances, each ratio must be divided by the spectrum amplitude at the particular frequency. These normalized ratios are listed in Table 4.6, and, in effect, represent the amplitudes at the output geophones (V4, V8, etc.) that would have been measured if all frequencies had been given the same input energy.

The assumption that all amplitudes equal 1.0 at V2 is arbitrary. The normalized amplitude ratio (NAR) is not an absolute amplitude but serves only as a relative value to compare attenuation of different frequencies from a common origin. Ideally, it is desirable to measure input amplitudes at exactly the source point. Practical experimental limitations preclude the gathering of attenuation data in this fashion.

Values of NAR are plotted as a function of distance from the source in Fig 4.30. Also included are several curves representing amplitude attenuation of Rayleigh waves for ranging from 0 to 0.25 ft^{-1}. Note that these curves originate from NAR = 1.0 at 2 ft. For clarity, only selected frequencies from Table 4.6 are shown. Sufficient scatter exists in the data to make it not possible to fit a specific attenuation curve to a given frequency. However, a general trend can be observed. As the frequency increases, the NAR shows more rapid decrease with distance. This trend is most clearly illustrated at a distance of 24 ft (measurement V2-V24). This behavior is not unexpected, since higher frequencies will have undergone more wavelengths (cycles) to reach a given distance.

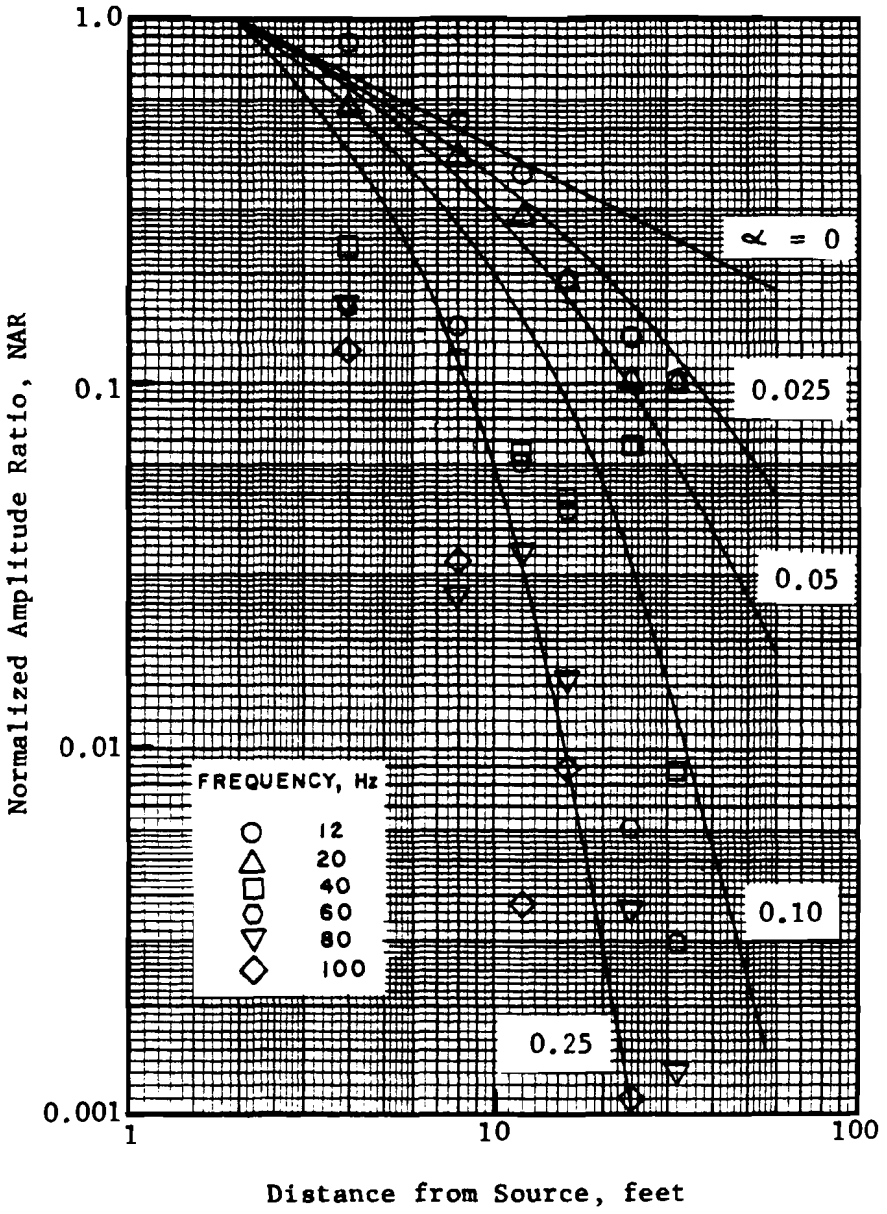

Fig 4.30. Relationship between normalized amplitude ratio (NAR) and distance from the source as a function of frequency.

The number of cycles or fractions thereof that a given frequency has undergone in a given distance can be calculated by

$$\text{Number of Cycles} = \Delta x / L_R \tag{4.7}$$

Calculations using Eq 4.7 are summarized in Table 4.6. Values of NAR are plotted as a function of number of cycles in Fig 4.31. Although some scatter still exists, it appears that all frequencies exhibit similar damping of wave energy when plotted as a function of number of cycles. This suggests that the material damping is independent of frequency (at least over the range of frequencies observed in these measurements).

The expression for R-wave attenuation (in a homogeneous, isotopic half-space) which includes both geometric and material damping was given in Chapter 2 as follows:

$$AR = \frac{A_2}{A_1} = \sqrt{\frac{r_1}{r_2}} \exp\left[-\alpha(r_2 - r_1)\right] \tag{4.8}$$

Rearranging terms to evaluate α , when all other variables are known, yields

$$\alpha = \frac{-\ln\left[AR\sqrt{\frac{r_2}{r_1}}\right]}{r_2 - r_1} \tag{4.9}$$

where α has dimensions of 1/distance and the same units as r_1 and r_2. Equation 4.9 was used to calculate values of α as a function of frequency. Values of ranged from 0.031 ft^{-1} to 0.435 ft^{-1}, with the larger values

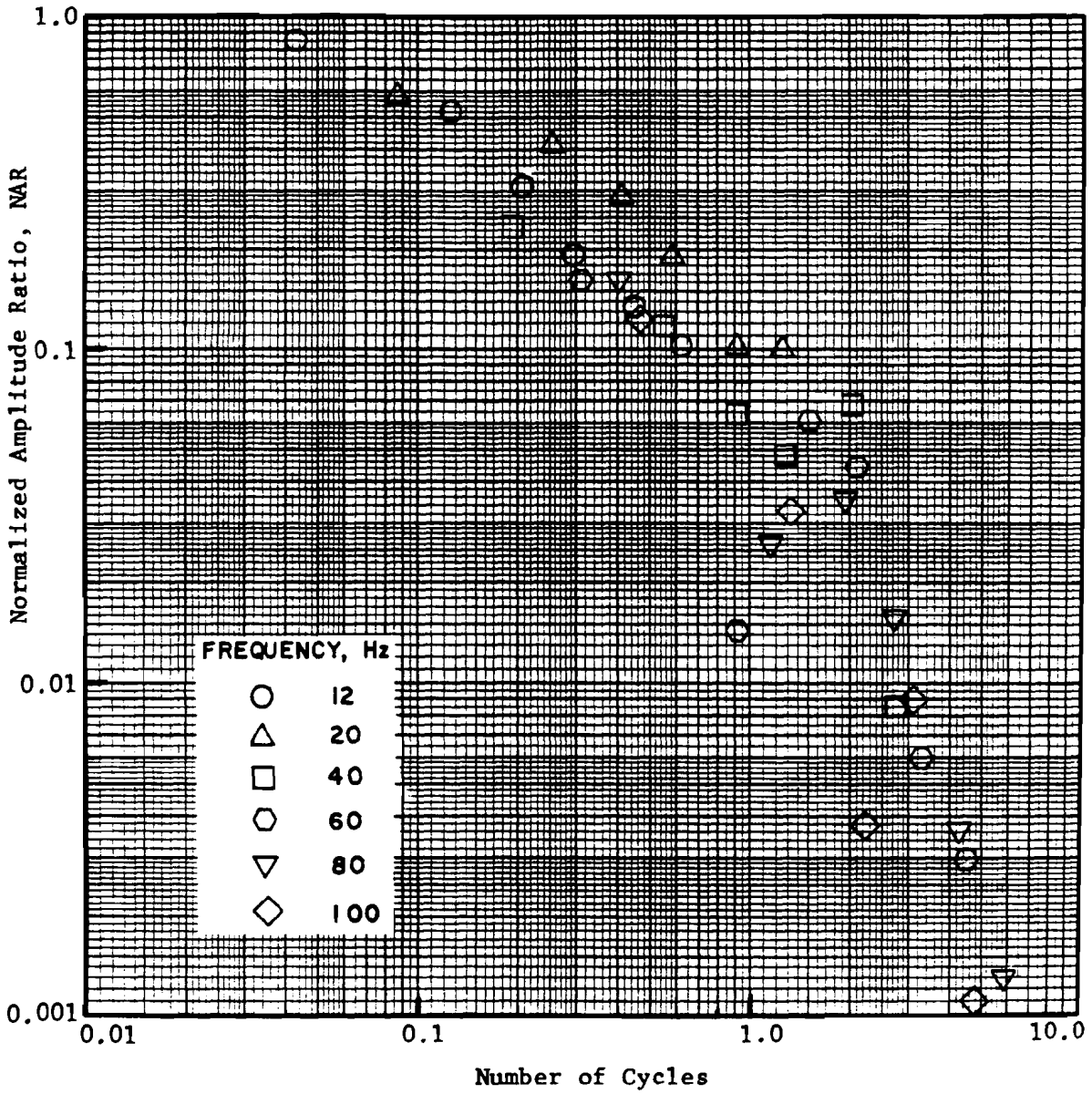

Fig 4.31. Relationship between normalized amplitude ratio (NAR) and number of cycles as a function of frequency.

resulting from measurements V2-V4 and V2-V8 where the waves had undergone only a small fraction of a cycle. Much of the scatter is reduced if values of are calculated only for waves that have travelled at least one-third of their wavelength at a given geophone location.

Using this criterion, the range in as a function of frequency is shown in Fig 4.32. Average values are indicated by the solid circles. Figure 4.32 shows that increases with frequency. This graph more clearly illustrates the trend observed in Fig 4.29. A linear regression analysis performed with the average values plotted in Fig 4.31 indicates the α is very nearly a linear function of frequency. A correlation coefficient of 0.97 was obtained for a line with a slope of 0.00173. Due to slight scatter in the data, a small intercept value was also obtained, although, theoretically, as f approaches zero (L_R approaches infinity), no attenuation should occur and α should equal zero.

The relationship $\alpha = 0.00173$ f was used to calculate values for α that did not exhibit the general scatter in the measured values of α. In addition, values of the logarithmic decrement δ and damping ratio D were calculated using the equations presented in Chapter 2. Each of these quantities is listed in Table 4.7.

The values of damping ratio (expressed as a percentage) do not vary significantly with frequency. This confirms the conclusion that was drawn from Fig 4.30, namely, that material damping is independent of frequency over the range from 0 to 100 Hz. Damping values ranging from about 11 to 17 percent are somewhat higher than those typically measured in the laboratory. There are at least two possible explanations for this discrepancy. First, it is possible that significant body wave energy was still present in the wave pulse at the reference geophone (V2). This energy would have dissipated due

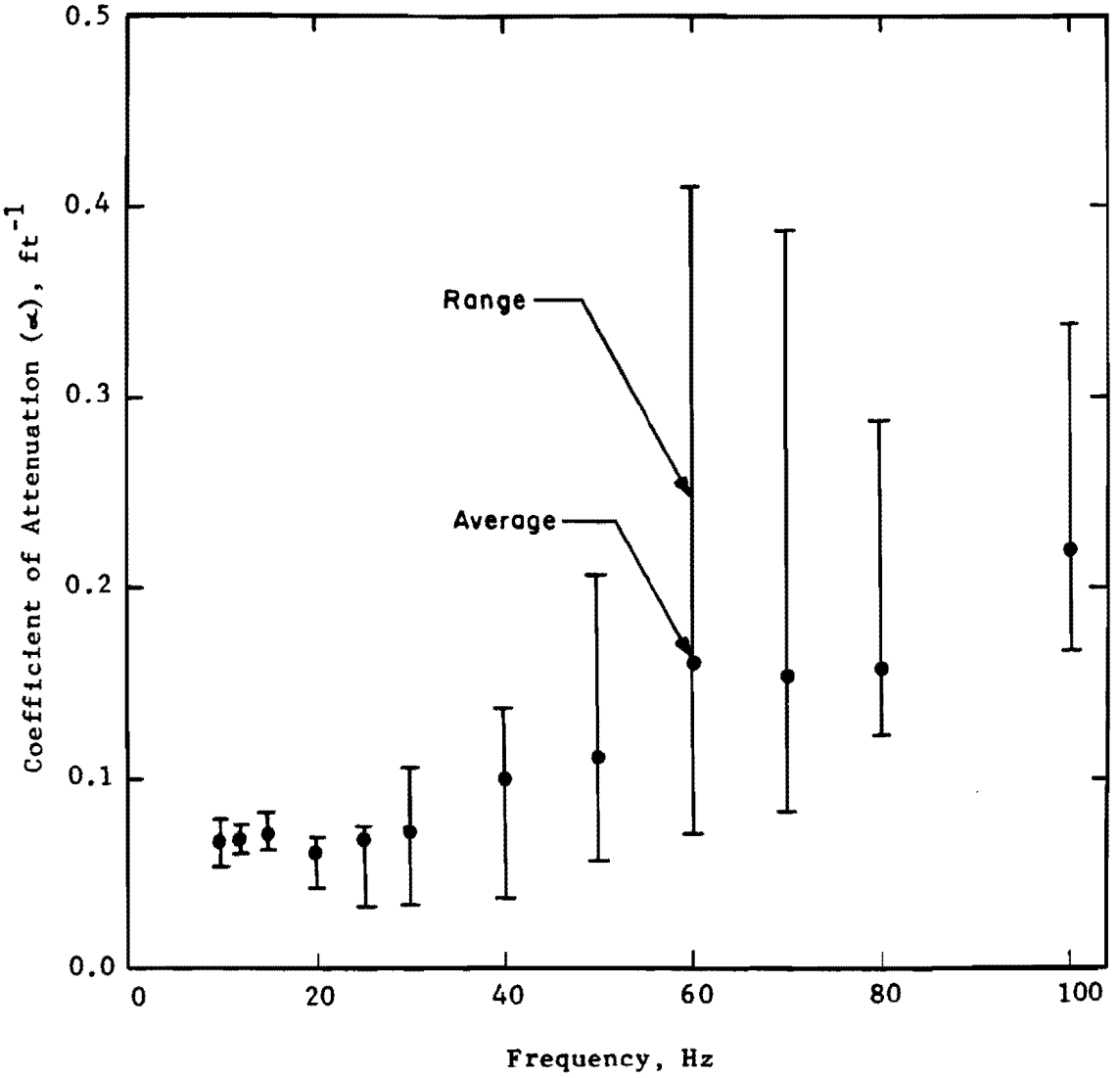

Fig 4.32. Variation of coefficient of attenuation with frequency at Walnut Creek site.

TABLE 4.7. RELATIONSHIP BETWEEN FREQUENCY AND DAMPING AT WALNUT CREEK SITE.

Frequency f(Hz)	Wavelength L_R(ft)	Coefficient of Attenuation $\alpha(ft^{-1})$	Logarithmic Decrement δ	Damping Ratio D(%)
10	62	0.017	1.07	16.8
12	48	0.021	1.00	15.7
15	34	0.026	0.88	13.9
20	24	0.035	0.83	13.1
25	18.4	0.043	0.80	12.6
30	14.9	0.052	0.77	12.2
40	10.9	0.069	0.75	11.9
50	8.6	0.087	0.74	11.7
60	6.6	0.104	0.69	10.9
70	5.7	0.121	0.69	10.9
80	5.1	0.138	0.71	11.2
100	4.5	0.173	0.78	12.3

to geometric damping at a greater rate than the surface wave energy by the time the wave pulse reached the far geophone. As a result, the far geophone would have interpreted some of the geometric damping of the body wave as material damping of the Rayleigh wave, thus yielding an erroneously high value for α . The other possible explanation is that the higher damping values are true properties of the in situ material. Factors such as non-homogeneities or reflection and refraction of wave energy due to layering may cause "backscattering" which yields a field damping that is somewhat higher than that measured in the laboratory sample.

It appears that attenuation, or damping, can be measured in the field with the use of the transfer function. Based on results at the Walnut Creek site, better attenuation data can be obtained by using a fixed reference geophone than by using an equally spaced arrangement of geophones. However, before such data can be used with confidence, the problems cited above should be resolved.

SUMMARY

Results and conclusions based on tests performed at Walnut Creek can be categorized in terms of measurement set-up, type of source, interpretation of velocity profile, and determination of damping.

In general, measurements made with five averages (transient events) will provide reliable data. Additional averages in the measurement are not warranted because they do not significantly improve the data. Frequency resolution is not a problem if the frequency bandwidth is commensurate with the geophone spacing. Close spacings near the source may use a higher frequency range (100 Hz to perhaps 800 Hz) while wide spacings farther from

the source should use a lower frequency range (25 to 100 Hz). Selection of a lower (narrower) frequency bandwidth will provide better resolution of long wavelengths needed to sample greater depths.

A source should be used which generates predominantly Rayleigh wave energy and minimizes body wave energy in the wave pulse. A vertical blow from a hammer which is in direct contact with the soil a good source. The magnitude of the input energy does not seem to be a critical factor as long as adequate energy is provided to excite low frequencies. The coupling of the source with the soil, which influences the transfer of energy, is an important factor. In this regard, the use of a plate between the hammer and soil should be avoided.

The velocity profile obtained from surface measurements will probably have some scatter. Better measurements can be obtained when the geophones are appropriately located from the source. Based on results at Walnut Creek, a spacing arrangement in which the first geophone is located at increasing distance from the source is more favorable than an arrangement in which the first geophone is fixed at a reference location close to the source. In addition, much of the scatter in the velocity profile can be reduced by filtering out data for wavelengths which are inappropriate for the spacing of the geophones. Wavelengths which are too short for a given spacing may attenuate excessively, whereas wavelengths which are too long for a given spacing may not have travelled a sufficient distance to sample adequately the depth proportional to the wavelength. Using the criteria discussed in this chapter, an appropriate range of L_R for a given spacing Δx was found to be

$$\frac{1}{2}\,\Delta x \leq L_R \leq 3 \cdot \Delta x \qquad (4.10)$$

Equation 4.10 was used to filter inappropriate wavelengths which resulted in a refined velocity profile.

The velocity profile obtained from cross spectrum measurements was compared with velocities from crosshole tests by applying depth criteria of $L_R/4$, $L_R/3$, and $L_R/2$. The comparison of profiles did not clearly indicate which depth criterion is most appropriate for surface measurements. Overall, the velocities plotted at a depth of $L_R/3$ appeared to correlate well with the crosshole velocities. On the average, the cross spectrum velocities were 10 to 20 percent lower than the crosshole velocities. However, this difference is considered tolerable for practical engineering applications.

Attenuation properties at the site were evaluated by means of transfer functions. The coefficient of attenuation α was found to be approximately a linear function of frequency and was estimated by $\alpha = 0.00173$ f. Values of logarithmic decrement and damping ratio were also calculated. Damping ranged from about 11 to 17 percent. These values are somewhat higher than those typically measured in the lab, possibly due to backscattering of wave energy caused by reflection from layer boundaries or anamolies at the site, or because there is excessive body energy at the near geophone which is located relatively close to the source.

CHAPTER 5. SOIL TESTING AT THE CROSSING SITE

SITE DESCRIPTION

The second soil site at which R-wave dispersion testing was performed was the Crossing site. The Crossing site is located about 4 miles (6.4 km) southeast of the campus of The University of Texas at Austin, as shown in Fig 5.1. The site is part of an open tract of land currently undergoing development. The actual test area is located about 1000 ft (300 m) from the city street (East Riverside Drive). Because the site is open and away from traffic, ambient noise at the site is minimal.

The site lies in the flood plain of the Colorado River, and, as a result, the topography of the site is relatively flat. The soil profile consists of a medium dark clay deposit underlain by sand. The clay extends to a depth of approximately 30 ft (9 m). During dry periods, the soil within a few feet of the surface becomes highly desiccated and undergoes extensive shrinkage cracking.

Because the site is not located near any structures, power to operate electrical equipment had to be supplied by a portable power generator.

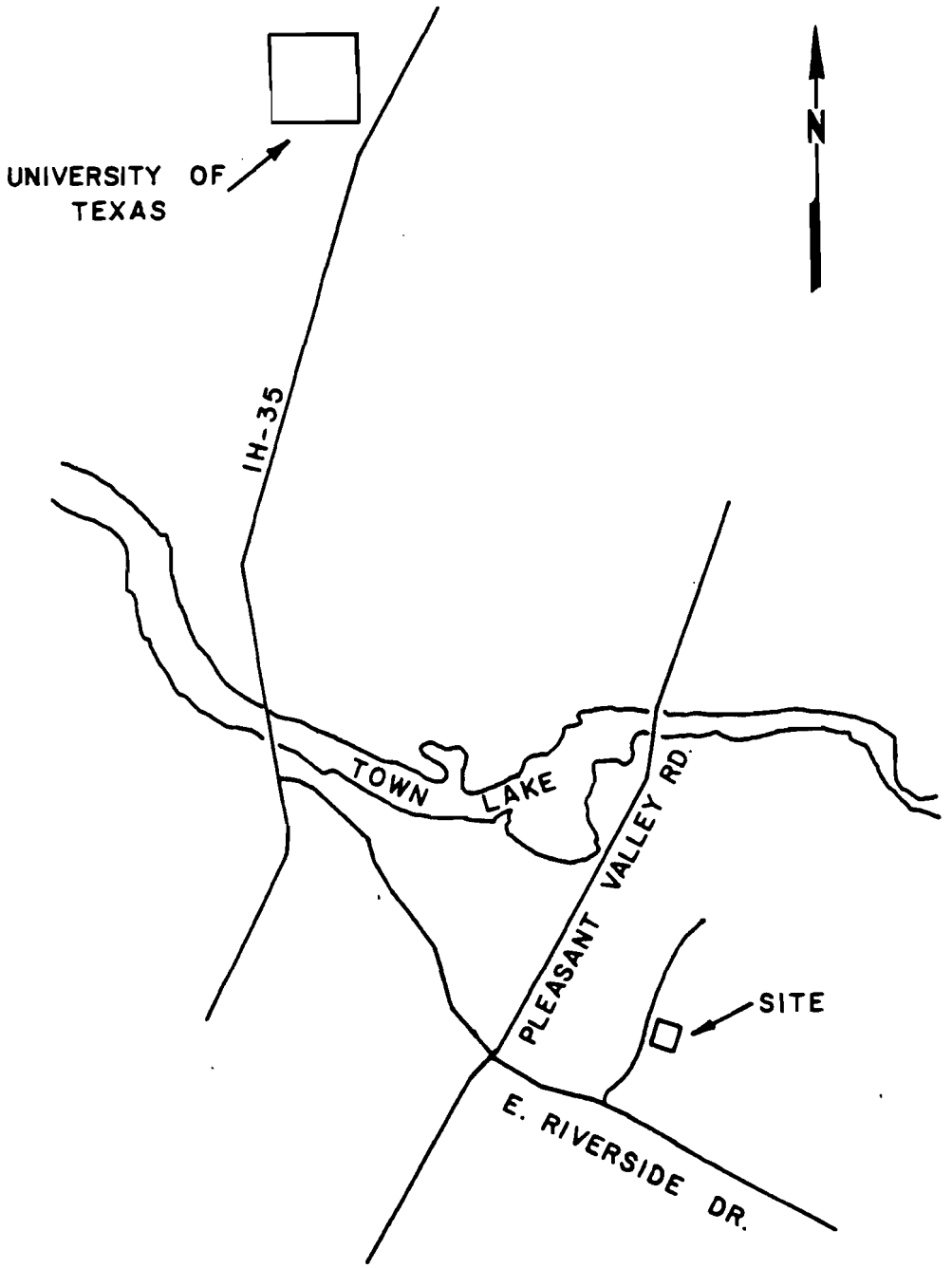

Fig 5.1. Location of the Crossing Site.

EXPERIMENTAL PROCEDURE

Testing at the Crossing site was conducted on May 28, 1981. The soil at the surface was soft (but not muddy) from heavy rainfall that had occurred during the previous week. The source used to generate wave energy was the drop hammer previously described in Section 4.3.1 and illustrated in Fig 4.7a. The drop hammer was used in direct contact with the soil surface.

Two vertical geophones were used to capture the time domain signal of the propagated wave. The geophones used at the Crossing were the same as those used at Walnut Creek for Test Series WC-1. Each geophone had an undamped natural frequency of about 8 Hz and had a shunt resistance which provided a damping of approximately 50 percent of critical damping. The transduction constant was in the range of 1 volt per in./sec (0.4 volt per cm/sec). The frequency response curves for the two geophones are shown in Fig 4.3.

The geophones were placed in augured holes to minimize background noise generated by the wind striking the geophones and to improve the geophone-soil contact. The holes were augured to a depth of 4 to 6 in. (10.2 to 15.2 cm). Each geophone was then embedded at the bottom of the hole by means of a steel spike on the end of the geophone and the remainder of the hole was backfilled with augured soil.

The locations of the geophones for the various measurements are shown in Fig 5.2. One set of measurements was performed with the near geophone located at increasing distance from the source and then spacing the far geophone at that same distance (source to near geophone) from the near geophone. In other words, the first geophone was located exactly midway between the source and the far geophone. (This arrangement is similar to

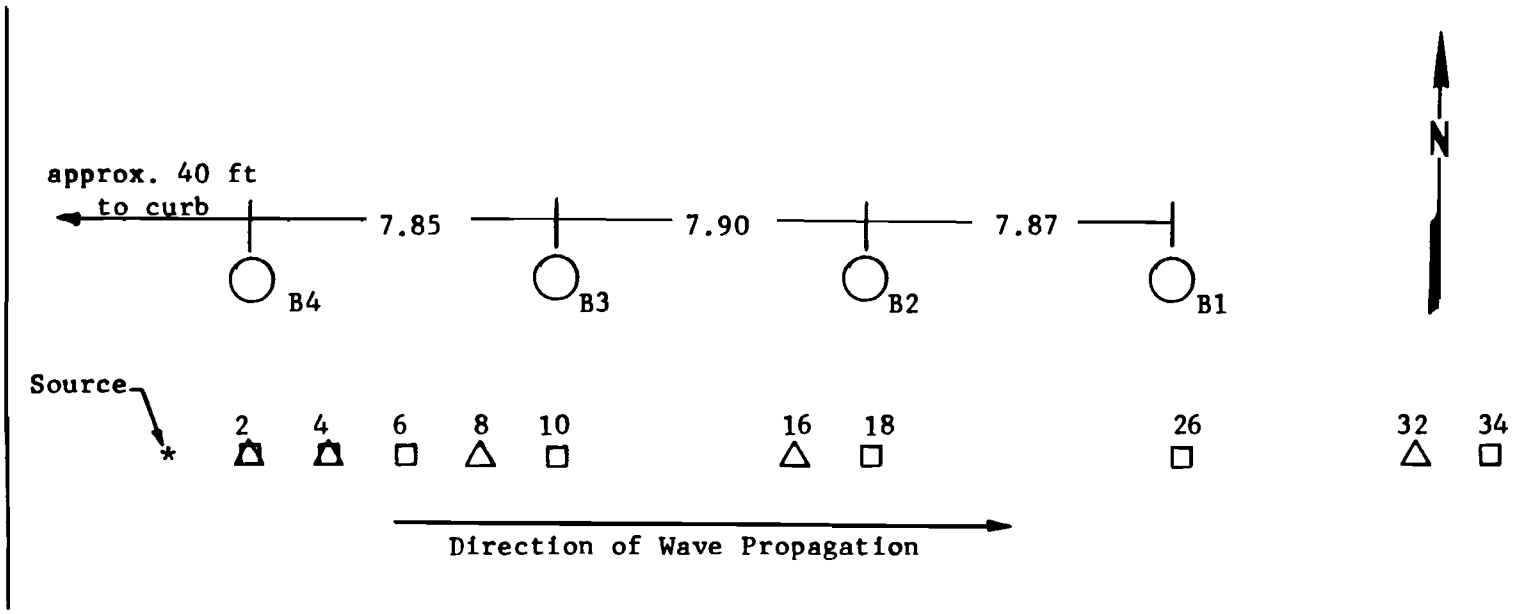

Legend

○ Existing boreholes used in work performed by Hoar (1981).

□ Location of geophones (with distance from source in feet) for measurements with a "reference" geophone at 2 ft.

△ Location of geophones (with distance from source in feet) for measurements with the near geophone located midway between the source and the far geophone.

Fig 5.2. Locations of source and geophones for testing at the Crossing Site.

that for test series WC-1.) Another set of measurements was performed with a reference geophone at 2 ft (0.6 m) from the source and with only the far geophone increasing in distance from the source. (This arrangement is similar to that for Test Series WC-2.) The location of the far geophone was selected so that the spacing between geophones was the same as that for measurements having the equally spaced arrangement.

A summary of the measurements performed at the Crossing is presented in Table 5.1. Hereafter, these measurements will be identified by the location of the pair of geophones. For example, measurement V16-V32 identifies the measurement recorded with the near vertical geophone (V) located at 16 ft (4.9 m) from the source and the far vertical geophone located at 32 ft (9.8 m) from the source.

SHEAR WAVE VELOCITY PROFILE

The shear wave velocity profile can be obtained from Rayleigh wave velocities if Poisson's ratio is known or assumed. If available, data from crosshole tests (both P- and S-wave velocities) can be used to calculate an estimate of Poisson's ratio. One of the reasons for selecting this site is that crosshole tests had been previously performed there by Hoar (Ref 11). The shear wave velocities at the site increase from about 500 fps (150 mps) at the surface to nearly 1000 fps (300 mps) at a depth of 30 ft (9 m). Values of S-wave and P-wave velocities (obtained by Hoar) at 3-ft (0.9-m) intervals are listed in Table 5.2.

The ratio of V_S/V_P was calculated at each depth, and by using Table 2.1, the corresponding value of Poisson's ratio was determined. Then ratios of V_R/V_S were determined using Poisson's ratios. Table 5.2 contains each of

TABLE 5.1. SUMMARY OF MEASUREMENTS AT THE CROSSING SITE

Record No. (Track No.)	Distance from Source to Geophones (ft)		Distance between Geophones (ft)	Source	Number of Averages	Bandwidth of Spectrum (Hz)	Computer Data File Identification
	Near	Far					
9(1)	2.0	4.0	2.0	Drop Hammer on Soil	5	1600	SHCR01
14(1)	2.0	4.0	2.0	" " " "	5	200	SHCR02
19(1)	2.0	6.0	4.0	" " " "	5	200	SHCR03
24(1)	2.0	10.0	8.0	" " " "	5	200	SHCR04
29(1)	2.0	18.0	16.0	" " " "	5	100	SHCR05
36(1)	2.0	26.0	24.0	" " " "	5	100	SHCR06
41(1)	2.0	34.0	32.0	" " " "	5	100	SHCR07
42(1)	2.0	34.0	32.0	" " " "	5	25	-
48(1)	4.0	8.0	4.0	" " " "	5	200	SHCR08
53(1)	8.0	16.0	8.0	" " " "	5	100	SHCR09
58(1)	16.0	32.0	16.0	" " " "	5	100	SHCR10
59(1)	16.0	32.0	16.0	" " " "	5	25	SHCR11

TABLE 5.2. SUMMARY OF CROSSHOLE TEST RESULTS AT THE CROSSING SITE (FROM HOAR, 1981)

Depth (ft)	S-Wave Velocity V_S(fps)*	P-Wave Velocity V_P(fps)*	V_S/V_P	Poisson's Ratio**	V_R/V_S**
3	509	1568	0.325	0.44	0.95
6	577	1611	0.358	0.43	0.95
9	636	1985	0.320	0.44	0.95
12	650	2008	0.324	0.44	0.95
15	689	2064	0.334	0.44	0.95
18	699	2146	0.326	0.44	0.95
21	666	2218	0.300	0.45	0.95
25	738	2149	0.343	0.43	0.95
30	978	5000	(Water Table)	-	-

* S-wave velocities and P-wave velocities from Hoar (1981).

** Poisson's ratios and V_R/V_S based on V_S/V_P using Table 2.1.

these ratios for each depth. At the Crossing site, Poisson's ratios range from 0.43 to 0.45. Over this range, the value of V_R/V_S is approximately 0.95. Hence, a value of 0.95 was assumed for the entire profile to convert Rayleigh wave velocities to shear wave velocities.

Velocity Profiles From Cross Spectrum Measurements

As a first approximation, a depth criterion of $L_R/3$ was used to represent the effective depth at which the R-wave sampled and, hence, the depth at which the R-wave velocity should be plotted. The relationship $V_S = V_R/0.95$ was then used to obtain shear wave velocities. Two profiles were developed using this approach: one using measurements made with the reference geophone arrangement and one using measurements made with the equally spaced geophone arrangement.

The S-wave velocity profile obtained using measurements made with the reference geophone is shown in Fig 5.3. A large amount of scatter exists over the entire profile, with values of velocity at a given depth varying by as much as three-fold, depending on which measurement is examined. Figure 5.4 shows the same profile after the data has been filtered using the criterion given by Eq 4.5 ($\frac{1}{2}\Delta x \leq L_R \leq 3\Delta x$). For the longest spacing (measurement V2-V34), Eq 4.5 excludes wavelengths above 96 ft (29 m) and depths below 32 ft (9.8 m). Comparison of Figs 5.3 and 5.4 indicates that filtering the data eliminates much of the scatter in the profile. However, significant scatter still exists from about 6 to 9 ft (1.8 to 2.7 m) and below about 22 ft (6.7 m).

The S-wave velocity profile obtained using measurements with equally spaced geophones is shown in Fig 5.5. Significant scatter in velocity exists

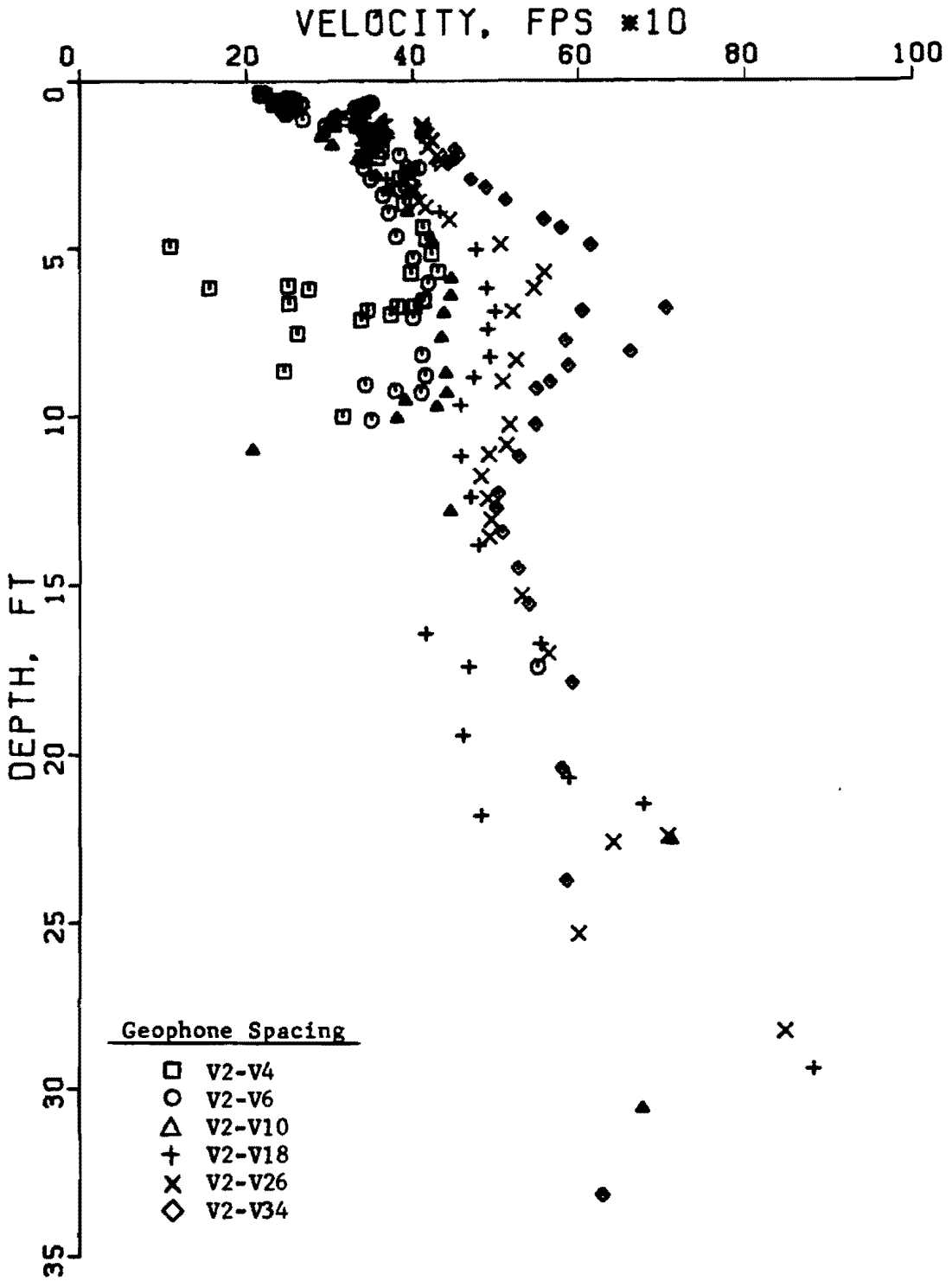

Fig 5.3. Unfiltered shear wave velocity profile for measurements using a reference geophone located 2 ft from the source.

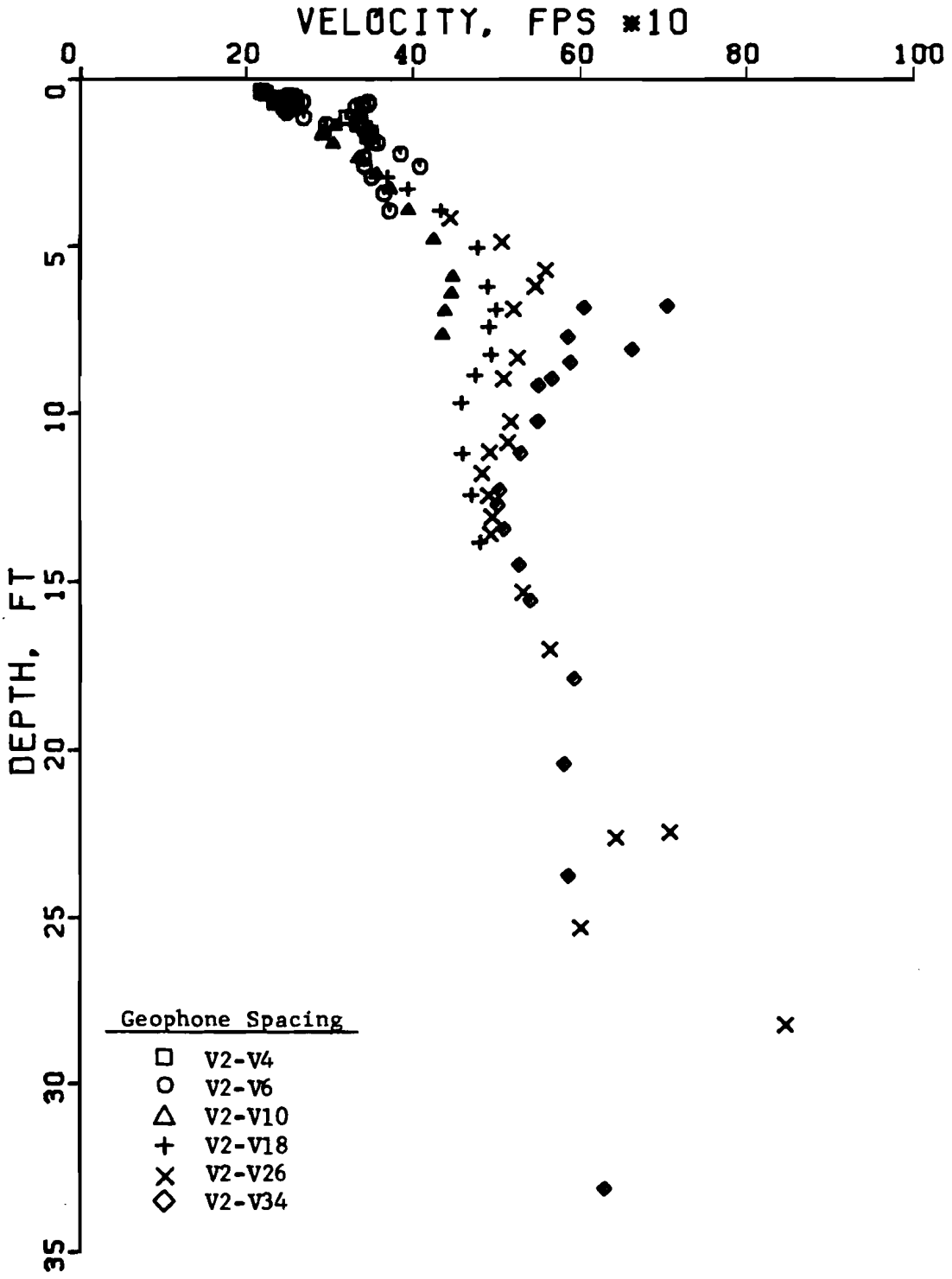

Fig 5.4. Filtered shear wave velocity profile for measurements using a reference geophone located 2 ft from the source.

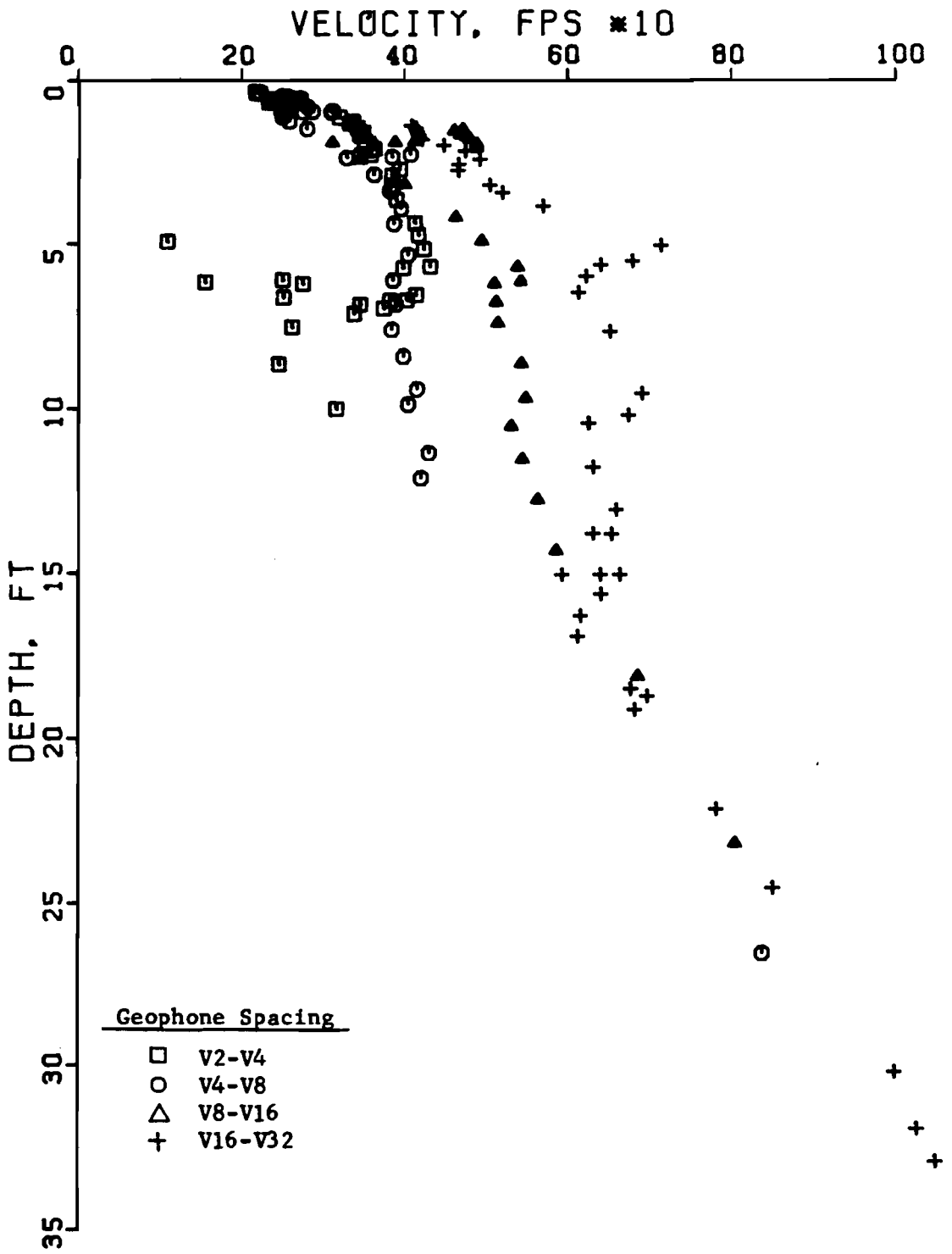

Fig 5.5. Unfiltered shear wave velocity profile for measurements using an arrangement of equally spaced geophones.

to a depth of about 15 ft (4.6 m). Figure 5.6 shows the same profile after the data has been filtered using the criterion given by Eq 4.5. For the longest spacing (measurement V16-V32), Eq 4.5 excludes wavelengths above 48 ft (14.6 m) and depths below 16 ft (4.9 m). For purposes of comparison with the reference geophone arrangement (Fig 4.5), wavelengths up to 96 ft (29 m) have been included in Fig 5.6.

Figures 5.4 and 5.6 can be used to compare the S-wave velocity profile obtained from a reference geophone arrangement and the velocity profile obtained from an equally spaced geophone arrangement. In general, velocities obtained using a reference geophone are lower than those obtained using equally spaced geophones. The difference in velocities becomes greater with increasing depth. A comparison of the two profiles with crosshole test results is presented in Section 5.3.2.

Further conclusions can be drawn regarding the location of the pair of geophones (and the spacing between the geophones). First, consider measurements with equal spacing Δx between geophones but with different locations of the near and far geophones relative to the source. Figure 5.7 shows measurement V2-V18 compared with measurement V16-V32, both having the same spacing, $\Delta x = 16$ ft. Data are plotted using a depth criterion of $L_R/3$ for $\frac{1}{2}\Delta x \leq L_R \leq 3\Delta x$. The measurement made with the reference geophone (V2-V18) yielded significantly lower velocities than the measurement with equally spaced geophones (V16-V32). Similar results were obtained for spacings of $\Delta x = 8$ ft (V2-V6 vs V4-V8). The differences in velocities decreased as the spacing decreased since the two geophone arrangements approached approximately the same measurement.

Second, consider measurements with different spacings but with the locations of the far geophones approximately the same. Figure 5.8 shows

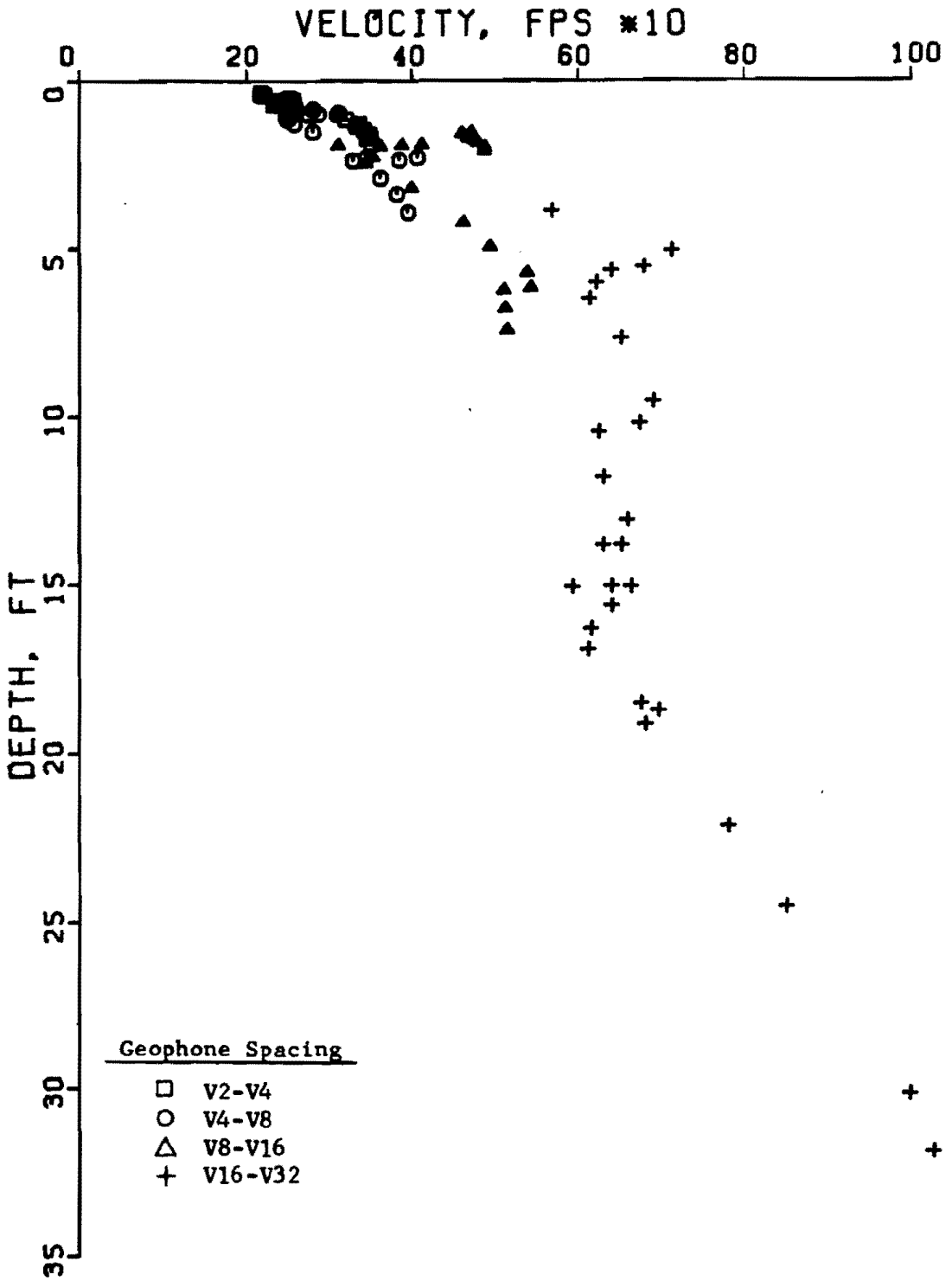

Fig 5.6. Filtered shear wave velocity profile for measurements using an arrangement of equally spaced geophones.

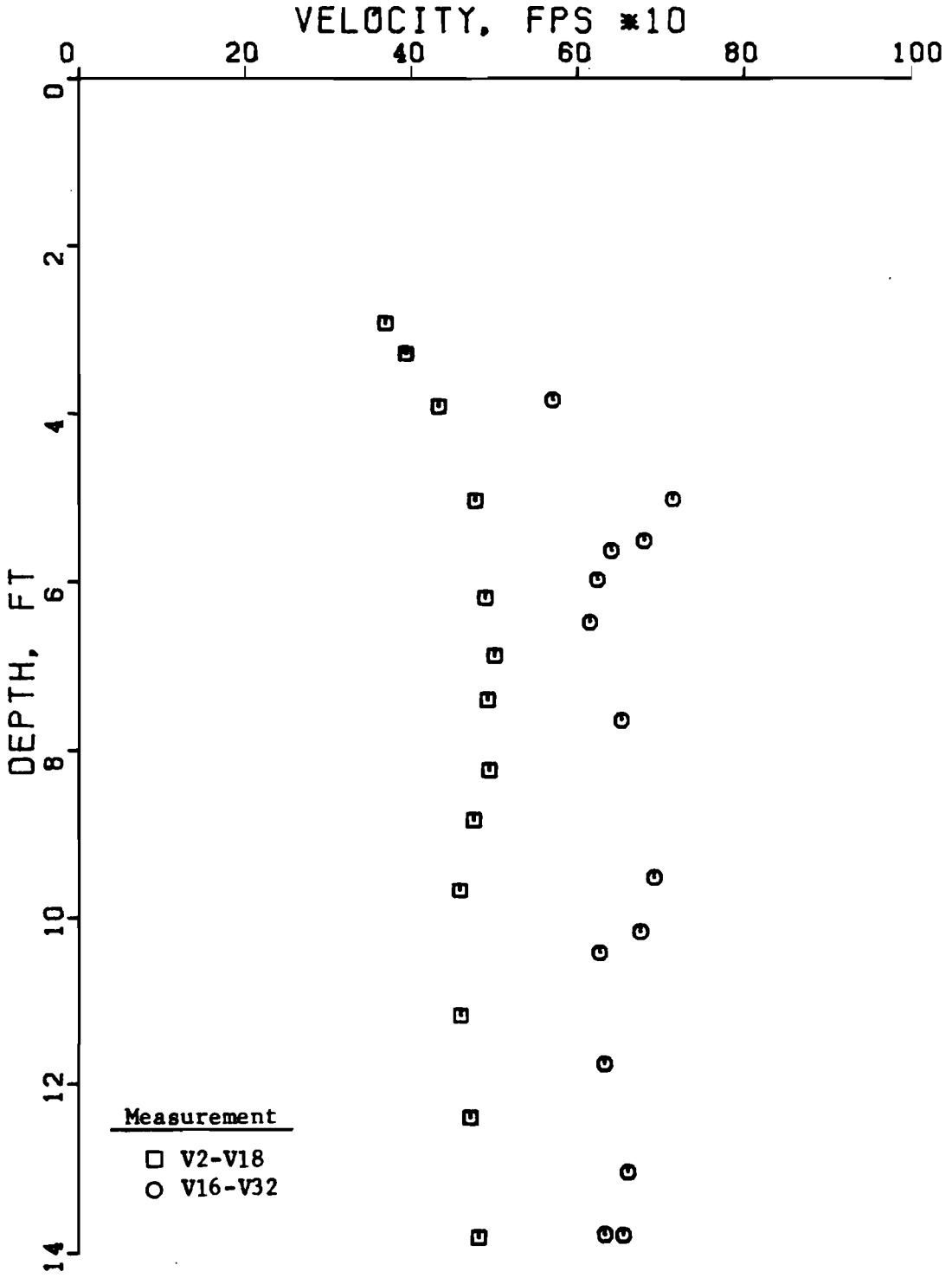

Fig 5.7. Comparison of reference geophone arrangement with equally spaced geophone arrangement for measurements with similar spacing between geophones.

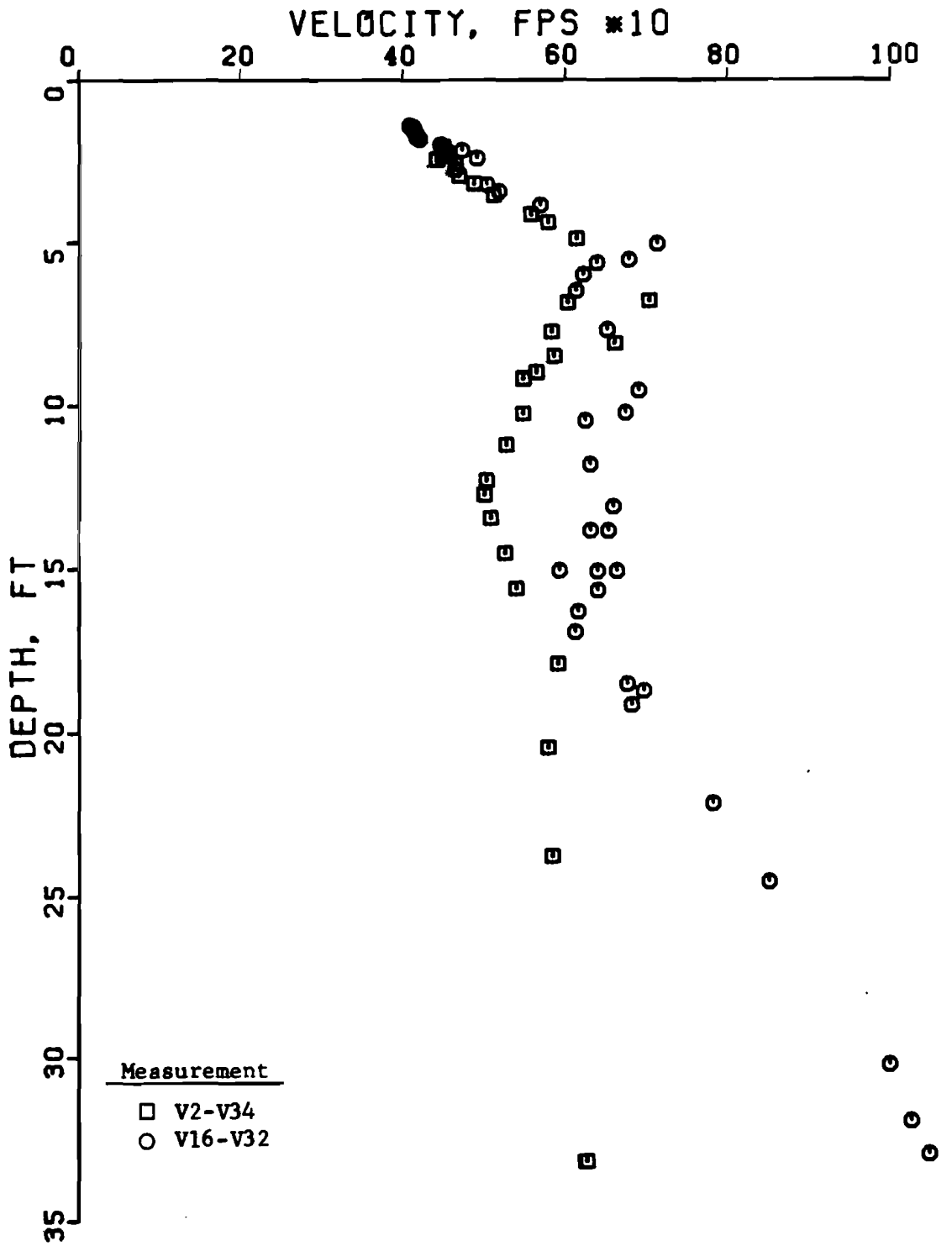

Fig 5.8. Comparison of reference geophone arrangement with equally spaced geophone arrangement for measurements with similar location of the far geophone.

measurement V2-V34 compared with measurement V16-V32. For each measurement the distance from the source to the far geophone is nearly equal. Again, the measurement with the reference geophone (V2-V34) yielded lower velocities than the measurement with equally spaced geophones (V16-V32).

Since different velocity profiles can be obtained from different geophone arrangements despite identical spacing Δ x between geophones and despite a similar location of the far geophone, it can be concluded that the location of the geophone nearer the source is a significant parameter. One approach to determine which geophone arrangement provides the better velocity profile is to compare velocities from cross spectrum measurements with velocities from crosshole tests. Also, a rational approach incorporating fundamentals of wave propagation can be considered. Both of these approaches are presented in the next section.

Comparison Between Cross Spectrum Measurements and Crosshole Results

The velocity profiles shown in Figs 5.4 and 5.6 are replotted in Fig 5.9 along with the velocity profile from crosshole test results obtained by Hoar (Ref 11). The velocities from the cross spectrum measurements have been adjusted to shear wave velocities and are plotted using a depth criterion of $L_R/3$. Based on the comparison of velocity profiles in Fig 5.9, it appears that measurements made using the equally spaced geophone arrangement correlate significantly better with the crosshole results than do the measurements made using the reference geophone arrangement. This conclusion is particularly evident at greater depths, where velocities from measurements made using the reference geophone arrangement are as much as 35 percent lower than velocities from crosshole tests.

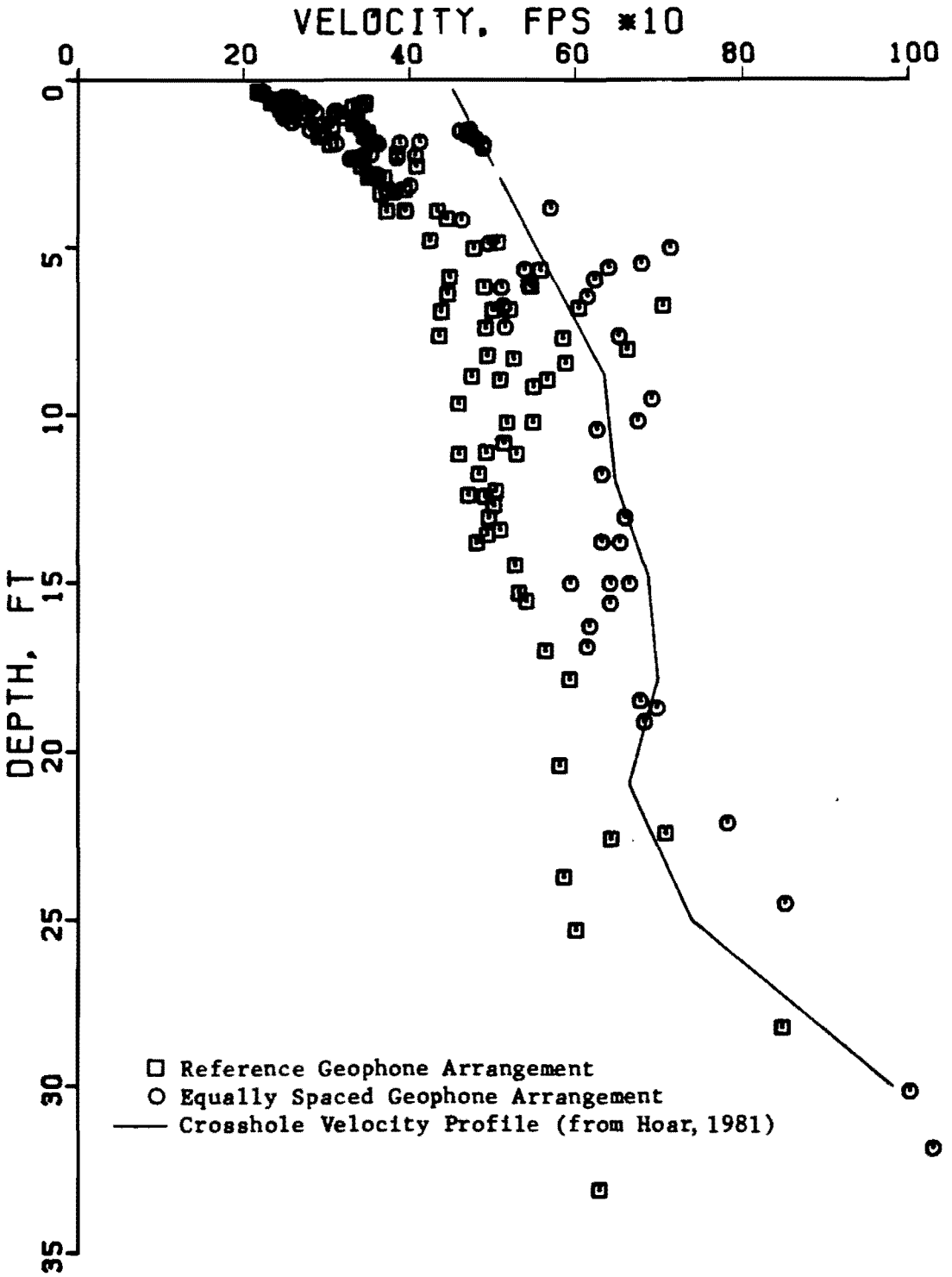

Fig 5.9. Comparison of crosshole results with shear wave velocity profiles from different geophone arrangements using as "Effective Sampling Depth" of $L_R/3$.

A rational approach involving concepts of wave propagation also supports the use of an equally spaced geophone arrangement. The geophone nearer to the source should be located at sufficient distance to allow proper sampling of material to a depth of approximately one wavelength. This distance also permits wavelengths of different frequencies to separate and enhances the capability of the spectral analyzer to measure an accurate cross spectrum. The use of a reference geophone close to the source does not provide sufficient distance to allow proper sampling to a depth of one wavelength. As a result, material properties near the surface are overweighted. For most soil sites, where the velocity (or modulus) increases with depth, the velocities obtained by using the reference geophone arrangement will be too low (since the lower-velocity material near the surface was overweighted). In general, then, the velocity profile obtained with the reference geophone arrangement will be lower than the actual profile (as determined by crosshole tests). This conclusion is shown quite clearly in Fig 5.9 for the tests performed at the Crossing.

The depth criterion of $L_R/3$, when applied to measurements made using the equally spaced geophone arrangement, provides good correlation with the crosshole results. In general, the cross spectrum velocities do not vary by more than 10 percent from the crosshole velocities. Variations near the surface may be due to seasonal differences in moisture content of the soil. The cross spectrum measurements were performed a few days after a period of heavy rainfall, and the lower velocities probably reflect the "softer" properties of the surficial soil.

A depth criterion of $L_R/2$ was also used to correlate the velocity profile with the crosshole results. This criterion provided a reasonably good correlation down to about 20 ft (6.1 m), as shown in Fig 5.10. Below

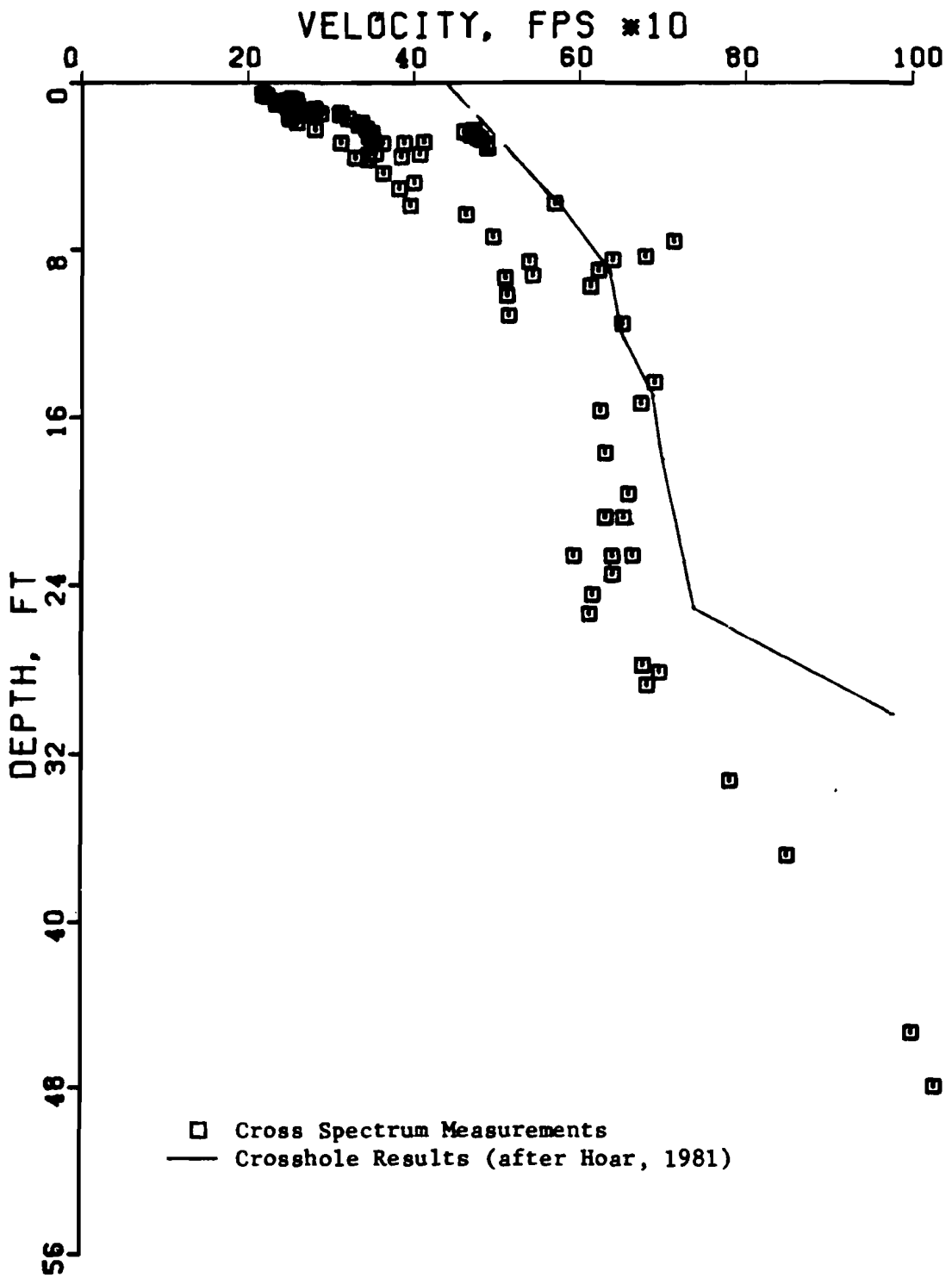

Fig 5.10. Comparison of crosshole results with shear wave velocity profile from measurements with equally spaced geophones using a depth criterion of $L_R/2$.

this depth, the velocity profile from cross spectrum measurements diverges markedly from the crosshole results. Inasmuch as crosshole test data exists only to 30 ft (9 m), it is difficult to assess how well either criterion ($L_R/2$ or $L_R/3$) correlates the cross spectrum velocities with crosshole velocities for depths greater than 30 ft (9 m).

ATTENUATION

Transfer function measurements were used to gather data on the attenuation properties at the site. The output/input ratio of wave magnitude (or energy) was obtained as a function of frequency over the range from 10 to 100 Hz. Transfer functions for measurements made using equally spaced geophones are shown in Fig 5.11a, and the corresponding coherence functions are shown in Fig 5.11b. The data exhibits several anomalies such as output/input ratios greater than unity. In some instances, transfer function magnitudes for a large spacing between geophones (e.g., V8-V16) are greater than magnitudes for a shorter spacing (e.g, V4-V8). This behavior is inconsistent with R-wave attenuation, since measurements with increased spacing should exhibit decreasing magnitudes. The erratic coherence, particularly above 45 Hz, also suggests that the transfer functions for measurements made using equally spaced geophones would not yield reliable attenuation data.

In contrast, transfer functions for measurements made using a reference geophone are shown in Fig 5.12a, and the corresponding coherence functions are shown in Fig 5.12b. The magnitudes of the transfer functions generally decrease with increased spacing between geophones, which is consistent with attenuation behavior. The coherence is also significantly better for

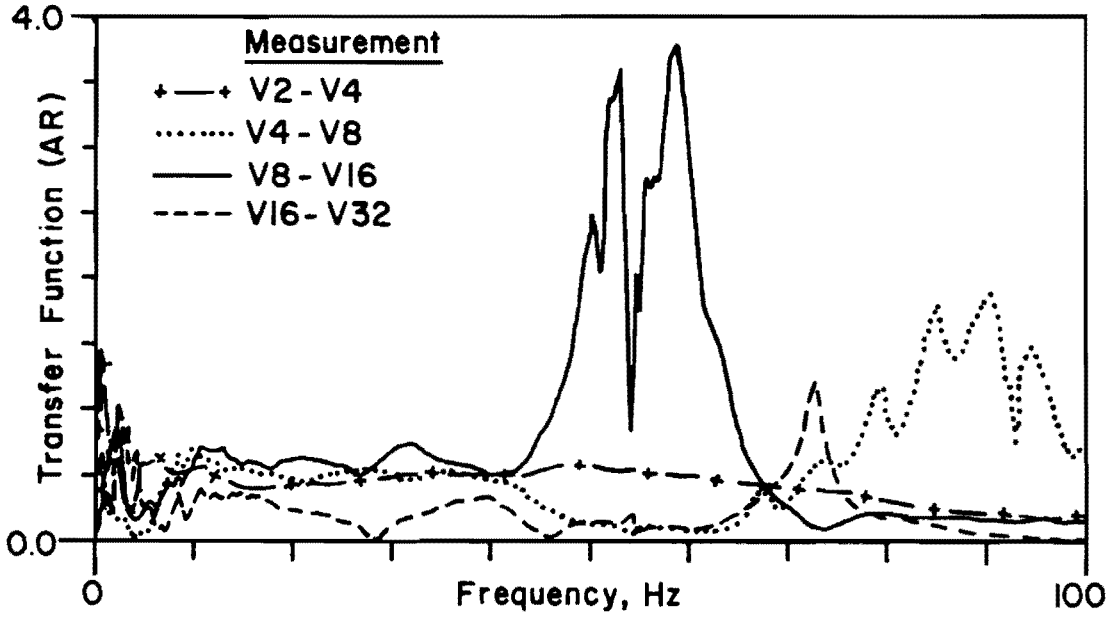

(a) Magnitude of Transfer Function

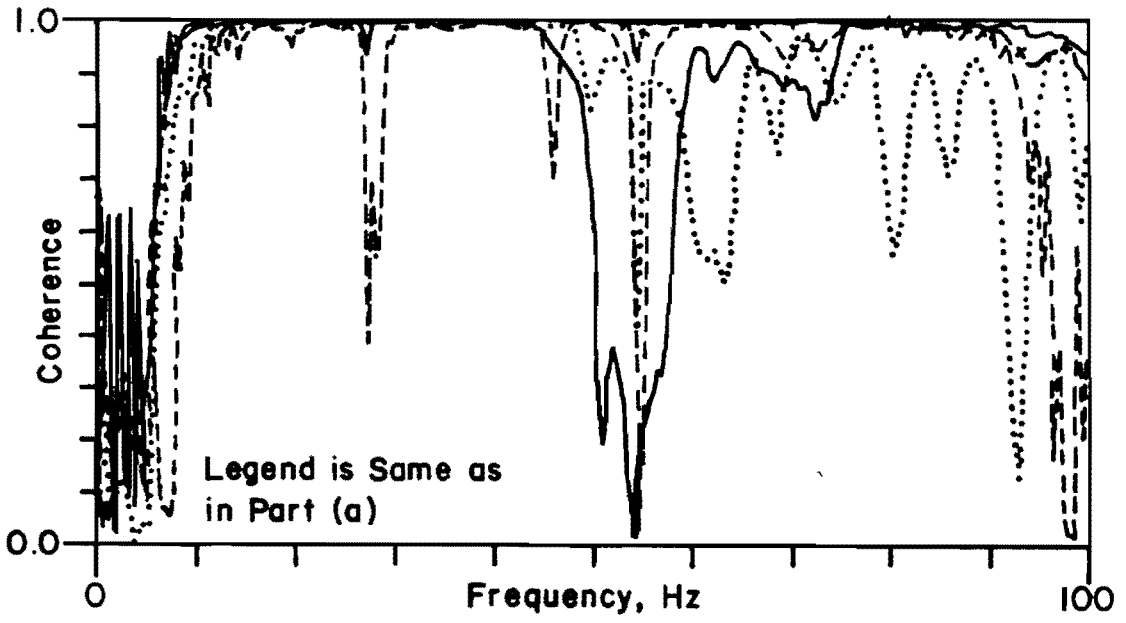

(b) Coherence Function

Fig. 5.11. Transfer Function and Coherence Function for Measurements with Equally Spaced Geophone Arrangement.

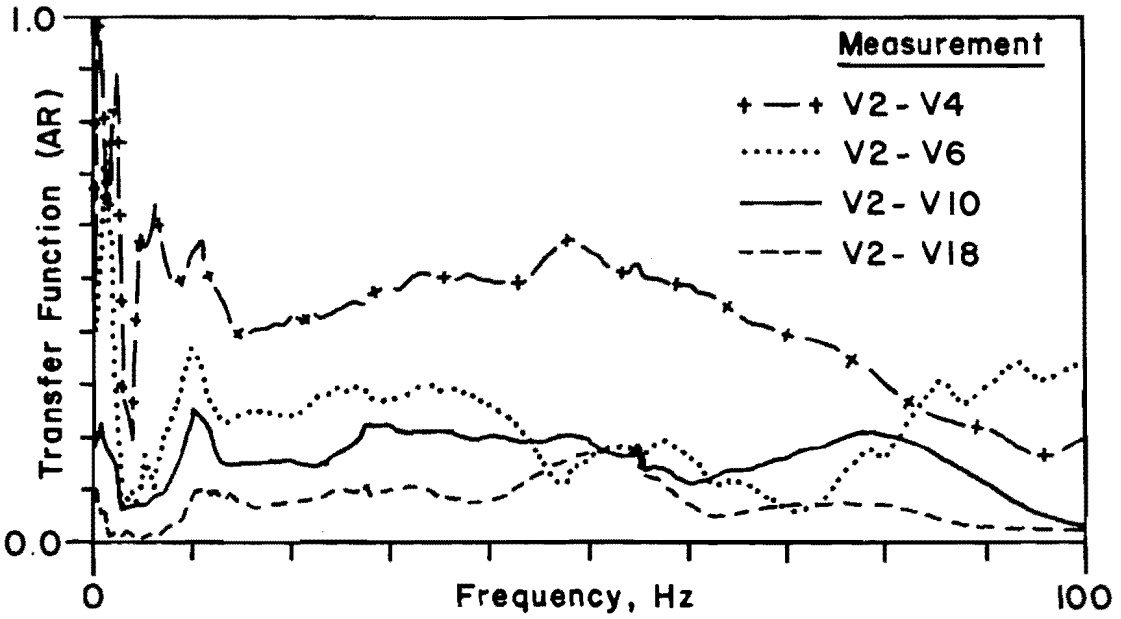

(a) Magnitude of Transfer Function

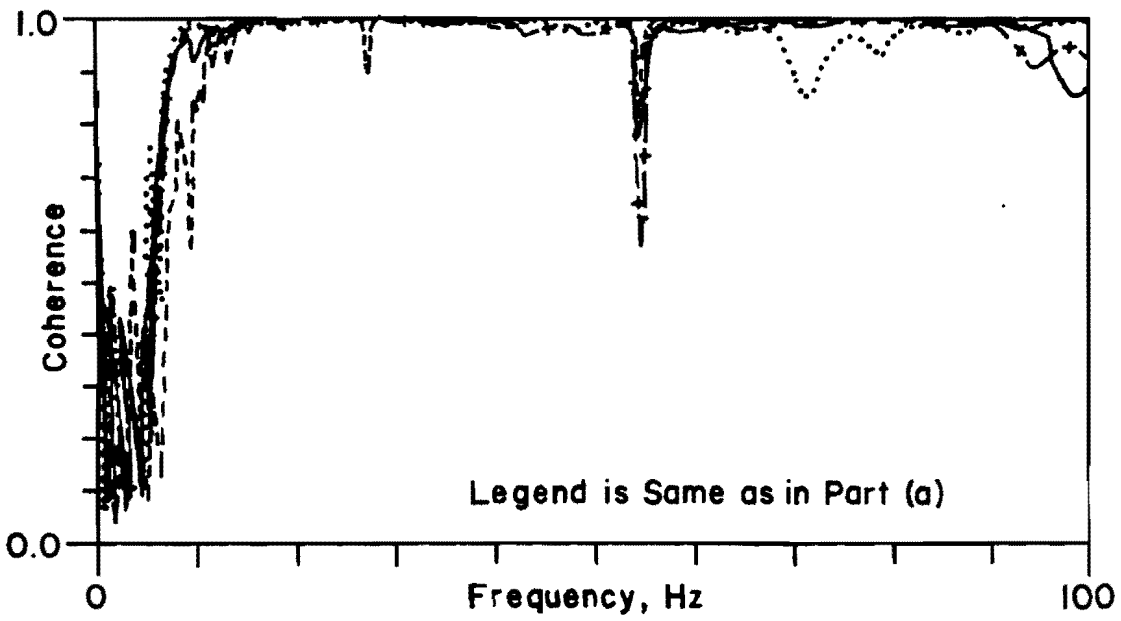

(b) Coherence Function

Fig. 5.12. Transfer Function and Coherence Function for Measurements with Reference Geophone Arrangement.

measurements made using the reference geophone. Although the equally spaced geophone arrangement provides better data for the velocity profile, the reference geophone arrangement appears to provide better data for attenuation calculations.

The output/input ratios, or amplitudes ratios (AR), are listed as a function of frequency and geophone location in Table 5.3. The input magnitude generated by the drop hammer varied as a function of frequency, as shown in Fig 5.13. Table 5.3 also contains values of the amplitude of the linear spectrum at V2 (the reference geophone) which were used to "normalize" the output at each frequency relative to the input magnitude. In addition, a frequency-wavelength plot (shown in Fig 5.14) based on measurements made using reference geophones was used to determine the values of L_R listed in Table 5.3.

Values of α, the coefficient of attenuation, were calculated using Eq 4.9 for each value of AR given in Table 5.3. Values of ranged from 0.042 ft^{-1} to 0.622 ft^{-1}, but only a few outlying points were above 0.300 ft^{-1}. Data for which the waves have traveled at least one-third of a wavelength were used to calculate average values of α as a function of frequency. (Only these data were used, so that scatter resulting from insufficient travel distance could be reduced.) The range in α and average values of α as a function of frequency are plotted in Fig 5.15. It appears that α increases approximately linearly with frequency. A linear regression analysis yielded a straight line with a slope of 0.00195 and a correlation coefficient of 0.98. A small intercept was also determined due to scatter in the low-frequency range (10 to 25 Hz). Ideally, no intercept should exist, since a wave of "infinite" length (zero frequency) would not undergo any attenuation.

TABLE 5.3. SUMMARY OF ATTENUATION FROM THE CROSSING AS A FUNCTION OF FREQUENCY AND GEOPHONE SPACING

f	L_R	L SPEC Ampl. at V2	V4, Δx = 2.0 ft			V6, Δx = 4.0 ft			V10, Δx = 8.0 ft			V18, Δx = 16.0 ft			V26, Δx = 24.0 ft			V34, Δx = 32.0 ft		
			AR*	NAR†	NoC‡	AR	NAR	NoC	AR	NAR	NoC	AR	NAR	NoC	AR	NAR	NoC	AR	NAR	NoC
10	64	2.693	.542	.2013	0.031	.361	.1341	0.063	.244	.0906	0.125	.082	.0304	0.250	.037	.0137	0.375	.023	.0084	0.500
12	42	3.374	.494	.1464	0.048	.261	.0774	0.095	.190	.0563	0.190	.097	.0287	0.381	.046	.0136	0.571	.029	.0087	0.762
14	34	3.836	.409	.1066	0.059	.233	.0607	0.118	.150	.0391	0.235	.086	.0224	0.471	.038	.0099	0.706	.025	.0066	0.941
16	30	4.226	.401	.0949	0.067	.244	.0577	0.133	.149	.0353	0.267	.065	.0154	0.533	.047	.0111	0.800	.022	.0053	1.067
20	24	5.051	.424	.0839	0.083	.235	.0465	0.167	.151	.0299	0.333	.078	.0154	0.667	.041	.0081	1.000	.015	.0030	1.333
25	18	6.212	.446	.0718	0.111	.294	.0473	0.222	.176	.0283	0.444	.095	.0153	0.889	.033	.0053	1.333	.013	.0021	1.778
30	14	7.873	.482	.0612	0.143	.265	.0337	0.286	.220	.0279	0.571	.095	.0124	1.143	.022	.0028	1.714	.008	.0010	2.286
40	9.5	10.535	.495	.0470	0.211	.259	.0246	0.421	.200	.0190	0.842	.078	.0074	1.684	.070	.0066	2.526	.021	.0020	3.368
50	7.1	15.209	.563	.0370	0.282	.158	.0104	0.563	.189	.0124	1.127	.170	.0112	2.254	.021	.0014	3.380	.015	.0010	4.507
60	5.1	22.290	.490	.0220	0.392	.164	.0074	0.784	.117	.0053	1.569	.069	.0031	3.137	.042	.0019	4.706	.010	.0004	6.275
80	3.3	27.266	.304	.0111	0.606	.167	.0061	1.212	.201	.0074	2.424	.070	.0026	4.848	.016	.0006	7.273	.005	.0002	9.697
100	2.6	23.330	.204	.0087	0.769	.342	.0147	1.538	.042	.0018	3.077	.025	.0011	6.154	.005	.0002	9.231	.000+	.0000+	12.308

* AR = Amplitude Ratio † NAR = Normalized Amplitude Ratio ‡ NoC = Number of Cycles

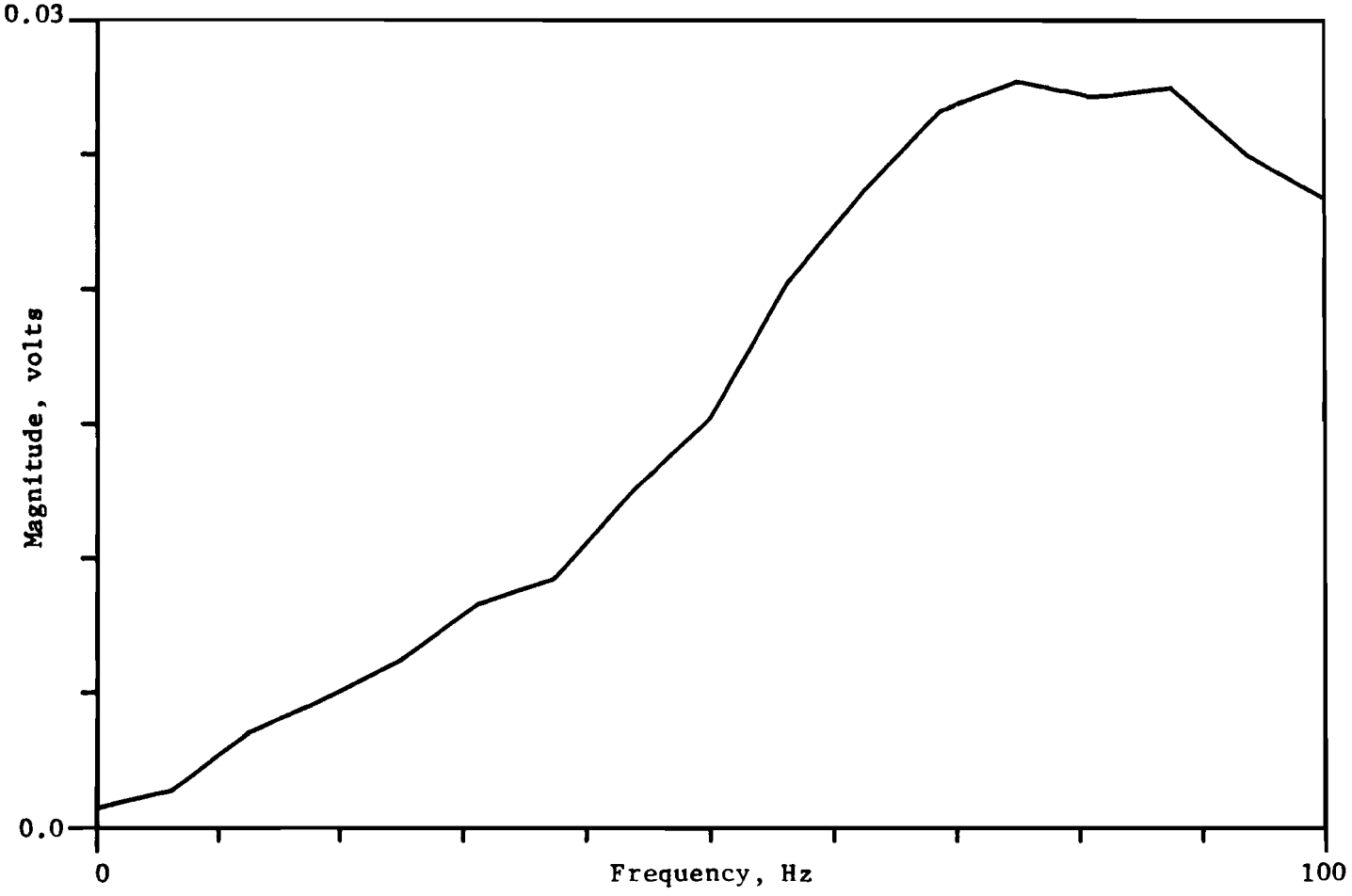

Fig 5.13. Input linear spectrum at V2 as a function of frequency.

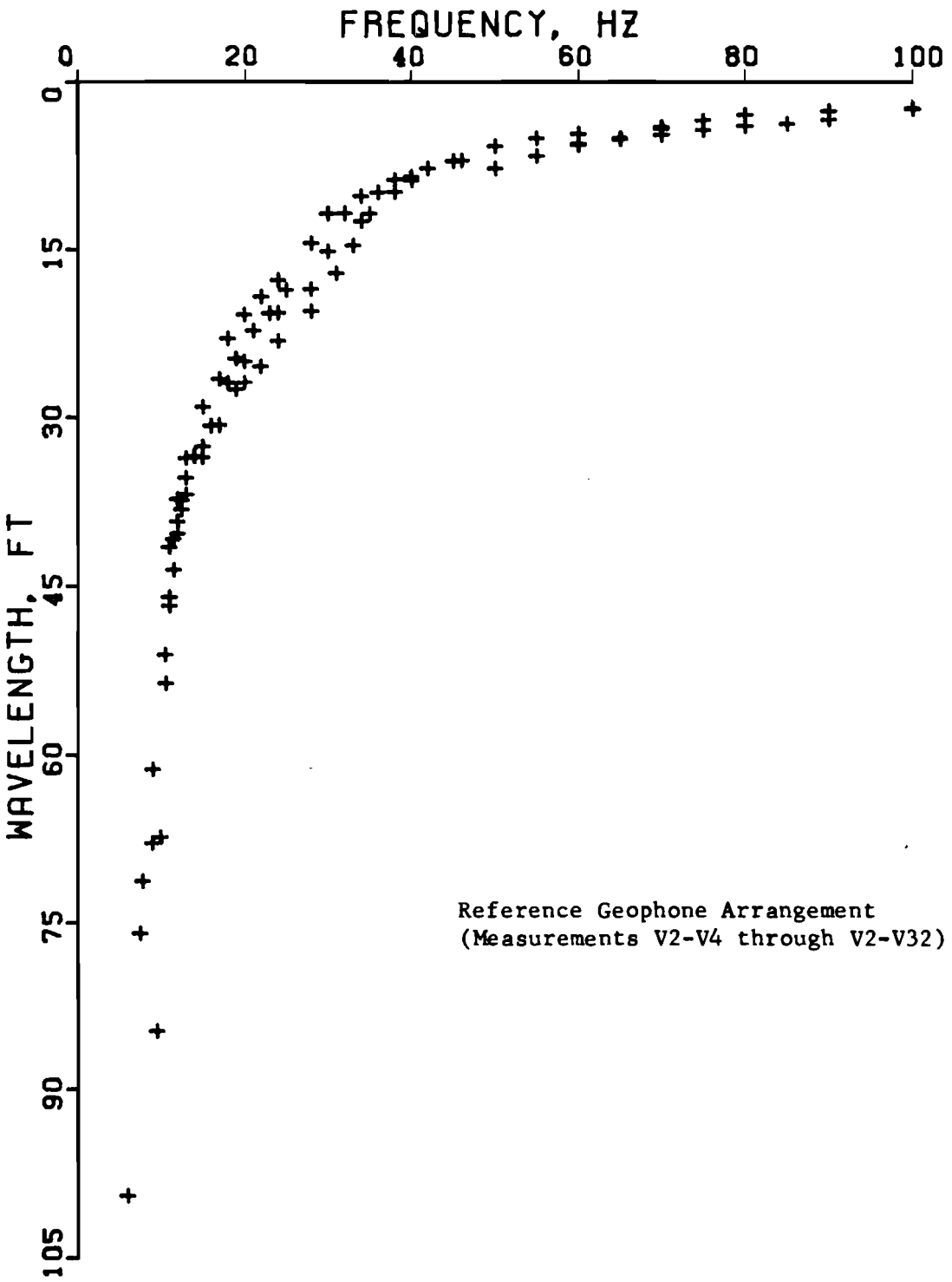

Fig 5.14. Frequency versus wavelength plot at the Crossing Site.

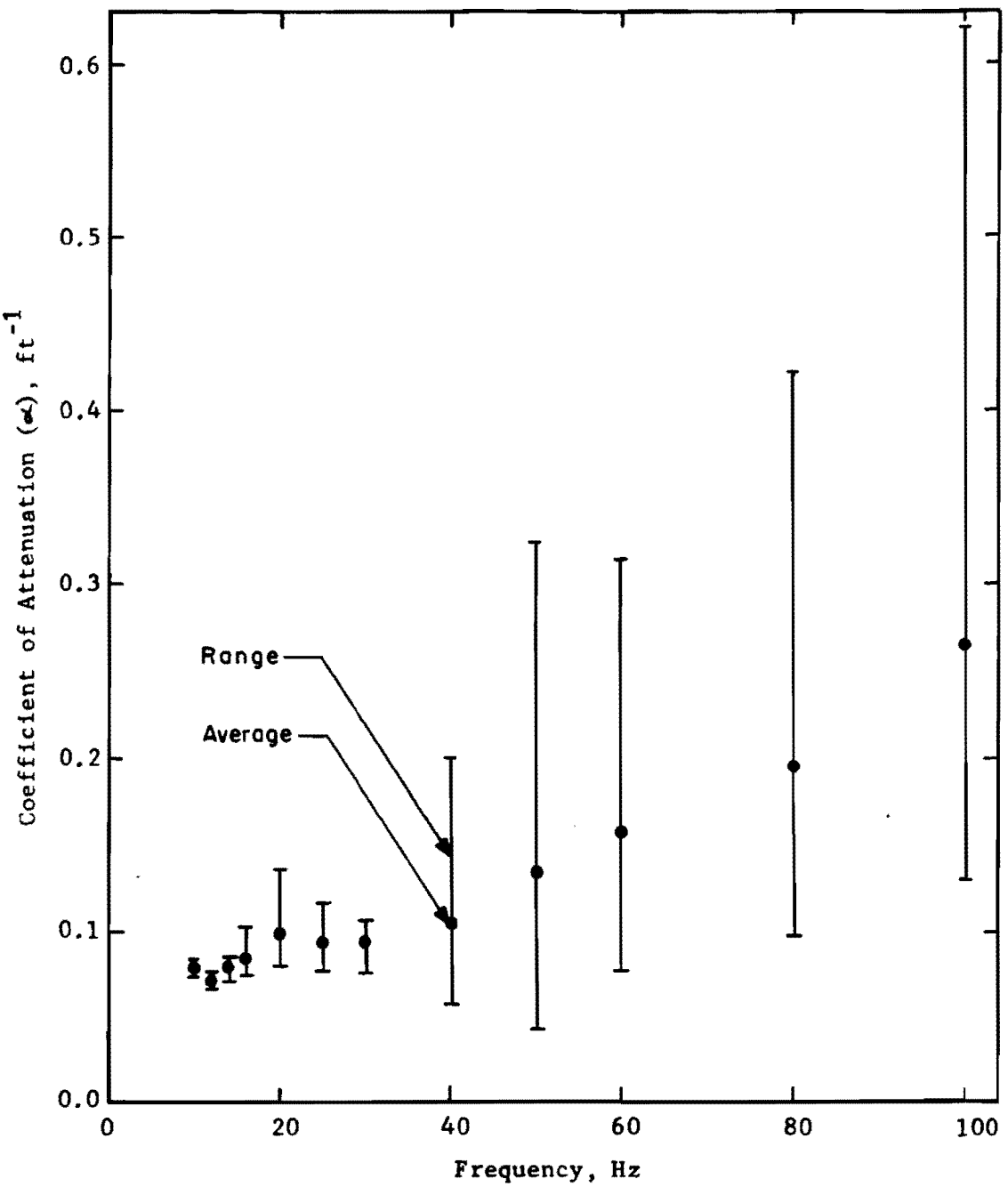

Fig 5.15. Variation of coefficient of attenuation with frequency at the Crossing Site.

Using the relationship $\alpha = 0.00195\ f$, values of α were calculated that did not exhibit the scatter associated with the measured values. In addition, values of the logarithmic decrement δ and damping ratio D were calculated using Eqs 2.9 and 2.10, respectively. Calculated values of α, δ, and D are listed in Table 5.4. The damping ratio is expressed in percentage and ranges from about 8 to 20 percent. The higher values associated with the lower frequencies may have resulted from insufficient input energy at those frequencies and/or from the fact that the longer wavelengths had not traveled enough to obtain a representative reading, even for the farthest location of geophones (measurement V2-V34).

The apparent large variation in damping as a function of frequency is probably not due to actual differences in soil properties but, rather, is a result of poorer data at the lower frequencies. To compare graphically the attenuation of R-wave amplitude as a function of frequency, it is necessary to establish a datum at which each frequency has the same initial magnitude. The reference geophone V2 is the most convenient initial point since it served as the input geophone for each measurement. For the sake of comparison, the amplitudes at each frequency are assumed to equal unity at V2, although the linear spectrum at V2 (Fig 5.13) indicates that the input amplitude varied as a function of frequency. To "normalize" the amplitude ratios at other distances, then, each ratio must be divided by the input spectrum amplitude at each particular frequency. These normalized amplitude ratios (NAR) are listed in Table 5.3, and, in effect, represent the amplitudes at the output geophones (V4, V6, V10, etc.) that would have been measured if all frequencies had been given the same input energy.

In addition, a provision must be made to account for the fact that higher frequencies will have undergone more wavelengths in a given distance

TABLE 5.4. RELATIONSHIP BETWEEN FREQUENCY AND DAMPING AT THE CROSSING SITE

Frequency f(Hz)	Wavelength L_R(ft)	Coefficient of Attenuation α(ft^{-1})	Logarithmic Decrement δ	Damping Ratio D(%)
10	64	0.020	1.25	19.5
12	42	0.023	0.98	15.4
14	34	0.027	0.93	14.6
16	30	0.031	0.94	14.8
20	24	0.039	0.94	14.8
25	18	0.049	0.88	13.9
30	14	0.059	0.82	12.9
40	9.5	0.078	0.74	11.7
50	7.1	0.098	0.69	10.9
60	5.1	0.117	0.60	9.5
80	3.3	0.156	0.51	8.1
100	2.6	0.195	0.51	8.1

than lower frequencies. Frequencies can be compared on an equal basis by using the number of cycles the wavelength has undergone as opposed to the actual travel distance. The number of cycles can easily be calculated from Eq 4.7 if the wavelength for a given frequency is known. Table 5.3 contains values for the number of cycles for each frequency at each geophone location. These values are plotted versus NAR for selected frequencies in Fig 5.16. The trend in the data indicates that all frequencies (from 10 to 100 Hz) exhibit the same damping behavior.

This conclusion was also drawn from the data at the Walnut Creek site which are shown in Fig 4.31. As was the case at Walnut Creek, it is difficult to determine whether the high values for D are excessive because of body wave energy present in the wave pulse at V2 or if the values are realistic estimates of field damping caused by backscattering that is indeed higher than damping measured in the laboratory. The former difficulty could possibly be avoided by using a reference geophone at 8 to 10 ft, thus allowing the body wave energy to dissipate prior to reaching the first geophone.

SUMMARY

Results and conclusions based on tests performed at The Crossing are quite similar to those found from soil testing at Walnut Creek.

Velocity profiles obtained from cross spectrum (surface) measurements tend to exhibit some scatter. Much of this scatter can be reduced by filtering out data for wavelengths which are inappropriate for the spacing of geophones. Using criteria developed from the Walnut Creek site, data from the Crossing site was filtered to produce a refined velocity profile.

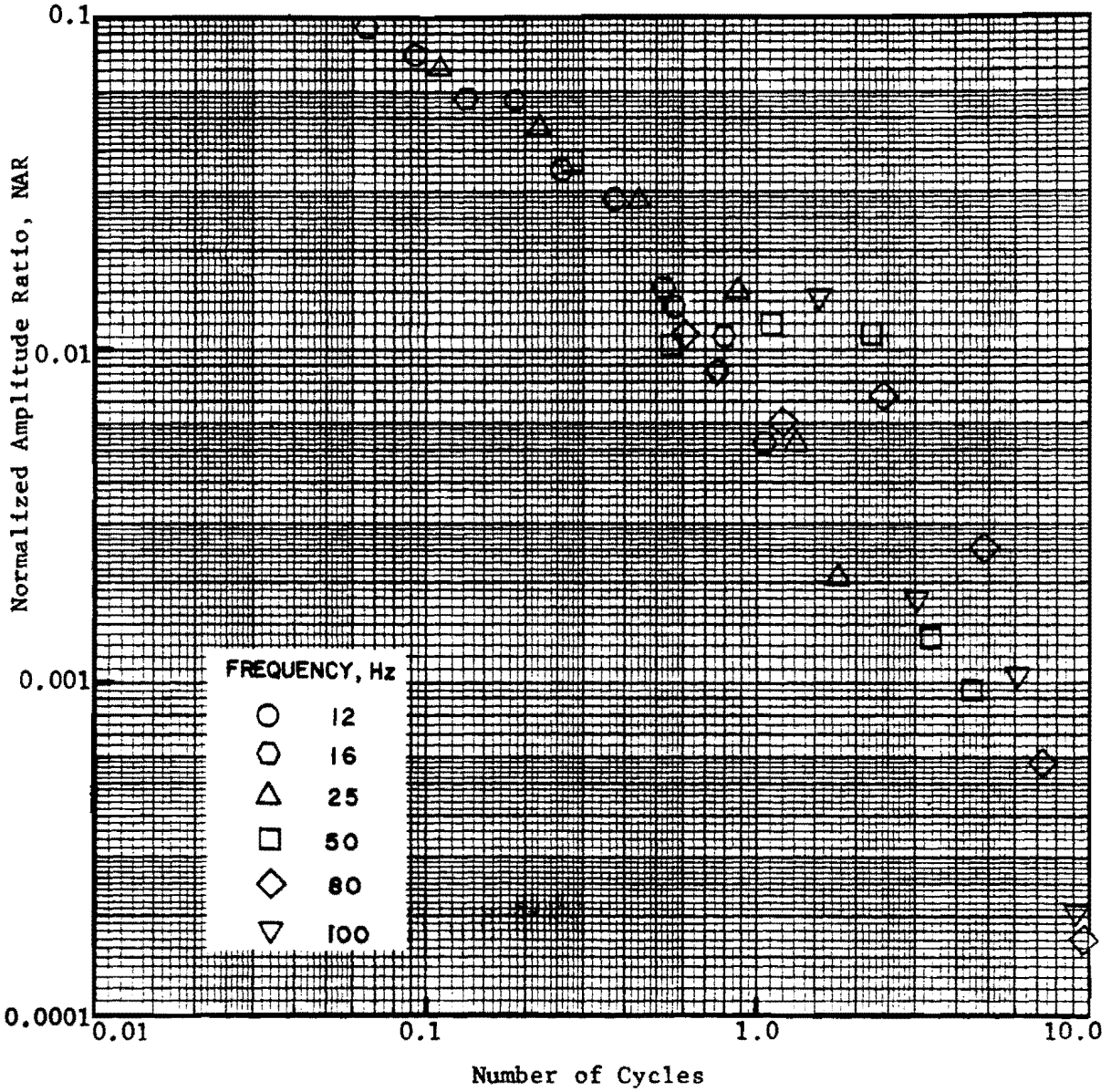

Fig 5.16. Relationship between normalized amplitude ratio (NAR) and number of cycles (NoC) as a function of frequency.

The velocities obtained from cross spectrum measurements using an equally spaced geophone arrangement were, on the average, higher than those obtained from measurements made using a reference geophone arrangement. The difference in velocities increased with increasing wavelength, suggesting that the reference geophone was located too close to the source to sample long wavelengths adequately. The velocity profile from measurements using equally spaced geophones correlated well with crosshole results when the profile was plotted using a depth criterion of $L_R/3$. In general, cross spectrum velocities did not vary by more than 10 percent from crosshole velocities.

Attenuation properties at the site were evaluated by means of transfer functions. For attenuation calculations, better data were obtained using the reference geophone arrangement than were obtained using the equally spaced geophone arrangement. The coefficient of attenuation was found to be approximately a linear function of frequency and was estimated by $\alpha = 0.00195\ f$. Values of logarithmic decrement and damping ratio were also calculated, with values of damping ranging from about 8 to 20 percent. These values are somewhat higher than those typically measured in laboratory tests, perhaps due to excessive body wave energy present at the near geophone (but not present at the far geophone). This problem could possibly be overcome by locating the reference (near) geophone at a distance of 8 to 18 ft from the source.

CHAPTER 6. PAVEMENT EVALUATION AT AUSTIN SITE

SITE DESCRIPTION

The Austin site is located about 2 miles (3.2 km) northeast of the campus of The University of Texas at Austin, as shown in Fig 6.1. The selected site is a flexible pavement section of IH 35 at Sta 670+00, which is located near Capital Plaza Shopping Center. All testing was conducted in the extreme right-hand lane on the northbound portion of the highway.

The longitudinal section profile is shown in Fig 6.2. The profile is based on borings which were made in conjunction with crosshole testing. The asphalt layer consists of a hot mix asphaltic concrete (HMAC) surface approximately 2.5 in. (6.4 cm) thick and an asphalt-stabilized base approximately 4 in. (10.2 cm) thick. The unit weights and Poisson's ratios of these materials were assumed to be 145 pcf and 0.35, respectively. The flexible base of crushed limestone was compacted in three layers, each approximately 5 in. (12.7 cm) thick, with a unit weight of 140 pcf and a Poisson's ratio of 0.40. The base course grades into a subbase of dense sand with a layer thickness of about one foot (0.3 m). The natural subgrade is a black stiff clay grading into a tan silty clay. The unit weight and Poisson's ratio of the subgrade were assumed to be 115 pcf and 0.40, respectively. Borings were terminated at a depth of 12.5 to 13 ft (3.8 to

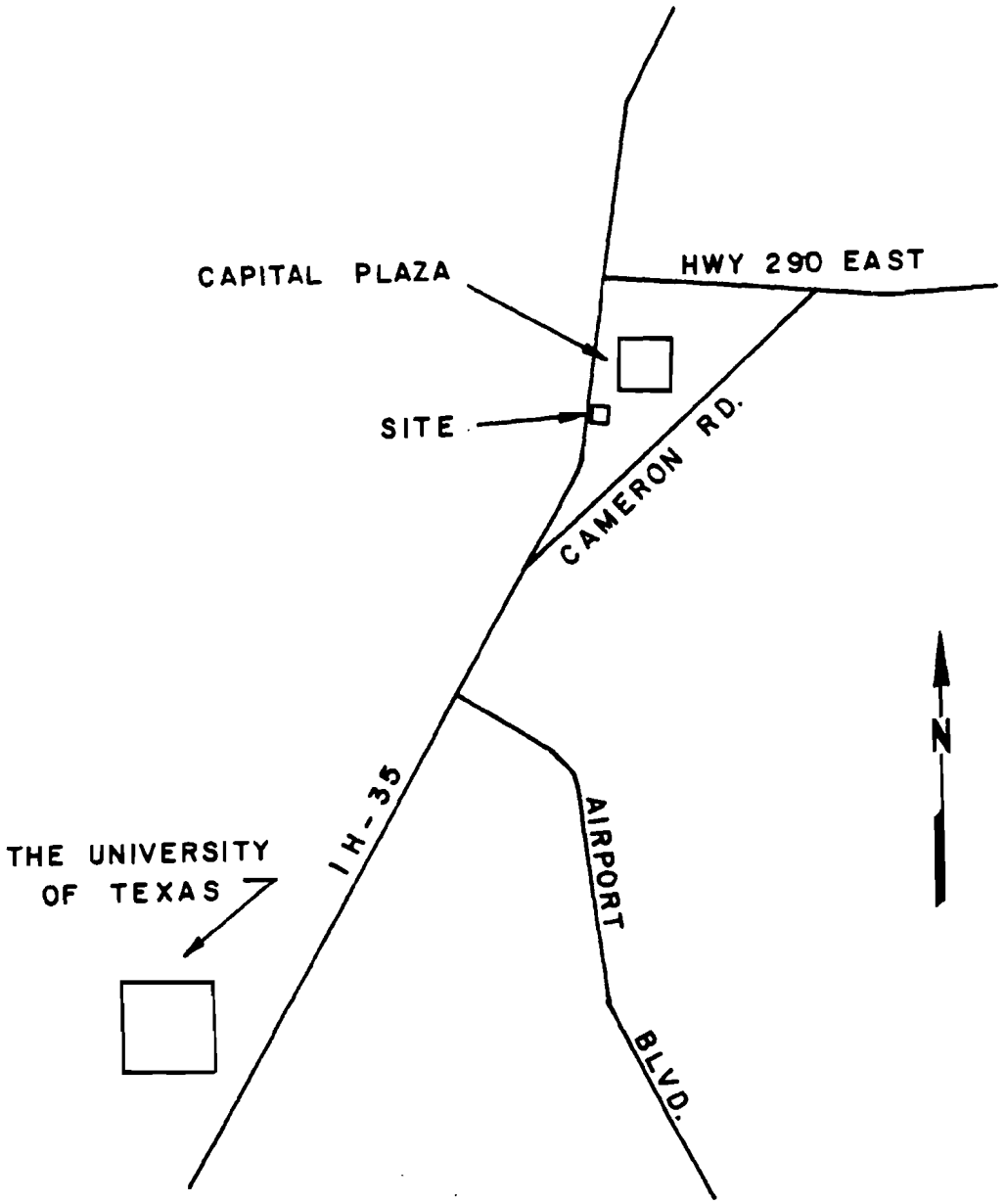

Fig 6.1. Location of Austin (IH 35) Pavement site.

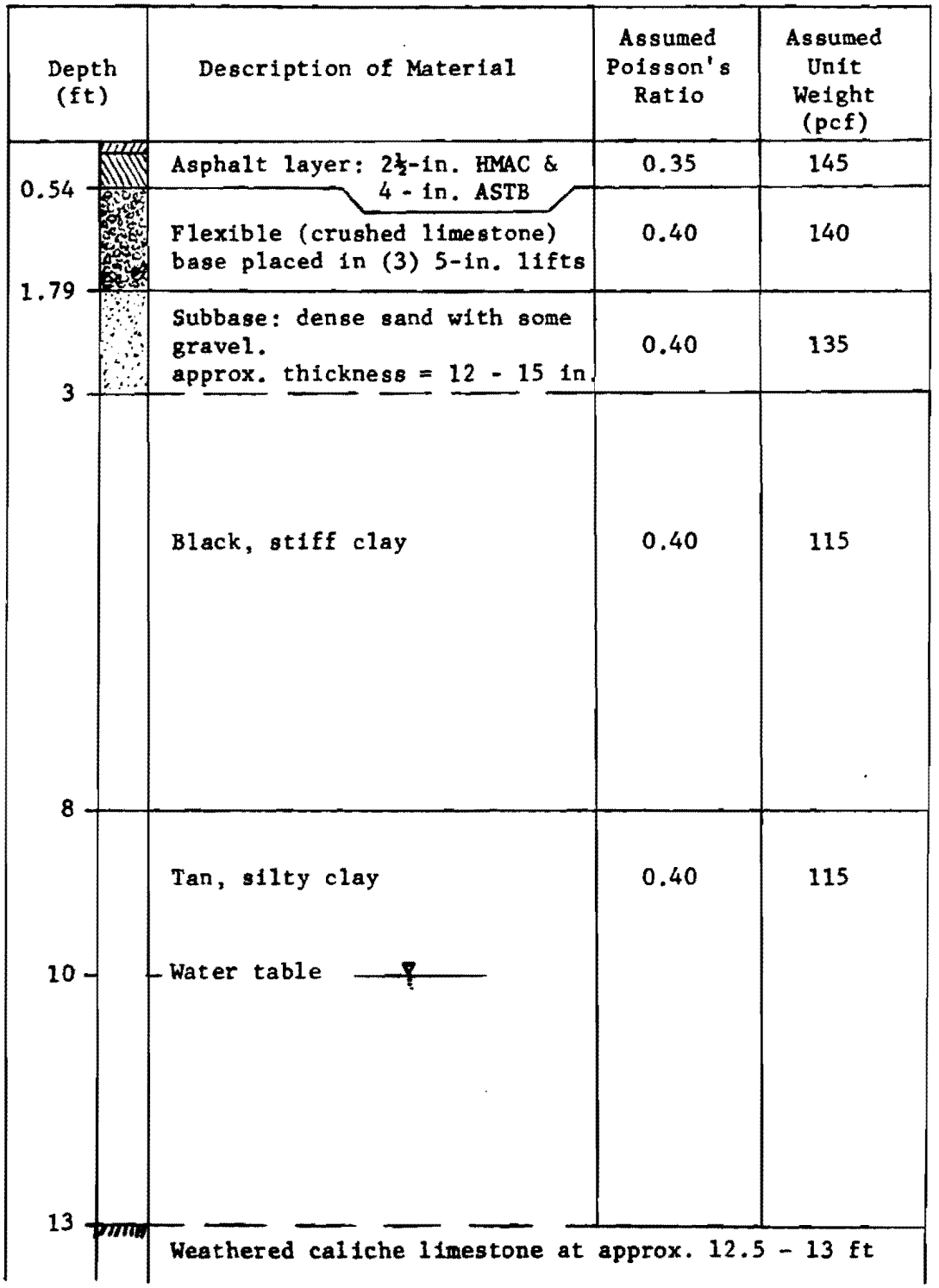

Fig 6.2. Longitudinal-section profile for Austin (IH 35) site.

4.0 m), the depth at which rock was encountered. The water table was located at a depth of about 10 ft (3 m).

Due to the heavy traffic at the site, a small amount of undesirable background noise was present during testing. In addition, power to operate electrical equipment had to be provided by a portable generator, which also contributed some background noise at the site.

EXPERIMENTAL PROCEDURE

Initially, only surface measurements were performed at the Austin site. These tests were conducted on May 19-20, 1980. No borings were made at this time, so as to keep within the restraint of nondestructive testing. Subsequently, crosshole tests (and borings) were performed on September 15, 1980, to verify the section profile as well as check the accuracy of the velocities obtained from surface measurements. The equipment and general procedure are discussed in the following sections.

Equipment

Two different sources were used to propagate waves through the pavement system. Each source generated an impulsive load on the surface of the pavement. Therefore, all signals were transient events. Truncation for digital analysis of the signals in the frequency domain was accomplished using a rectangular window.

The primary source was a Falling Weight Deflectometer (FWD), similar to the Phoenix Falling Weight Deflectometer manufactured in Denmark (Ref 3). This device was mounted on a two-wheel trailer that could be towed on the

highway by a passenger vehicle. The hammer was a falling mass which weighed 150 kg (331 lb) and could be dropped from various heights. Cross spectrum measurements were triggered internally by using the signal from the receiver closest to the source.

The second source was the drop hammer previously described in Chapter 4. The drop hammer was a falling mass which weighed about 12 lb (5.4 kg) and could be dropped from various heights. Measurements were triggered with a resistance-capacitance (RC) trigger which is discussed in detail by Hoar and Stokoe (Ref 12). The RC trigger permits accurate determination of the direct arrival time of the wave from the source to the receiver.

Velocity transducers, commonly called geophones, were used to detect wave propagation through the pavement system. Both vertical and horizontal geophones were employed to allow sensitivity for several different types of waves and directions of motion. The geophones were mounted on steel blocks with a largest dimension of 2.75 in. (7.0 cm). The blocks were epoxied to the asphalt surface to ensure adequate coupling. Geophones used at this site had natural frequencies of 8 and 14 Hz with an approximately linear response over the range of 20 to 1600 Hz. Since only wave propagation velocities were calculated, no calibration factor was determined to relate voltage to absolute particle velocity.

The primary instrument used to record the signals was the Hewlett-Packard Model 5420A Digital Signal Analyzer. The instrument includes a set of signal filters, an analog-to-digital converter (ADC), a dual-channel digital oscilloscope, and a magnetic cassette tape for storage and recall of permanent records. The analyzer can directly measure all of the time domain and frequency domain measurements previously discussed. In addition, the type of signal, type and number of averages, bandwidth (or time length), and

trigger conditions can all be specified by the operator. The analyzer can be easily interfaced with an x-y plotter to provide a hard copy of the data.

An auxiliary instrument, the Nicolet Instrument Corporation Model 2090C Digital Storage Oscilloscope, was used, for convenience, to make additional time records. This oscilloscope is also dual-channel, but it cannot perform frequency analysis of signals. Records are stored on magnetic disks, and the oscilloscope can be interfaced with an x-y plotter to produce a hard copy of the data.

Measurement Setup and Analysis

The general configuration of the source, geophones, and recording equipment used in these tests is shown in Fig 6.3. The geophones were placed in a linear array to minimize anisotropic effects that might influence wave propagation. The line of geophones extended parallel to the direction of the roadway. Vertical geophones (subsequently identified by the symbol V) were located approximately 1, 2, 5, and 10 ft (0.3, 0.6 7.5, and 3.0 m) from the source. Horizontal geophones (subsequently identified by the symbol H) were located at the same positions and were aligned radially from the source so as to detect wave motion occurring in the direction of wave propagation. Hereafter, measurements are identified by the type of geophone which was used (V or H) and the location of the geophone(s) from the source (1, 2, 5, or 10 ft). For example, measurement V2-V5 used vertical geophones which were located at 2 ft (0.6 m) and 5 ft (1.5 m) from the source.

Measurements were made using only two geophones for any one impulse, since the recording instruments were dual-channel devices. Emphasis was placed on obtaining data for the FWD source, with supplemental data provided

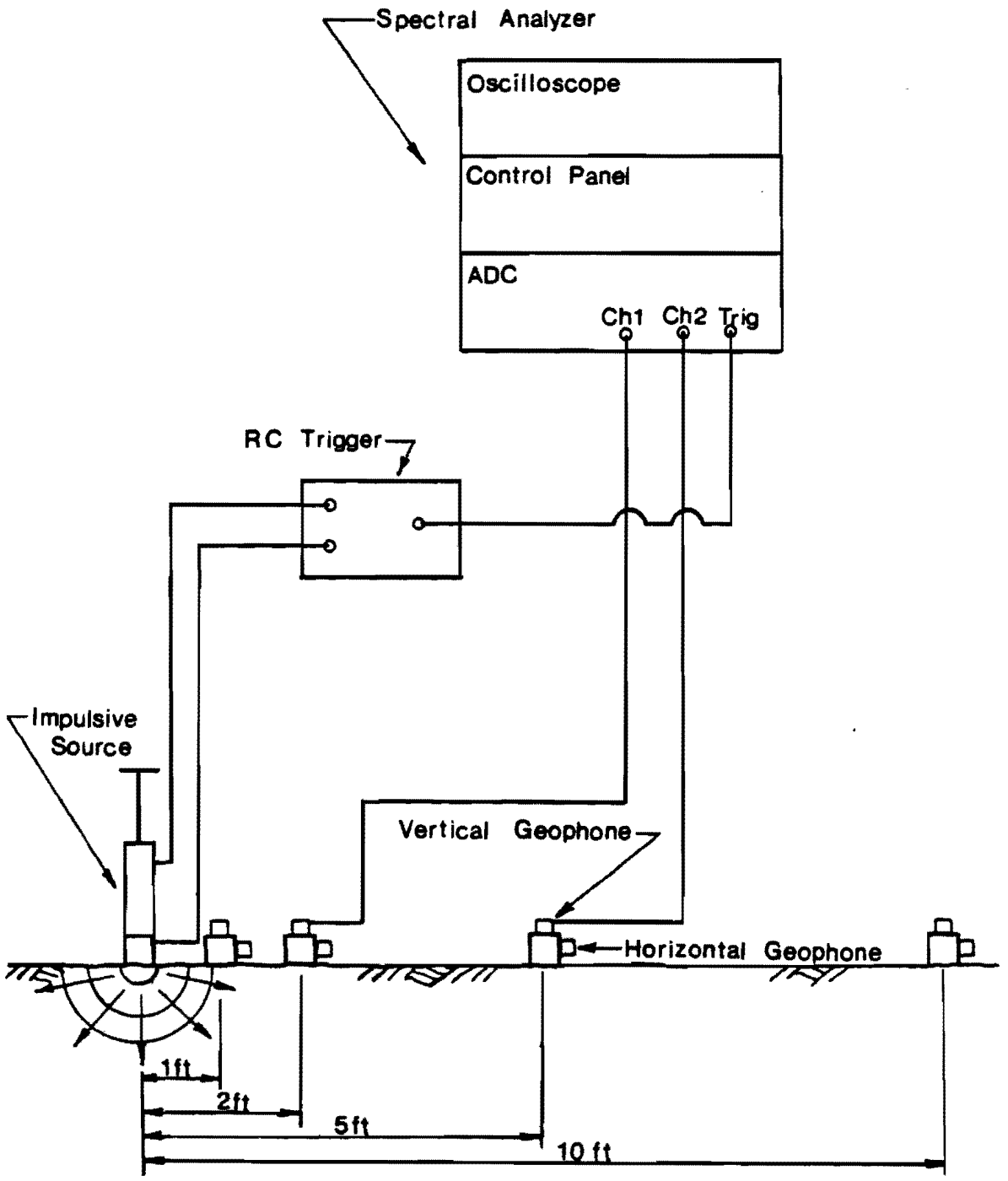

Fig 6.3. Schematic diagram of experimental setup.

by the drop hammer source. Both time domain and frequency domain measurements were recorded, although the thrust of the data acquisition was toward spectral analysis. Table 6.1 contains a listing of the various pairings of geophones, the exact distances between the geophones, the source, and the bandwidth for each measurement. Time domain measurements included time record averaging, autocorrelation, and cross-correlation. Frequency domain measurements included the linear spectrum, autospectrum, cross spectrum, transfer function, and coherence function.

The analysis of the cross spectrum data followed the general procedure outlined in Appendix A. Various parameters were studied to determine their influence on the cross spectrum measurements. Records with one average and five averages were used to compare the advantages of averaging. Comparative measurements were made for responses of both vertical and horizontal geophones. The effectiveness of each source was also investigated. Results of these comparisons are presented in the following section.

RESULTS FROM SURFACE MEASUREMENTS

Comparisons for both time and frequency domain measurements indicate that there are no significant differences between one-average records and five-average records. This is probably a result of the high reproducibility of the impulse. However, one-average records occasionally exhibited apparent anomalies. To avoid anomalies, all analyses were performed using five-average records.

TABLE 6.1. SUMMARY OF MEASUREMENTS AT THE AUSTIN (IH 35) SITE

Record No.	Channel Input		Distance between Geophones (ft)	Source	Number of Averages	Bandwidth of Spectrum (Hz)	Computer Data File Identification
	#1	#2					
22	V5	V10	5.02	Falling Weight Deflectometer	1	400	SHCP3
29	V1	V2	1.00	" " "	5	200	SHCP1
51 & 55	V2	V5	3.08	" " "	1 & 5	100	SHCP2
101 & 106	V2	V5	3.08	" " "	1 & 5	1600	SHCP2
59 & 64	H2	H5	3.08	" " "	1 & 5	100	SHCP5
69 & 74	H2	H10	8.10	" " "	1 & 5	100	SHCP6
79 & 84	V2	V10	8.10	" " "	1 & 5	100	SHCP4
91 & 96	V2	V10	8.10	" " "	1 & 5	1600	-
114	H2	H5	3.08	Drop Hammer	5	1600	SHCP8
119	V2	V5	3.08	" "	5	1600	SHCP7

Comparison of Horizontal and Vertical Geophones

In general, the coherence functions were similar for measurements with the same geophone locations, regardless of whether the geophones were oriented horizontally or vertically. The range of frequencies measured by the cross spectrum was also similar regardless of geophone orientation. Based on the magnitudes of the cross spectrums for measurements with the drop hammer as the source, the levels of excitation energy in the horizontal and vertical directions are of the same order of magnitude. In contrast, for measurements with the FWD as the source, the magnitudes of the cross spectrums for measurements using vertical geophones were approximately 100 times greater than the magnitudes for measurements using horizontal geophones. This result is not unexpected, since the FWD is designed to input a large force in the vertical direction to create a deflection basin.

Although the range of frequency response was similar for both orientations of geophones, the velocities obtained from measurements using horizontal geophones were significantly higher than those obtained from measurements using vertical geophones. This trend was true for measurements made with both the FWD and the drop hammer. Since the horizontal geophones are much more sensitive to P-wave motion than the vertical geophones, it is quite likely that spectrums for measurements using horizontal geophones contain some higher-velocity P-wave energy which leads to an overall higher velocity for the (apparent) R-wave.

Such a hypothesis can be checked, at least in part, by comparing time records of wave pulses obtained from horizontal and vertical geophones. Figure 6.4a shows time records obtained with the Nicolet oscilloscope for horizontal geophones H2 and H10 (FWD source). For the interval travel time

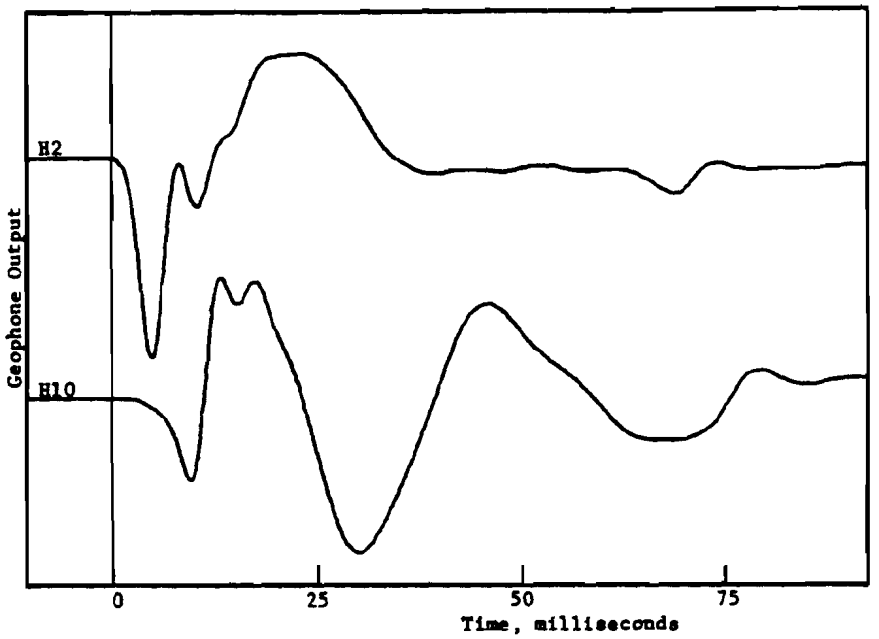

(a) Measurements with horizontal geophones.

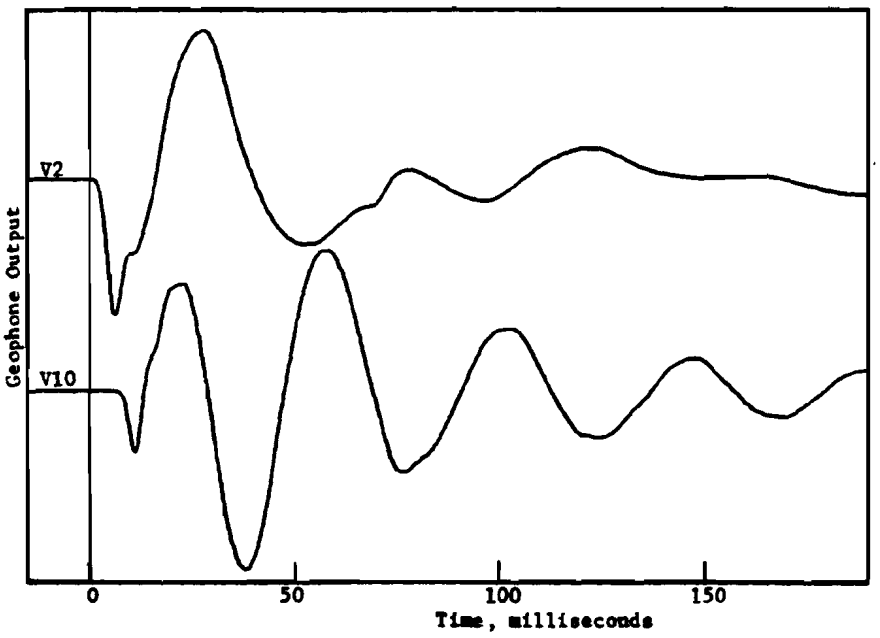

(b) Measurements with vertical geophones.

Fig 6.4. Comparison of time records obtained with horizontal and vertical geophones using the FWD source.

between the initial arrival of the wave pulse at H2 and the initial arrival of the wave pulse at H10, the calculated wave velocity is 3180 fps (970 m/sec). For the same wave pulses, the interval travel time based on trough-to-trough (of the first half-sine wave) yields a velocity of 1705 fps (570 m/sec). This latter velocity is within the range of S-wave (or R-wave) velocities for asphalt whereas the former velocity is within the range of P-wave velocities for asphalt. Since the P-wave travels much faster than the S-wave, the influence of the P-wave is greatest at the initial arrival of the pulse, and, based on the calculated velocities, the influence is greatly diminished by the first trough in the pulse.

In contrast, Fig 6.4b shows time records for vertical geophones V2 and V10 (FWD source). For the interval travel time between the initial arrival of the wave pulse at V2 and V10, the calculated wave velocity is 1305 fps (400 m/sec). For the same wave pulses, the interval travel time based on trough-to-trough (of the first half-sine wave) yields a velocity of 1655 fps (505 m/sec). Both of these velocities are within the range of S-wave velocities for asphalt, suggesting that the vertical geophones do not measure any significant influence of the P-wave.

It is difficult to assess solely on the basis of time records how much the P-wave influences measurements made with horizontal geophones. Time records of surface measurements, in general, are difficult to interpret, particularly for layer systems with markedly different properties. This difficulty is evidenced by the substantial difference in S-wave velocities based on different interval travel times even for measurements with vertical geophones (Fig 6.4b). Because different wavelengths travel at different velocities, the time record of the wave pulse may change substantially from one geophone location to the next. Indeed, this is the reason why the

spectral analyzer is used to isolate the propagation of individual frequencies within the measurement bandwidth.

The phase plots of the cross spectrums for measurements V2-V10 and H2-H10 are shown in Fig 6.5. In general, the phase for a particular frequency is less for measurement H2-H10 than the phase at the same frequency for measurement V2-V10. A lesser phase translates into a lesser travel time and, hence, a greater velocity for the wavelength at the particular frequency. For example, at 30 Hz, the phase for measurement H2-H10 is 111.01 degrees, which yields a velocity of 788 fps (240 m/sec), while the phase for measurement V2-V10 is 149.44 degrees, which yields a velocity of 586 fps (179 m/sec) for a difference in velocities of 34 percent.

The most important and conclusive comparison involves the velocity profile obtained with measurements using vertical geophones versus the profile obtained with measurements using horizontal geophones. Figure 6.6 compares the velocity profiles (using $L_R/3$ as the "effective" depth) for measurements V2-V5 and H2-H5 using the drop hammer source. In each layer, the velocities from H2-H5 are distinctly greater than velocities from V2-V5. The velocity profile from V2-V5 correlates extremely well with shear wave velocities from crosshole tests verifying that measurements with vertical geophones are more reliable than those with horizontal geophones. As a result, nearly all of the analysis for the Austin site (and subsequent testing at other sites) included only measurements made with vertical geophones.

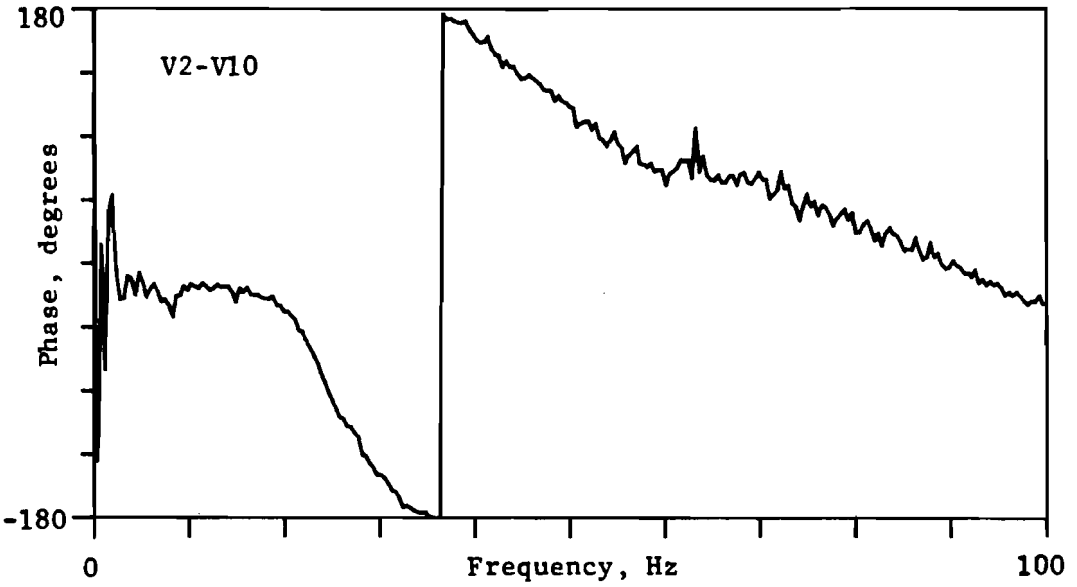

(a) Recorded with vertical geophones

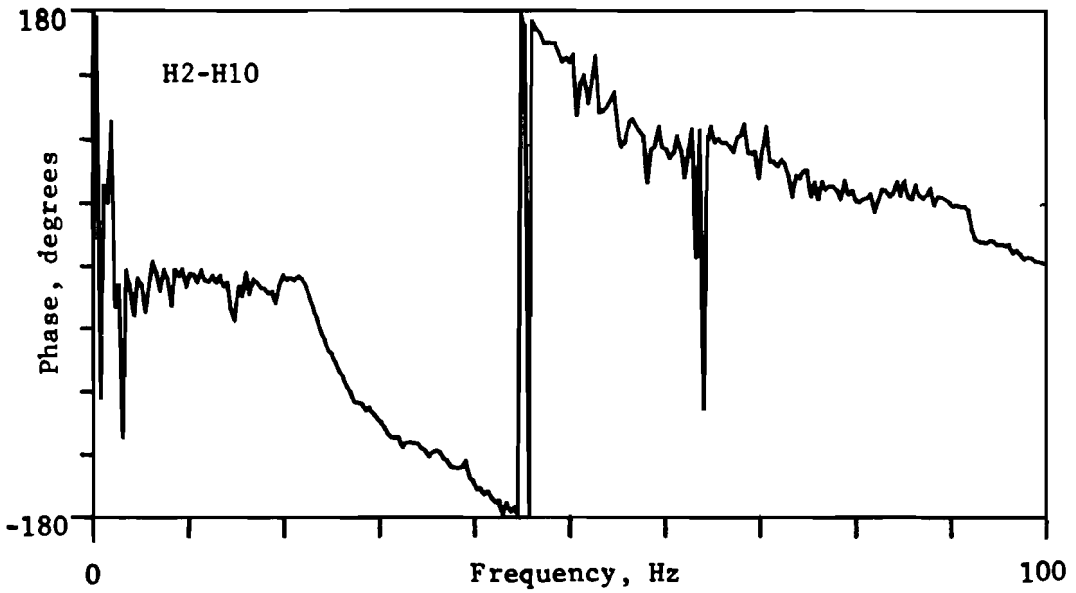

(b) Recorded with horizontal geophones

Fig 6.5. Comparison of the phase of the cross spectrum from vertical and horizontal geophones using the FWD.

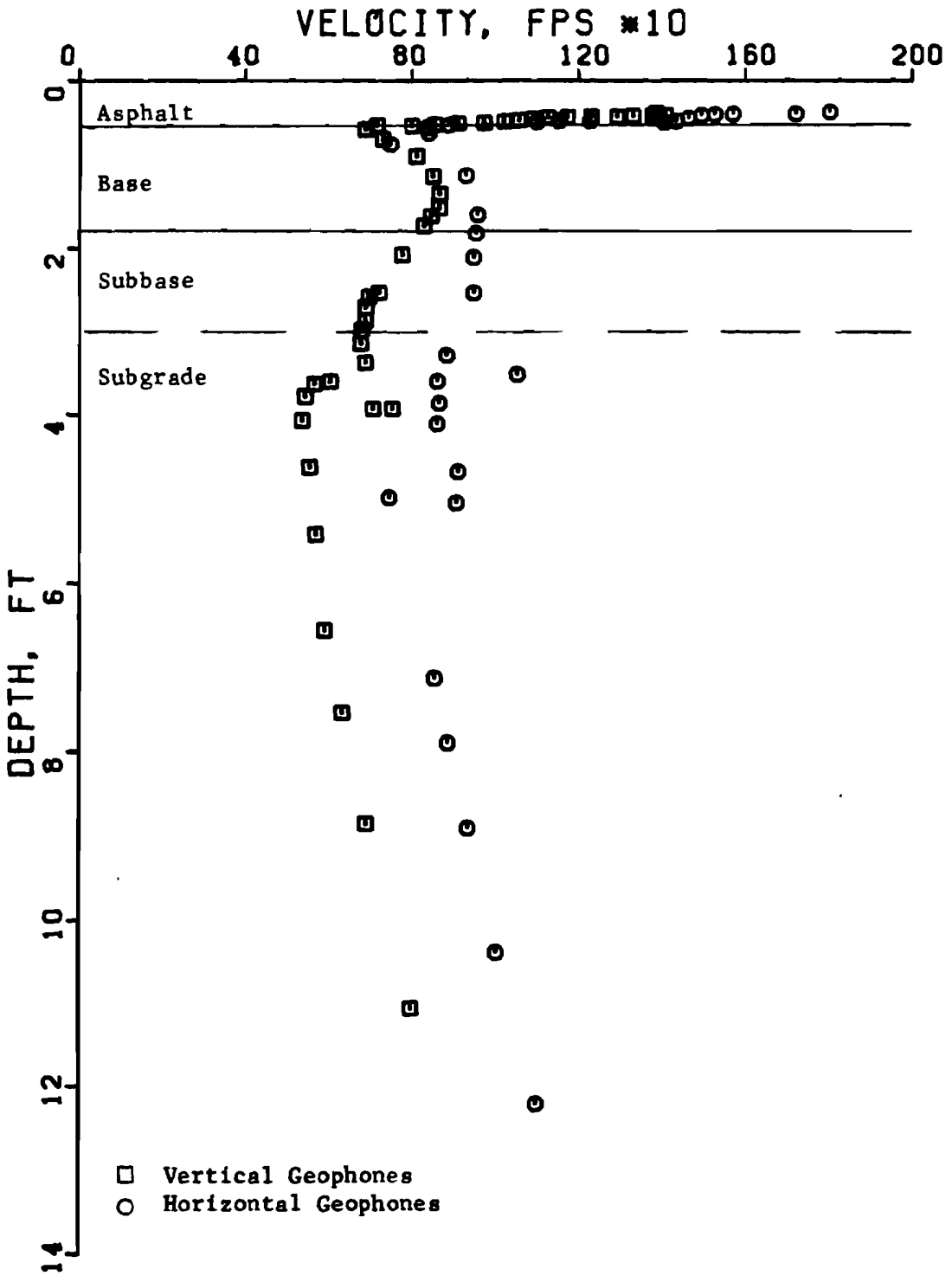

Fig 6.6. Comparison of velocity profiles obtained with vertical and horizontal geophones using the Drop Hammer source.

Analysis of the Falling Weight Deflectometer

The complete time history of the falling weight is shown in Fig 6.7a. The signal was recorded from a geophone attached to the base of the FWD. The signal was triggered (t = 0) with the initial downward hit of the weight. A pre-trigger delay was used to capture the "negative time" part of the signal. (The use of a pre-trigger delay to capture the signal is discussed in Appendix A). The small upward displacement at approximately t = -0.25 sec is due to the slight rebound of the base plate when the weight is released to undergo free fall. Multiple impacts occur for about eight or nine rebounds of the weight. These additional impacts do not interfere with the initial pavement response, because all data is collected from each impulse before the next impulse occurs. The time interval for a wave travelling from 2 to 10 ft (0.6 to 3.0 m) is on the order of 10 milliseconds, whereas the interval time between the first and second impacts of the weight is approximately 450 milliseconds.

The Fourier transform of the time signal, the linear spectrum, is shown in Fig 6.7b. The major frequency component excited by the falling weight is approximately 21 Hz. This corresponds quite closely to the pulse created by the first trough of the signal in the time domain. This pulse width is approximately 25 milliseconds, yielding a predominant period T = 50 milliseconds, or a predominant frequency of 20 Hz. The level of excitation greatly decreases with increasing frequencies.

The response of the pavement using the FWD for measurement V2-V5 is shown in Fig 6.8. Both the transfer function and the cross spectrum indicate that most of the response centers about the predominant frequency of

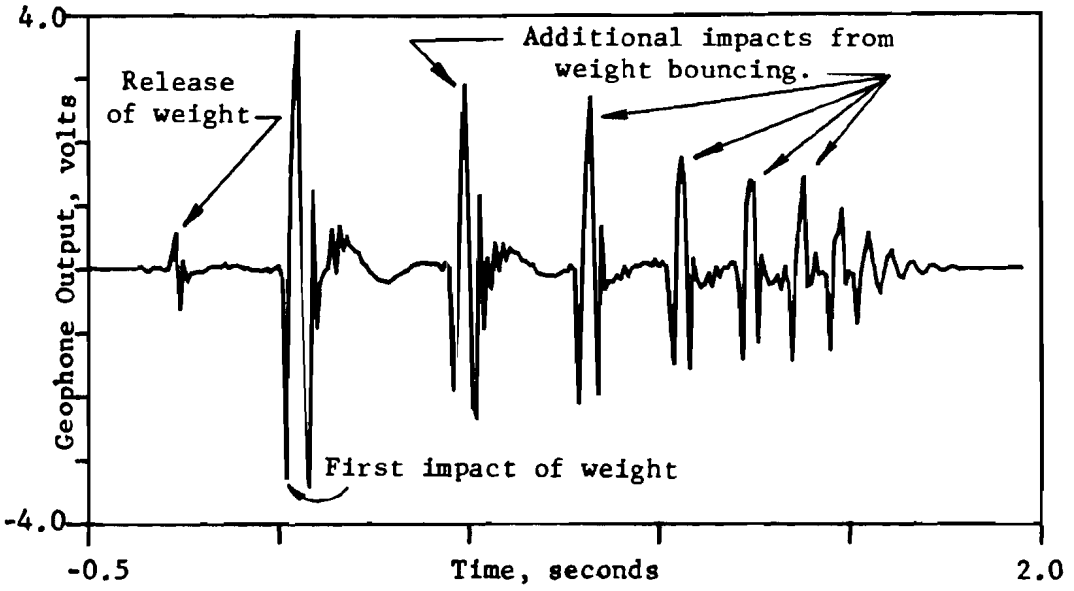

(a) Time-history of motion

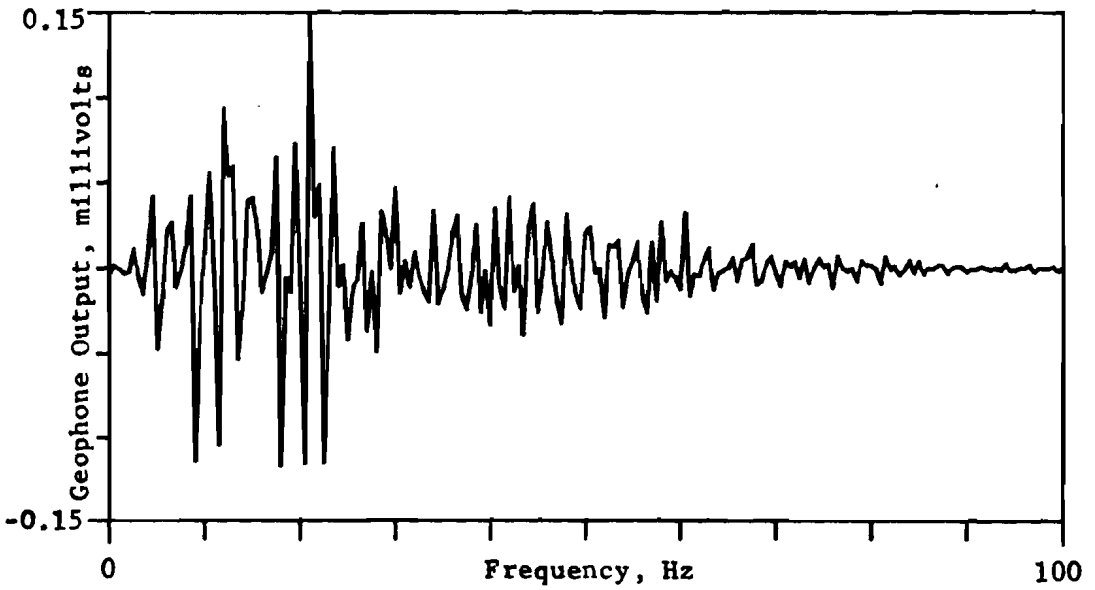

(b) Linear spectrum of motion

Fig 6.7. Impulsive loading created by the Falling Weight Deflectometer.

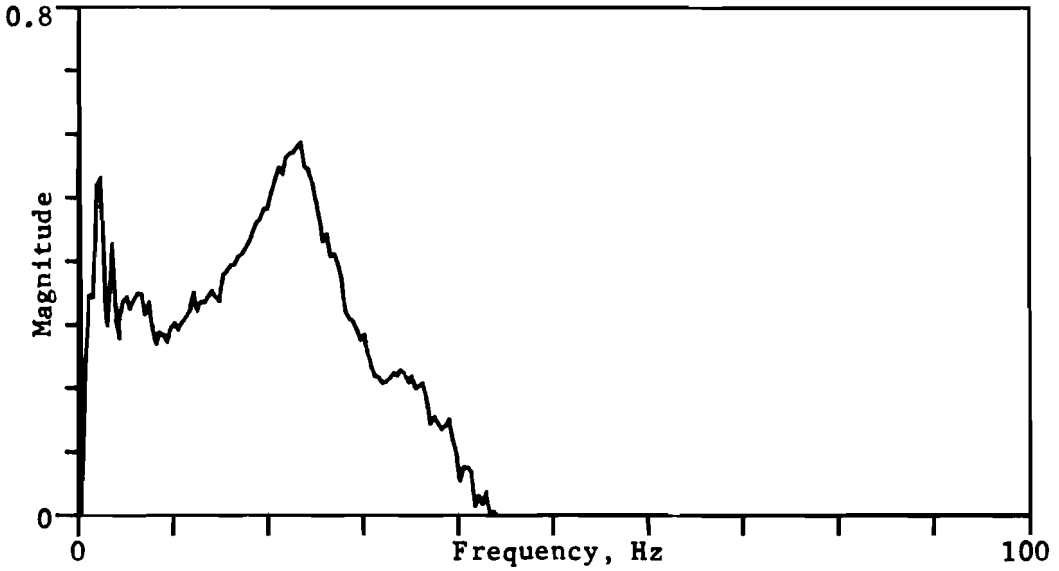

(a) Transfer Function

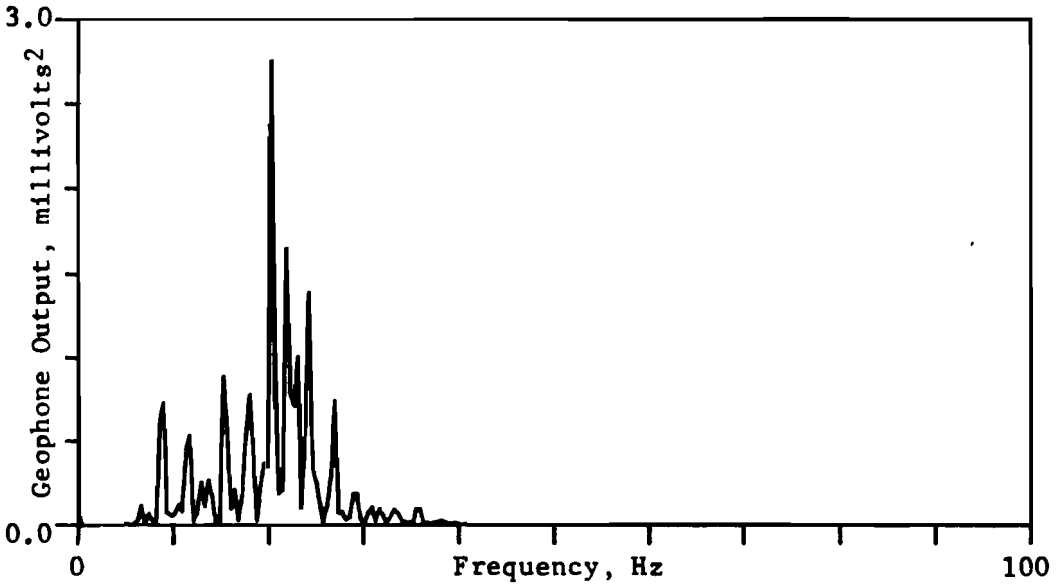

(b) Cross Spectrum

Fig 6.8. Pavement Response for measurement V2-V5 using the FWD source.

excitation of the source itself (21 Hz). Similar responses were obtained for other combinations of receivers.

The velocity profile for measurements with the FWD was determined from phase information of the cross spectrum obtained from plots such as the one in Fig 6.5a. A typical set of calculations is shown in Table 6.2. Depths given in the table were calculated using the one-third wavelength criterion. The resulting profile is shown in Fig 6.9.

There is some scatter in the velocities for measurement V1-V2. This scatter may be due to the fact that the geophones are located too close to the source to sample properly the wavelengths which travel primarily in the base and subgrade. As a result, the phase difference is small between the two geophones, and the measurement is more sensitive to the experimental limitations of the spectral analyzer (see Chapter 4). Also, the longer wavelengths will not have travelled far enough to be influenced adequately by the material properties at a depth which the wave(s) supposedly sampled. The velocities will then be overweighted by the material properties near the surface, particularly by the higher-velocity asphalt surface layer.

Based on Fig 6.9, R-wave velocities in the base and subgrade were estimated to be 800 fps (270 m/sec) and 580 fps (175 m/sec), respectively. In the zone where the base course grades into the sandy subbase, the velocity contrast is not as distinct, but it appears that a reasonable estimate of the R-wave velocity in the subbase is about 700 fps (215 m/sec). Velocities could not be determined (with the FWD as the source) for the upper 15 in. (38 cm) of the profile. For typical velocities of pavement materials, the FWD cannot excite frequencies high enough to generate the short wavelengths needed to sample the upper layers.

TABLE 6.2. CALCULATIONS FROM THE PHASE OF THE CROSS SPECTRUM FOR DETERMINING THE VELOCITY VERSUS DEPTH PROFILE

DISTANCE BETWEEN GEOPHONES = 8.104 FEET

FREQUENCY (HZ)	PHASE (DEGREES)	TRAVEL TIME (MSEC)	VELOCITY (FPS)	WAVELENGTH (FT)	DEPTH L/3 (FT)
12,000	18.35	4.248	1907.9	158.992	52,997
14,000	16.57	3.288	2465.0	176.071	58,690
16,000	17.17	2.981	2718.7	169.919	56,640
18,000	24.98	3.855	2102.3	116.793	38,931
20,000	34.31	4.765	1700.7	85.034	28,345
22,000	50.11	6.327	1280.9	58.222	19,407
24,000	81.28	9.407	861.5	35.894	11,965
26,000	109.30	11.677	694.0	26.693	8,898
28,000	130.89	12.985	624.1	22.290	7,430
30,000	149.44	13.837	585.7	19.523	6,508
32,000	164.78	14.304	566.6	17.705	5,902
34,000	175.84	14.366	564.1	16.592	5,531
36,000	179.80	13.873	584.1	16.226	5,409
38,000	187.92	13.737	590.0	15.525	5,175
40,000	198.78	13.804	587.1	14.677	4,892
45,000	228.95	14.133	573.4	12.743	4,248
50,000	248.71	13.817	586.5	11.731	3,910
54,000	275.96	14.195	570.9	10.572	3,524
59,750	293.72	13.655	593.5	9.933	3,311
65,000	300.91	12.859	630.2	9.696	3,232
69,500	300.18	11.998	675.5	9.719	3,240
75,000	310.71	11.508	704.2	9.390	3,130
79,000	323.33	11.369	712.8	9.023	3,008
83,000	343.29	11.489	705.4	8.499	2,833
90,000	361.33	11.152	726.7	8.074	2,691
95,000	374.94	10.963	739.2	7.781	2,594
100.000	388.62	10.795	750.7	7.507	2.502

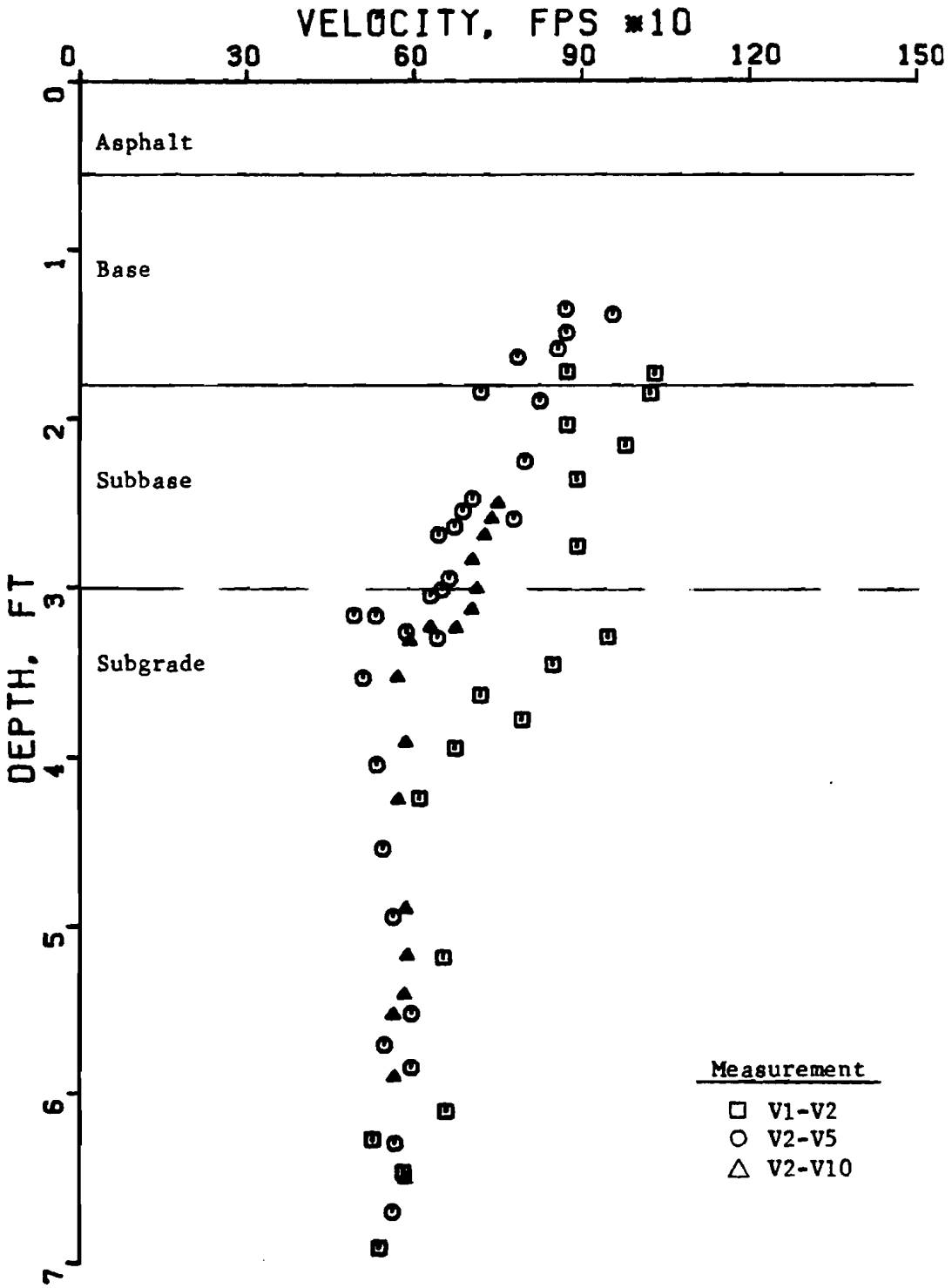

Fig 6.9. Velocity profile obtained from measurements using the FWD source.

Previously, it was shown that the level of excitation of the FWD decreased with increasing frequency (Figs 6.7 and 6.8). This trend is illustrated even more clearly by comparison of the autospectrum over different bandwidths shown in Fig 6.10. Nearly all of the energy of excitation is contained within 100 Hz and essentially no frequencies are excited above 250 Hz. Figure 6.11 shows the cross spectrum and coherence for measurement V2-V5 over a 1600-Hz bandwidth. Above 250 Hz, the phase of the cross spectrum becomes erratic. Similarly, the coherence displays irregularities above 250 Hz. These plots indicate that the FWD does not sufficiently excite the necessary frequencies to test the entire pavement system.

Analysis of the Drop Hammer

Measurements with the drop hammer source were made using one pair of horizontal geophones, H2-H5, and one pair of vertical geophones, V2-V5. Figure 6.12 shows the autospectrum of the signal at geophone V2. The magnitude indicates that all of the frequencies up to about 1600 Hz are sufficiently excited to determine a valid pavement response for all layers of the system. The phase of cross spectrum and the coherence function for measurement V2-V5 are shown in Fig 6.13. Although the cross spectrum looks fine up to 1600 Hz, the coherence function drops off sharply at about 1300 to 1400 Hz, suggesting that data above 1300 Hz should be used with caution.

The velocity versus depth profile is shown in Fig 6.14. This profile is based on the phase information from measurement V2-V5 (Fig 6.13a) and is plotted using $L_R/3$ as the depth criterion.

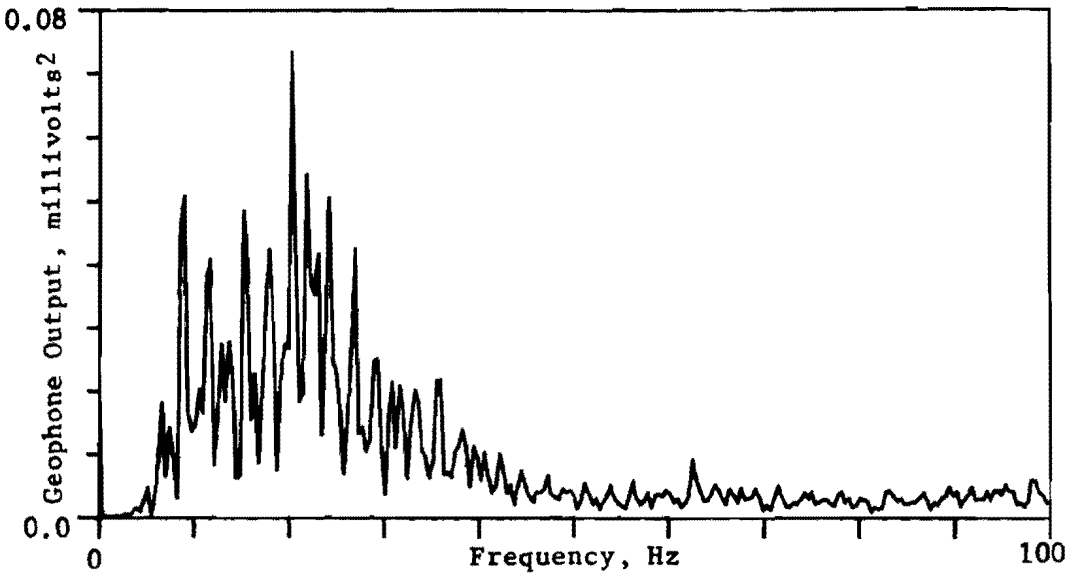

(a) Bandwidth equal to 100 Hz

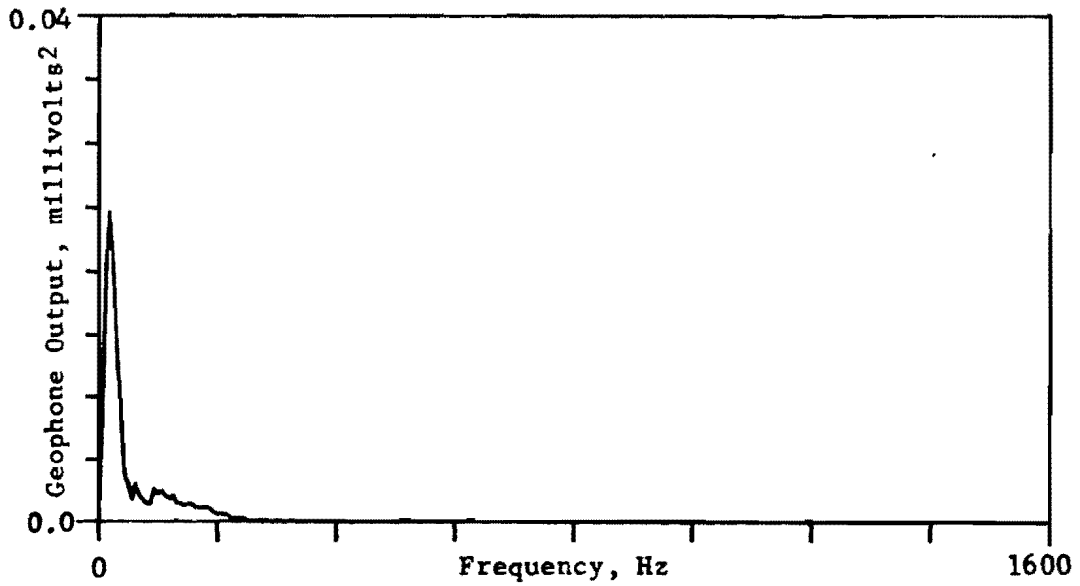

(b) Bandwidth equal to 1600 Hz

Fig 6.10. Comparison of autospectrums for geophone V2 for different measurement bandwidths using the FWD source.

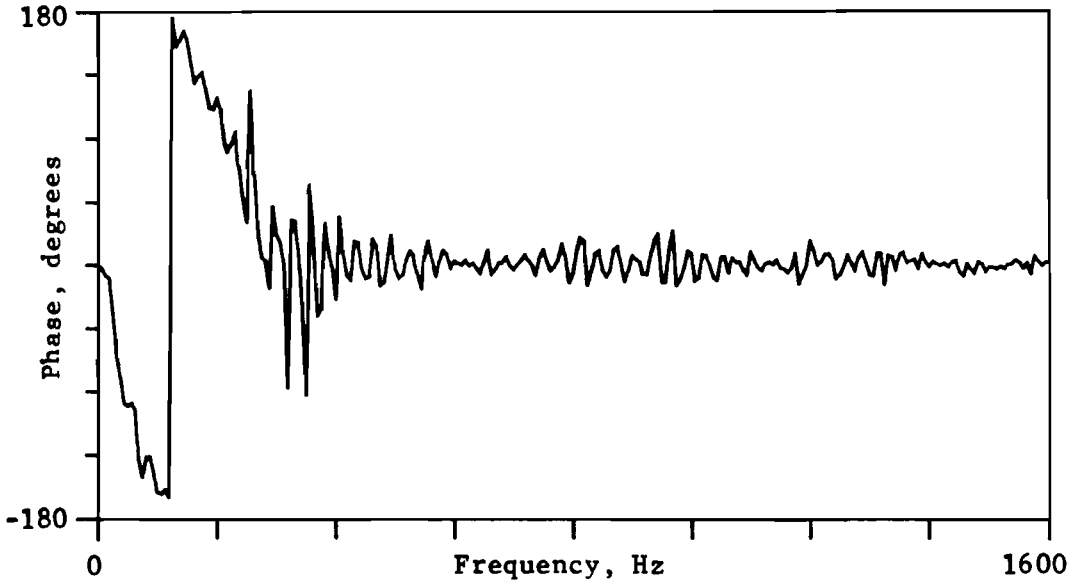

(a) Phase of cross spectrum

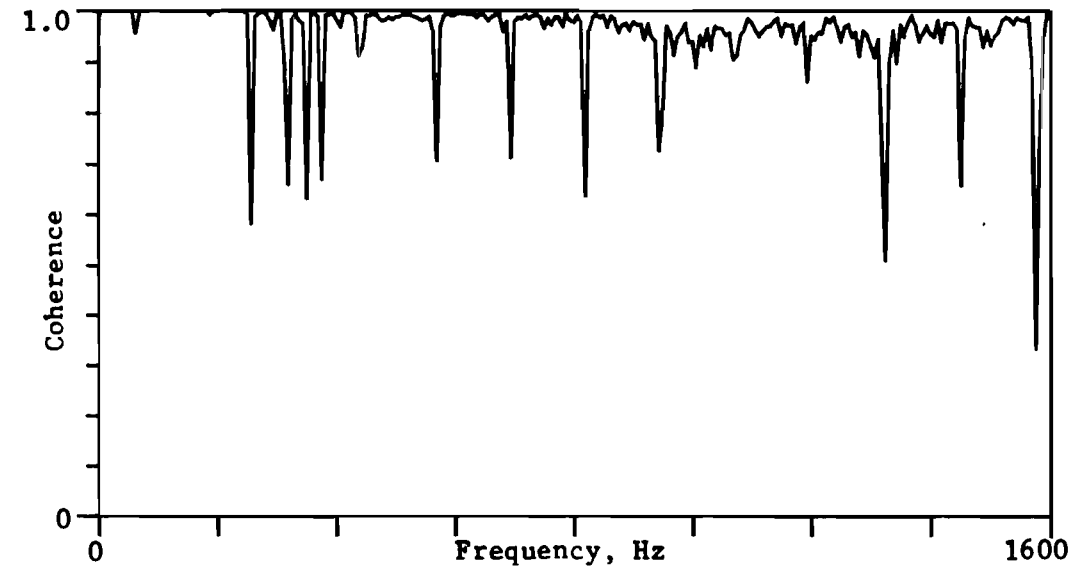

(b) Coherence function

Fig 6.11. Cross spectrum phase and coherence function for measurement V2-V5 using the FWD source.

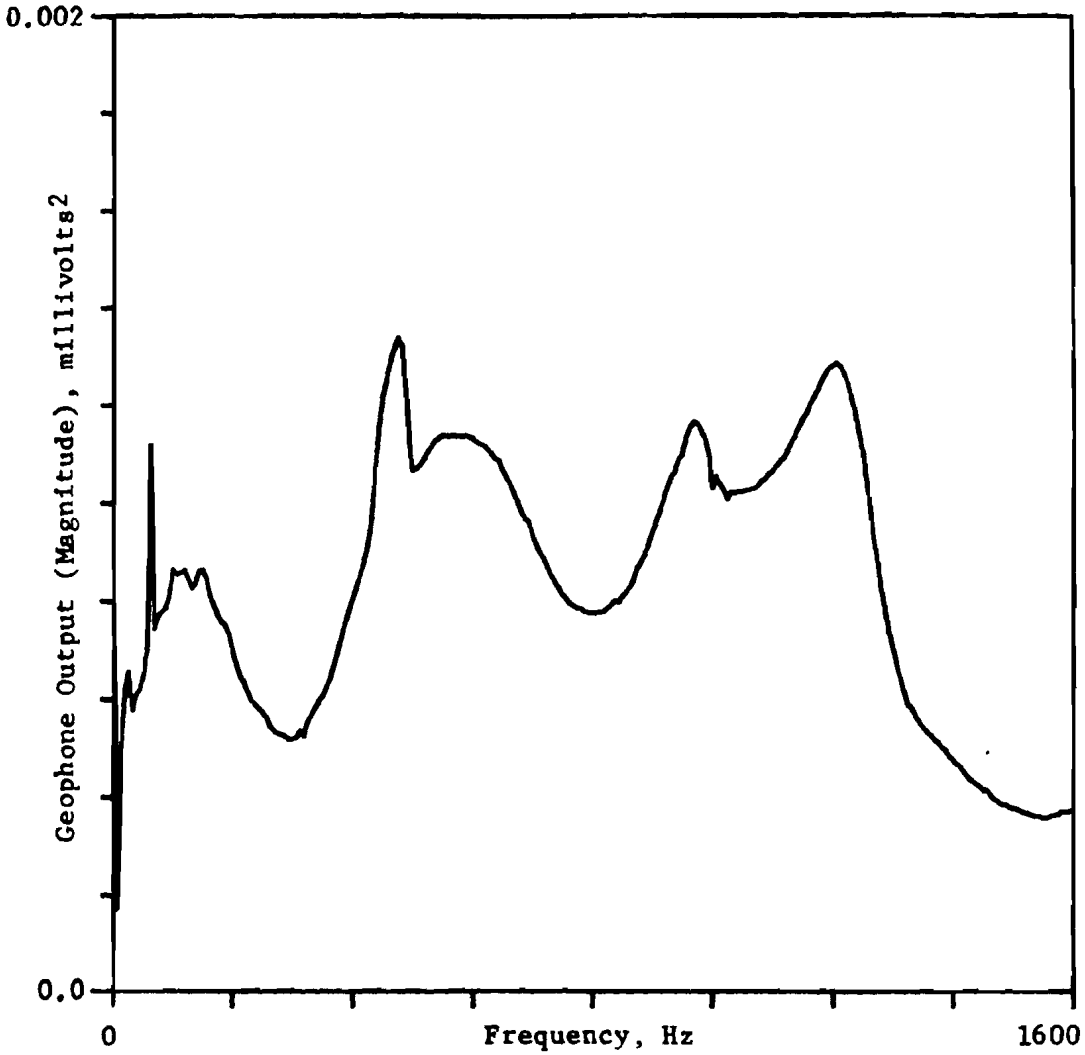

Fig 6.12. Magnitude of the autospectrum for geophone V2 using the Drop Hammer source.

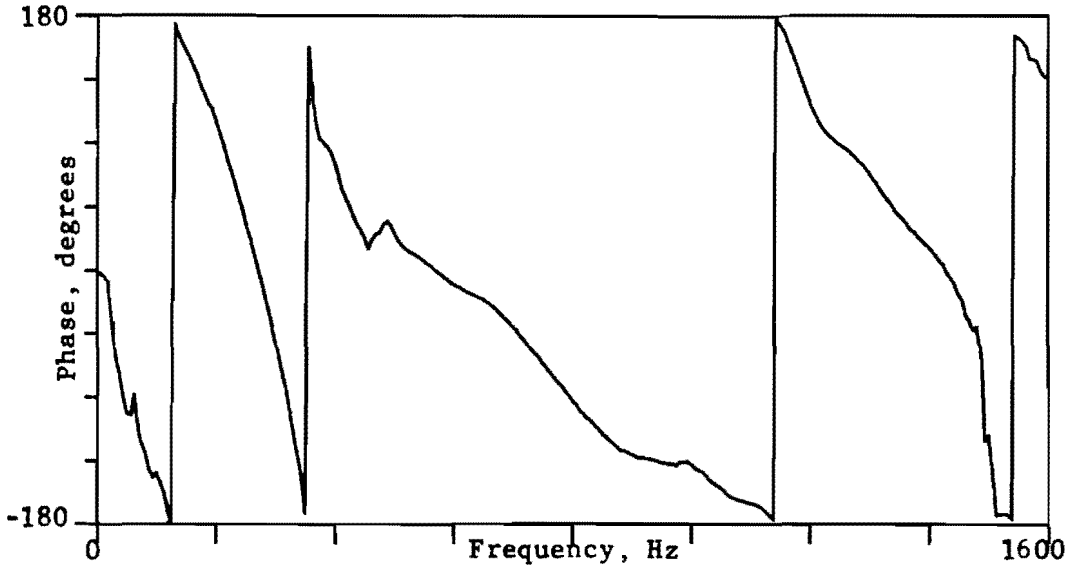

(a) Phase of the cross spectrum

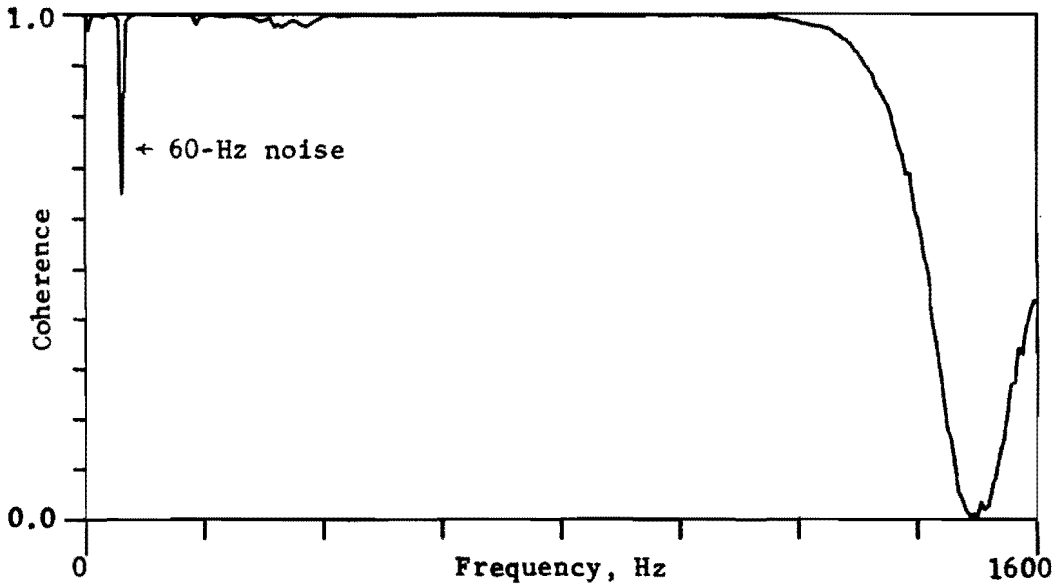

(b) Coherence function

Fig 6.13. Cross spectrum phase and coherence function for measurement V2-V5 using the Drop Hammer source.

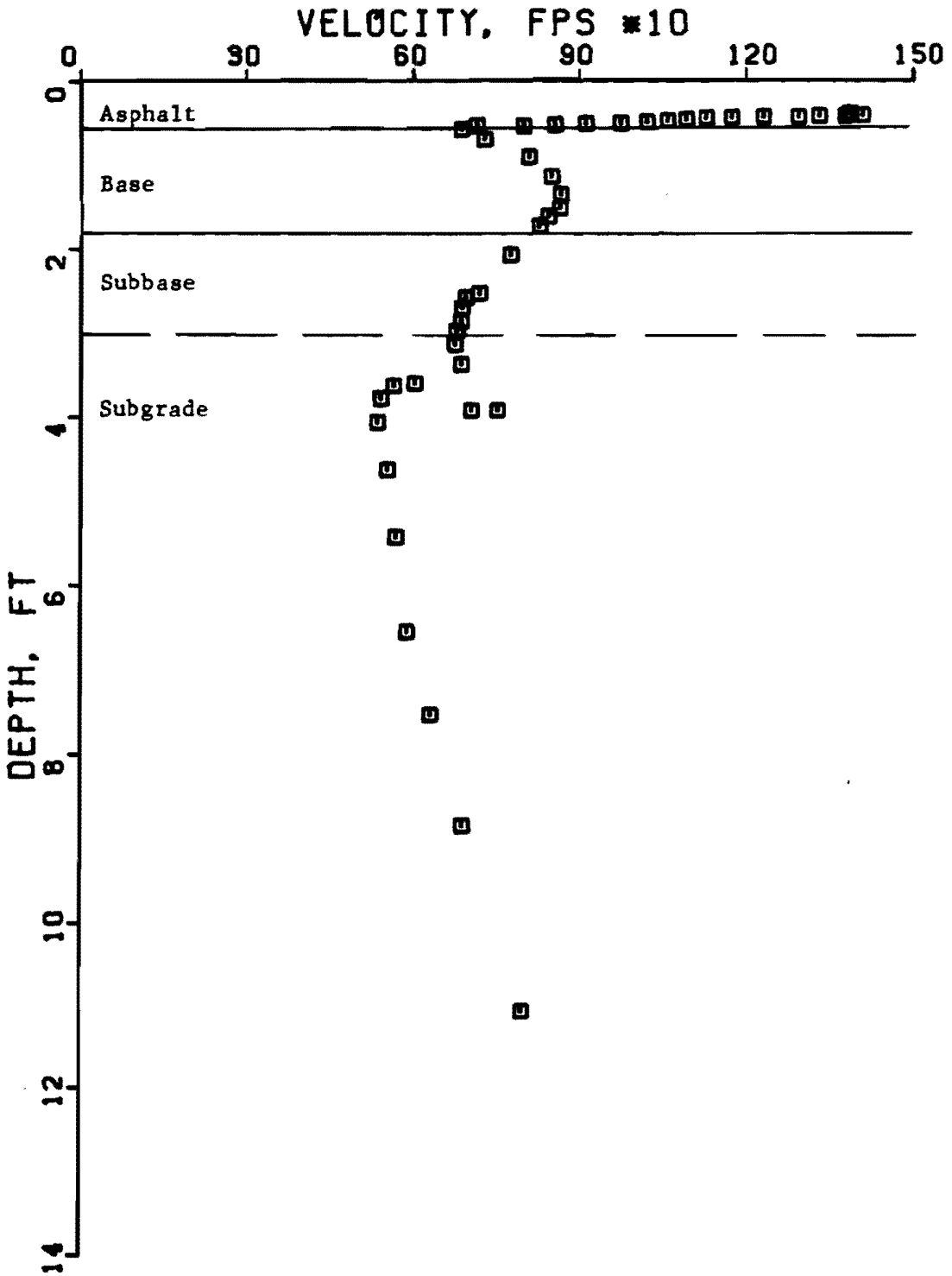

Fig 6.14. Velocity profile obtained using the Drop Hammer source.

The layering in the velocity profile (based on velocity contrasts) correlates well with the actual profile when the cross spectrum velocities are plotted at a depth of $L_R/3$. The subbase can be readily identified as a separate layer. The subgrade shows an increase in velocity with depth which probably is due to the influence of the underlying, higher-velocity rock. Based on the profile in Fig 6.14, R-wave velocities were estimated as 1400, 860, 690, and 560 fps (425, 260, 210, and 170 m/sec) for the surface layer, base, subbase, and subgrade, respectively.

Comparison of the FWD and the Drop Hammer

The usefulness of an impact hammer for measuring wave velocities depends on how well the hammer excites the frequencies required to analyze the pavement system. Figure 6.15 contains the Fourier transforms, or linear spectrums, of the wave pulse generated by the FWD and the drop hammer sources. The dashed lines in part (a) are the limits of the plot in part (b). The FWD focuses its excitation energy about 20 to 25 Hz, while the drop hammer does a significantly better job of exciting frequencies over the entire 1600-Hz bandwidth. Similar trends were shown in the autospectrums for both vertical and horizontal receivers at various distances from the source.

Figure 6.16 compares the magnitude of the cross spectrums for measurement V2-V5 for the FWD and the drop hammer. Based on areas under the plots in Fig 6.16, the total energy in the cross spectrum of the FWD is roughly 35 times the energy in the cross spectrum of the drop hammer. However, this is not a critical factor, since total energy is only an indirect index of the stress level induced by the impact. More important is the relative distribution of the energy. As expected from previous

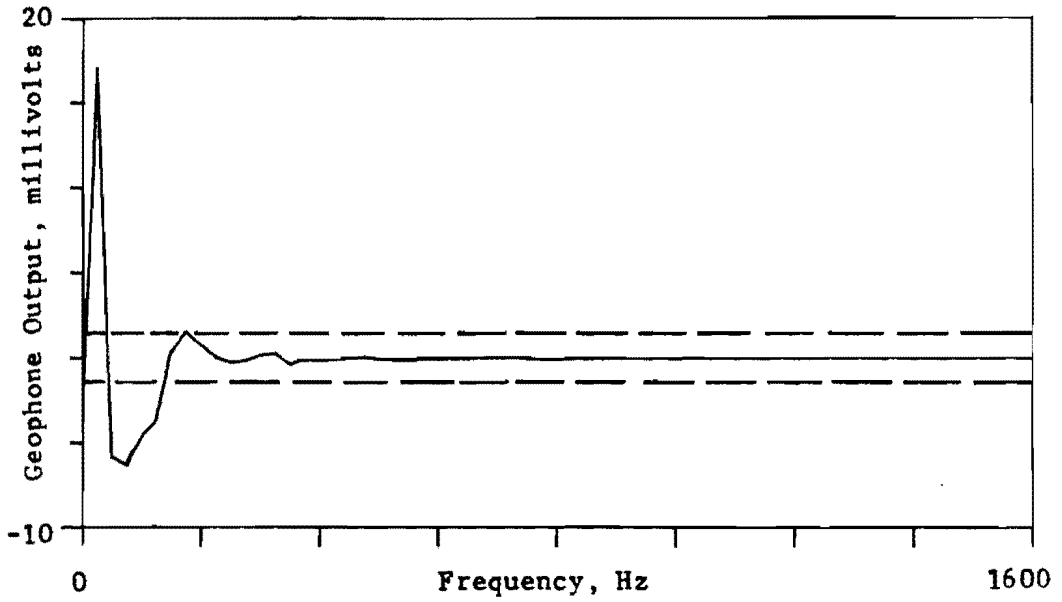

(a) Falling Weight Deflectometer

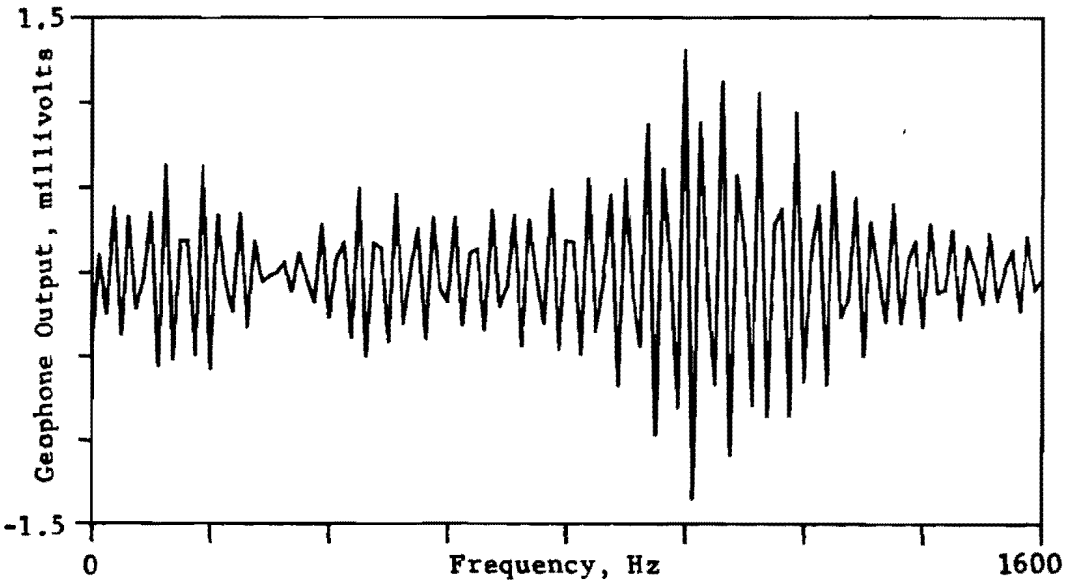

(b) Drop hammer source

Fig 6.15. Comparison of the linear spectrums for different sources.

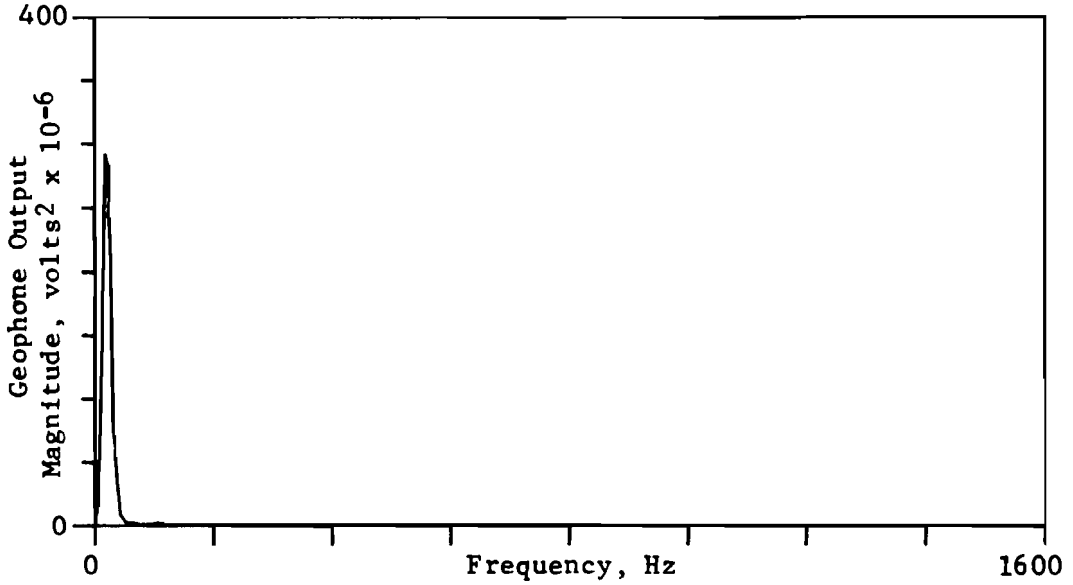

(a) Falling Weight Deflectometer

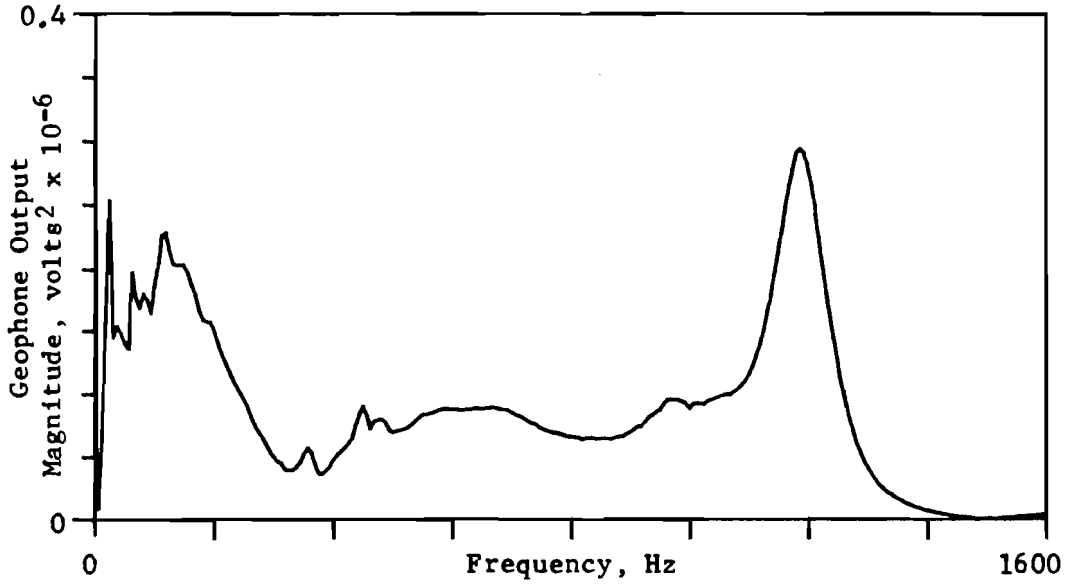

(b) Drop hammer source

Fig 6.16. Comparison of the magnitudes of the cross spectrums for measurement V2-V5 using different sources.

examination of the autospectrum, the energy of excitation is distributed better by the drop hammer. Over 98 percent of the energy in the FWD spectrum is contained within the first 100 Hz of the band, whereas only 11 percent of the energy in the drop hammer spectrum is contained in the first 100 Hz of the band.

Another comparison involves the phase of the cross spectrum. Figure 6.17a indicates that the FWD does not provide discernible information above 250 Hz, while Fig 6.17b shows that the drop hammer provides unambiguous data over the entire 1600-Hz bandwidth. As noted previously, the FWD cannot adequately sample the surface layer. Although the FWD is a good impulse source for deflection measurements due to its high stress levels, the drop hammer is better suited for determination of wave velocities in the surface layers.

The R-wave velocities obtained from the FWD and the drop hammer sources are listed in Table 6.3. Despite the large difference in the input energy, the velocities obtained from measurements using the two sources are virtually the same. This suggests that a large, heavy source is not necessary for determining wave velocities or moduli. In addition, over the range of stresses induced by the drop hammer up to those induced by the FWD, the moduli of the materials are not stress (or strain) sensitive. Average values of the R-wave velocities were determined from which S-wave velocities were calculated. The shear wave velocities in Table 6.3 are based on cross spectrum (surface) measurements and can be compared directly with the shear wave velocities from crosshole tests presented in the next section.

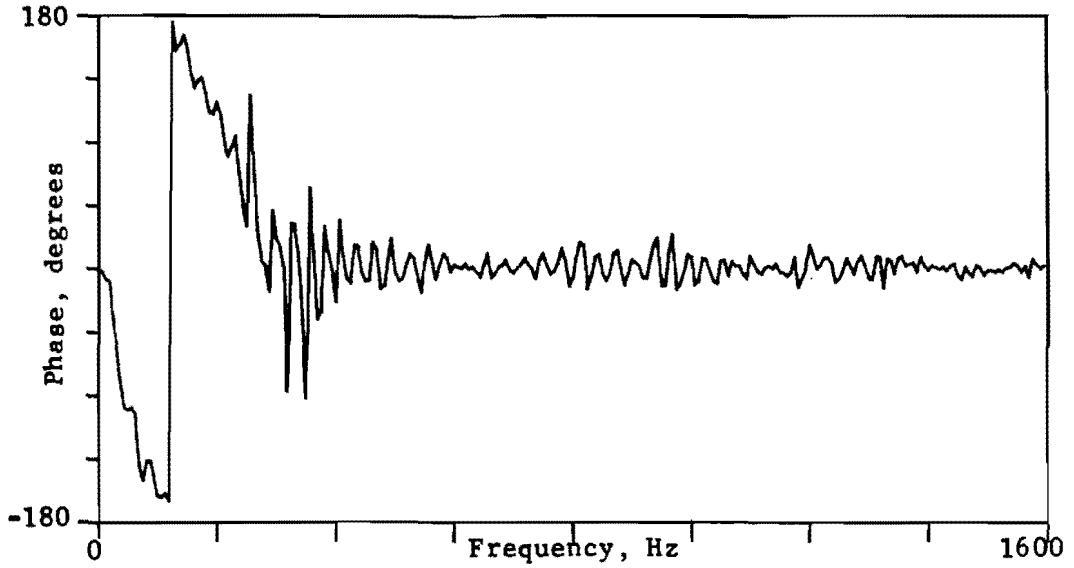

(a) Falling Weight Deflectometer.

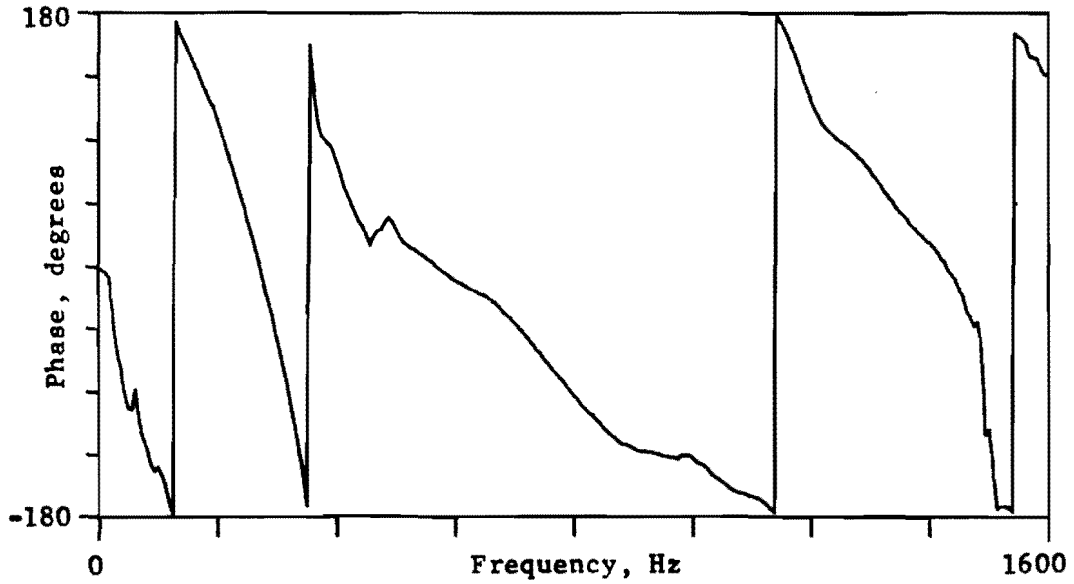

(b) Drop hammer source.

Fig 6.17. Comparison of the phase of the cross spectrums for measurement V2-V5 using different sources.

TABLE 6.3. SUMMARY OF R-WAVE VELOCITIES DETERMINED FROM CROSS SPECTRUM MEASUREMENTS AT AUSTIN (IH 35) SITE

Material	Approximate Thickness (in.)	Unit Weight (pcf)	Poisson's Ratio	R-Wave Velocity (fps)			S-Wave Velocity (fps)
				FWD	Drop Hammer	Average	
Asphalt	6.5	145	0.35	-	1400	1400	1500
Base	15	140	0.40	880	860	870	925
Subbase	12 to 15	135	0.40	700	690	695	740
Subgrade	120	115	0.40	580	560	570	605

RESULTS FROM CROSSHOLE TESTING

Crosshole testing was conducted at the Austin site approximately four months after the surface measurements were made. During the interim period, the right lane of northbound IH 35 remained closed to traffic. Thus, both sets of measurements were performed on the section as constructed. The following paragraphs briefly describe aspects of crosshole testing particular to the Austin site. A more general discussion of the crosshole seismic method is presented by Stokoe and Hoar (Ref 12).

Description of Test Procedure

A diagram of the crosshole test setup is shown in Fig 6.18. The boreholes were advanced in stages so that both the source(s) and geophones could be situated at the bottom of the holes for selected depths, as shown in Fig 6.18. Two holes, approximately 8 ft (2.4 m) apart, were drilled to a depth of about 12.5 to 13 ft (3.8 to 4.0 m). One of these holes served as the source hole for measurements made in the subbase and subgrade. The other hole served as the receiver (geophone) hole. An additional hole, located 4 ft (1.2 m) from the receiver hole, was drilled to a depth of approximately 1.5 ft (0.5 m) and served as a source hole for measurements in the asphalt and base course. This additional source hole was used to avoid refracted waves from the higher-velocity surface layer.

Two sources were used to generate body waves (P- and S-waves) in the various layers. Within 1.5 ft (0.5 m) of the surface, the drop hammer was used. The drop hammer was placed so that its base plate rested on the bottom of the hole. Measurements were triggered with an RC trigger. Below 1.5 ft

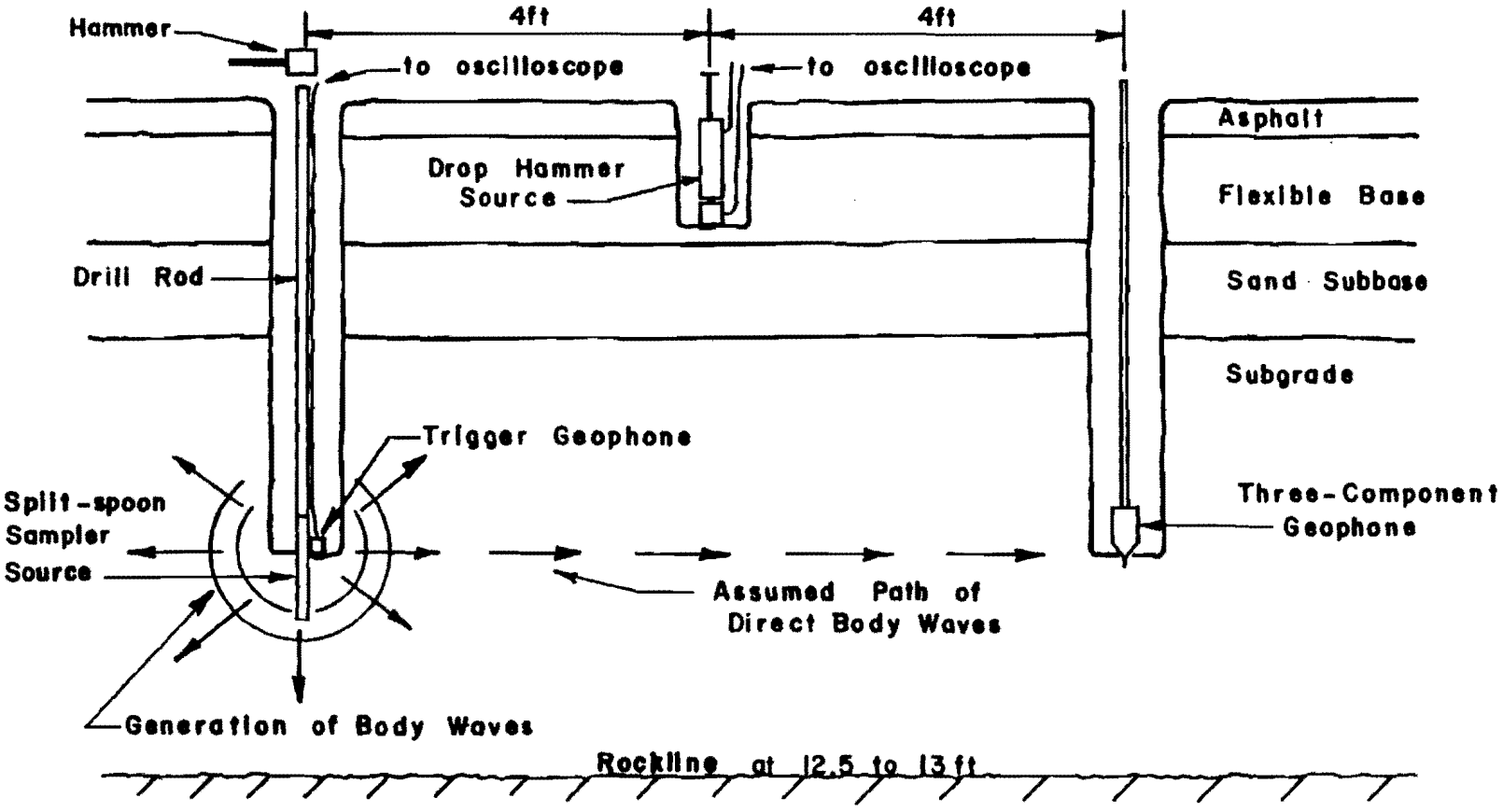

Fig 6.18. Schematic diagram of crosshole test setup.

(0.5 m), a split-spoon sampler attached to the end of the drill rod was used as the source. For a given measurement, the source hole was advanced slightly less than the receiver hole. Then, the split-spoon sampler was driven into the soil about 6 in. (15 cm) so that the source and geophones were at essentially the same depth. Measurements were triggered by the signal from a geophone fixed to the spoon at the point where the wave energy from the hammer pulse was generated in the soil.

A package of three geophones was enclosed in a single case which was attached to the bottom of a rod used to lower the geophones into the borehole. The geophone case rested on the bottom of the borehole and was coupled to the soil by means of a short, steel spike. One geophone was oriented in the vertical direction and was used to determine the arrival of the S-wave. Another geophone was oriented in the horizontal (longitudinal) direction and was used to determine the arrival of the P-wave. The third geophone, oriented in the horizontal (transverse) direction, was not used in the testing. The depths at which the geophones were located are listed in Table 6.4.

The time records of the wave pulses were recorded with the Nicolet digital oscilloscope and were stored on magnetic floppy disks. One record of the S-wave arrival and one record of the P-wave arrival were obtained at each measurement depth.

Analysis of Crosshole Data

Velocities for both P-waves and S-waves were calculated from direct arrival times. For measurements using the drop hammer, t=0 was defined by the time at which the hammer impacted the base of the source. For

TABLE 6.4. SUMMARY OF CROSSHOLE TEST RESULTS AT AUSTIN (III 35) SITE

Material	Depth (ft)	S-Wave Velocity (fps)	P-Wave Velocity (fps)	V_S/V_P	Poisson's Ratio
Asphalt	0.33	1610	5230	0.308	0.45
Base	1.17	801	1980	0.405	0.40
	1.46	826	1810	0.456	0.37
	1.46	843	1970	0.428	0.39
Subbase-Dense Sand	2.21	753	1160	0.649	0.14
	2.96	733	1130	0.649	0.14
Subgrade-Stiff Clay	3.79	483	1130	0.427	0.39
	4.92	523	1370	0.381	0.41
	7.04	577	1480	0.390	0.41
Silty Clay	9.33	679	1740	0.390	0.41
	11.29	-	5000	(Water Table at 10 ft)	
Rock	13.04	3110	7730	0.402	0.40

measurements using the split-spoon sampler, t=0 was defined by the time at which the wave pulse excited the trigger geophone. Direct arrival times were then based on the elapsed time between the initial excitation of the trigger geophone and the initial arrival point of the wave at the geophone in the receiver borehole.

A typical record for S-wave analysis is shown in Fig 6.19. The upper, irregular trace represents the response of the trigger geophone. The initial excitation is described by the sharp, downward break and this point defines t=0. The lower, smoother trace represents the motion recorded by the vertical geophone in the receiver borehole. The arrival of the S-wave is defined by the first, large, downward break in the wave pulse. For the measurement shown in Fig 6.19, the distance between the source and receiver was 7.96 ft (2.43 m), and the direct arrival time was determined as 10.86 milliseconds, yielding an S-wave velocity of 733 fps (224 m/s).

The results of the crosshole tests (both P- and S-wave velocities) are summarized in Table 6.4. Using calculated ratios of V_S/V_P and Table 2.1, estimates were obtained for Poisson's ratios of the various materials in the pavement system. For the base course and the subgrade, Poisson's ratios determined from this approach agreed quite closely with those assumed for the respective materials (see Fig 6.2). For the dense sand (subbase), the Poisson's ratio was found to be 0.14, which is considerably lower than the assumed value (0.40). However, the value of 0.14 is not unlikely for a dense sand undergoing low shearing strains. In either case, the difference in shear wave velocities (converted from the R-wave velocity as a function of Poisson's ratio) is less than 5 percent, and the difference in moduli is only about 10 percent. For consistency, a value of 0.40 was used for all calculations involving the subbase.

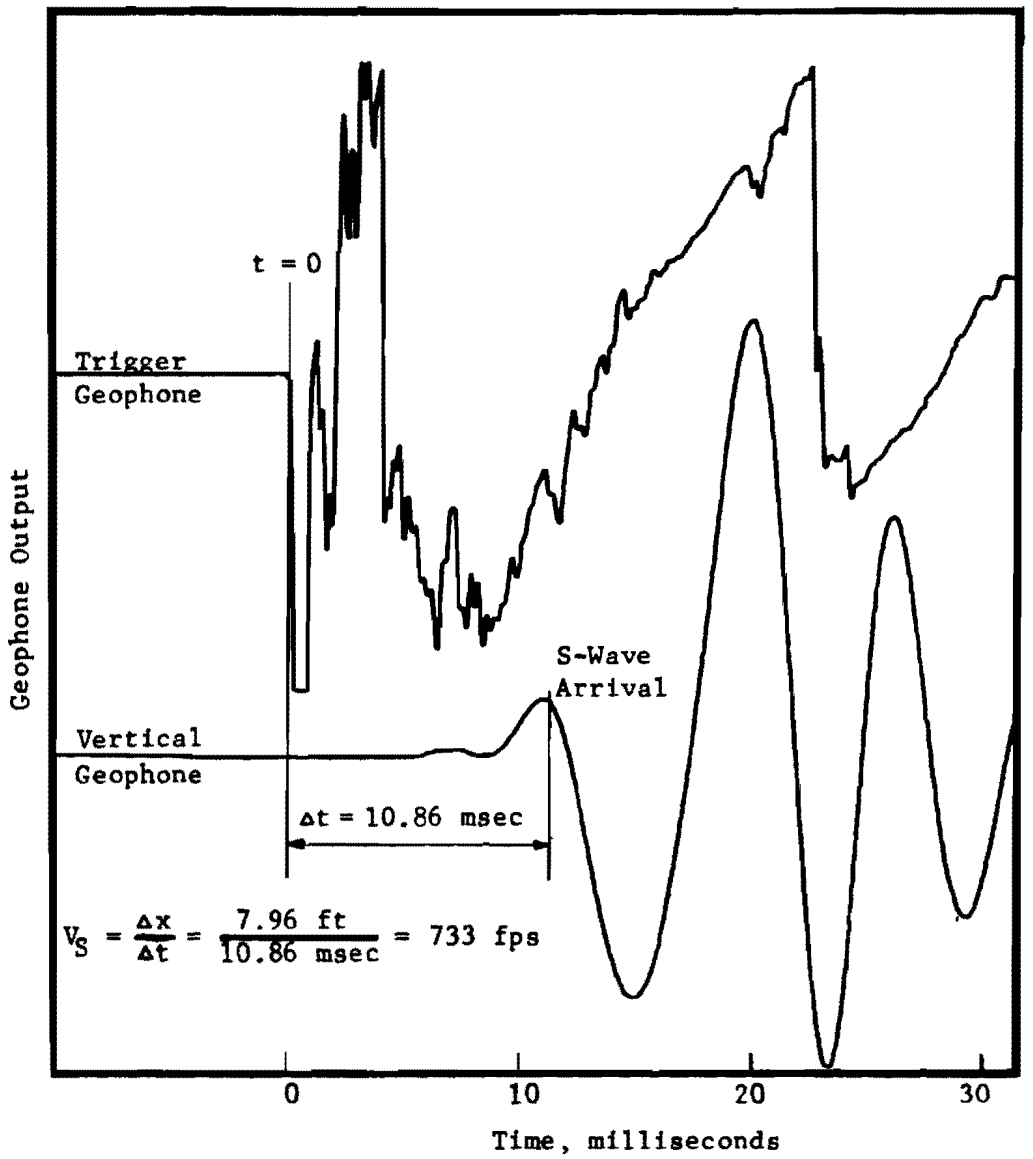

Fig 6.19. Determination of shear wave velocity from crosshole data.

Poisson's ratio determined for the asphalt (using V_R/V_S) is 0.45, which is somewhat higher than the range typically assumed for asphalt ($0.25 \leq \nu \leq 0.35$). One possible reason for this difference is the difficulty in measuring an accurate value for the P-wave velocity. Since the P-wave velocity is relatively high in the asphalt and the distance between the source and the geophone is only a few feet, the travel time of the wave pulse is quite short. Therefore, any errors introduced by triggering which lead to an inaccurate definition of t=0 may significantly effect determination of the travel time. In view of this possibility, and an apparent P-wave velocity of 3180 fps (970 m/s) from the measurement shown in Fig 6.4a, it appears that the P-wave velocity of 5230 fps (1594 m/s) obtained from crosshole testing is not correct. Using V_P = 3180 fps (970 m/s) in the asphalt, the ratio of V_S/V_P is 0.506, which in turn yields a Poisson's ratio of 0.33 from Table 2.1. It seems, then, that the assumed value of Poisson's ratio (0.35) is valid, and this value is used for all calculations involving the asphalt layer.

The crosshole S-wave velocities listed in Table 6.4 are plotted and compared with the velocity profile obtained from cross spectrum measurements in Fig 6.20. The R-wave velocities from cross spectrum measurements were converted to S-wave velocities using the appropriate relationship of V_R/ V_S (as a function of Poisson's ratio) listed in Table 2.1. Figure 6.20 indicates that the cross spectrum velocities agree quite well with the crosshole velocities.

A further comparison that includes S-wave velocities from both methods is presented in Table 6.5. Average values of V_S from cross spectrum measurements (from Table 6.3) and average values of V_S from crosshole tests (determined from Table 6.4) are compared for each material at the site. The

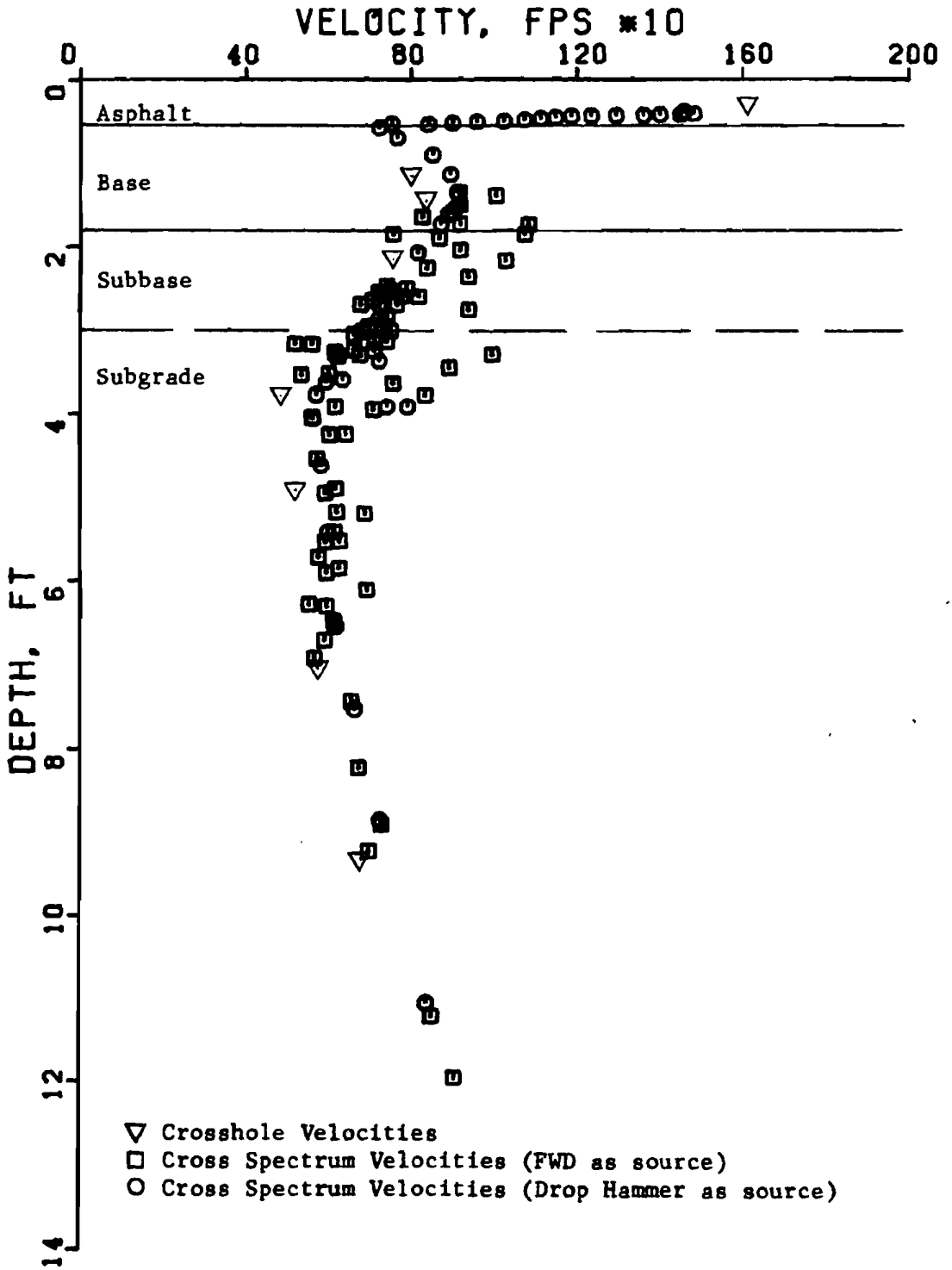

Fig 6.20. Comparison of crosshole velocities with shear wave velocity profile obtained using cross spectrum (surface) measurements.

TABLE 6.5. COMPARISON BETWEEN S-WAVE VELOCITIES FROM CROSS SPECTRUM MEASUREMENTS VERSUS CROSSHOLE TESTS

Material	S-Wave Velocity (fps)		Percent Difference
	Cross Spectrum Measurements	Crosshole Tests	
Asphalt	1500	1610	6.8
Base	925	823	12.4
Subbase	740	743	0.4
Subgrade	605	565	7.1

TABLE 6.6. COMPARISON BETWEEN ELASTIC MODULI CALCULATED FROM WAVE VELOCITIES VERSUS DEFLECTION MEASUREMENTS (ELSYM5)

Material	Shear Modulus (psi)	Young's Modulus, E (psi)	
		Wave Propagation	Deflection Method*
Asphalt	70,000	190,000	250,000
Base	26,000	72,000	108,000
Subbase	16,000	45,000	40,000
Subgrade	9,000	25,000	17,000

*Moduli were backcalculated from fitted deflection basin using elastic theory (ELSYM5).

difference in velocities ranges from as little as 0.4 percent to no more than 12.4 percent, with an average difference of about 7 percent. These differences are certainly acceptable for engineering applications, suggesting that the surface technique using cross spectrum measurements is a reliable way to obtain the shear wave velocity profile.

DETERMINATION OF MODULI

Based on the shear wave velocities listed in Table 6.3, a shear modulus was calculated for each layer using Eq 2.6. Young's modulus was then calculated from Eq 2.3 using the Poisson's ratios given in Table 6.3. The moduli based on wave propagation (cross spectrum velocities) are listed in Table 6.6. The Young's modulus for each layer fall in the range of moduli typical of the respective materials.

Young's moduli were also determined from deflection measurements provided by the Dynaflect device operated by the Texas State Department of Highways and Public Transportation (SDHPT). Moduli are backcalculated using a computer program (ELSYMS) which incorporates elastic layer theory. The moduli are obtained by a trial-and-error solution which converges when the calculated deflection basin matches (within a given tolerance) the deflection basin measured under the Dynaflect loading.

The analysis at the Austin site (provided by SDHPT) incorporated four layers: asphalt surface, flexible base, sand subbase, and subgrade, with layer thicknesses of 6.5, 15, 15, and 120 inches, respectively. A rigid base was assumed on the basis of the rockline at approximately 13 ft. The moduli determined by the deflection method using ELSYM5 are listed in Table 6.6. These moduli differ by 11 to 33 percent from those calculated from wave

propagation velocities. This agreement is reasonably good, considering the markedly different approaches for determining Young's moduli.

Another way to compare the two methods is to use ELSYM5 to calculate deflections using the moduli determined by wave propagation and then compare those deflections with the measured (Dynaflect) deflections. The calculated deflection basin (for geophone locations of 0, 1, 2, 3, and 4 ft from the source point) was 0.53, 0.40, 0.26, 0.18, and 0.13 mils, respectively. These deflections were slightly less than the measured deflections, which were 0.53, 0.44, 0.32, 0.22, and 0.18 mils, respectively. The calculated deflections differ from the measured deflections by no more than 30 percent in the worst case. The calculated deflections appear to be lower than the measured deflections as a result of the stiffer modulus (relative to the one backcalculated by ELSYM5) associated with the subgrade.

The relatively good agreement between the moduli (or deflections) determined by the two methods indicates that the wave propagation method (using cross spectrum measurements) is a valid method for determining Young's moduli of the various layers in the pavement system. It should be noted that the wave propagation method does not require knowledge or assumptions about the layer thicknesses (which the ELSYM5 program requires), but in fact can provide a good approximation of layer thicknesses as a part of the analysis.

SUMMARY

Based on test results at the Austin pavement site, conclusions were obtained regarding geophones, sources, and the overall validity of the wave propagation (cross spectrum measurements) method to evaluate the moduli of a pavement system.

Comparisons between measurements using vertical and horizontal geophones indicate that vertical geophones are more desirable for determining Rayleigh-wave velocities. Horizontal geophones are much more sensitive to P-wave motion, and the result is velocities which are somewhat higher than those obtained from vertical geophones. Comparisons with crosshole test results indicate that measurements using vertical geophones agree closely with S-wave velocities measured with the crosshole method.

It also appears that some scatter may occur in the velocity profile if the location of the geophones from the source is not commensurate with the wavelengths being sampled. For pavement systems, which have higher-velocity layers at the surface, measurements using geophones spaced too closely to the source may yield velocities in the subgrade which are too high because the apparent long wavelengths have been overweighted by material properties of the surface layers. In general, by increasing the spacing of the geophones from the source, this problem can be eliminated or minimized.

Comparison measurements were also made using the Falling Weight Deflectometer and a drop hammer source. Over the range of frequencies (or wavelengths) excited by both sources, the velocity profiles agreed quite closely. Since the input energy of the two sources is significantly different, the close agreement suggests that the velocities (and moduli) are not stress-sensitive, at least up to and including the stresses generated by the FWD. However, the FWD could not excite frequencies high enough to sample the asphalt surface. The sharper, quicker impact of the drop hammer did generate the high frequencies needed to sample the asphalt. Based on these results, it appears that the significant criterion for a source is the range of frequencies which it can excite, and <u>not</u> the stress level induced by the impact.

Velocities obtained by cross spectrum measurements compare closely with crosshole velocities. The differences were not greater than 12.4 percent and averaged about 7 percent, which is quite acceptable for engineering purposes. These results indicate that the surface (cross spectrum) measurements provide a reasonably accurate shear wave velocity profile without drilling or coring. The good correlation in the subbase and subgrade indicates that the stiffer, upper layers in a flexible pavement system do not adversely effect the surface measurements.

A comparison of Young's moduli obtained from wave propagation velocities with the moduli from deflection measurements using ELSYM5 indicates that the wave propagation method (using spectral analysis) is a valid way to determine moduli. The differences in moduli ranged up to about 35 percent, which is quite good considering the markedly different approaches of the two methods. It is difficult to say which method is more accurate, although the wave propagation method seems more desirable, since it determines the moduli for each layer directly whereas the deflection method must find moduli by trial-and-error which yield deflections that match deflections measured from a composite influence of all the layers in the pavement system. In addition, it is not clear how well the elastic layer theory incorporated into ELSYM5 applies to low-strain, dynamic (transient) loading.

CHAPTER 7. PAVEMENT EVALUATION AT GRANGER SITE

SITE DESCRIPTION

The Granger site is located about 5 miles (8 km) east of Granger, Texas, on Farm to Market Road 971. The test section is located approximately 80 to 100 ft (24 to 30 m) east of the eastern abutment of a newly constructed bridge (Structure S19T50). The location of the site is shown in Fig 7.1.

The pavement section consists of a two-course surface treatment. The flexible base course consists of 11 in. (28 cm) of crushed limestone placed in two lifts with thicknesses of approximately 7 in. (18 cm) and 4 in. (10 cm). The subgrade is a compacted fill used to construct the embankments on either side of the bridge. The upper 6 in. (15 cm) of the subgrade is lime stabilized.

The embankment was constructed with approximately 18 to 20 ft (5.5 to 6.0 m) of compacted clay fill. The upper half of the fill was stiff tan clay (Taylor marl), while the lower half was stiff black clay (gumbo clay). The underlying natural soil is also gumbo clay. Construction of the embankment occurred in the spring of 1977. The fill was placed at a water content of approximately 27 percent and a dry unit weight of about 97 pcf.

The pavement and soil profile is shown in Fig 7.2. The unit weights and Poisson's ratios shown are estimated values typical of the construction materials which are used at the Granger site.

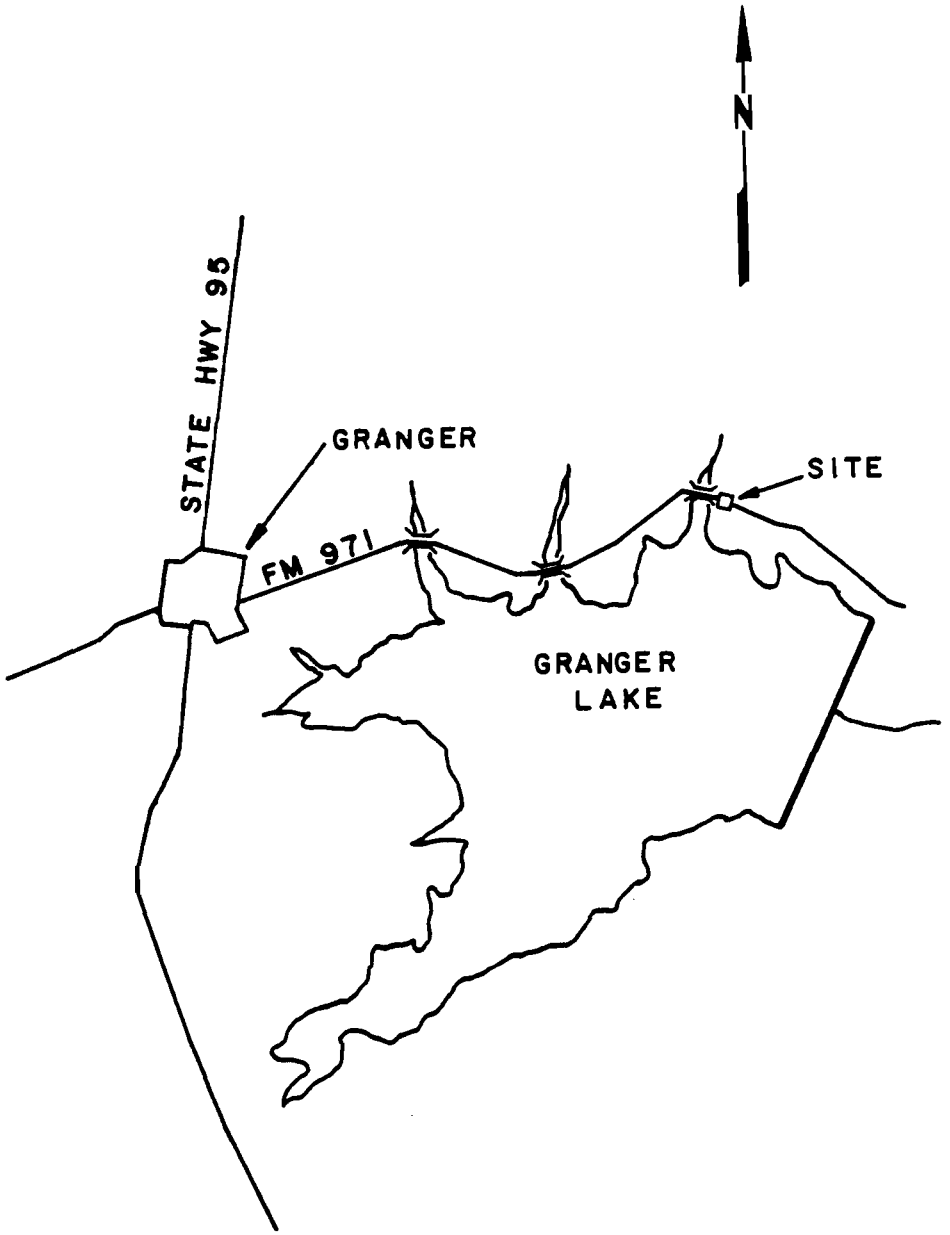

Fig 7.1. Location fo Granger (FM 971) pavement site.

Depth (ft)	Description of Material	Assumed Poisson's Ratio	Assumed Unit Weight (pcf)
0.085	Two-course surface treatment	0.30	145
1.0	Flexible base (total of 11 in.)	0.35	140
	6-in. lime-stabilized subgrade	0.40	125
	Compacted fill: stiff, tan clay (Taylor marl)	0.45	125
10	Compacted fill: stiff, tan and black clay (mixed)	0.45	125
12	Compacted fill: stiff, black clay (Gumbo clay)	0.45	125
19	Natural soil: firm, black clay (Gumbo clay)		

Fig 7.2. Longitudinal-section profile at Granger (FM 971) site.

EXPERIMENTAL PROCEDURE

The procedure used at the Granger site was similar to the procedure used at the IH 35 site and followed the general procedure discussed in Appendix A. The drop hammer was the only source of input energy used at the Granger site. Based on the results from the testing conducted at IH 35, which showed that horizontal geophones are too sensitive to undesirable P-wave energy, only vertical geophones were utilized. The geophones were mounted on steel blocks which were then epoxied to the pavement surface to permit adequate coupling.

Measurements were made with the geophones located along the centerline of the road and along the right (exterior) wheelpath of the eastbound lane. Table 7.1 contains a listing of the measurements including the distance from the source to the geophones and the bandwidth used for each measurement. Measurements along the centerline included a series of geophone spacings with the near geophone located 1 ft (0.3 m) from the source and a series of geophone spacings with the near geophone located midway between the source and the far geophone. Hereafter, measurements will be referred to by the location of the geophones from the source.

In addition, deflection readings were obtained from the Dynaflect device which was made available by the Texas State Department of Highways and Public Transportation (SDHPT). Measurements were performed at four locations along both the centerline and the right wheelpath. Data were collected at distances of 53, 78, 103, and 128 ft (16, 24, 31, and 39 m) from the bridge abutment. Results of these tests are presented herein.

TABLE 7.1. SUMMARY OF MEASUREMENTS AT THE GRANGER (FM 971) SITE

Record No. (Track No.)	Distance from Source to Geophones (ft)		Distance between Geophones (ft)	Location of Geophones	Number of Averages	Bandwidth of Spectrum (Hz)	Computer Data File Identification
	Near	Far					
5(1)	0.5	1.0	0.5	Centerline of Road	5	3200	SHGR1
14(1)	1.0	2.0	1.0	" " "	5	1600	SHGR6
19(1)	1.0	2.0	1.0	" " "	5	100	-
24(1)	1.0	2.0	1.0	" " "	5	400	-
25(1)	1.0	2.0	1.0	" " "	5	3200	-
31(1)	1.0	5.0	4.0	" " "	5	800	-
38(1)	1.0	5.0	4.0	" " "	5	400	SHGR7
43(1)	1.0	9.0	8.0	" " "	5	400	SHGR8
44(1)	1.0	9.0	8.0	" " "	5	50	-
50(1)	1.0	16.0	15.0	" " "	5	200	SHGR9
55(1)	8.0	16.0	8.0	" " "	5	200	SHGR4
60(1)	4.0	8.0	4.0	" " "	5	400	SHGR3
67(1)	2.0	4.0	2.0	" " "	5	400	SHGR2
74(1)	5.0	9.0	4.0	" " "	5	400	SHGR5
5(2)	5.0	9.0	4.0	Right Ext. Wheel Path	5	400	SHGR12
10(2)	1.0	5.0	4.0	" " " "	5	800	SHGR11
15(2)	1.0	2.0	1.0	" " " "	5	1600	SHGR10
20(2)	7.0	15.0	8.0	" " " "	5	400	SHGR13

DETERMINATION OF VELOCITY PROFILE

For comparative purposes, cross spectrum measurements were divided into three groups: measurements along the centerline of the road with the near geophone located midway between the source and far geophone, measurements along the centerline of the road with the near geophone fixed at a distance 1 ft (0.3 m) from the source, and measurements along the right wheelpath. Velocity profiles obtained from these three sets of measurements are shown in Figs 7.3, 7.4, and 7.5, respectively. These profiles include data over the entire frequency range for which interpretable phase information existed, regardless of the level of coherence for the measurements.

The velocity profiles shown in Figs 7.3 and 7.5 indicate that the R-wave velocity in the subgrade ranges from approximately 400 to 450 fps (120 to 140 m/sec) for measurements along the centerline of the road as well as along the wheelpath. However, the velocity profile shown in Fig 7.4 indicates that the R-wave velocity in the subgrade is somewhat higher, ranging from 450 to 700 fps (140 to 215 m/sec). This large difference is not a result of varying soil properties since the profile shown in Fig 7.3 represents the same centerline location. The difference is most likely related to the location of the pair of geophones, particularly the geophone nearer to the source. In the case where the near geophone is fixed close to the source (Fig 7.5), there is not a sufficient distance for the long wavelengths which sample the subgrade (L_R greater than about 6 ft, (2 m)) to disperse, i.e., separate and travel at a velocity commensurate with the material that the full wavelength would sample. As a result, the low-frequency waves are influenced disproportionately by the material near the surface. For pavement systems, the materials near the surface have higher velocities (more stiffness) than

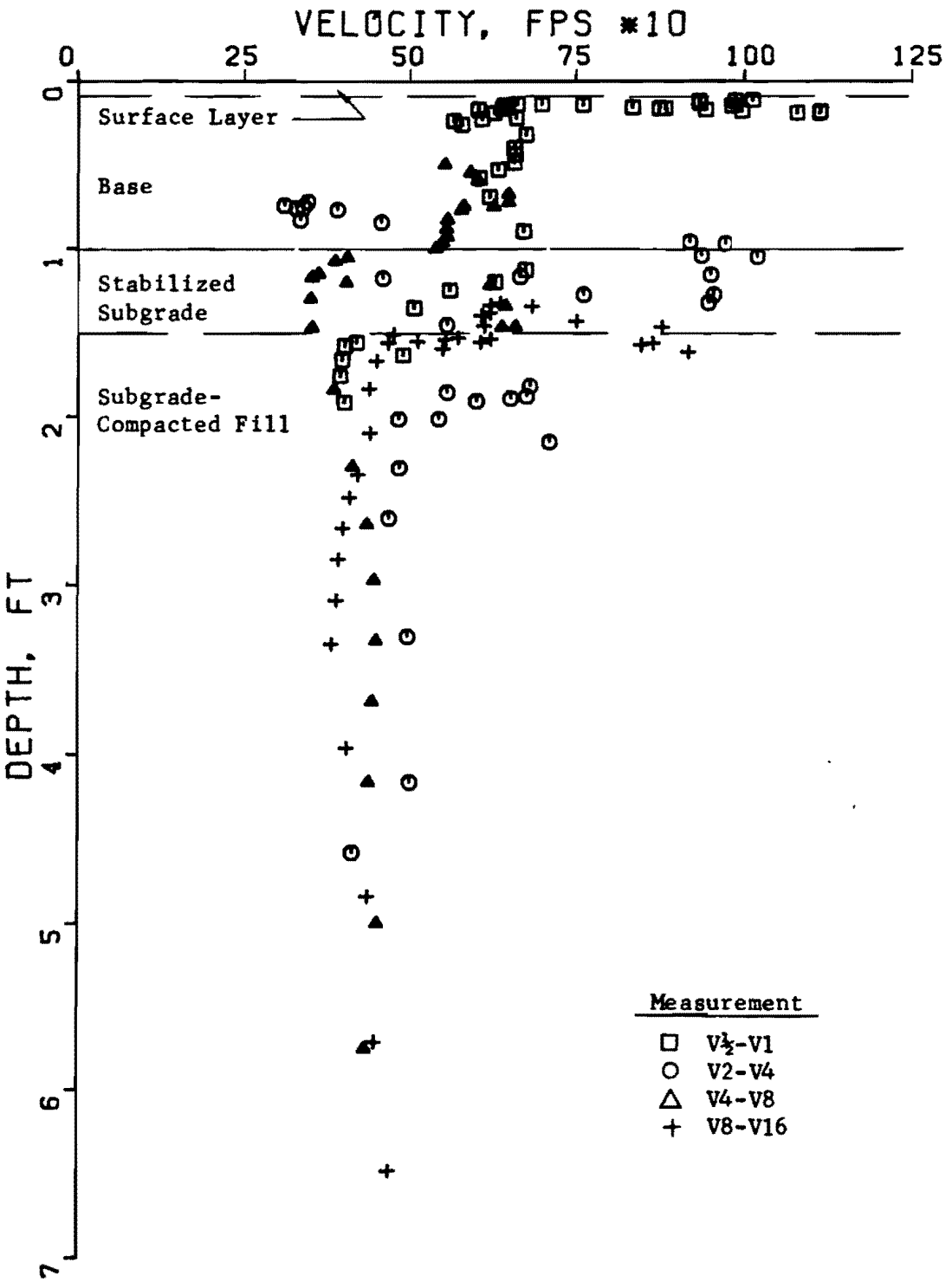

Fig 7.3. Unfiltered velocity profile for measurements along the centerline using equally spaced geophones.

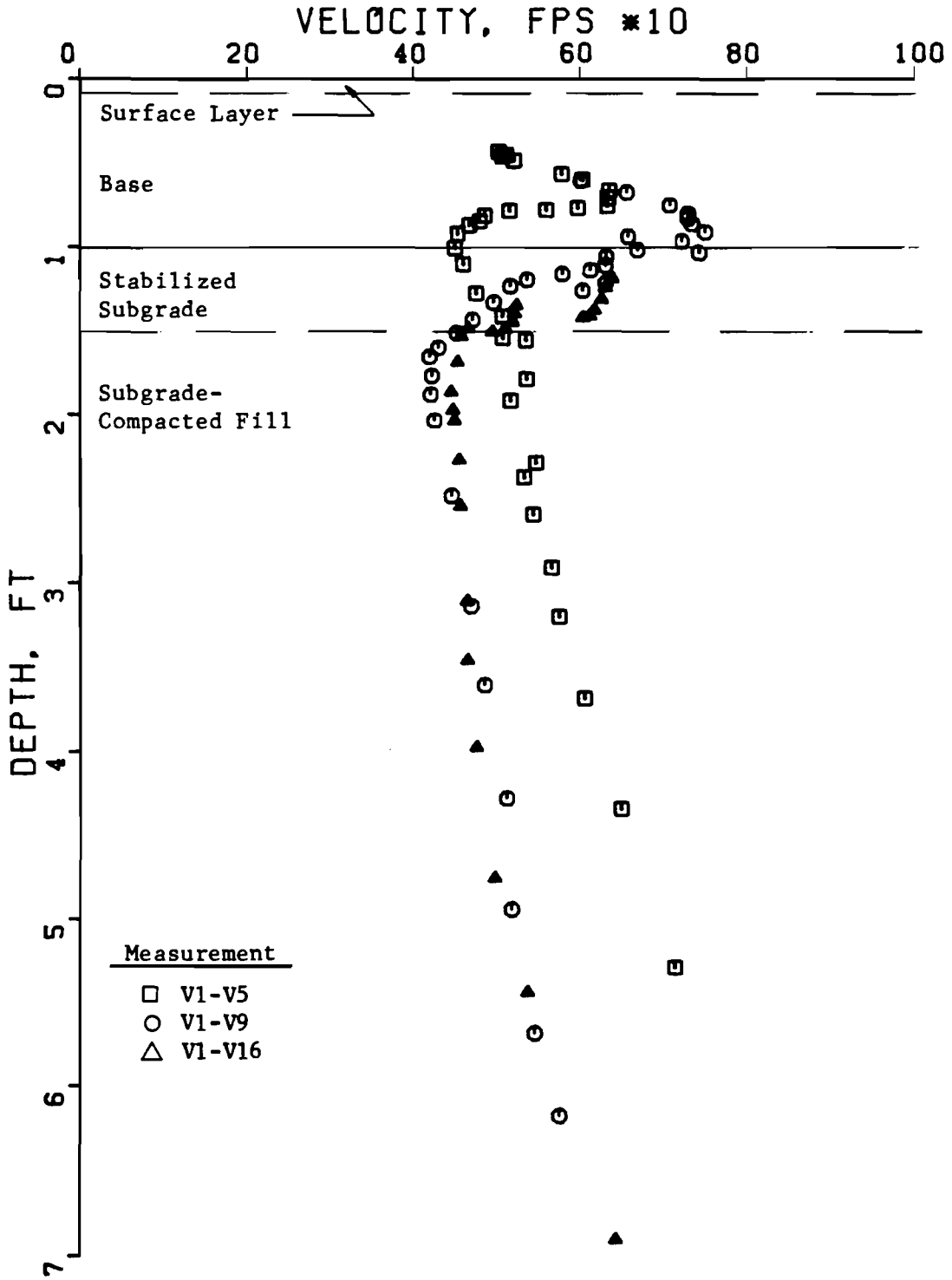

Fig 7.4. Unfiltered velocity profile for measurements along the centerline using a reference geophone located 1 ft from the source.

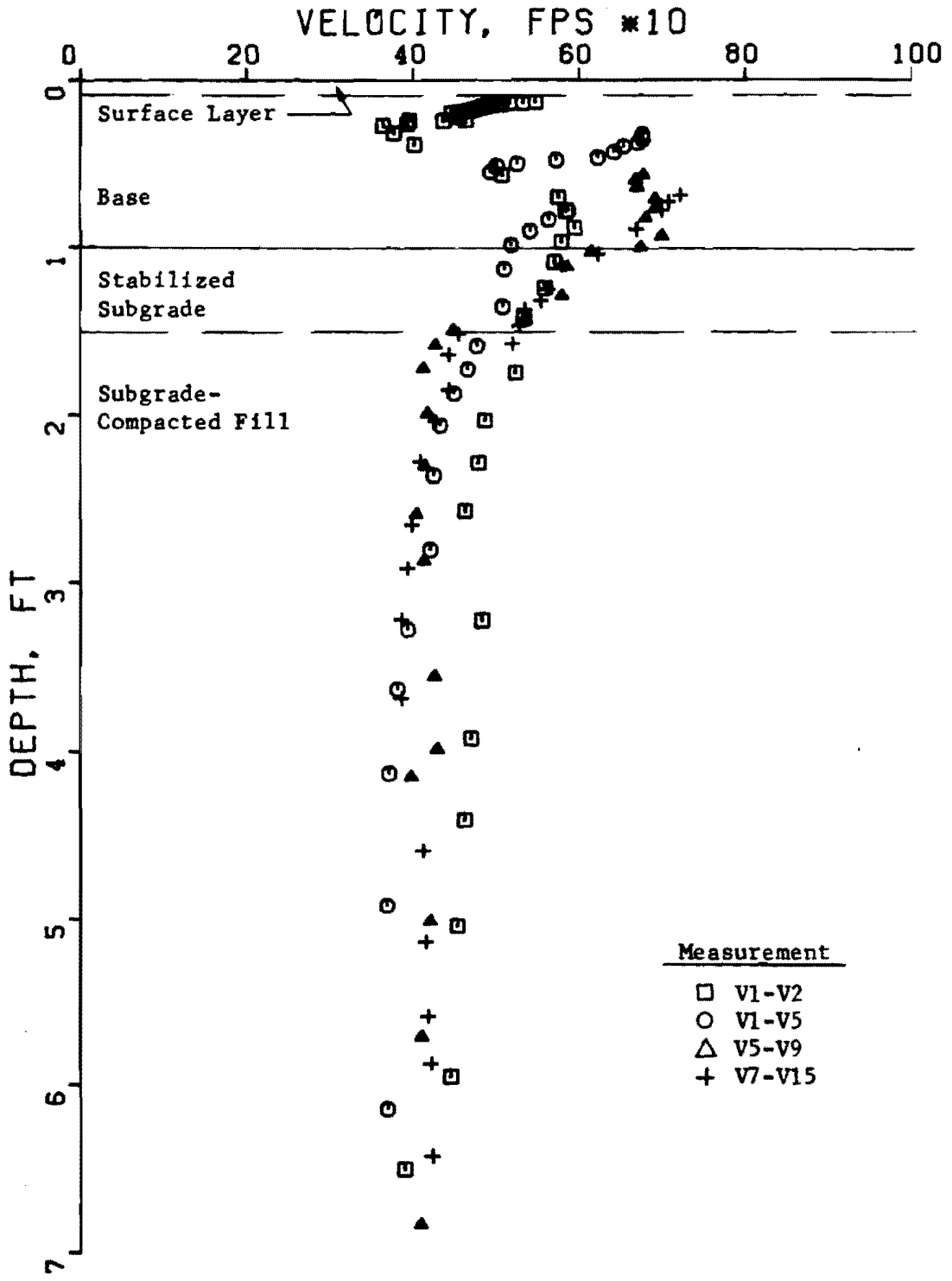

Fig 7.5. Unfiltered velocity profile for measurements along the right wheelpath.

the subgrade. Consequently, the apparent subgrade velocity will be higher than it should be when the near geophone is located an adequate distance from the source. This phenomenon is observed in Fig 7.4. The problem is minimized by locating the near geophone at an increasing distance from the source to sample increasing wavelengths (depths), such as shown in Fig 7.3.

All of the velocity profiles show considerable scatter within 2 ft (0.6 m) of the surface. The upper part of the profile contains several relatively thin layers having significantly different properties. For example, the layer boundary between the surface and the base course can be observed by the line of velocities plotted at about 0.1 to 0.15 ft (3.0 to 4.6 cm). This layer boundary is clearly shown in Fig 7.3 and is partially developed in Fig 7.5. However, the layer boundary between the base course and the subgrade can only be estimated. Because the section of lime-stabilized subgrade probably has a stiffness between that of the underlying nonstabilized subgrade and the overlying base course, the transition between layers is difficult to define.

The scatter in the upper part of the velocity profile is probably due to the presence of layering which causes some wavelengths to be reflected or refracted at layer boundaries. Reflected and refracted waves may influence the phase of the cross spectrum and, in turn, may complicate the interpretation of velocities which are based on direct travel distance between the geophones on the surface.

In general, the phase plots obtained at the Granger site were quite difficult to interpret. A typical example of the difficulty is shown in Fig 7.6a for measurement V4-V8. Over the range of frequencies from about 100 to 200 Hz, various "glitches" occur in the phase plot which are not normally expected in a more continuous relationship such as that shown over the range

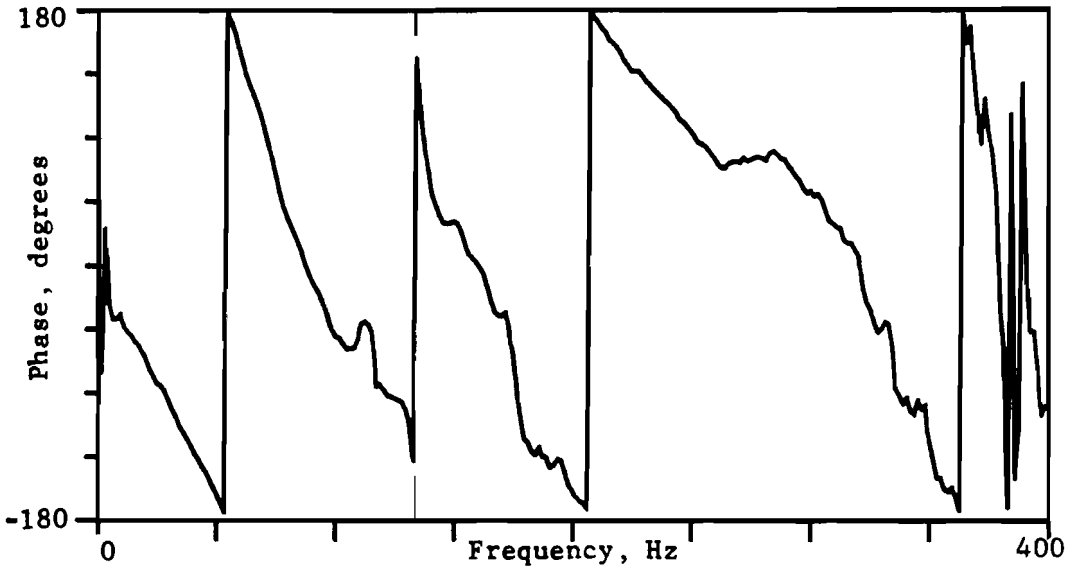

(a) Phase of the cross spectrum.

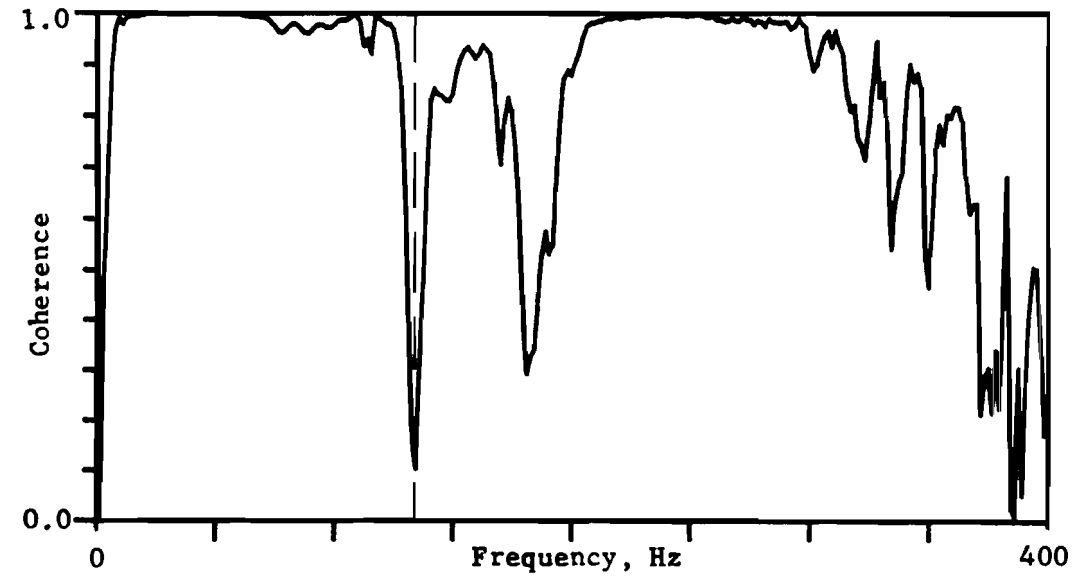

(b) Coherence function.

Fig 7.6. Relationship between phase of the cross spectrum and coherence for measurement V4-V8.

from 10 to 100 Hz. In particular, there appears to be a 360-degree phase shift at about 134 Hz, similar to the shifts occurring at about 53 and 207 Hz. (These shifts are usually a plotting phenomenon; see the discussion in Appendix A.) However, if the apparent shift at 134 Hz is interpreted as a 360-degree shift, the velocities obtained for frequencies above 134 Hz are much too low for the base material which those frequencies (or wavelengths) supposedly sampled. In this case, the sharp break in continuity is due to actual behavior (rather than just a plotting phenomenon) of waves having frequencies in the neighborhood of 134 Hz.

The coherence function for measurement V4-V8, shown in Fig 7.6b, exhibits a sharp spike of poor coherence at 134 Hz which corresponds exactly to the sharp break in phase shown in Fig 7.6a. In addition, there is another wider spike of poor coherence at approximately 182 Hz. Analysis of the reduced data indicates that both of these frequencies correspond to sharp demarcations in velocities.

Further examination of phase plots and coherence functions from other measurements revealed that similar spikes or depressions of poor coherence occurred over frequency ranges where the phase was atypical and/or difficult to interpret. The sharpness of the spike or depression, as well as the level of coherence, varied somewhat from measurement to measurement. However, regardless of the location of the geophones, each measurement showed poor coherence at the same frequency or range of frequencies (within the measurement bandwidth). In each case, the frequencies corresponded to sharp demarcations in velocities. These frequencies and the approximate depths associated with the velocity contrasts are summarized in Table 7.2. In turn, it was found that these depths correlate quite closely with layer boundaries in the profile. This suggests that reflection and refraction of certain

TABLE 7.2. RELATIONSHIP BETWEEN FREQUENCIES WITH LOW COHERENCE AND DEPTH OF LAYER BOUNDARIES

Measurement	Frequency (Hz)	Approximate Depth** (ft)	Layer Boundary
V½-V1	1750-2100	0.14-0.18	surface course / base course
V½-V1	550	0.4	1st lift / 2nd lift of base
V2-V4	183	1.0	base / stabilized subgrade
V4-V8	182	1.0	" " "
V4-V8	134	1.5	stabilized subgrade / subgrade
V8-V16	105-135	1.55	" " "
V1-V16	105-115	1.5	" " "
V1-V2 (WP) *	1225+	0.14	surface course / base course
V5-V9 (WP)	185-240	1.0	base / stabilized subgrade
V7-V15 (WP)	105-110	1.55	stabilized subgrade / subgrade

* Measurements in wheel path denoted by (WP).

** Depths based on $L_R/3$ criterion; L_R is wavelength for particular frequency.

waves due to layering does influence the phase of the cross spectrum as well as the coherence function.

Although measurements with poor coherence are not desirable, it may be advantageous, when possible, to use the spikes or depressions of poor coherence to identify layering. Such a possibility is shown in Fig 7.7. The phase of the cross spectrum for measurement V½-V1, shown in Fig 7.7a, exhibits a broad peak from about 1700 to 2300 Hz. The presence of the peak indicates that the phase is decreasing although the frequency is increasing. As the phase decreases, the time for the wave to travel between the geophones decreases, and the velocity increases significantly. The sharp change in velocity suggests the influence of a layer boundary. Figure 7.7b shows the coherence function for the measurement, and, as could be expected, there is a marked drop in the level of coherence over the frequency range of the peak in Fig 7.7a. The detection of layers using frequencies may also be enhanced by examining the magnitude of the cross spectrum plotted on a logarithmic scale as in Fig 7.7c. Small but distinct dips in magnitude can be observed at 1900 Hz (corresponding to the coherence function) as well as at 550 Hz. This latter point is barely distinguishable in the phase plot (Fig 7.7a) and is not well-defined in the coherence function (Fig 7.7b) in view of the fact that several similar short spikes of poor coherence also exist up to about 1000 Hz. The sensitivity of the logarithmic scale to small dips in magnitude shows the dip at 550 Hz, which corresponds to a depth of about 0.4 ft, or about 5 in. (12 cm). This depth appears to correspond to the boundary between the first and second lifts of the base course. Since the material properties (and, hence, the velocities) are essentially the same in both lifts, no distinction is observed in the phase plot.

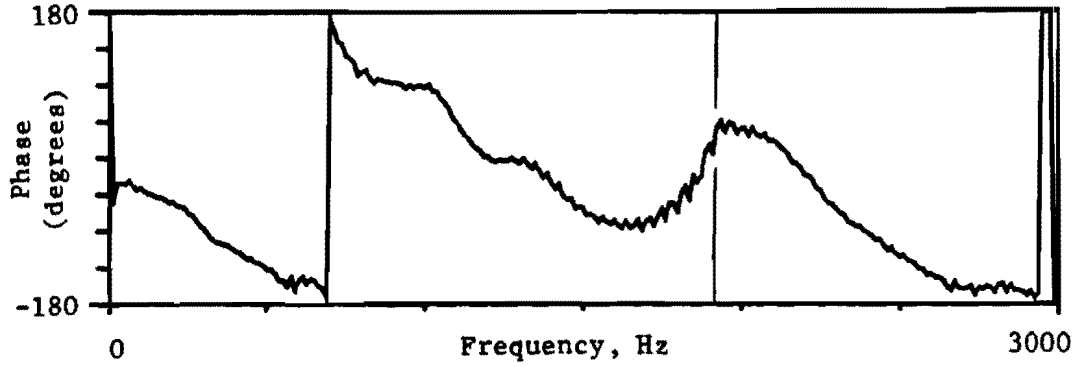

(a) Phase of the cross spectrum.

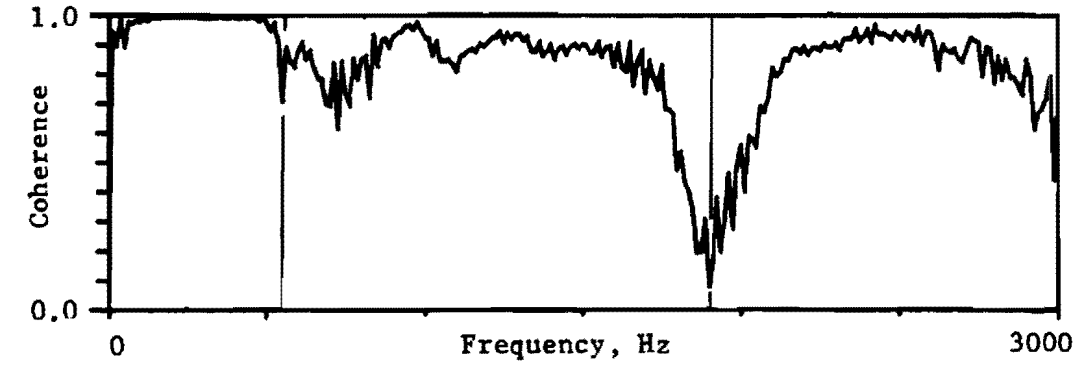

(b) Coherence function.

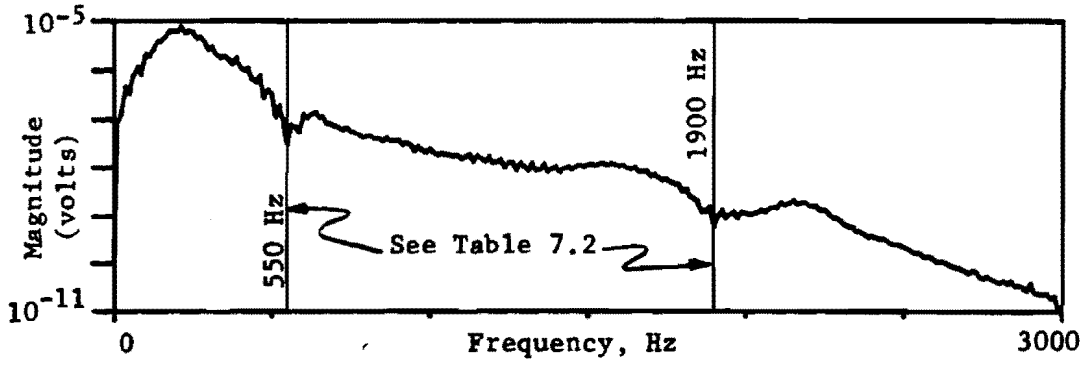

(c) Magnitude (logarithmic scale) of the cross spectrum

Fig 7.7. Detection of layer boundaries using spectral measurements.

Although the major layer boundaries can be approximated, there is still the problem of assigning a velocity to the base course, where excessive scatter exists in the data (Figs 7.3-7.5). For soil sites, such scatter could be identified and filtered out using the criterion developed in Chapter 4. For pavement sites, a general equation (such as Eq 4.5) cannot be readily applied because the various materials have significantly different properties. However, the same approach can be applied; data for frequencies with poor coherence are rejected and thereby filtered out of the velocity profile. The definition of "poor" coherence is somewhat arbitrary. Analysis of the various measurements indicates that data for which $\gamma^2 < 0.90$ should be filtered out.

Using this criterion, the velocity profiles were filtered and replotted. Figure 7.8 shows the profile to a depth of 7 ft (2.1 m) for measurements along the wheelpath. Figure 7.9 shows the profile to a depth of 14 ft (4.3 m) for measurements along the centerline. Both profiles still show some scatter, which is probably remnant of the reflection and refraction problems previously discussed. The transition zone is still present at the depth of the stabilized subgrade.

Rayleigh wave velocities can be determined for the subgrade and the base using Fig 7.8, and R-wave velocities can be determined for the subgrade, the base, and the surface layer using Fig 7.9. A "mean value" for the velocity in each layer was selected by graphically fitting a straight line through the data which are least influenced by the layer boundaries. In the subgrade, a velocity of 420 fps (128 m/sec) was obtained from measurements along the wheelpath and a velocity of 440 fps (134 m/sec) was obtained from measurements along the centerline, yielding an average value of 430 fps (131 m/sec). In the base course, a velocity of 680 fps (207 m/sec) was

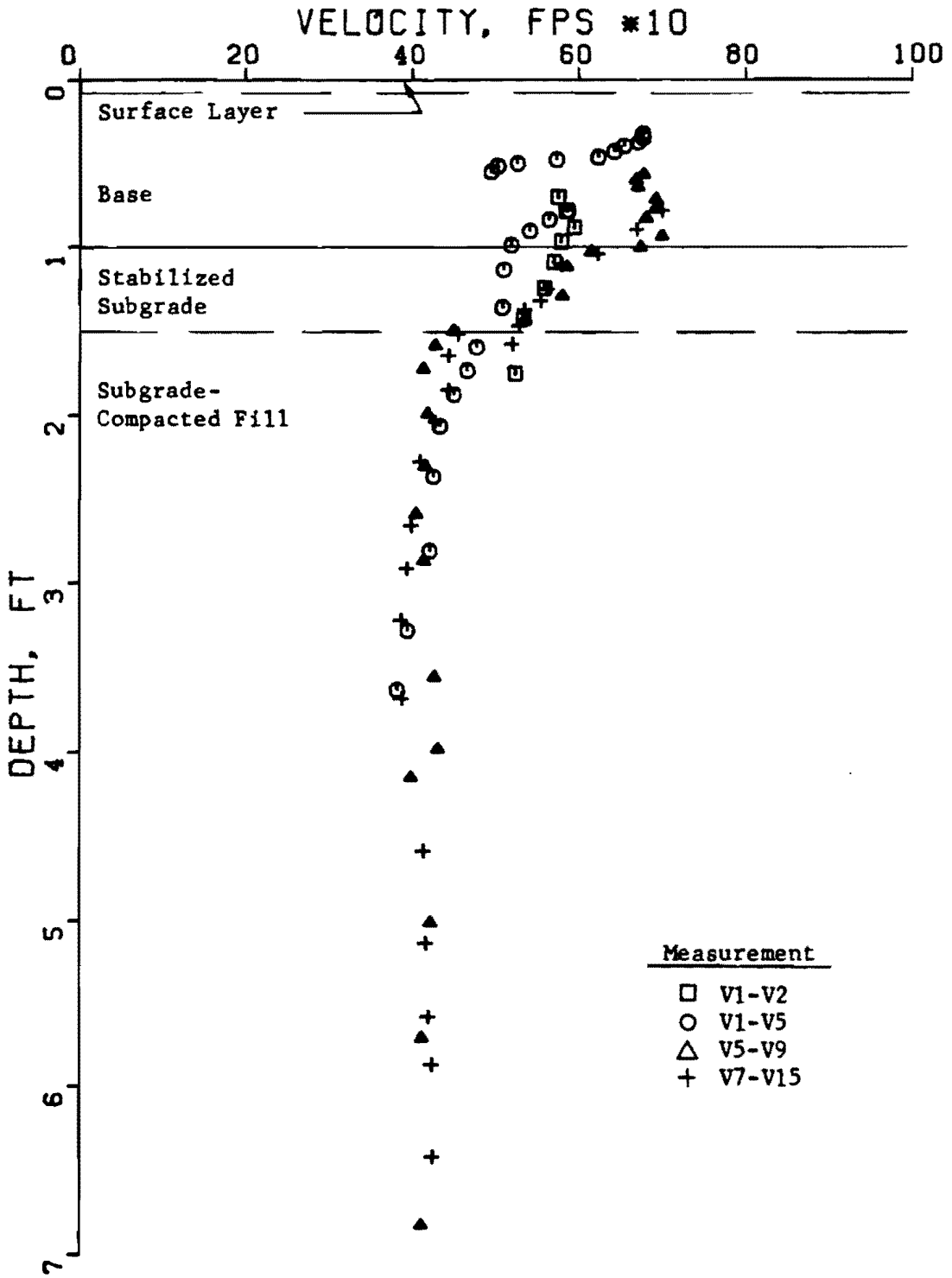

Fig 7.8. Filtered Rayleigh wave velocity profile for measurements along the right wheelpath.

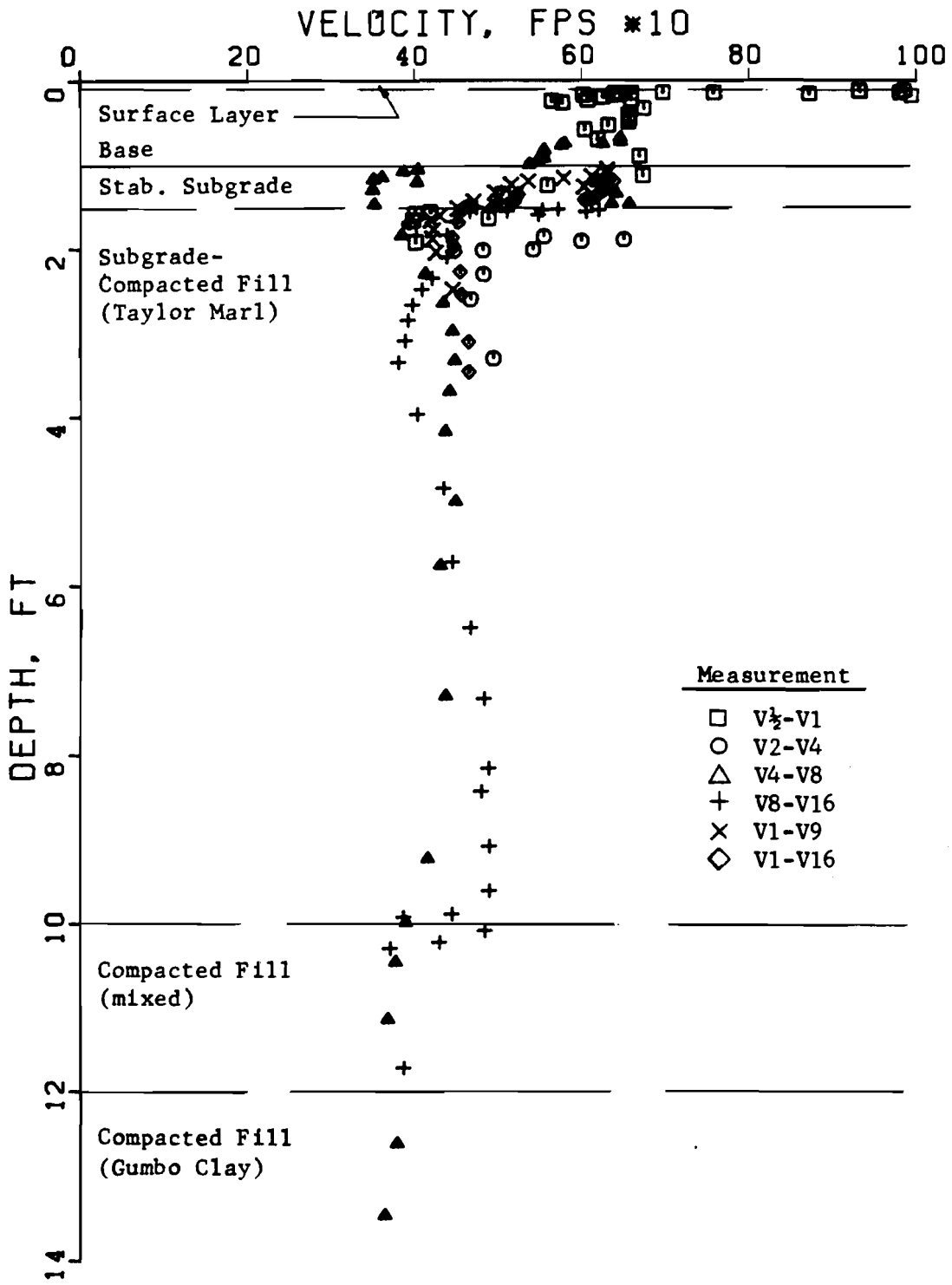

Fig 7.9. Filtered rayleigh wave velocity profile for measurements along the centerline.

obtained from measurements along the wheelpath and a velocity of 660 fps (201 m/sec) was obtained from measurements along the centerline, yielding an average value of 670 fps (204 m/sec). The velocity in the surface layer was determined from centerline measurements only and was estimated to be 980 fps (299 m/sec).

The subgrade velocity obtained from cross spectrum measurements can be compared with crosshole velocities obtained by Long (1980) immediately after the construction of the embankment. Long obtained shear wave velocities in the fill material ranging from about 515 to 530 fps (157 to 162 m/sec). From cross spectrum measurements, the R-wave velocity of 430 fps (131 m/sec) converts to an S-wave velocity of 453 fps (138 m/sec) for a clay with Poisson's ratio of about 0.45. Thus, the S-wave velocity from cross spectrum measurements is about 15 percent lower than the S-wave velocities from crosshole tests. Since the cross spectrum measurements were made after a period of wet weather, the lower velocities may reflect a greater moisture content than when the crosshole tests were performed (several years earlier).

The velocity profile in Fig 7.9 shows a small but marked decrease in velocity at about 10 ft (3 m). This depth corresponds with the depth at which the compacted fill material changes from Taylor marl to gumbo clay. This close correlation between the velocity profile and soil profile suggests that the $L_R/3$ criterion for depth is appropriate for the Granger site. Again, the lower velocity below 10 ft (3 m) may be a result of the heavy rainfall and subsequent increase in elevation of the water table due to impoundment of Granger Lake. Borings were not performed to obtain samples or determine water contents at the time the cross spectrum measurements were made.

DETERMINATION OF MODULI

Using the values for R-wave velocities determined from cross spectrum measurements and estimated values for unit weights and Poisson's ratios, values for S-wave velocities, shear moduli, and Young's moduli were calculated for the surface layer, base, and subgrade. These values are listed in Table 7.3. Young's moduli for the surface layer, base, and subgrade were determined to be 91,000 psi, 42,000 psi, and 16,000 psi, respectively. These values fall within the range typical of the respective materials. In addition, a Young's modulus for the stabilized subgrade was calculated to be 23,000 psi based on an estimated R-wave velocity.

Moduli were backcalculated (by SDHPT) from Dynaflect data using ELSYM5 as described in Chapter 6. Four layers were assumed, including a surface course, flexible base, and lime-stabilized subgrade having layer thicknesses of 1 in., 11 in., and 6 in., respectively, and a subgrade of infinite extent. The moduli from deflection measurements are listed in Table 7.3. These moduli are considerably lower (by as much as 1/2 to 1/3) than those calculated from wave propagation velocities.

Deflections were also calculated (by ELSYM5) using the moduli determined from wave velocities. The calculated deflections were 1.39, 1.20, 0.67, 0.47, and 0.35 mils for locations of 0, 1, 2, 3, and 4 ft from the source. In comparison, the measured deflections (based on an average for 7 readings) were 2.27, 1.59, 0.95, 0.61, and 0.44 mils, respectively. The calculated deflections are approximately 20 to 40 percent lower than the measured deflections, which would be expected since the moduli from wave propagation velocities were higher than the moduli found by using ELSYM5.

TABLE 7.3. SUMMARY OF WAVE VELOCITIES AND ELASTIC MODULI DETERMINED AT GRANGER (FM 971) SITE

Material	Unit Weight (pcf)	Poisson's Ratio	R-Wave Velocity (fps)	S-Wave Velocity (fps)	Shear Modulus (psi)	Young's Modulus, E (psi)	
						Wave Propagation	Deflection Method*
Surface	145	0.30	980	1060	35,000	91,000	50,000
Base	140	0.35	670	720	15,700	42,000	13,000
Stabilized Subgrade	125	0.40	520	550	8,100	23,000	12,500
Subgrade	125	0.45	430	450	5,500	16,000	12,000

*Moduli were backcalculated from fitted deflection basin using elastic layer theory (ELSYM5).

The agreement between the wave propagation method and the deflection method is not particularly good. The differences in moduli (or deflections) suggest that the methods are not equivalent or interchangeable. It is difficult to assess which method is more "accurate." Perhaps the assumptions of elastic layer theory used in ELSYM5 are not reasonable for older, deteriorating, or cracked pavements such as the sections at the Granger site. In contrast, the wave propagation method did provide fairly good correlation with the profile layering and crosshole velocities at the site.

SUMMARY

Analyses of the cross spectrum measurements made at the Granger pavement site were generally more difficult to interpret than measurements made at the Austin pavement site. In particular, there was significant scatter in the velocity profile in the surface layer and base course. Examination of the coherence function, along with erratic patterns in the phase of the cross spectrum, indicated that marked depressions or spikes of low coherence occurred at frequencies whose wavelengths corresponded to depths of layer boundaries. Identification of these frequencies and layer boundaries permitted better interpretation of the cross spectrum phase plots.

Much of the scatter was reduced by filtering out data for frequencies which displayed a value of coherence less than 0.90. Also, data were not used for which the wavelengths were too long to sample effectively an appropriate depth of material (when the geophones were located too close to the source). The filtered velocity profile correlated well with the site profile. The S-wave velocity for the subgrade was about 15 percent lower than that obtained from crosshole tests performed during the construction of

the embankment, possibly because the cross spectrum measurements reflected a greater moisture content following a period of wet weather.

Young's moduli obtained from the wave propagation velocities were considerably greater (up to 2 or 3 times) than those backcalculated from deflection measurements using ELSYM5. Conversely, deflections using moduli from the wave propagation method were 20 to 40 percent less than the measured (Dynaflect) deflections. Inasmuch as the cross spectrum measurements provided a velocity profile which correlated closely with the site profile and crosshole velocities, the differences in moduli between the two methods suggest that the elastic layer theory used in ELSYM5 may not apply well to thin, surface layered pavement.

CHAPTER 8. SUMMARY, CONCLUSIONS, AND RECOMMENDATIONS

SUMMARY

A method to determine elastic moduli at soil and pavement sites was proposed and tested. Criteria which guided the development of this method included the restraint of non-destructive testing, accuracy of moduli for all layers regardless of thicknesses, and quickness and efficiency for rapid, extensive testing. To meet these criteria, surface receivers were utilized to evaluate the Rayleigh-wave motion created by a vertical impulsive source that could excite a wide range of frequencies with a single impact. Analysis was facilitated by using a portable spectral analyzer to study the magnitude and phase of the frequency content of the recorded wave pulse.

Phase information from the cross spectrum function was used to calculate Rayleigh wave velocities which were converted to shear wave velocities. Elastic moduli (shear moduli and Young's moduli) were then calculated from the shear wave velocities. Results from field testing at two pavement sites and two soil sites indicate that the spectral analysis of surface waves provides an accurate estimation of the velocity (and, hence, modulus) profile of a site. The following sections present general conclusions regarding test-related variables, as well as specific conclusions and recommendations particular to testing at soil sites and pavement sites.

GENERAL CONCLUSIONS REGARDING TEST-RELATED VARIABLES

Several transient events, or impacts, should be averaged together to obtain a representative cross spectrum measurement. The number of averages may vary somewhat with the reproducibility of the source, but, typically five averages will provide a representative measurement. Additional averages do not seem to improve the measurement sufficiently to warrant the extra testing time.

Several sources were investigated. Results show that the stress (or strain) level is not necessarily the critical parameter for selecting an appropriate impact hammer. Selection should be based on the range of frequencies that can be sufficiently excited to sample the site profile adequately. Energy of excitation should not be focused on a few frequencies but should be distributed over all frequencies in the bandwidth. On this basis, a light hammer producing a sharp impulse is much more suited than a large weight which produces a relatively "cushioned" impulse, particularly for testing pavement sites.

Signals recorded with velocity transducers, or geophones, appear to provide valid cross spectrum measurements up to frequencies of at least 3 KHz. Based on tests performed on pavements, vertical geophones provide a more accurate R-wave velocity profile than horizontal geophones. Velocities obtained from measurements using horizontal geophones were generally too high, probably due to the greater sensitivity of horizontal geophones to the higher velocity P-waves.

The spacing of the geophones from the source also is important. In general, an "equally spaced" arrangement, where both the near geophone and the far geophone are located at increasing distances from the source, is more

desirable than a "reference" arrangement, where the near geophone is fixed at a location close to the source and only the far geophone is located at increasing distances from the source. The former arrangement provides a more accurate velocity profile, particularly at greater depths (greater wavelengths). The equally spaced arrangement appears to be better than the reference arrangement because the near geophone is located at a sufficient distance from the source, which allows the different frequencies to disperse (by travelling at different velocities) as well as permitting the longer wavelengths to travel through a depth of material which the wave(s) supposedly sampled.

Velocities for given frequencies were assigned to depths from wavelength criteria corresponding to an "effective sampling depth" of material properties. Based on comparisons with S-wave velocity profiles from crosshole testing, a depth criterion of $L_R/3$ provided a velocity profile which correlated best with the crosshole profile. Velocities from cross spectrum (surface) measurements did not differ from crosshole velocities by more than 20 percent in the extreme and were typically within less than 10 percent. Inasmuch as crosshole data did not exist for depths greater than 30 ft (9 m), it is not certain if the $L_R/3$ criterion is applicable for long wavelengths.

The surface technique is restricted to using an average velocity and the determination of a velocity profile based on wavelength criteria is somewhat empirical. The problem of averaging is particularly evident at layer boundaries. Although the empirical approach provides reasonably good correlation with the site profile and crosshole data, it is desirable to incorporate a more rigorous and "accurate" approach for determining the velocity profile from surface measurements. Such an approach involves

Rayleigh-wave inversion and extensive numerical techniques to "back out" the velocity (or modulus) profile and to eliminate or minimize the problems associated with averaging. This approach could be used to refine the analysis of measurements from surface testing.

In addition to the cross spectrum function, other functions may be helpful in the analysis of data. The coherence function is most definitely needed to assess the range of frequencies over which quality data were obtained for a given measurement. The linear spectrums or autospectrums can indicate which frequencies are adequately excited to measure a good response. Lastly, the transfer function may be used to calculate attenuation properties at a site.

CONCLUSIONS AND RECOMMENDATIONS FOR SOIL INVESTIGATION

For typical soil sites, frequencies up to about 100 to 200 Hz should be excited. For depths greater than about 25 to 30 ft (7.6 to 9.1 m), the measurement bandwidth should be reduced to at least 25 Hz to obtain adequate resolution of low frequencies. Geophones with low resonant frequencies, or perhaps accelerometers, should be used to obtain a "flat" transducer response over the range from 0 to 10 Hz.

The source should be adequately coupled with the soil to ensure transfer of wave energy over the necessary range of frequencies. The source should also be large enough to excite low-frequency waves sufficiently enough to sample depths well below the surface. For depths to about 30 ft (9 m), the drop hammer appears to be adequate. For greater depths, a larger source is desirable to provide sufficient energy at low frequencies. This additional

wave energy would also permit greater spacing of the geophones from the source, which is necessary to sample the longer wavelengths accurately.

Testing should include a series of various geophone spacings so that all wavelengths are accurately sampled during at least one measurement. For spacings close to the source, short wavelengths will be accurately sampled but long wavelengths will not have travelled a sufficient distance to measure properties to an adequate depth. Conversely, for spacings farther from the source, long wavelengths will be accurately sampled but short wavelengths may have attenuated too much for a valid frequency response to be obtained. Based on the coherence function, criteria can be established for a given site whereby inappropriate wavelengths (or frequencies) can be filtered from the velocity profile. Filtering reduces much of the scatter in the data, and using a series of measurements, will result in some overlap in the profile. This overlap of several measurements provides a more-representative profile than a single measurement would permit.

Attenuation and damping data were calculated from transfer function measurements. The coefficient of attenuation α for Rayleigh waves could be approximated as a linear function of frequency. Values of damping ratio were calculated from α and ranged from about 8 to 20 percent, depending on the particular site. These values are somewhat higher than those typically measured with laboratory samples. Possible reasons for the higher in situ values may be that the field measurement may have erroneously interpreted geometrical damping of body wave energy as material damping and/or the field measurement accurately reports backscattering of wave energy caused by material anomalies, voids, reflections, or refractions. The former problem could be resolved by locating the near geophone at 8 to 10 ft (2.4 to 3.0 m) from the source, thereby allowing adequate distance for the geometric damping

of body waves. Results from this investigation certainly show potential application of spectral analysis in the determination of attenuation and damping.

CONCLUSIONS AND RECOMMENDATIONS FOR PAVEMENT EVALUATION

For pavement sites consisting of a flexible (AC) surface, frequencies up to 2 to 5 kHz should be excited. This upper bound will vary depending on the thickness and stiffness of the surface layer. Higher frequencies are necessary for thinner, stiffer pavements. Based on tests at two pavement sites, it appears that geophones provide good response up to at least 3 kHz. For higher frequencies, it may be necessary to use accelerometers.

Cross spectrum measurements should be made for a series of various geophone spacings from the source so that all wavelengths can be accurately sampled. Spacings close to the source are better for measuring higher frequencies, which sample the surface layer and base course. Spacings farther from the source are better for measuring low frequencies, which sample the subgrade. By using a series of spacings, some overlap of measurements will occur, which will minimize the possibility of misinterpreting reflections or refractions of waves at layer boundaries. The coherence function should also be used in conjunction with the cross spectrum to identify poor data. Spikes or depressions of low coherence may be associated with layer boundaries, and their identification may be helpful in analyzing the phase of the cross spectrum.

Comparisons between moduli calculated from wave propagation velocities and moduli backcalculaed (by ELSYM5) from measured Dynaflect deflection basins indicate that the wave propagation method is a valid method to

determine Young's modulus for each layer in a pavement system. Agreement between the two methods was quite good at the Austin site, where the pavement was newly constructed, but was not as good at the Granger site, where the pavement was several years old and showed signs of deterioration. The poorer comparison at the Granger site may result from assumptions in the elastic layer program that are not reasonable for thin layered pavement. In general, it is not clear how applicable the elastic layer theory incorporated into ELSYM5 is for low-strain (less than 0.001 percent) dynamic loading.

Shear wave velocities in the subgrade obtained from surface measurements correlated well with those obtained from crosshole testing, suggesting that the spectral analysis (surface) method is not hindered by the relatively stiff asphalt layer at the surface. However, both of the pavement systems investigated in this research consisted of flexible surface layers, with stiffnesses about 5 to 10 times those for the subgrade. For rigid (PC) pavements, the stiffness of the surface layer is considerably greater and may complicate the analysis of subgrade velocities and moduli. Further research is necessary to determine if the surface method is applicable for rigid pavements.

REFERENCES

1. Ballard, R. F., Jr., "Determination of Soil Shear Moduli at Depth by In-Situ Vibratory Techniques," Waterways Experiment Station, Misc. Paper No. 4-691, December 1964.

2. Ballard, R. F., Jr., and D. R. Casagrande, "Dynamic Foundation Investigations, TAA-2A Radar Site, Cape Kennedy, Florida," Waterways Experiment Station, Misc. Paper No. 4-878, February 1967.

3. Bohn, A., P. Ullidtz, R. Stubstad, and A. Sorenson, "Danish Experiments with the French Falling Weight Deflectometer," Proceedings, Third International Conference on the Structural Design of Asphalt Pavements, Vol. 1, pp 1119-1128, 1972.

4. Bolt, B. A., Nuclear Explosions and Earthquakes, W. H. Freeman and Company, San Francisco, California, 1976.

5. Brigham, E. O., The Fast Fourier Transform, Prentice-Hall, Englewood Cliffs, New Jersey, 1974.

6. Ewing, W. M., W. S. Jardetzky, and F. Press, Elastic Waves in Layered Media, McGraw-Hill Book Company, New York, 1957.

7. Fry, Z. B., "Development and Evaluation of Soil Bearing Capacity, Foundations of Structures," Waterways Experiment Station, Technical Report No. 3-632, Report No. 1, July 1963.

8. Heukelom, W., "Auscultation Dynamique de Constructions Routieres," La Propagation des Ebranlements dans les Milieux Heterogenes, Colloques Internationeaux du Centre National de la Recherche Scientifique, No. 111, Marseille, France, pp 129-141, September 1961.

9. Heukelom, W., and C. R. Foster, "Dynamic Testing of Pavements," Journal of the Soil Mechanics and Foundations Division, American Society of Civil Engineers, Vol. 86, No. SM1, pp 1-28, February 1960.

10. Hewlett-Packard Company, "Digital Signal Analysis - Time and Frequency Domain Measurements," Application Note 240-0, Hewlett-Packard, August 1977.

11. Hoar, R. J., "In Situ Seismic Velocity and Attenuation Measurements for Dynamic Analyses," Ph.D. Dissertation, The University of Texas at Austin, 1981.

12. Hoar, R. J., and K. H. Stokoe, II, "Generation and Measurement of Shear Waves In Situ," Dynamic Geotechnical Testing, ASTM STP 654, American Society for Testing and Materials, 1978.

13. Jones, R., "Surface Wave Technique for Measuring the Elastic Properties and Thicknesses of Roads: Theoretical Development," British Journal of Applied Physics, Vol. 13, pp 21-29, 1962.

14. Kudo, K., and E. Shima, "Attenuation of Shear Waves in Soil," Bulletin of the Earthquake Research Institute, Vol. 48, Part 2, pp 145-158, March 1970.

15. Long, L. G., "Comparison of Field and Laboratory Dynamic Soil Properties," Master's Thesis, The University of Texas at Austin, 1980.

16. Lytton, R. L., W. M. Moore, and J. P. Mahoney, Pavement Evaluation: Phase I Pavement Evaluation Equipment, Report No. FHWA-RD-75-78, Federal Highway Administration, Washington, D. C., 1975.

17. McDonal, F. J., F. A. Angona, R. L. Millis, R. L. Sengbush, R. G. Van Nostrand, and J. E. White, "Attenuation of Shear and Compressional Waves in Pierre Shale," Geophysics, Vol. 23, pp 421-439, 1958.

18. Miller, G. F., and H. Pursey, "On the Partition of Energy Between Elastic Waves in a Semi-Infinite Solid," Proceedings Royal Society, London, Series A, Vol. 233, pp 55-69, 1955.

19. Newland, D. E., Random Vibrations and Spectral Analysis, Longman, London, 1975.

20. Patel, N. S., "Generation and Attenuation of Seismic Waves in Downhole Testing," Master's Thesis, The University of Texas at Austin, 1981.

21. Rao, H. A. B., and D. Harnage, "Evaluation of Rigid Pavements by Nondestructive Tests," Highway Research Record No. 407: Pavement Technology, Highway Research Board, pp 76-86, 1972.

22. Rayleigh, Lord, "On Waves Propagated Along the Plane Surface of an Elastic Solid," London Mathematical Society Proceedings, Vol. 17, pp 4-11.

23. Richart, F. E., Jr., J. R. Hall, Jr., and R. D. Woods, Vibrations of Soils and Foundations, Prentice-Hall, Englewood Cliffs, New Jersey, 1970.

24. Stokoe, K. H., II, and R. J. Hoar, "Variables Affecting In Situ Seismic Measurements," Earthquake Engineering and Soil Dynamics, Vol. II, American Society of Civil Engineers, pp 919-939, 1978.

25. Stoneley, R., "Elastic Waves at the Surface of Separation of Two Solids," Proceedings of the Royal Society of London, Series A, Vol. 106, pp 416-428, December 1924.

26. Szendrei, M. E., and C. R. Freeme, "Road Responses to Vibration Tests," Journal of the Soil Mechanics and Foundations Division, American Society of Civil Engineers, Vol. 96, SM6, pp 2099-2124, November 1970.

APPENDIX A

DISCUSSION OF EXPERIMENTAL PROCEDURES AND DATA ANALYSIS

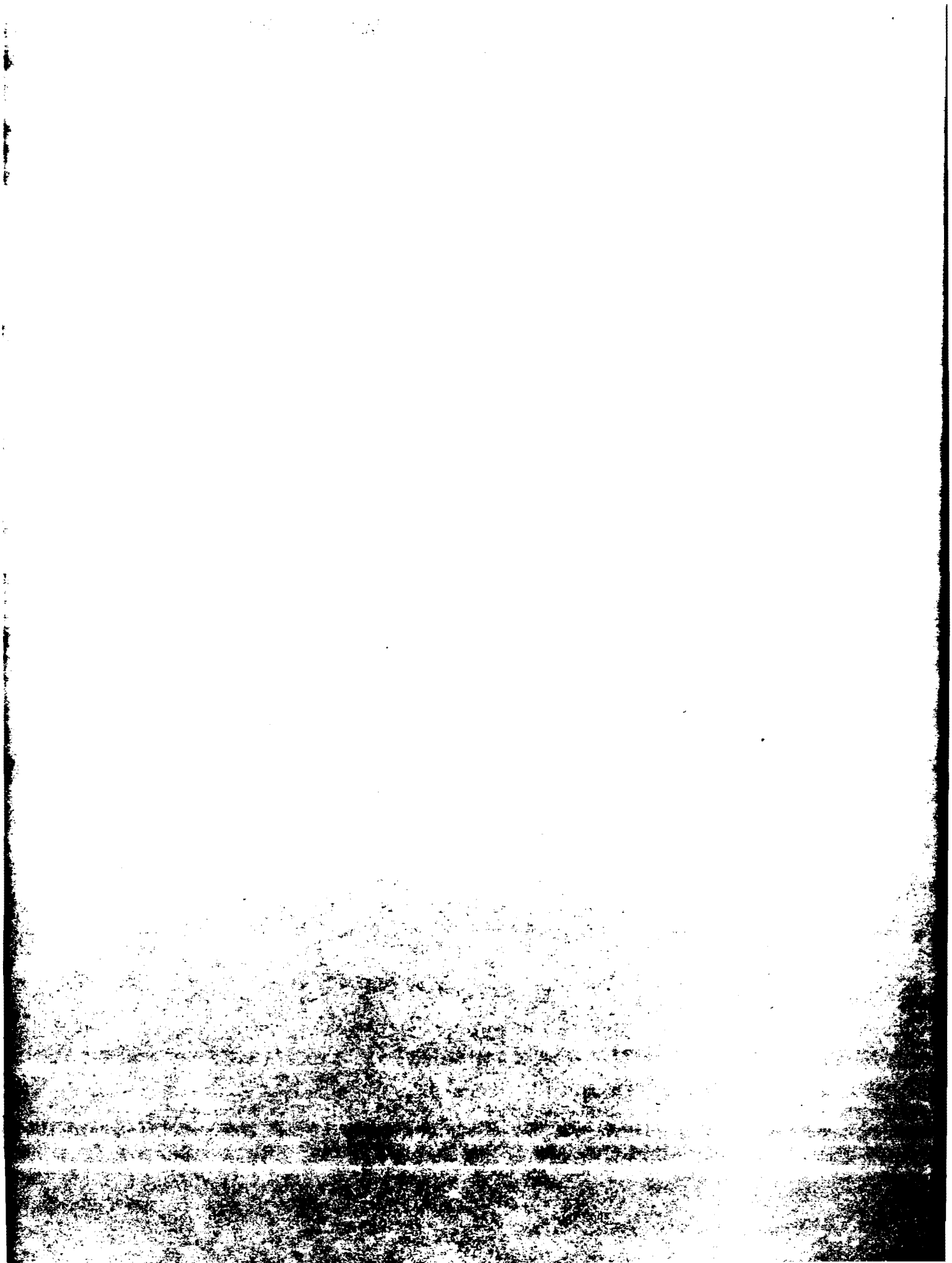

APPENDIX A

DISCUSSION OF EXPERIMENTAL PROCEDURES AND DATA ANALYSIS

This appendix outlines the steps involved in the acquisition and analysis of frequency data to obtain a V_S-versus-depth profile. It is assumed that the reader is familiar with the basic operation of the Hewlett-Packard 5423A Analyzer.

FIELD PROCEDURE FOR DATA ACQUISITION

Frequency data can be acquired directly in the field with the Hewlett-Packard 5423A Structural Dynamics Analyzer, shown in Fig A.1. The HP 5423A Analyzer consists of three portable units having a net weight of 115 lb (52.2 kg). The three units stack together vertically during operation and are interconnected by means of appropriate cables. Complete performance specifications as well as operator instructions are contained in the three volumes of the Hewlett-Packard 5423A Users' Guide.

Analyzer Set-up

The analyzer must be "programmed" for a particular measurement state. The format (and typical set-up) of the measurement state is shown in Fig A.2. The measurement state is displayed in three sections which include:

Fig A.1. Hewlett-Packard 5423A Structural Dynamics Analyzer (from Hewlett-Packard Company, 1979).

MEASUREMENT STATE

MEASUREMENT :	TRANSFER FUNCTION
AVERAGE :	5 , STABLE
SIGNAL :	IMPACT
TRIGGER :	INTERNAL , CHNL 1

CENT FREQ :	0.0 HZ	ΔF :	390.625 mHZ
BANDWIDTH :	100.000 HZ		
TIME LENGTH :	2.56000 S	ΔT :	2.50000 mS

CHAN #	RANGE	AC/DC	DELAY	CAL (EU/V)
* 1	2.5 V	DC	-20.0000 mS	1.00000
* 2	2.5 V	DC	-20.0000 mS	1.00000

Fig A.2. Format and typical setup of a measurement state.

(1) the type of measurement and how it will be obtained,

(2) the frequency bandwidth or time length information specified, and

(3) the selected parameters for the analog-to-digital conversion of the input signals.

To obtain data for determining wave propagation velocities, the measurement should be specified in accord with the following guidelines.

The transfer function should be specified as the desired measurement although the cross-spectrum measurement would provide the necessary information. When the transfer function is specified, the analyzer also provides the coherence function, the cross-spectrum, and the autospectrums of each input signal. The additional measurements may aid in the subsequent analysis of the data. As a general rule, five "averages" should be used to construct the measurement. Stable averaging should be used in order to give each event in the ensemble equal weight. The signal type should be specified as "Impact," which allows for the acceptance or rejection of a particular transient event. In this way, poor impulses can be eliminated from the overall average.

The trigger type may vary depending on the available equipment. The most convenient method is simply to trigger internally off the signal going into the first channel. The trigger level can be adjusted to fix a starting point (t=0) in the first half sine wave of the impulse as it passes by the first geophone. A pre-trigger delay must be used to capture the initial portion of the impulse that would otherwise be lost prior to triggering. Since only the relative phase between the signals of the two geophones is required, an external trigger is not necessary.

The selection of the measurement bandwidth or time length depends on several considerations, including the spacing between geophones, the desired resolution in the frequency spectrum, the attenuation properties of the site, and the range of wavelengths needed to investigate the site to a desired depth. The interdependence of these variables is discussed in detail in Chapter 4. For most soil sites, a bandwidth of 100 to 200 Hz should adequately cover the range of frequencies needed to "sample" within a foot or two of the surface. For pavement systems, frequencies from 1.6 to 3.2 Hz may be required to sample the thin, high-velocity layer at the surface. In each case the "center frequency" should be specified as zero, so that the measurement is made in the "baseband" mode, i.e., the bandwidth ranges from 0 to, say, 100 Hz. Note also that the selection of a bandwidth or a time length automatically establishes the other. Since frequency and period are inversely related, both bandwidth and time length cannot be specified independently. Additionally, because the HP 5423A uses a fixed number of points to digitize the signal, selection of a bandwidth or time length automatically establishes Δf and Δt, the resolution or precision of the measurement in the frequency domain and the time domain, respectively.

The parameters pertaining to the analog-to-digital converter (ADC) can differ between input channels 1 and 2. However, in general, only the range should differ. The specification of the range for each channel is related to the voltage output of each geophone. The value for range should be as small as possible to increase the sensitivity of the ADC. When the voltage output from the geophone(s) exceeds the specified range, a caution message will appear: "ADC OVERFLOW, IMPACT AGAIN." Subsequent signals can be utilized by increasing the range to an appropriate value (not exceeding + 10 volts). For both channels, DC coupling should be specified. For measurement of wave

propagation velocities, a calibration factor need not be specified as long as the frequency response curves for each geophone are nearly identical.

Lastly, when triggering internally with the signal from the near geophone, a trigger delay must be specified. The same trigger delay should be specified for each channel so as not to introduce an internal time or phase delay for measurements incorporating both signals. The exact value of the delay will vary somewhat with the velocity of the material at the site as well as the distance beteen the source and the near geophone. In general, a delay of 5 to 50 milliseconds should prove adequate. Note that the delay is negative, since the pre-trigger (before t=0) portion of the signal is to be captured.

Measurement Acquisition

Prior to the measurement of the transfer function, the input time signals should be checked. This can be done before each impact event is accepted (or rejected) for the measurement ensemble. However, in the case of narrow bandwidth measurements (say, 100 to 200 Hz), the time signal may be compressed and/or have poor resolution as shown in Fig A.3a. In such cases, it is beneficial to perform initially a "time record average" with a relatively wide bandwidth (say, 1600 Hz) to verify that the geophones are connected properly to the ADC. This preliminary measurement can be used to check that the trigger delay is appropriate, that the entire transient event is being captured, and that both geophones are connected with the same polarity (i.e., a "downward" impact produces an initial downward impulse in the time signal of both geophones). The benefit of using a wide bandwidth measurement to check the input signal(s) is shown in Fig A.3b.

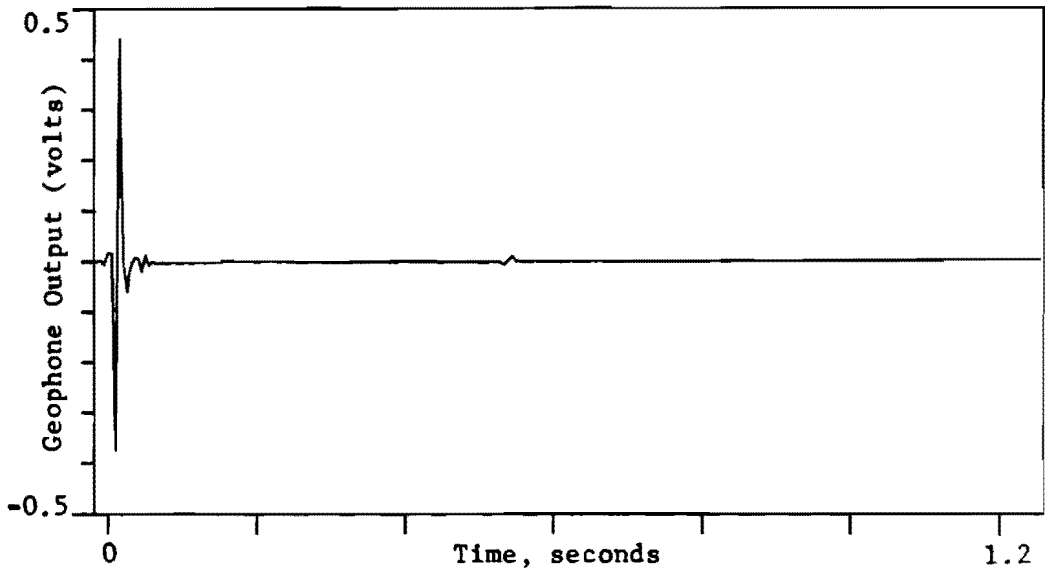

(a) Narrow-bandwidth (BW = 200 Hz) measurement

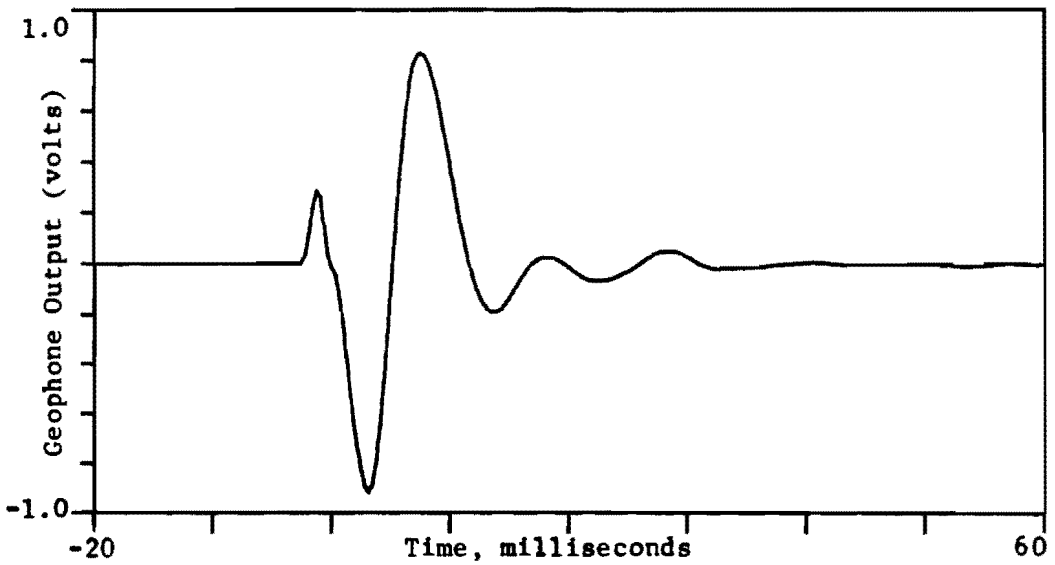

(b) Wide-bandwidth (BW = 1600 Hz) measurement

Fig A.3. Comparison of time records obtained from measurements with narrow and wide bandwidths.

Once the input time signals have been checked, the transfer function can be measured. After the measurement is completed, the coherence function should be examined to confirm that a "good" measurement was obtained over the desired bandwidth. Such a check may indicate that the bandwidth should be lengthened or shortened to optimize the range or resolution of frequency information. The range of frequencies providing useful information (good coherence) will vary somewhat with the distance between the geophones. In general, wider spacings between geophones will lead to attenuation of high frequencies. Each new measurement should be checked and adjusted accordingly.

In addition, the phase of the cross-spectrum should be examined to confirm that meaningful information has been gathered. Finally, it may be useful to compare the autospectrums from each geophone to determine which frequencies have been excited sufficiently enough to provide good transfer function data. In particular, the autospectrum from the geophone farthest from the source may indicate the upper limit of frequencies which can be excited at that particular distance.

Permanent Data Storage

When a satisfactory measurement has been obtained and checked, each available function should be recorded on magnetic tape. The available functions should include the transfer function, the coherence function, the cross-spectrum, and both autospectrums. Although the two autospectrums could be used to reconstruct the other three functions, it is most convenient to save all five functions directly while in the field.

Additionally, it may be desirable to save the "measurement state" associated with the measurement. In general, this probably will not be necessary if the measurement state follows the specifications given in Fig A.2. Usually only the bandwidth will vary (and possibly the range), then only the particular bandwidth for the measurement needs to be recorded. The only pertinent information that needs to be recorded is the location of the geophones for each measurement in order to calculate the distance between the geophones. For convenience, the tape record number should be listed for each function as it is saved. A typical field log containing the necessary information is shown in Fig A.4.

IN-HOUSE DATA ANALYSIS

The reduction and analysis of the data can be divided into three major processes:

(1) preparation of frequency and phase arrays to be used as input data for computer programs,

(2) execution of computer programs to reduce data and provide output tables and plots, and

(3) analyses of the tables and plots to determine the shear wave velocity profile.

Each of these processes is discussed in the following paragraphs. Complete listings of the computer programs and an explanation of their use are contained in Appendix B.

DATE: 3/19/81 LOCATION: Walnut Creek

TAPE IDENTIFICATION: WC-2 TAPE TRACK NO.: 1

SETUP STATE NUMBER	DATA RECORD NUMBER	TYPE OF FUNCTION	DESCRIPTION OF CHANNEL #1 INPUT	DESCRIPTION OF CHANNEL #2 INPUT
1	1	TM REC	V. Geo @ 2' from	source, T=80 msec
2	2	TM REC	V. Geo @ 2' from	source, T=1.28 sec
3	3	TRANS	V. Geo @ 2'	V. Geo @ 4'
BW=1600	4	COHER		
	5	AUTO 1		
	6	AUTO 2		
	7	CROSS		
4	8	TRANS	V. Geo @ 2'	V. Geo @ 8'
BW=100	9	COHER		
	10	AUTO 1		
	11	AUTO 2		
	12	CROSS		
5	13	TRANS	V. Geo @ 2'	V. Geo @ 16'
BW=100	14	COHER		

Fig A.4. Example of typical field log.

Preparation of Data Arrays

The computer programs are designed to convert phase data to velocity and wavelength information for selected frequencies. Currently, the input arrays are dimensioned to handle 50 pairs of frequency and phase data (f,θ).

The selected frequencies can range over the entire bandwidth for which the measurement was obtained. However, in general, the selected frequencies should not be evenly distributed over the bandwidth if a well-distributed velocity profile is desired. More concentration should be given to the lower frequencies (about 5 to 40 Hz) than to the higher frequencies (about 80 Hz or greater) since a few Hz increase between selected frequencies may represent a large percentage increase in the low frequency range. This effect is best illustrated by considering a simple profile which has a constant velocity of 500 fps to a depth well beyond the region of interest. Then, frequencies of 10 and 20 Hz yield wavelengths of 50 and 25 ft, respectively, while frequencies of 100 and 110 Hz yield wavelengths of 5 and 4.5 ft, respectively. In both cases, the difference between the selected frequencies is 10 Hz. However, in the low frequency range this difference represents a difference in wavelength of 25 ft. In the higher frequency range, the same 10-Hz difference represents a difference in wavelength of only 0.5 ft. To obtain an even distribution of wavelengths so that the velocity profile is well distributed, the difference between selected frequencies should be quite small (only 1 or 2 Hz) at low frequencies and should gradually increase to a relatively large difference (perhaps 10 to 100 Hz) at higher frequencies.

The determination of the phase of the cross-spectrum is facilitated by using the x-cursor with the display. The x-cursor is located by specifying a selected frequency, at which time the y-value (phase) at the intersection of

the cursor and plot is also displayed. It is not necessary to scale off values from a hard copy.

The coherence function should be used in conjunction with selecting frequency and phase. If the cross-spectrum and coherence are displayed in an "over and under" fashion as shown in Fig A.5, zones can be readily identified where the phase data may be suspect. If possible, zones of frequencies which exhibit poor coherence should be avoided when selecting phase information. For example, in Fig A.5, frequencies below about 12 Hz and above about 85 Hz exhibit poor coherence, and phase data in these regions should be used with caution. Occasionally such zones are unavoidable. When data of poorer quality must be used, such data should be closely examined throughout the analysis process.

By design, the HP 5423A displays phase information between the limits of +180 degrees to -180 degrees, as shown in Fig A.6a. When phase values pass between the second and third quadrants of a circle, the value and sign are adjusted accordingly to maintain all phase data between these limits. For example, a phase value of -190 degrees would actually be displayed as 170 degrees. The computer programs are constructed to accept the phase data exactly as it appears in the display. However, when the data is reduced by the computer, it must be "unravelled" as if it were displayed as shown in Fig A.6b.

Special attention must be given to regions where the phase fluctuates about 180 degrees (or -180 degrees). The plots in Fig A.6 illustrate such a region from about 75 to 95 Hz. In Fig A.6a, there appear to be two complete (360 degrees) phase shifts within only a few Hz. However, this is a result of the graphic limitations of the display. Figure A.6b indicates that the

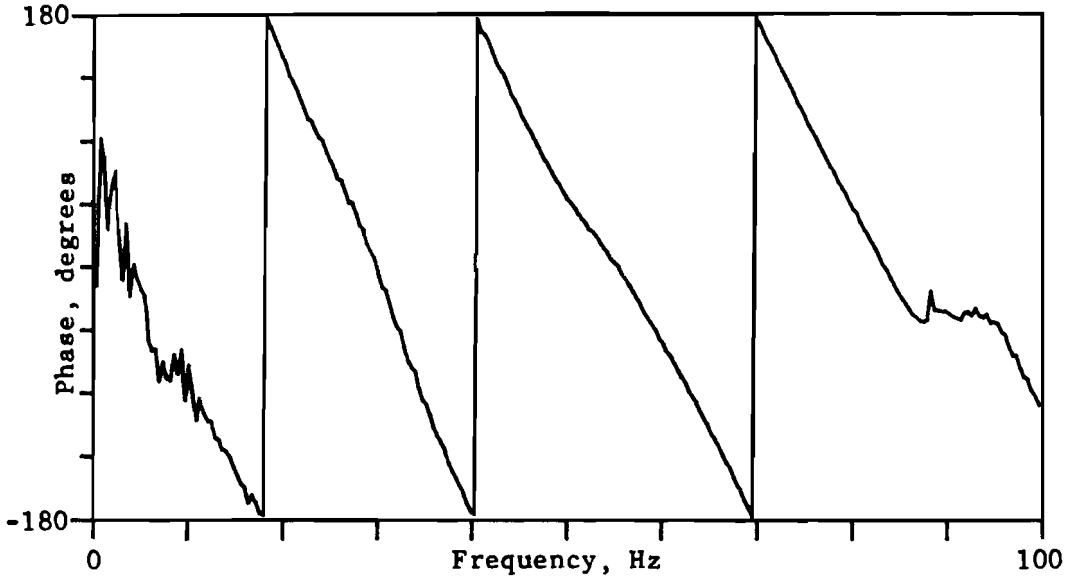

(a) Phase of the cross spectrum

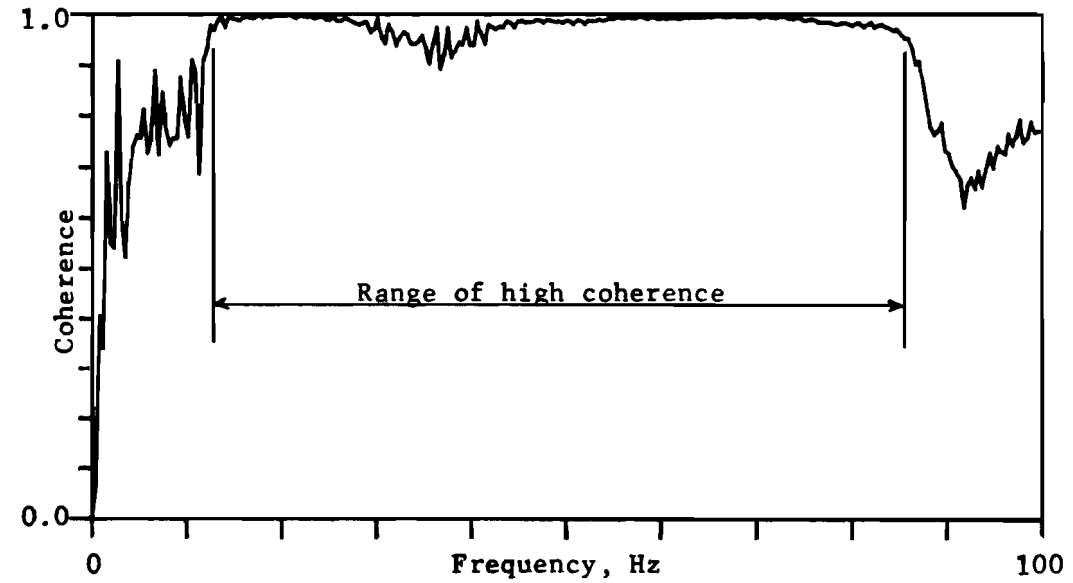

(b) Coherence function

Fig A.5. Use of the coherence function in conjunction with the phase of the cross spectrum.

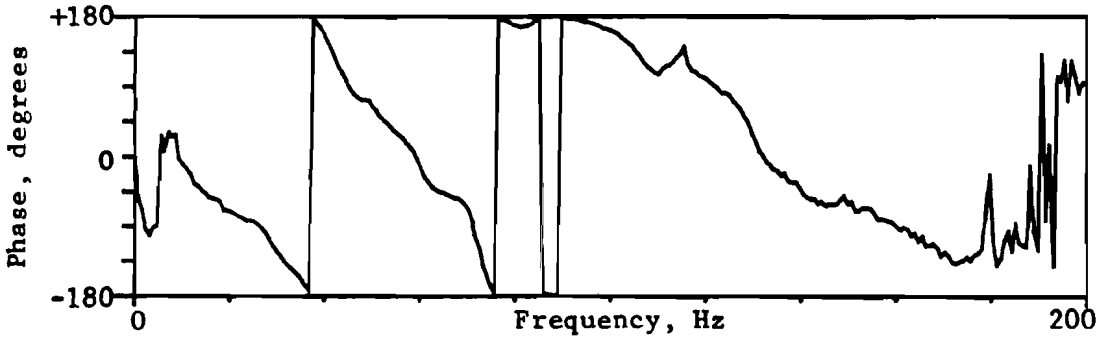

(a) Original ("Displayed") phase plot.

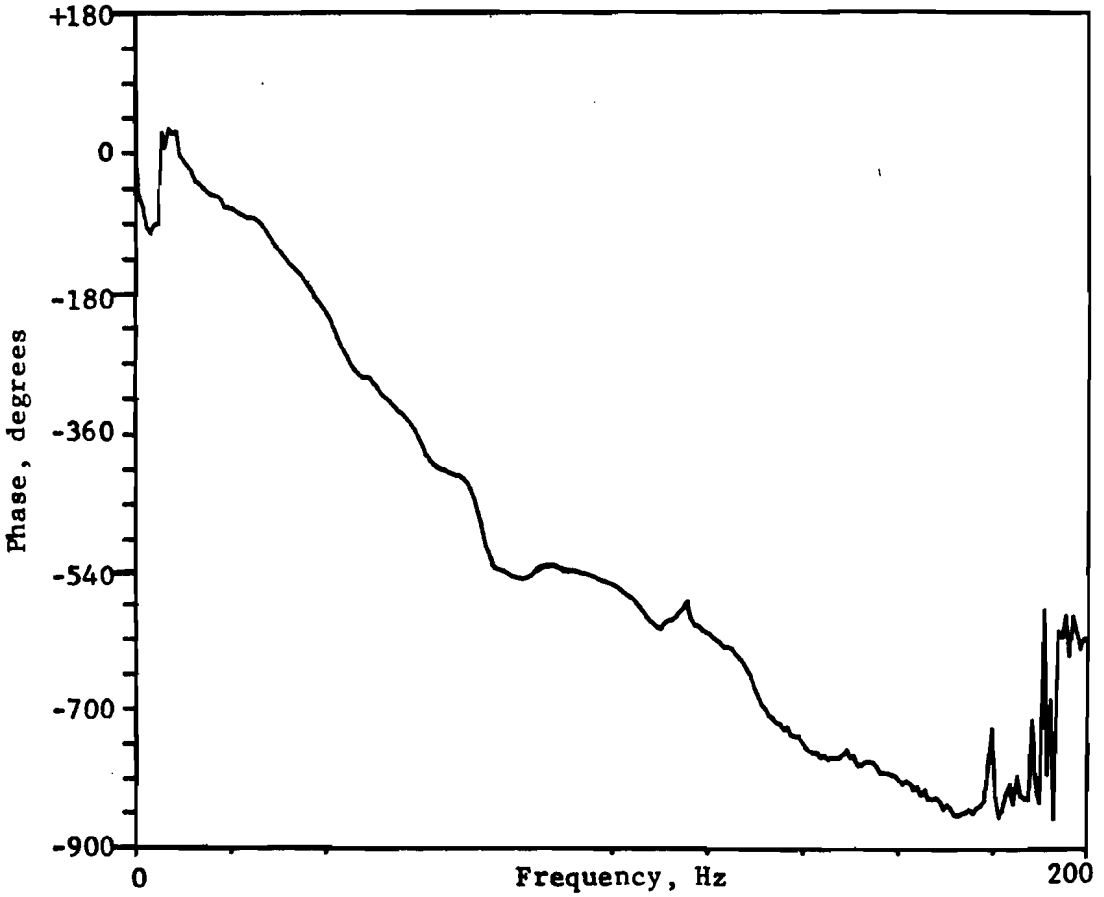

(b) True ("Unraveled") phase plot.

Fig A.6. Comparison of "Displayed" and "Unraveled" phase plots.

apparent shifts result from slight variations in the phase and are not actual phenomena.

Utilization of Computer Programs

The computer programs used to reduce data and plot results do not contain complicated algorithms. The purpose of the programs is to perform a large number of repetitive calculations which would require significantly more time to perform by hand. The plot routines also feature the flexibility to compare the influence of various parameters on the velocity profile. Details of how each program functions and what data each requires are given in Appendix B. For the most part, only the role of each program as it relates to the analysis process is discussed in this section.

The first step is to reduce all of the available records (measurements) using program PHAS. PHAS uses the phase information from the cross-spectrum to calculate a travel time for each frequency that is given. The phase difference, θ, between the signals of the input and output geophones represents the time lag or travel time, Δt, for an R-wave (of frequency f and velocity V_R) to propagate over the distance between the two geophones. The phase difference is 360 degrees for a travel time equal to the period of wave, T. With T/360 as a proportionality factor, the relationship for travel time is

$$\Delta t = \frac{T}{360^\circ}\,\theta \qquad (A.1)$$

Because the frequency is the inverse of the period, travel time can be written as

$$\Delta t = \frac{\theta}{360^\circ} \frac{1}{f} \qquad (A.2)$$

The distance Δx between the geophones is a known parameter, and, therefore, the velocity is readily calculated by

$$V_R = \frac{\Delta x}{\Delta t} \qquad (A.3)$$

Now both frequency and velocity are known and the wavelength of the R-wave can be calculated by

$$L_R = \frac{V_R}{f} \qquad (A.4)$$

PHAS also calculates approximate depths for each calculated velocity using both $L_R/2$ and $L_R/3$ as criteria for depth.

A plot of frequency versus wavelength can be obtained by using program FWPL. This plot serves as a guide for determining which frequencies should be used to develop the velocity profile. Since depth is related to wavelength, the plot can be used to approximate the depth to which meaningful data is available.

Program VDPL yields a velocity versus depth plot using nearly the same input as program PHAS. The depth is determined by specifying a fraction of the wavelength such as $L_R/2$ or $L_R/3$. The appropriate criterion can be first estimated by examining the output from PHAS. If distinct layering is present at the site, then program VDPL should graph relatively distinct contrasts in velocity for each layer. The appropriate depth criterion can be established when the layer boundaries indicated by the plot occur at the same depths as those at the site.

In addition to VDPL, layering may also be depicted in a plot of frequency versus velocity provided by program FVPL. Lines which separate contrasting velocity layers and which pass through the origin will have a slope of $1/L_R$. From the slope, wavelengths (and subsequently, depths) can be calculated for each layer boundary.

Analysis of Results

Analysis of the results must coincide with the use of the programs and plot routines in order to determine the velocity profile. The selection of an appropriate depth factor for the plot programs relies on an analysis of the calculated velocities and corresponding layering.

In addition, any apparent anomalies in the velocity profile should be checked. The frequency and phase which yielded an unusually low or high velocity should be traced back to the cross-spectrum from which they came. The corresponding coherence function should be re-examined to verify the quality of the measurement at that particular frequency. The phase plot should also be rechecked to make sure regions which exhibit apparent phase shifts (the effect of the 180-degree limit) have been interpreted correctly.

Finally, the velocity profile may be refined by eliminating some of the scatter associated with wavelengths not suitable for the spacing between geophones for a particular measurement. A workable criterion was developed in Chapter 4 and was given (Eq 4.5) as

$$\tfrac{1}{2}\Delta x \leq L_R \leq 3\Delta x \qquad (A.5)$$

Wavelengths (or frequencies) which do not fall within the constraints of Eq 4.5 can be screened out by checking the output from PHAS. Inappropriate data can be excluded from the final data arrays prior to using VDPL for the final velocity profile.

APPENDIX B

COMPUTER PROGRAMS AND PLOT ROUTINES

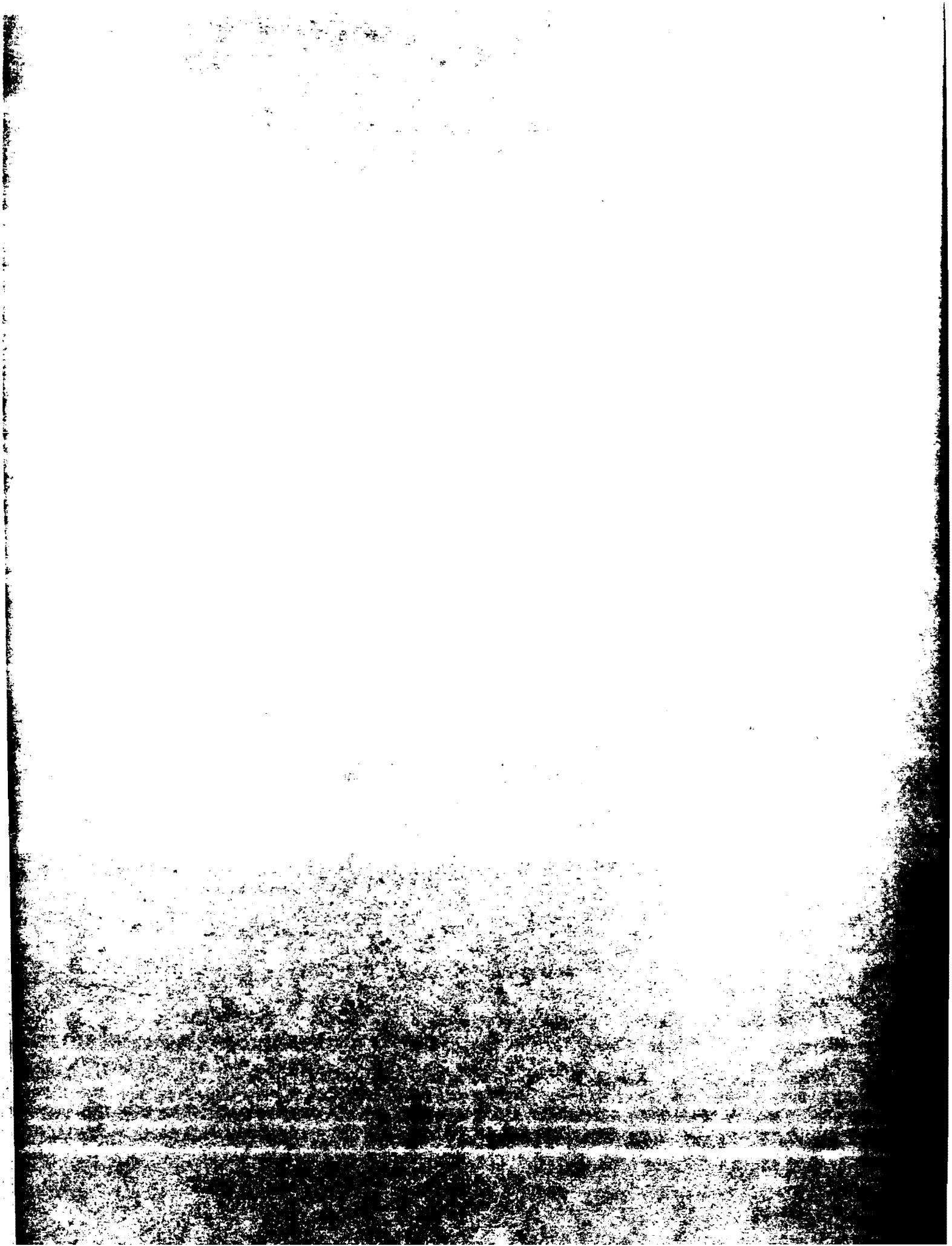

APPENDIX B

COMPUTER PROGRAMS AND PLOT ROUTINES

This appendix includes a listing of each computer program and plot routine used in the reduction and analysis of cross-spectrum data. In addition, a brief description of the capabilities, limitations, and input requirements precedes each program. Sample input and output are included for the reader's benefit.

B.1. PROGRAM PHAS

Program PHAS is the foundation program for the reduction of frequency-phase data. A major portion of PHAS also serves as a first state in each of the plot routines. The input data file for program PHAS can be readily modified to use with any of the plot programs.

Principal variables in PHAS are defined in the variable list of the program listing. Input variables include: NREC, DATFIL, RECN, TRKN, X1, X2, BW, SOURCE, and the primary data arrays FR (frequency) and PH (phase). All data can be input with free-field format with the exception of the alphanumeric titles DATFIL and SOURCE. Input of a negative number for a value of frequency terminates the input of (f,θ) pairs and concludes the input of data for that particular record. A sample input data file is shwn in Fig B.1.

Details on how to select values of frequency and phase are given in Appendix A. The input phase (PH) is that value which was obtained directly from the frequency-phase display. The computer program calculates the "true" phase or "unravelled" phase by tracking the switch from -180 degrees to +180 degrees by means of the integer variable NP. The value of NP is initialized as zero and is increased by 1 each time the 180-degree switch occurs. The limits on the switch are quite liberal; if the present value of PH is greater than 45 degrees and the previous value of PH was less than -90 degrees, the program assumes that the -180 degrees to +180 degrees switch has occurred. These limits provide minimal restraint if θ is changing rapidly as a function of frequency. However, input data should be checked to make sure that erroneous switches cannot be interpreted from a particular sequence of phase values.

```
      PROGRAM PHAS(INPUT,OUTPUT,TAPE1=INPUT)
C
C     THIS PROGRAM USES PHASE INFORMATION FROM
C         THE CROSS POWER SPECTRUM TO DEVELOP A
C         VELOCITY VS DEPTH PROFILE
C
C*************************************************************************
C                          VARIABLE LIST
C*************************************************************************
C   BW       BANDWIDTH (RANGE OF FREQUENCIES) OF MEASUREMENT
C   CNVRT    VALUE USED TO CONVERT R-WAVE VELOCITY TO S-WAVE VELOCITY
C   DATFIL   TITLE FOR IDENTIFICATION OF SINGLE DATA FILE
C   DELF     FREQUENCY RESOLUTION OF MEASUREMENT
C   DELT     TIME RESOLUTION OF MEASUREMENT
C   DELX     DISTANCE BETWEEN GEOPHONES
C   DL2      DEPTH CALCULATED USING WAVELENGTH DIVIDED BY 2
C   DL3      DEPTH CALCULATED USING WAVELENGTH DIVIDED BY 3
C   FR( )    FREQUENCY INPUT ARRAY
C   FRACT    NUMBER BY WHICH WAVELENGTH IS DIVIDED TO OBTAIN DEPTH
C   NP       PARAMETER USED TO UNRAVEL FREQUENCY-PHASE PLOT
C   NREC     NUMBER OF RECORDS TO BE READ FOR A GIVEN RUN OF PROGRAM
C   PH( )    PHASE INPUT ARRAY
C   PHADJ    ADJUSTED PHASE VALUE AFTER UNRAVELING
C   RECN     RECORD NUMBER (FROM HP5423A TAPE) TO IDENTIFY DATA
C   SOURCE   TITLE FOR SOURCE USED TO MAKE MEASUREMENT
C   TITLE    TITLE FOR FIGURE OF RESULTANT PLOT
C   TMLEN    TIME LENGTH OF MEASUREMENT
C   TRKN     TRACK NUMBER (FROM HP5423A TAPE) TO IDENTIFY DATA
C   TT       CALCULATED TRAVEL TIME OF WAVE
C   TTM      CALCULATED TRAVEL TIME IN MILLISECONDS
C   VEL      CALCULATED VELOCITY
C   WL1      CALCULATED WAVELENGTH; WL( ) IS USED IN PLOT PROGRAMS
C   X1       DISTANCE FROM SOURCE TO FIRST (NEAR) GEOPHONE
C   X2       DISTANCE FROM SOURCE TO SECOND (FAR) GEOPHONE
C*************************************************************************
      INTEGER DATFIL(5),SOURCE(10),RECN,TRKN
      DIMENSION FR(50),PH(50)
      READ (1, ) NREC
      DO 116 IREC=1,NREC
      PRINT 100
  100 FORMAT (=1=,3X)
      READ  101,(DATFIL(N),N=1,5)
      READ (1, ) RECN,TRKN
      READ (1, ) X1,X2,BW
      READ  102,(SOURCE(N),N=1,10)
  101 FORMAT (X,A3,9A4)
  102 FORMAT (X,A3,9A4)
      DELX=X2-X1
      DELF=BW/256.0
      TMLEN=1.0/DELF
      DELT=TMLEN*1000.0/1024.0
      PRINT 103,(DATFIL(N),N=1,5),RECN,TRKN
  103 FORMAT(X,10HDATA FILE:,X,A3,4A4,3X,17HTAPE RECORD NO.: ,
     1    I2,1H(,I1,1H))
      PRINT 104,X1,X2
  104 FORMAT (X,21HGEOPHONES LOCATED AT ,F6.2,8H FT AND ,F6.2,3H FT)
      PRINT 105,DELX
  105 FORMAT (X,28HDISTANCE BETWEEN GEOPHONES: ,F6.2,3H FT)
      PRINT 106,(SOURCE(N),N=1,10)
  106 FORMAT (X,7HSOURCE:,X,A3,9A4)
      PRINT 107,BW,DELF
```

```
107 FORMAT (X,14HBANDWIDTH=,F8.2,3H HZ,8X,11HRESOLUTION=,F8.4,3H HZ)
    PRINT 108,TMLEN,DELT
108 FORMAT (X,11HTIMELENGTH=,F7.2,4H SEC,7X,11HRESOLUTION=,F8.4,
   1    5H MSEC)
    IO=1
109 READ (1, ) FR(IO),PH(IO)
    IF(FR(IO).LT.0.0) GO TO 110
    IO=IO+1
    GO TO 109
110 IOF=IO-1
    PRINT 111
111 FORMAT (//2X,9HFREQUENCY,4X,5HPHASE,3X,16HTRAVEL  VELOCITY,
   1    2X,10HWAVELENGTH,6X,5HDEPTH)
    PRINT 112
112 FORMAT (20X,4HTIME,26X,3HL/2,5X,3HL/3)
    PRINT 113
113 FORMAT (9X,4H(HZ),5X,16H(DEGREES) (MSEC),3X,5H(FPS),
   1    7X,4H(FT),6X,4H(FT),4X,4H(FT))
    PRINT
    NP=0
    DO 115 IO=1,IOF
    IF(PH(IO).GT.45.0.AND.PH(IO-1).LT.-90.0) NP=NP+1
    RNP=NP
    PHADJ=(RNP-(PH(IO)/360.0))*360.0
    TT=PHADJ/360.0/FR(IO)
    TTM=TT*1000.0
    VEL=DELX/TT
    WL1=VEL/FR(IO)
    DL2=WL1/2.0
    DL3=WL1/3.0
    PRINT 114,FR(IO),PHADJ,TTM,VEL,WL1,DL2,DL3
114 FORMAT (2X,F8.3,3X,F7.2,F9.3,F9.1,4X,F7.3,2X,2(2X,F6.3))
115 CONTINUE
116 CONTINUE
    END
```

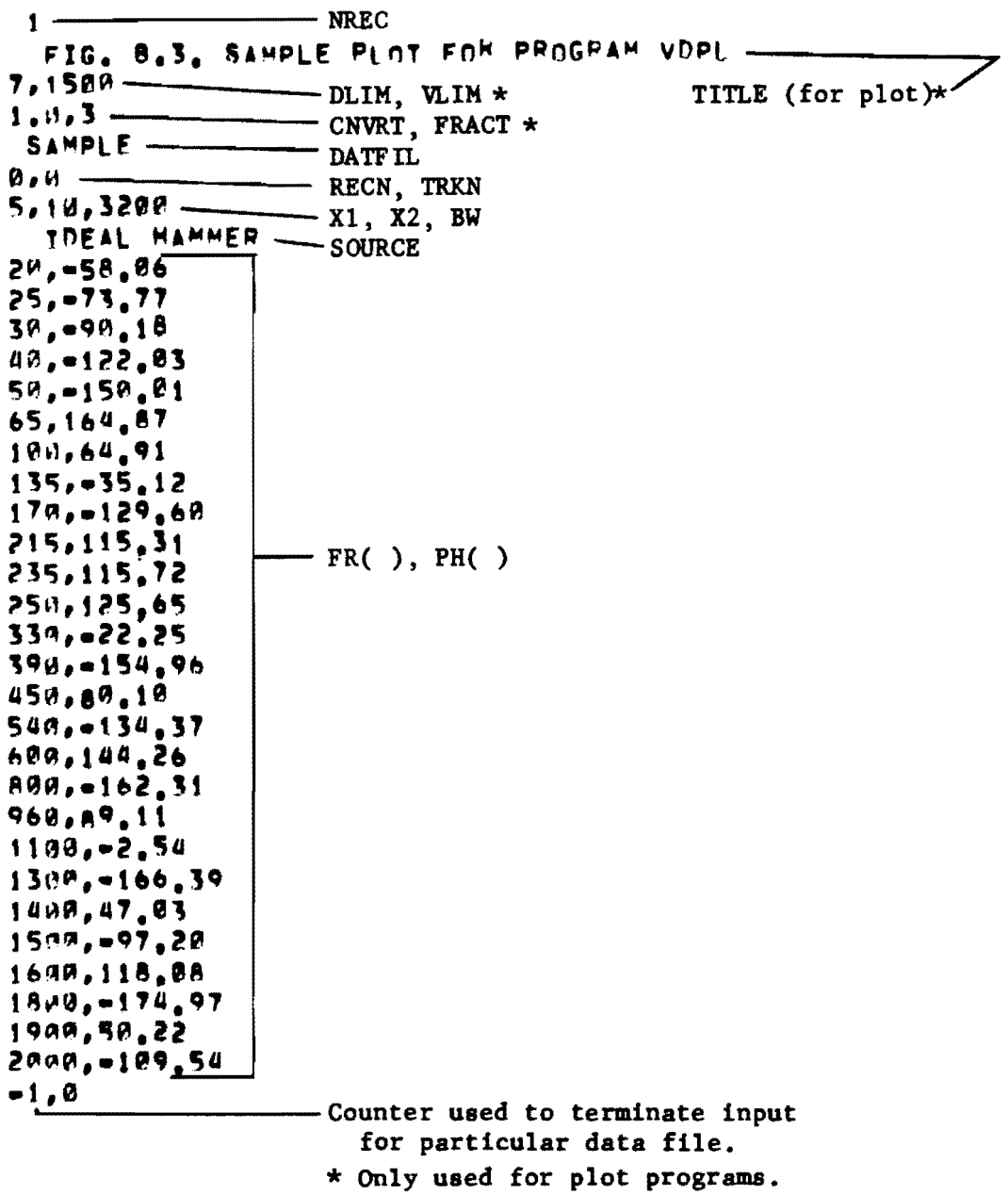

Fig B.1. Sample input data file.

The reduced data and calculations are output in a table which includes frequency, "true" phase, and the travel time, velocity, and wavelength of the wave associated with each particular frequency. Values of depth based on $L_R/2$ and $L_R/3$ are also listed. Each new record yields a summary table, such as Table B.1., beginning on a new page. There is no limit to the number of records (NREC) which can be reduced in a single run of PHAS.

DATA FILE: SAMPLE TAPE RECORD NO.: #(0)
GEOPHONES LOCATED AT 5.00 FT AND 10.00 FT
DISTANCE BETWEEN GEOPHONES: 5.00 FT
SOURCE: IDEAL HAMMER
BANDWIDTH: 3200.00 HZ RESOLUTION: 12.5000 HZ
TIMELENGTH: .08 SEC RESOLUTION: .0781 MSEC

FREQUENCY (HZ)	PHASE (DEGREES)	TRAVEL TIME (MSEC)	VELOCITY (FPS)	WAVELENGTH (FT)	DEPTH L/2 (FT)	DEPTH L/3 (FT)
20.000	58.06	8.064	620.0	31.002	15.501	10.334
25.000	73.77	8.197	610.0	24.400	12.200	8.133
30.000	90.18	8.350	598.8	19.960	9.980	6.653
40.000	122.03	8.474	590.0	14.750	7.375	4.917
50.000	150.01	8.334	600.0	11.999	6.000	4.000
65.000	195.13	8.339	599.6	9.225	4.612	3.075
100.000	295.09	8.197	610.0	6.100	3.050	2.033
135.000	395.12	8.130	615.0	4.556	2.278	1.519
170.000	489.60	8.000	625.0	3.676	1.838	1.225
215.000	604.69	7.813	640.0	2.977	1.488	.992
235.000	684.28	7.143	700.0	2.979	1.489	.993
250.000	594.35	6.604	757.1	3.029	1.514	1.010
330.000	742.25	6.248	800.3	2.425	1.213	.808
390.000	874.96	6.232	802.3	2.057	1.029	.686
450.000	999.90	6.172	810.1	1.800	.900	.600
540.000	1214.37	6.247	800.4	1.482	.741	.494
600.000	1295.74	5.999	833.5	1.389	.695	.463
800.000	1602.31	5.564	898.7	1.123	.562	.374
960.000	1710.89	4.950	1010.0	1.052	.526	.351
1100.000	1802.54	4.552	1098.4	.999	.499	.333
1300.000	1966.39	4.202	1190.3	.915	.458	.305
1400.000	2112.97	4.192	1192.6	.852	.426	.284
1500.000	2257.20	4.180	1196.2	.797	.399	.266
1600.000	2401.92	4.170	1199.0	.749	.375	.250
1800.000	2694.97	4.159	1202.2	.668	.334	.223
1900.300	2829.78	4.137	1208.6	.636	.318	.212
2000.000	2989.54	4.152	1204.2	.602	.301	.201

Table B.1. Sample output from program PHAS.

B.2 PROGRAM FWPL

Program FWPL uses the reduced frequency and phase data to plot frequency versus wavelength. There is no limit to the number of records which can be stacked together for a single plot. However, each record is plotted with the same symbol. The data input is nearly identical to the one used for PHAS. Three new variables (TITLE, FLIM, and WLIM) are required and are input immediately after NREC, prior to reading the first record. The alphanumeric variable TITLE is an overall title which serves as a caption for the plot. Variables FLIM and WLIM are used to establish the limits of the plot.

Values of frequency are scaled to a 5-inch horizontal axis while values of wavelength are scaled to a 7-inch vertical axis. In order to avoid the irregular bounds set up by the plot commands, a sorting routine is used to establish rational bounds and to screen out data outside these bounds. Both variables, wavelength and frequency, have lower bounds of zero. The maximum value of frequency is not fixed and must be input as variable FLIM. Similarly, the maximum value of wavelength must be input as WLIM. The scale(s) for the plot are then determined as 1 inch = FLIM/5 and 1 inch = WLIM/7. Appropriate selection of FLIM and WLIM will yield a plot which can be conveniently used with an engineer°s scale. A sample plot for program FWPL is shown in Fig B.2.

```
      PROGRAM FWPL(INPUT,OUTPUT,TAPE1=INPUT,PLOTR)
C
C     THIS PROGRAM USES PHASE INFORMATION FROM
C         THE CROSS POWER SPECTRUM TO DEVELOP A
C         FREQUENCY VS WAVELENGTH PLOT
C
C*****************************************************************************
C          INITIALIZES PROGRAM TO REDUCE AND PLOT NREC NUMBER OF
C             RECORDS STACKED TOGETHER
C*****************************************************************************
      INTEGER TITLE(8),DATFIL(5),SOURCE(10),RECN,TRKN
      DIMENSION FR(50),PH(50),WL(50),PFR(50),PWL(50)
      READ (1, ) NREC
      READ  100,(TITLE(N),N=1,8)
  100 FORMAT (8A10)
      READ (1, ) FLIM,WLIM
      CALL PLOTS (0.2,0.0,5HPLOTR)
      CALL PLOT (1.8,2.0,-3)
      DO 120 IREC=1,NREC
C*****************************************************************************
C          READS DATA FOR CURRENT RECORD
C*****************************************************************************
      READ  101,(DATFIL(N),N=1,5)
      READ (1, ) RECN,TRKN
      READ (1, ) X1,X2,BW
      READ  102,(SOURCE(N),N=1,10)
  101 FORMAT (X,A3,8A4)
  102 FORMAT (X,A3,9A4)
      DELX=X2-X1
      DELF=BW/256.0
      TMLEN=1.0/DELF
      DELT=TMLEN*1000.0/1024.0
      PRINT 103,(DATFIL(N),N=1,5),RECN,TRKN
  103 FORMAT(X,10HDATA FILE:,X,A3,4A4,3X,17HTAPE RECORD NO.: ,
     1    I2,1H(,I1,1H))
      PRINT 104,X1,X2
  104 FORMAT (X,21HGEOPHONES LOCATED AT ,F6.2,8H FT AND ,F6.2,3H FT)
      PRINT 105,DELX
  105 FORMAT (X,28HDISTANCE BETWEEN GEOPHONES: ,F6.2,3H FT)
      PRINT 106,(SOURCE(N),N=1,10)
  106 FORMAT (X,7HSOURCE:,X,A3,9A4)
      PRINT 107,BW,DELF
  107 FORMAT (X,10HBANDWIDTH:,F8.2,3H HZ,8X,11HRESOLUTION:,F8.4,3H HZ)
      PRINT 108,TMLEN,DELT
  108 FORMAT (X,11HTIMELENGTH:,F7.2,4H SEC,7X,11HRESOLUTION:,F8.4,
     1    5H MSEC)
      PRINT
      IO=1
  109 READ (1, ) FR(IO),PH(IO)
      IF(FR(IO).LT.2.0) GO TO 110
      IO=IO+1
      GO TO 109
  110 IOF=IO-1
C*****************************************************************************
C          CALCULATES FREQUENCY, VELOCITY, AND WAVELENGTH INFORMATION
C*****************************************************************************
      NP=0
      DO 111 IO=1,IOF
      IF(PH(IO).GT.45.0.AND.PH(IO-1).LT.-90.0) NP=NP+1
      RNP=NP
      PHADJ=(RNP-(PH(IO)/360.0))*360.0
```

```
      TT=PHADJ/360.0/FR(IO)
      VEL=DELX/TT
      WL(IO)=VEL/FR(IO)
  111 CONTINUE
C*************************************************************************
C           SORTS FREQUENCY AND WAVELENGTH ARRAYS TO PREPARE FOR
C              DESIRED PLOT FROM CURRENT RECORD
C*************************************************************************
      PRINT 112
      PRINT
  112 FORMAT (3X,17HDATA FOR PLOTTING)
      DO 113 IO=1,IOF
      IF(WL(IO).LT.WLIM) GO TO 114
  113 CONTINUE
  114 IOB=IO
      DO 115 IO=1,IOF
      IF(FR(IO).GT.FLIM) GO TO 116
  115 CONTINUE
      IO=IOF+1
  116 IOE=IO-1
      IOP=1
      DO 118 IO=IOB,IOE
      PFR(IOP)=FR(IO)
      PWL(IOP)=WL(IO)
      PRINT 117,IOP,PFR(IOP),PWL(IOP)
  117 FORMAT (2X,I4,2(5X,F10.2))
      IOP=IOP+1
  118 CONTINUE
C*************************************************************************
C           SETS UP PARAMETERS AND EXECUTES PLOT FOR CURRENT RECORD
C*************************************************************************
      NPTS=IOP-1
      KCYCLE=1
      PFR(NPTS+1)=0.0
      FINC=FLIM/5.0
      PFR(NPTS+2)=FINC
      PWL(NPTS+1)=WLIM
      WINC=WLIM/7.0
      PWL(NPTS+2)=WINC
      IF(IREC.GT.1) GO TO 119
      CALL SYMBOL (-.5,-1.0,.12,TITLE,0.0,80)
      CALL AXIS (0.0,7.0,13HFREQUENCY, HZ,13,5.0,0.0,0.0,FINC)
      CALL AXIS (0.0,0.0,18HWAVELENGTH, FT,18,7.0,90.0,WLIM,WINC)
  119 CALL LINE (PFR,PWL,NPTS,KCYCLE,-1,3)
C*************************************************************************
C           RESETS FOR NEW RECORD
C*************************************************************************
      PRINT
  120 CONTINUE
C*************************************************************************
C           CLOSES PLOT AND TERMINATES PROGRAM
C*************************************************************************
      CALL PLOT (8.5,0.0,999)
      END
```

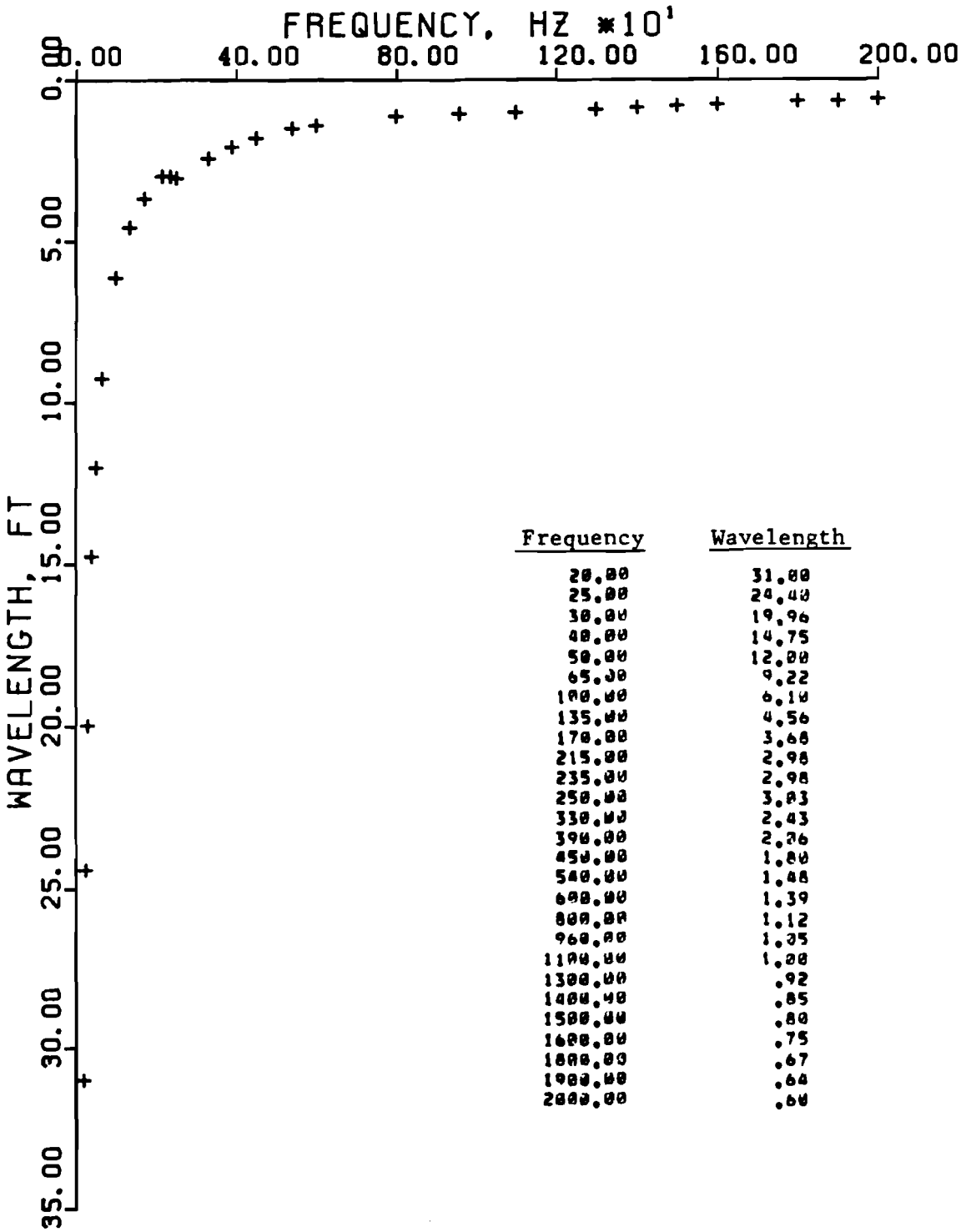

Frequency	Wavelength
20.00	31.00
25.00	24.40
30.00	19.96
40.00	14.75
50.00	12.00
65.00	9.22
100.00	6.10
135.00	4.56
170.00	3.68
215.00	2.98
235.00	2.98
250.00	3.03
330.00	2.43
390.00	2.06
450.00	1.80
540.00	1.48
690.00	1.39
800.00	1.12
960.00	1.05
1100.00	1.00
1300.00	.92
1400.00	.85
1500.00	.80
1600.00	.75
1800.00	.67
1900.00	.64
2000.00	.60

Fig B.2. Sample plot for program FWPL.

B.3 PROGRAM VDPL

Program VDPL uses the reduced frequency and phase data to plot velocity versus depth. There is no restriction on the number of records which can be incorporated into a single plot. However, each record is designated by a different symbol (for comparison purposes) and it is not practical to use more than six records on a single plot because this is the maximum number of easily recognizable symbols. The program designates symbols as follows:

□ First Record

○ Second Record

△ Third Record

\+ Fourth Record

X Fifth Record

◇ Sixth Record

Variables which must be input into VDPL include DLIM, VLIM, CNVRT, and FRACT. These variables must be input prior to reading in the first record. The variables DLIM and VLIM are used to set the maximum limits of the plot for depth and velocity, respectively. Values for DLIM are selected on the basis of which depth criterion is being used. Velocities are scaled to a 5-inch horizontal axis and depths are scaled to a 7-inch vertical axis. Appropriate selection of VLIM and DLIM will yield a plot which can be conveniently used with an engineer°s scale. For instance, convenient values of VLIM might be 750, 1000, or 1500 fps, depending on the material properties at a particular site. A sample plot for program VDPL is shown in Fig B.3.

Variables CNVRT and FRACT are found only in program VDPL. Since program PHAS calculates the Raleigh wave velocity, the calculated velocity must be

```
      PROGRAM VDPL(INPUT,OUTPUT,TAPE1=INPUT,PLOTR)
C
C     THIS PROGRAM USES PHASE INFORMATION FROM
C         THE CROSS POWER SPECTRUM TO DEVELOP A
C         VELOCITY VS DEPTH PLOT
C         DEPTH DETERMINED AS FRACTION OF WAVELENGTH
C
C*************************************************************************
C          INITIALIZES PROGRAM TO REDUCE AND PLOT NREC NUMBER OF
C             RECORDS STACKED TOGETHER
C*************************************************************************
      INTEGER TITLE(8),DATFIL(5),SOURCE(10),RECN,TRKN
      DIMENSION FR(50),PH(50),VEL(50),WL(50),PVEL(50),PWF(50)
      READ (1, ) NREC
      READ  100,(TITLE(N),N=1,8)
  100 FORMAT (8A10)
      READ (1, ) DLIM,VLIM
      READ (1, ) CNVRT,FRACT
      CALL PLOTS (0.0,0,0.0,5HPLOTR)
      CALL PLOT (1.0,2.0,-3)
      ILETT=0
      DO 120 IREC=1,NREC
C*************************************************************************
C          READS DATA FOR CURRENT RECORD
C*************************************************************************
      READ  101,(DATFIL(N),N=1,5)
      READ (1, ) RECN,TRKN
      READ (1, ) X1,X2,BW
      READ  102,(SOURCE(N),N=1,10)
  101 FORMAT (X,A3,9A4)
  102 FORMAT (X,A3,9A8)
      DELX=X2-X1
      DELF=BW/256.0
      TMLEN=1.0/DELF
      DELT=TMLEN*1000.0/1024.0
      PRINT 103,(DATFIL(N),N=1,5),RECN,TRKN
  103 FORMAT(X,10HDATA FILE:,X,A3,4A4,3X,17HTAPE RECORD NO.: ,
     1    I2,1H(,I1,1H))
      PRINT 104,X1,X2
  104 FORMAT (X,21HGEOPHONES LOCATED AT ,F6.2,8H FT AND ,F6.2,3H FT)
      PRINT 105,DELX
  105 FORMAT (X,28HDISTANCE BETWEEN GEOPHONES: ,F6.2,3H FT)
      PRINT 106,(SOURCE(N),N=1,10)
  106 FORMAT (X,7HSOURCE:,X,A3,9A4)
      PRINT 107,BW,DELF
  107 FORMAT (X,10HBANDWIDTH:,F8.2,3H HZ,8X,11HRESOLUTION:,F9.4,3H HZ)
      PRINT 108,TMLEN,DELT
  108 FORMAT (X,11HTIMELENGTH:,F7.2,4H SEC,7X,11HRESOLUTION:,F8.4,
     1    5H MSEC)
      PRINT
      IO=1
  109 READ (1, ) FR(IO),PH(IO)
      IF(FR(IO).LT.0.0) GO TO 110
      IO=IO+1
      GO TO 109
  110 IOF=IO-1
C*************************************************************************
C          CALCULATES FREQUENCY, VELOCITY, AND WAVELENGTH INFORMATION
C*************************************************************************
      NP=0
      DO 111 IO=1,IOF
```

```
      IF(PH(IO).GT.45.0.AND.PH(IO-1).LT.-90.0) NP=NP+1
      RNP=NP
      PHADJ=(RNP-(PH(IO)/360.0))*360.0
      TT=PHADJ/360.0/FR(IO)
      VEL(IO)=DELX/TT
      WL(IO)=VEL(IO)/FR(IO)
  111 CONTINUE
C*************************************************************************
C           SORTS VELOCITY AND WAVELENGTH ARRAY TO PREPARE FOR DESIRED
C              PLOT FROM CURRENT RECORD
C*************************************************************************
      WLIM=FRACT*DLIM
      PRINT 112
      PRINT
  112 FORMAT (3X,17HDATA FOR PLOTTING)
      DO 113 IO=1,IOF
      IF(WL(IO).LT.WLIM.AND.VEL(IO).LT.VLIM) GO TO 114
  113 CONTINUE
  114 IOB=IO
      DO 115 IO=IOB,IOF
      IF(VEL(IO).GT.VLIM) GO TO 116
  115 CONTINUE
      IO=IOF+1
  116 IOE=IO-1
      IOP=1
      DO 118 IO=IOB,IOE
      PVEL(IOP)=VEL(IO)/CNVRT
      PWF(IOP)=WL(IO)/FRACT
      PRINT 117,IOP,PVEL(IOP),PWF(IOP)
  117 FORMAT (2X,I4,2(5X,F10.2))
      IOP=IOP+1
  118 CONTINUE
      IOPT=IOP-1
C*************************************************************************
C           SETS UP PARAMETERS AND EXECUTES PLOT FOR CURRENT RECORD
C*************************************************************************
      NPTS=IOPT
      KCYCLE=1
      PVEL(NPTS+1)=0.0
      VINC=VLIM/5.0
      PVEL(NPTS+2)=VINC
      PWF(NPTS+1)=DLIM
      DINC=-DLIM/7.0
      PWF(NPTS+2)=DINC
      IF(IREC.GT.1) GO TO 119
      CALL SYMBOL (-.5,-1.0,.12,TITLE,0.0,80)
      CALL AXIS (0.0,7.0,13HVELOCITY, FPS,13,5.0,0.0,0.0,VINC)
      CALL AXIS (0.0,0.0,9HDEPTH, FT,9,7.0,90.0,0.0,DLIM,DINC)
  119 CALL LINE (PVEL,PWF,NPTS,KCYCLE,-1,ILETT)
C*************************************************************************
C           RESETS FOR NEW RECORD
C*************************************************************************
      ILETT=ILETT+1
      PRINT
  120 CONTINUE
C*************************************************************************
C           CLOSES PLOT AND TERMINATES PROGRAM
C*************************************************************************
      CALL PLOT (8.5,0.0,999)
      END
```

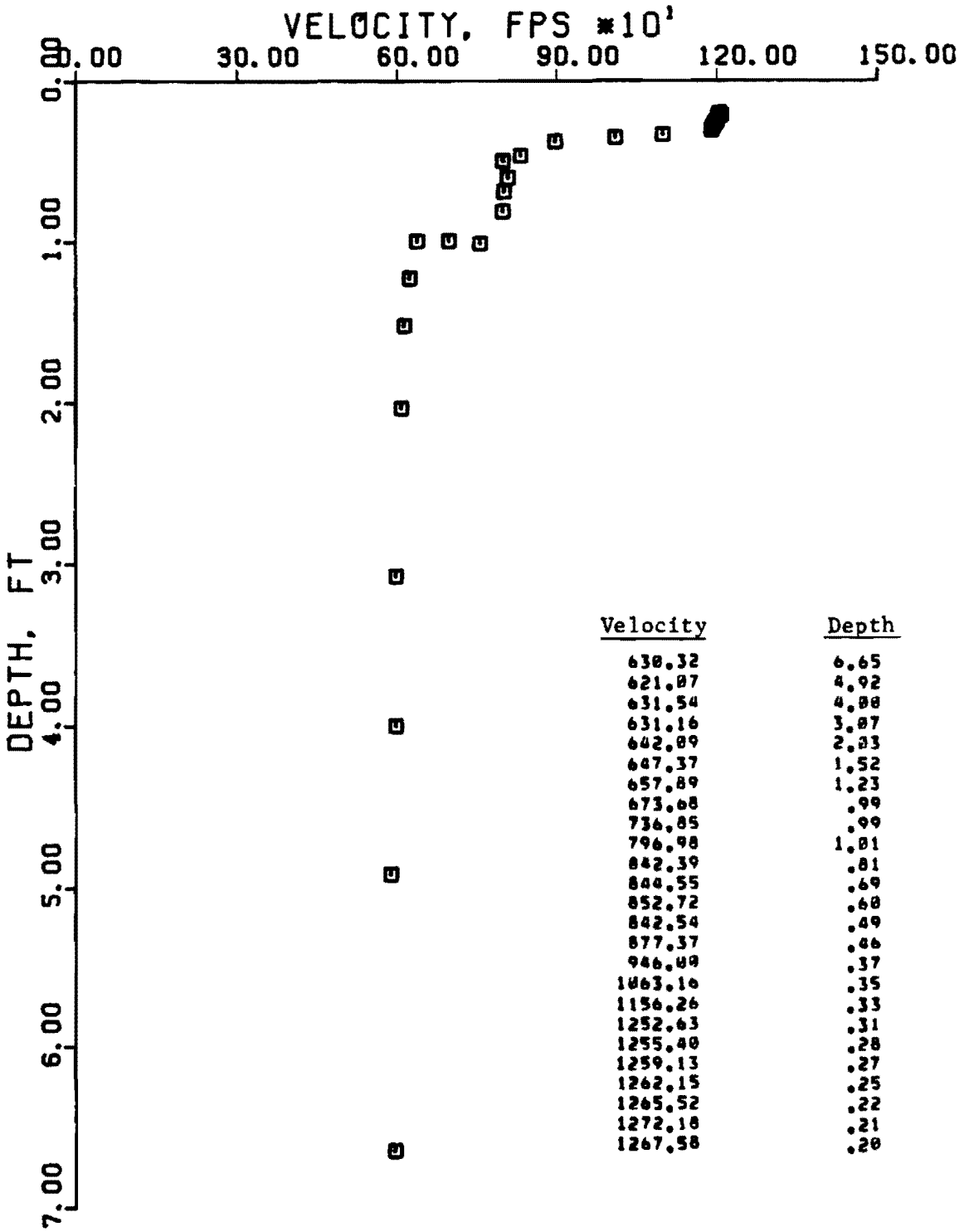

Fig B.3. Sample plot for program VDPL.

converted to a shear wave velocity. The conversion factor CNVRT is a function of Poisson's ratio and is given by

$$CNVRT = V_R / V_S$$

The value of CNVRT will always be less than 1.0. Additionally, the depth z which is associated with a particular velocity is defined by a fraction of the wavelength where

$$z = L_R / FRACT$$

The value of FRACT is always greater than or equal to 1.0. When FRACT = 1.0, the program provides a velocity versus wavelength plot.

B.4 PROGRAM FVPL

Program FVPL uses the reduced frequency and phase data to plot frequency versus velocity. The velocity that is plotted is the calculated Rayleigh wave velocity. There is no limit to the number of records which can be used for a single plot. However, it is not practical to use more than six records, since each record is designated by a different symbol as in program VDPL. Values for FLIM and VLIM must be input to establish plot limits. Frequencies are scaled to a 7-inch vertical axis while velocities are scaled to a 5-inch horizontal axis. A sample plot for program FVPL is shown in Fig B.4.

```
      PROGRAM FVPL(INPUT,OUTPUT,TAPE1=INPUT,PLOTR)
C
C     THIS PROGRAM USES PHASE INFORMATION FROM
C         THE CROSS POWER SPECTRUM TO DEVELOP A
C         FREQUENCY VS VELOCITY PLOT
C
C*****************************************************************
C          INITIALIZES PROGRAM TO REDUCE AND PLOT NREC NUMBER OF
C             RECORDS STACKED TOGETHER
C*****************************************************************
      INTEGER TITLE(8),DATFIL(5),SOURCE(10),RECN,TRKN
      DIMENSION FR(50),PH(50),VEL(50),WL(50),PVEL(50),PFR(50)
      READ (1, ) NREC
      READ  100,(TITLE(N),N=1,8)
  100 FORMAT (8A10)
      READ (1, ) FLIM,VLIM
      CALL PLOTS (0.0,0.0,0.0,5HPLOTR)
      CALL PLOT (1.9,2.5,-3)
      ILETT=0
      DO 120 IREC=1,NREC
C*****************************************************************
C          READS DATA FOR CURRENT RECORD
C*****************************************************************
      READ  101,(DATFIL(N),N=1,5)
      READ (1, ) RECN,TRKN
      READ (1, ) X1,X2,BW
      READ  102,(SOURCE(N),N=1,10)
  101 FORMAT (X,A3,4A4)
  102 FORMAT (X,A3,9A4)
      DELX=X2-X1
      DELF=BW/256.0
      TMLEN=1.0/DELF
      DELT=TMLEN*1000.0/1024.0
      PRINT 103,(DATFIL(N),N=1,5),RECN,TRKN
  103 FORMAT (X,10HDATA FILE:,X,A3,4A4,3X,17HTAPE RECORD NO.: ,
     1    I2,1H(,I1,1H))
      PRINT 104,X1,X2
  104 FORMAT (X,21HGEOPHONES LOCATED AT ,F6.2,4H FT AND ,F6.2,3H FT)
      PRINT 105,DELX
  105 FORMAT (X,20HDISTANCE BETWEEN GEOPHONES: ,F6.2,3H FT)
      PRINT 106,(SOURCE(N),N=1,10)
  106 FORMAT (X,7HSOURCE:,X,A3,9A4)
      PRINT 107,BW,DELF
  107 FORMAT (X,10HBANDWIDTH:,F8.2,3H HZ,8X,11HRESOLUTION:,F8.4,3H HZ)
      PRINT 108,TMLEN,DELT
  108 FORMAT (X,11HTIMELENGTH:,F7.2,4H SEC,7X,11HRESOLUTION:,F8.4,
     1    5H MSEC)
      PRINT
      IO=1
  109 READ (1, ) FR(IO),PH(IO)
      IF(FR(IO).LT.0.0) GO TO 110
      IO=IO+1
      GO TO 109
  110 IOF=IO-1
C*****************************************************************
C          CALCULATES FREQUENCY, VELOCITY, AND WAVELENGTH INFORMATION
C*****************************************************************
      NP=0
      DO 111 IO=1,IOF
      IF(PH(IO).GT.45.0.AND.PH(IO-1).LT.-90.0) NP=NP+1
      RNP=NP
```

```
      PHADJ=(RNP-(PH(IO)/360.0))*360.0
      TT=PHADJ/360.0/FR(IO)
      VEL(IO)=DELX/TT
      WL(IO)=VEL(IO)/FR(IO)
  111 CONTINUE
C*************************************************************************
C           SORTS VELOCITY AND FREQUENCY ARRAY TO PREPARE FOR DESIRED
C              PLOT FROM CURRENT RECORD
C*************************************************************************
      PRINT 112
      PRINT
  112 FORMAT (3X,17HDATA FOR PLOTTING)
      DO 113 IO=1,IOF
      IF(VEL(IO).LT.VLIM) GO TO 114
  113 CONTINUE
  114 IO8=IO
      DO 115 IO=IO8,IOF
      IF(FR(IO).GT.FLIM.OR.VEL(IO).GT.VLIM) GO TO 116
  115 CONTINUE
      IO=IOF+1
  116 IOE=IO-1
      IOP=1
      DO 118 IO=IO8,IOE
      PVEL(IOP)=VEL(IO)
      PFR(IOP)=FR(IO)
      PRINT 117,IOP,PVEL(IOP),PFR(IOP)
  117 FORMAT (2X,I4,2(5X,F10.2))
      IOP=IOP+1
  118 CONTINUE
      IOPT=IOP-1
C*************************************************************************
C           SETS UP PARAMETERS AND EXECUTES PLOT FOR CURRENT RECORD
C*************************************************************************
      NPTS=IOPT
      KCYCLE=1
      PVEL(NPTS+1)=0.0
      VINC=VLIM/5.0
      PVEL(NPTS+2)=VINC
      PFR(NPTS+1)=0.0
      FINC=FLIM/7.0
      PFR(NPTS+2)=FINC
      IF(IREC.GT.2) GO TO 119
      CALL SYMBOL (-.5,-1.5,.12,TITLE,0.0,80)
      CALL AXIS (0.0,0.0,13HVELOCITY, FPS,-13,5.0,0.0,0.0,VINC)
      CALL AXIS (0.0,0.0,13HFREQUENCY, HZ,13,7.0,90.0,0.0,FINC)
  119 CALL LINE (PVEL,PFR,NPTS,KCYCLE,-1,ILETT)
C*************************************************************************
C           RESETS FOR NEW RECORD
C*************************************************************************
      ILETT=ILETT+1
      PRINT
  120 CONTINUE
C*************************************************************************
C           CLOSES PLOT AND TERMINATES PROGRAM
C*************************************************************************
      CALL PLOT (0.5,0.0,999)
      END
```

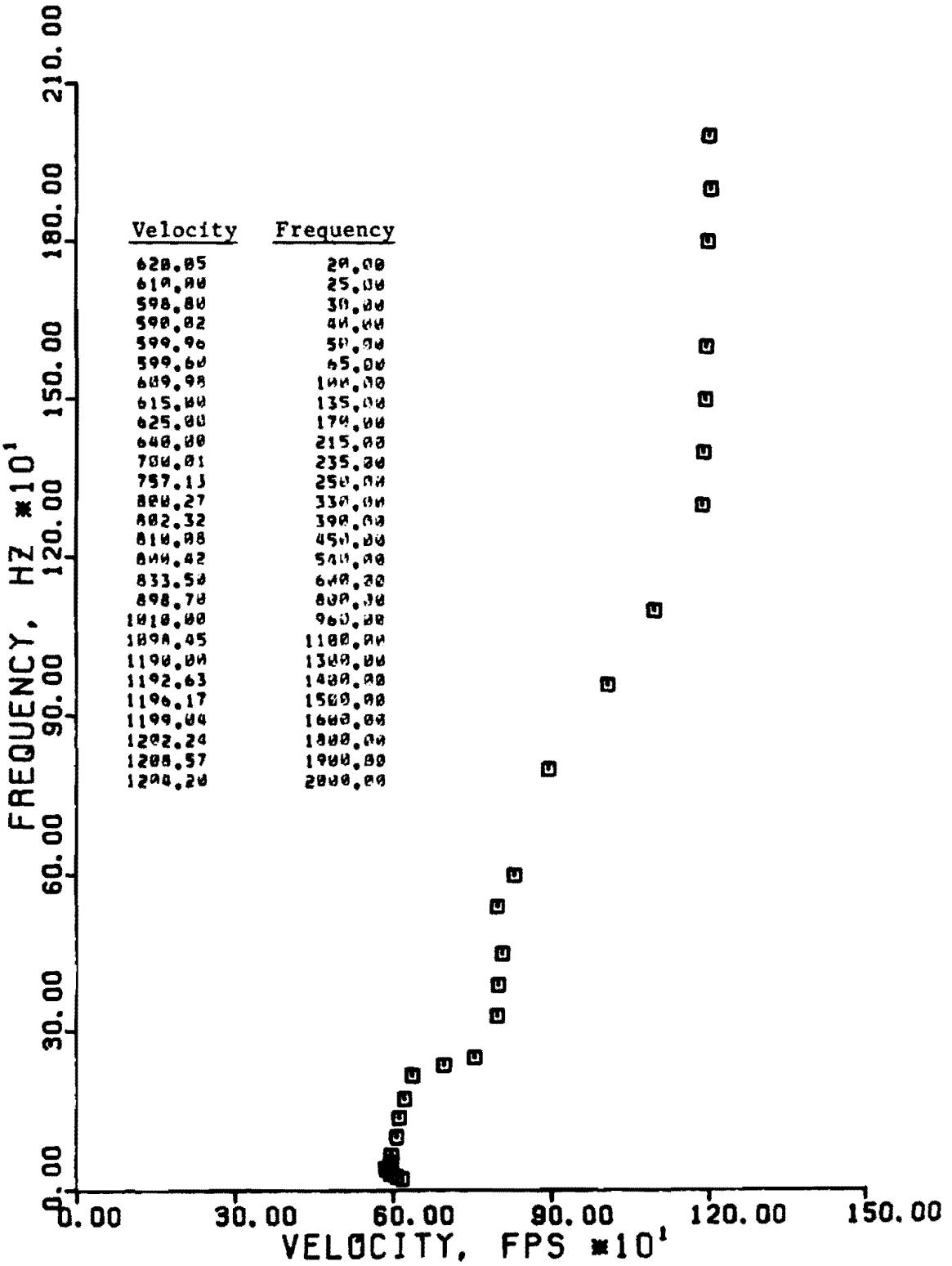

Fig B.4. Sample plot for program FVPL.

THE AUTHORS

J. Scott Heisey was born in Lancaster, Pennsylvania, on October 16, 1956. After graduating from Elizabethtown Area High School, Elizabethtown, Pennsylvania, in 1974, he entered Drexel University in Philidelphia. He received the degree of Bachelor of Science in Civil Engineering from Drexel University in June 1979. In Sepetember 1979, he entered The Graduate School of The University of Texas at Austin.

Kenneth H. Stokoe, II joined the faculty of the College of Engineering at The University of Texas at Austin in 1973. He is presently an Associate Professor of Civil Engineering and is actively involved with several on-going research projects. He has been working in the areas of in situ seismic measurement, laboratory measurement of dynamic soil properties, and the relationship between field and laboratory dynamic measurements for the past fifteen years. He was instrumental in developing the in situ crosshole seismic method for shear wave velocity and shear modulus measurements to the method that is presently used by most geotechnical engineering firms.

In addition to his teaching and research activities, Dr. Stokoe has served as a consultant to federal, state and private organizations in the areas of soil dynamics and geophysics. He is currently serving as a

consultant to the Civil Engineering Division and the Earthquake Hazards Mitigation Program of the National Science Foundation.

W. Ronald Hudson is a Professor of Civil Engineering at The University of Texas at Austin. He has a wide variety of experience as a research engineer with the State Department of Highways and Public Transportation and the Center for Transportation Research at The University of Texas at Austin and was Assistant Chief of the Rigid Pavement Research Branch of the AASHO Road Test. He is the author of numerous publications and was the receipient of the ASCE J. James R. Croes Medal. He is presently concerned with research in the areas of (1) design of pavement management systems, (2) measurement of pavement roughness and performance, (3) rigid pavement slab analysis and design, and (4) low volume roads.

A. H. Meyer is a Senior Lecturer in the Department of Civil Engineering at The University of Texas at Austin. He serves as an investigator on several continuing projects through the Center for Transportation Research. Before coming to The University of Texas in 1980, he was with the Civil Engineering Department and the Texas Transportation Institute at Texas A & M University. His area of specialization is in pavements (construction, evaluation, and maintenance) and pavement materials (portland cement concrete, rapid setting cements, and polymer concrete).

In addition to his teaching and research duties, Dr. Meyer is active in several professional and technical societies including the Texas Society of Professional Engineers, the American Society of Civil Engineers and the

Transportation Research Board. He is a licensed professional engineer in Texas and has published more than 30 research reports and papers.